



<https://theses.gla.ac.uk/>

Theses Digitisation:

<https://www.gla.ac.uk/myglasgow/research/enlighten/theses/digitisation/>

This is a digitised version of the original print thesis.

Copyright and moral rights for this work are retained by the author

A copy can be downloaded for personal non-commercial research or study,  
without prior permission or charge

This work cannot be reproduced or quoted extensively from without first  
obtaining permission in writing from the author

The content must not be changed in any way or sold commercially in any  
format or medium without the formal permission of the author

When referring to this work, full bibliographic details including the author,  
title, awarding institution and date of the thesis must be given

Enlighten: Theses

<https://theses.gla.ac.uk/>  
[research-enlighten@glasgow.ac.uk](mailto:research-enlighten@glasgow.ac.uk)

# **Adhesion Characterisation of Bonded Steel/Composite Cleavage Joints**

by

**Muhammad Shahid**

A thesis submitted to  
the Department of Mechanical Engineering  
University of Glasgow



**UNIVERSITY  
of  
GLASGOW**

in fulfilment of the requirement for  
the Degree of Doctor of Philosophy

© **Muhammad Shahid**, December 2000

ProQuest Number: 10647750

All rights reserved

INFORMATION TO ALL USERS

The quality of this reproduction is dependent upon the quality of the copy submitted.

In the unlikely event that the author did not send a complete manuscript and there are missing pages, these will be noted. Also, if material had to be removed, a note will indicate the deletion.



ProQuest 10647750

Published by ProQuest LLC (2017). Copyright of the Dissertation is held by the Author.

All rights reserved.

This work is protected against unauthorized copying under Title 17, United States Code  
Microform Edition © ProQuest LLC.

ProQuest LLC.  
789 East Eisenhower Parkway  
P.O. Box 1346  
Ann Arbor, MI 48106 – 1346

GLASGOW  
UNIVERSITY  
LIBRARY

12222

COPY 2

**Dedicated to my Parents**

## *Abstract*

There are an increasing number of applications for adhesive bonding in structural design with thick adherends. These include hybrid metal/composite materials, particularly in the marine, construction, and automotive industries. Failure of such connections normally arises from cleavage stresses. This study is largely experimental with theoretical aspects. The overall aims and objectives are: to improve the understanding of local cleavage strength and failure of bonded steel and composite adhesive joints, to develop a suitable experimental technique for evaluating the mechanical adhesion mechanism between steel and composite and to establish simplified theoretical models to assess critical stresses in cleavage joints, with reference to bonding parameters.

The experimental programme to evaluate cleavage specimens was based on the method described in BS 5350:Part C1:1986<sup>1</sup>. Mild steel and glass-fibre reinforced epoxy composite (GRE) adherends and a two-part toughened epoxy adhesive were used. The composite laminates were produced in-house by hot press moulding, from prepregs. The standard cleavage specimen was modified by inserting a GRE laminate between the steel adherends to allow testing of the cleavage joint between steel and composite, to prevent delamination failure. The specimens were tested to destruction on a universal tensile testing machine to examine the effect of adherend pre-treatments and surface conditions such as roughness and fibre orientation (in composites). Elastic finite element analyses (FEA) were performed to assess cleavage stresses in the adhesive at various conditions. A partial FEA modelling technique based on idealised butt joints was also used to study surface roughness and composite geometric and material details. Visual and light microscopic examination of the failure surfaces was used to verify the analyses. Mathematical relations based on classic mechanics and FEA results were developed to calculate the cleavage strength of standard joints.

The work shows that: (i) the modified cleavage specimen is a good specimen for testing composite/metal joints, (ii) grit-blasting of steel produces better and more consistent strengths than polishing, (iii) polished epoxy composite produces a joint strength consistently higher than that of both grit-blasted and polished steel, (iv) cleavage strength increases with the roughness level and profile area of adherends' surfaces and, (v) partial modelling of cleavage joints into elements of butt joints provides a useful evaluation technique.

## *Contents*

<b>Abstract</b>	3
<b>List of Figure</b>	9
<b>List of Tables</b>	15
<b>Nomenclature</b>	16
<b>Acknowledgements</b>	18
<b>1. Introduction</b>	
1.1. General Introduction	19
1.2. Aims and Objectives	22
1.3. Adhesion and Adhesives	23
1.4. Composites	27
1.5. Adhesive Bonding: Process and Applications	30
<b>2. Theoretical Aspects and Literature Review</b>	
2.1. General Review	43
2.2. Adhesion Mechanisms and Theories	44
2.2.1. Adsorption and Wetting	44
2.2.2. Mechanical Adhesion	47
2.2.3. Electrostatic Theory	47
2.2.4. Diffusion Theory	49
2.2.5. Real Solution	50
2.3. Factors Affecting Bond Strength	50
2.3.1. Effect of Adherend Surface Pre-treatment	51
2.3.1.1. Effect of Surface Roughness	54
2.3.1.2. Effect of Adhesive Thickness	58
2.3.2. Effect of Geometric Parameters	60
2.4. Adhesive Joints	60
2.4.1. Type of Joints	61

	5
2.4.2. Mechanical Behaviour	61
2.4.3. Mechanical Testing	62
2.4.4. Modes of Failure	64
2.5. Failure Analysis	66
2.5.1. Classical Mechanics (Analytical) Analysis	68
2.5.2. Numerical (Finite Element) Analysis	72
<b>3. Properties of the Materials</b>	
3.1. Introduction	89
3.2. Model Materials	89
3.3. Adhesive Selection	90
3.4. Production and Testing of Bulk Adhesive	90
3.5. Production of Laminates	92
3.6. Properties of the Materials	93
<b>4. Surface Profilometry</b>	
4.1. Introduction	100
4.2. Roughness Parameters	100
4.3. Talysurf	103
4.3.1. Basic Principle	103
4.3.2. Measurements of Specimens	104
4.3.3. Results	104
4.4. Atomic Force Microscope	105
4.4.1. Basic Principle	105
4.4.2. Measurements of Specimens	108
4.4.3. Results	108
4.5. Michelson's Interferometer	108
4.5.1. Basic Principle	109
4.5.2. Measurements of Specimens	110
4.5.3. Results	110

**5. Testing of Steel/Steel Cleavage Specimens**

5.1.	Introduction	128
5.2.	Specifications of Specimens	128
5.3.	Experimental Programme	128
5.4.	Grit-blasting of Adherends	129
5.5.	Polishing of Adherends	129
5.6.	Natural Oxidation of Adherends	130
5.7.	Control of Adhesive Thickness	130
5.8.	Bonding of Specimens	130
5.9.	Testing of Specimens	131
5.10.	Results	131
5.10.1.	Influence of Adhesive Thickness	131
5.10.2.	Influence of Natural Oxidation	132
5.10.3.	Influence of Bonding Area	133
5.10.4.	Influence of Surface Roughness	133
5.10.4.1.	Effect of $R_a$	134
5.10.4.2.	Effect of $R_{iu}^2$	134
5.10.5.	Influence of Over-curing	135

**6. Testing of Steel/Composite Cleavage Specimens**

6.1.	Introduction	152
6.2.	Specification of Specimens	152
6.3.	Experimental Details	152
6.4.	Pre-treatment of Adherends	153
6.5.	Bonding of Specimens	154
6.6.	Testing	154
6.7.	Results	155
6.7.1.	No Surface Pre-treatment (as moulded)	155
6.7.2.	Acetone Cleaning	155

	7
6.7.3. Roughening with Emery Paper	156
6.7.4. Grit-blasting	156
6.7.5. Influence of Polishing	157
6.7.6. Influence of Peel Ply	157
6.7.7. Influence of Fibre Directions	157
6.7.8. Influence of Matrix Material	158
6.7.9. Influence of Insert on Joint Strength	158
<b>7. Stress Analyses</b>	
7.1. Introduction	169
7.2. Software Packages	170
7.3. Numerical Analysis	171
7.3.1. Steel/Steel Cleavage Specimen	171
7.3.2. Steel/Composite/Steel Hybrid Cleavage Specimen	173
7.3.3. Partial Modelling of Joints	175
7.3.3.1. Modelling of Surface Roughness	176
7.3.3.2. Hybrid Steel/Composite/Steel Joint	177
7.4. Development of Equations for Maximum Cleavage Stress	180
7.4.1. Classic Mechanics Approach	180
7.4.2. Finite Element Approach	182
<b>8. Discussion</b>	
8.1. Adhesive Selection	231
8.2. Process Variables for Composite Moulding	232
8.3. Roughness Measurements	233
8.4. Effect of Adhesive Thickness	234
8.5. Effect of Corrosion	236
8.6. Effect of Surface Roughness	237
8.7. Effect of Surface Pre-treatment of Composites	241
8.8. Effect of Fibre Directions	243

8.9.	FE Modelling	245
8.10.	Loci of Failure	249
8.11.	Final Comments	251
<b>9.</b>	<b>Conclusions and Recommendations for Future Work</b>	
9.1.	Conclusions	253
9.2.	Recommendations for Future Work	254
	<b>References</b>	256
	<b>Appendices</b>	273

## *List of Figures*

Figure 1.1	Cleavage failure in an adhesively bonded panel (1.2 m x 1.2 m x 8mm).....	34
Figure 1.2	Load distribution in different joints (a) a welded joint; (b) a riveted joint; (c) an adhesive joint.....	35
Figure 1.3	Schematic representation of the function of elastomeric spheres.....	36
Figure 1.4	(a) Supported core sandwich constructions; (b) Core/laminate bonds for foams and honeycombs.....	36
Figure 1.5	Applications of adhesive and sealant in a modern car.....	37
Figure 1.6	Suspension link with composite shaft and aluminium ends.....	38
Figure 1.7	Ford Ranger/Explorer cross wheel beam (two component moulded and bonded composite).....	38
Figure 1.8	(a) Police car door (composite ballistic armour); (b) Composite hood of Alfa Romeo; (c) Delphi SuperPlug <sup>®</sup> door modular consolidated sixty parts to one module; (d) Rivet-less composite container; (e) Composite rail car; (f) A composite cycle fork.....	39
Figure 1.9	Utilisation of composite and/or adhesive technology in the structures of B-2 bomber (top) and Fokker 100 (bottom).....	40
Figure 1.10	a) Velocity aircraft; (b) Floor panel of Sea Hawk helicopter; (c) Bearing- free composite blade and yoke in Bell helicopter 430; (d) Floor panel of Black Hawk helicopter; (e) C-141 Tail Cone with aluminium honeycomb core and composite skins; (f) Spoiler made of honeycomb core with formed aluminium skin.....	41
Figure 1.11	(a) A composite electrical transmission tower; (b) Jacketing of free way columns using adhesively bonded composite sheets; (c) A composite bridge.....	42
Figure 1.12	(a) Composite golf clubs; (b) A composite leisure boat; (c) A composite tennis racket.....	42
Figure 2.1	Isolated contact points leading to weak adhesion between two rigid rough surfaces.....	79
Figure 2.2	Correlation between wetting angle and behaviour of adhesives.....	79
Figure 2.3	Schematic representation of mechanical hooking.....	80
Figure 2.4	Schematic representation of bond formation by electrostatic attraction.....	80
Figure 2.5	Schematic representation of bond formation by molecular entanglement.....	81
Figure 2.6	Schematic representation of various impurities present on an untreated metallic surface.....	81

	<b>10</b>
Figure 2.7	Correlation between adhesive strength and surface roughness.....82
Figure 2.8	Diversion of stresses- lock and key effect. ....82
Figure 2.9	Schematic representation of trapped air under the adhesive.....83
Figure 2.10	Void-free ideal interfacial contact with a low viscosity adhesive.....83
Figure 2.11	Four basic types of joints: (a) angle; (b) tee; (c) butt; (d) surface.....84
Figure 2.12	Stresses in adhesively bonded joints.....84
Figure 2.13	Idealisation of a tubular joint into a lap shear joint.....85
Figure 2.14	Failure modes in adhesive joint: (a) cohesion; (b) adhesion; (c) mixed mode; (d) adherend. ....86
Figure 2.15	Comparison between analytical and finite element results for a double lap joint with composite adherends. ....86
Figure 3.1	Sketch of bulk adhesive tensile test specimen and dimensions .....94
Figure 3.2	Production of dog-bone specimens.....95
Figure 3.3	Strain gauge mounted dog-bone specimen .....95
Figure 3.4	Experimental set-up for testing dog-bone specimen.....96
Figure 3.5	Load extension graph from the testing of a bulk adhesive specimen .....96
Figure 3.6	Mould for the production of laminates .....97
Figure 3.7	Micrograph showing (a) a good laminate; (b) a bad laminate .....97
Figure 3.8	Hydraulic heated platen used for moulding laminates.....98
Figure 4.1	Graphical representation of $R_a$ .....111
Figure 4.2	Graphical representation of $R_t$ .....111
Figure 4.3	Graphical representation of linear profile length, $R_{lo}$ .....112
Figure 4.4	Graphical representation of $R_{dq}$ .....112
Figure 4.5	Taylor and Hobson's Talysurf Series 2 50i surface profiler .....113
Figure 4.6	Schematic layout of a typical Talysurf instrument .....113
Figure 4.7	A typical inductive gauge and its working principle .....114
Figure 4.8	A 3D surface profile of grit-blasted (40/60) steel as characterised by Talysurf.....114
Figure 4.9	A 3D surface profile of polished Fibredux (WR) surface as characterised by Talysurf.....115
Figure 4.10	Roughness profile of polished steel surface.....116
Figure 4.11	Roughness profile of polished Tufnol surface.....117
Figure 4.12	Roughness profile of polished Fibredux (UD) surface .....118
Figure 4.13	Schematic diagram of the overall operation of a typical AFM.....119
Figure 4.14	The beam-bounce detection scheme .....119
Figure 4.15	The working cycle of AFM.....120
Figure 4.16	AFM set-up for operation in liquid environment.....120

Figure 4.17 AFM profile of a polished steel surface.....121

Figure 4.18 AFM profile of a polished Fibredux (WR) surface.....122

Figure 4.19 Nikon Corporation’s OPTIPHOT interference microscope.....123

Figure 4.20 Working principle of a double-beam interference microscope .....123

Figure 4.21 Disturbance fringes .....124

Figure 4.22 Interferometric profile of a polished steel surface .....125

Figure 5.1 Standard cleavage test specimen.....136

Figure 5.2 Thick adherend lap-shear specimen.....136

Figure 5.3 Typical grit-blasted steel surface .....137

Figure 5.4 Typical polished steel surface .....137

Figure 5.5 Specimen with attached wire spacers.....138

Figure 5.6 Mixing of adhesive by manual mixing gun .....138

Figure 5.7 Jig used for bonding cleavage specimens .....139

Figure 5.8 Partially bonded cleavage specimen with debond at the rear end .....139

Figure 5.9 Testing of cleavage specimens.....140

Figure 5.10 Fractured surface of polished steel joint showing unbonds .....140

Figure 5.11 Fractured surfaces of grit-blasted cleavage specimen showing mixed mode failure (0.1mm adhesive) .....141

Figure 5.12 Fractured surfaces of grit-blasted cleavage specimen showing mixed mode failure (0.5mm adhesive) .....141

Figure 5.13 Fractured surfaces of polished cleavage specimen showing adhesion failure (0.1mm adhesive) .....142

Figure 5.14 Fractured surfaces of polished cleavage specimen showing adhesion failure (0.5mm adhesive) .....142

Figure 5.15 Fractured surfaces of a lap-shear specimen showing mixed mode failure (0.1mm adhesive).....143

Figure 5.16 Fractured surface of a lap-shear specimen showing adhesive shearing (0.5mm adhesive).....143

Figure 5.17 Fractured surfaces of rusted steel cleavage specimen (a) grit-blasted; (b) polished.....144

Figure 5.18 Fractured surfaces of partially bonded (50%) steel cleavage specimen (a) grit-blasted; (b) polished.....145

Figure 5.19 Fractured surface of grit-blasted cleavage joint showing stress whitening in the initial joint region.....146

Figure 5.20 Fractured surface of grit-blasted steel cleavage specimen showing failure initiation from the edge.....146

Figure 5.21 Variation of cleavage strength with average roughness,  $R_a$ .....147

Figure 5.22	Variation of cleavage strength with effective area of bonding (experimental results) .....	147
Figure 6.1	Configuration of modified cleavage specimens.....	159
Figure 6.2	Typical grit-blasted surface of a GRE laminate.....	159
Figure 6.3	Typical polished GRE surface .....	160
Figure 6.4	Jig for the bonding of hybrid cleavage specimens.....	160
Figure 6.5	Fractured surfaces of a hybrid joint made with solvent cleaned laminate showing adhesion failure .....	161
Figure 6.6	Fractured surfaces of a hybrid joint made with emery paper roughened laminate.....	161
Figure 6.7	Fractured surfaces of a hybrid joint made with grit-blasted Fibredux laminate showing failure initiation at the composite surface.....	162
Figure 6.8	Fractured surfaces of a hybrid joint made with grit-blasted Tufnol laminate showing failure initiation at the composite surface.....	162
Figure 6.9	Fractured surfaces of a hybrid joint made with polished composite showing failure initiation at the steel surface (a) with Fibredux laminate; (b) with Tufnol laminate .....	163
Figure 6.10	Fractured surface of a hybrid joint using Fibredux composite made with peel ply.....	164
Figure 6.11	Fractured surface of a hybrid joint made with polyester laminate showing interlaminar failure .....	164
Figure 6.12	Fractured surfaces of a hybrid joint made with 90 <sup>0</sup> unidirectional Fibredux laminate.....	165
Figure 7.1	Schematic details of types of numerical models.....	184
Figure 7.2	Cleavage specimens (a) standard; (b) simplified (Model S).....	185
Figure 7.3	Finite element model (Model S) .....	186
Figure 7.4	Possible failure sites in the adhesive line.....	187
Figure 7.5	Minimum principal stress distribution in adhesive line of Model S (see Fig. 7.4) (a) full length; (b) initial 2mm.....	188
Figure 7.6	Maximum principal stress distribution in adhesive line of Model S (see Fig. 7.4) (a) full length; (b) initial 2mm.....	189
Figure 7.7	Axial stress distribution in adhesive line of Model S (see Fig. 7.4) (a) full length; (b) initial 2mm .....	190
Figure 7.8	Normal tensile stress distribution in adhesive line of Model S (see Fig. 7.4) (a) full length; (b) initial 2mm.....	191
Figure 7.9	Shear stress distribution in adhesive line of Model S (see Fig. 7.4) (a) full length; (b) initial 2mm .....	192

Figure 7.10	Von Mises stress distribution in adhesive line of Model S (see Fig. 7.4) (a) full length; (b) initial 2mm .....	193
Figure 7.11	Contour plot of normal stress ( $S_{22}$ ) in Model S.....	194
Figure 7.12	Contour plot of von Mises in Model S.....	195
Figure 7.13	Fractured surfaces of steel/steel cleavage specimen showing failure initiation at the surface (a) polished steel; (b) grit-blasted steel .....	196
Figure 7.14	Modified hybrid cleavage specimen (Model H) .....	197
Figure 7.15	Finite element model (Model H).....	197
Figure 7.16	Possible failure sites in Model H .....	198
Figure 7.17	Contour plot of normal stress ( $S_{22}$ ) in Model H.....	199
Figure 7.18	Contour plot of normal stress ( $S_{22}$ ) in adhesive line of Model H.....	200
Figure 7.19	Normal stress distribution in adhesive line of Model H (with isotropic laminate properties) (see Fig. 7.16) (a) full length; (b) initial 2mm .....	201
Figure 7.20	Fractured surfaces of hybrid cleavage specimen showing failure initiation at steel surface and then apparent shift towards bulk adhesive layer.....	202
Figure 7.21	Normal stress distribution in adhesive line of Model H (with orthotropic properties) (see Fig. 7.16) (a) full length; (b) initial 2mm.....	203
Figure 7.22	Tensile stress ( $S_{22}$ ) distribution in adhesive line of Model H (with steel insert - see Fig. 7.16) (a) full length; (b) initial 2mm .....	204
Figure 7.23	Representation of cleavage joint as multiple butt joints .....	205
Figure 7.24	Actual surface profile of grit-blasted surface as seen by Talysurf.....	205
Figure 7.25	Schematic diagram of the roughness models (a) Model P1; (b) Model P2 ....	206
Figure 7.26	Numerical model of the surface roughness (Model P2).....	206
Figure 7.27	Possible failure sites in the roughness models (Models P1 and P2).....	207
Figure 7.28	Transformation of normal stress at the rough surface.....	207
Figure 7.29	Normal stress distribution in adhesive line (see Figure 7.27) (a) Model P1; (b) Model P2.....	208
Figure 7.30	Normal stress distribution in the first millimetre of adhesive line (a) Model P1; (b) Model P2 .....	209
Figure 7.31	Fractured surfaces of grit-blasted cleavage joint showing failure initiation at the loaded edge .....	210
Figure 7.32	Details of partial hybrid model (Model P3).....	211
Figure 7.33	Schematic diagram of partial hybrid model (Model P4).....	212
Figure 7.34	Model P3 (Numerical model) .....	213
Figure 7.35	Possible failure sites in Model P3.....	214
Figure 7.36	Contour plot of normal stress ( $S_{22}$ ) in the adhesive line of Model P3 .....	215
Figure 7.37	Contour plot of normal stress ( $S_{22}$ ) in the laminate matrix of Model P3 .....	216

Figure 7.38	Normal stress ( $S_{22}$ ) distribution in adhesive line of Model P3 (see Fig. 7.35) (a) full length; (b) initial 1mm.....	217
Figure 7.39	Normal stress ( $S_{22}$ ) distribution at the glass cylinder surface in Model P3.....	218
Figure 7.40	Model P4 (Black spots showing first matching nodes).....	219
Figure 7.41	Possible failure sites (Model P4) .....	220
Figure 7.42	Contour plot of normal stress ( $S_{22}$ ) in the adhesive line of Model P4 .....	221
Figure 7.43	Normal stress ( $S_{22}$ ) distribution in adhesive line of Model P4 (see Fig. 7.41) (a) full length; (b) initial 1mm.....	222
Figure 7.44	Stresses through thickness at first matching nodes in Model P4 (see Figures 7.40 and 7.41) .....	223
Figure 7.45	Idealisation of cleavage forces as triangular distributed load .....	224
Figure 7.46	Calculated stresses from triangular load in cleavage joint.....	225
Figure 7.47	FE and calculated normal stresses in Model S.....	225
Figure 7.48	FE and calculated stresses in Model H (a) full joint length; (b) initial 2mm..	226
Figure 7.49	Variation of edge node stress with changing adhesive modulus of elasticity .....	227
Figure 7.50	Normal tensile stress ( $S_{22}$ ) distribution in adhesive line of Model H with double adhesive modulus (see Fig. 7.16) (a) full length; (b) initial 2mm.....	228
Figure A1	Stress-strain curve obtained from the tensile testing of bulk adhesive dog-bone specimen.....	274
Figure A2	Triangular load distribution along a 12.5mm beam (Model S).....	275
Figure A3	Triangular load distribution along a 15mm beam (Model H).....	277

## *List of Tables*

Table 2.1	Parameters influencing the strength of adhesive joints.....	87
Table 2.2	Typical surface pre-treatment processes.....	87
Table 2.3	Various surface pre-treatment methods.....	88
Table 2.4	Effect of surface topography on peel load.....	88
Table 3.1	Properties of bulk adhesive (Araldite 420A/B).....	99
Table 3.2	Properties of laminate in warp direction.....	99
Table 3.3	Properties of mild steel.....	99
Table 4.1	Surface roughness of adherends measured by Talysurf.....	126
Table 4.2	Surface roughness of adherends measured by AFM.....	127
Table 4.3	Surface roughness of adherends measured by Interferometer.....	127
Table 5.1	Effect of adhesive thickness on cleavage strength of steel specimens.....	148
Table 5.2	Effect of adhesive thickness on lap-shear strength of steel specimens.....	148
Table 5.3	Effect of corrosion on cleavage strength of steel specimens.....	149
Table 5.4	Effect of variable bonding area on cleavage strength of steel specimens.....	150
Table 5.5	Cleavage strength with different surface finishes of steel.....	151
Table 5.6	Effect of over-curing on cleavage strength of steel specimens.....	151
Table 6.1	Effect of surface treatment of GRE laminate on cleavage strength of hybrid specimens.....	166
Table 6.2	Cleavage strength of hybrid specimens with GRP laminate.....	168
Table 6.3	Cleavage strength of hybrid specimens with steel insert.....	168
Table 7.1	Comparison of stresses in the roughness models (Models P1 and P2).....	209
Table 7.2	Properties of adherends and adhesive.....	229
Table 7.3	Isotropic properties of laminate.....	229
Table 7.4	Orthotropic properties of laminate.....	230
Table A	Stress-strain measurements from bulk adhesive specimen.....	273

## Nomenclature

$\theta_R$	contact angles of sessile drop on rough surface ( $^{\circ}$ )
$\theta_0$	contact angles of sessile drop on smooth horizontal surface ( $^{\circ}$ )
$W_R$	Wenzel's roughness factor (true area/nominal area)
$\alpha_m$	maximum slope of the surface roughness at the liquid periphery ( $^{\circ}$ )
$W_B$	work required to break the adhesive bond ( $J/m^2$ )
$\sigma_u^2$	surface charge density ( $mC/m^2$ )
$h_B$	separation of surfaces at electrical breakdown ( $\mu m$ )
$E_c$	energy stored in the capacitor ( $J/m^2$ )
$\psi$	total adhesion
$\psi_M$	mechanical component of adhesion
$\psi_A$	adsorption component of adhesion
$\psi_D$	diffusion component of adhesion
$\psi_E$	electrical component of adhesion
$\alpha$	mixing constant for adhesion
$\beta$	mixing constant for adhesion
$\gamma$	mixing constant for adhesion
$\delta$	mixing constant for adhesion
$V$	voltage (V)
$R_a$	average roughness ( $\mu m$ )
$S_m$	mean spacing ( $\mu m$ )
$L$	sampling length (mm)
$l_n$	evaluation length (mm)
$R_q$	root mean square roughness ( $\mu m$ )
$R_t$ or $R_{y_{max}}$	maximum peak to valley height ( $\mu m$ )
$R_{lo}$	linear profile length (mm)
$R_{dq}$	root mean square slope ( $^{\circ}$ )
RMS	root mean square roughness ( $\mu m$ )
$\theta$	slope of the profile at any given point ( $^{\circ}$ )
$\lambda$	wavelength of the light source (nm)
SP1	minimum principal stress (MPa)
SP2	maximum principal stress (MPa)

$S_{11}$	normal stress along x-axis ( <i>MPa</i> )
$S_{22}$	normal stress along y-axis ( <i>MPa</i> )
$S_{12}$	shear stress ( <i>MPa</i> )
$F_Y$	force components along x-axis ( <i>kN</i> )
$M_A$	moment of force ( <i>kNm</i> )
$\sigma$	cleavage stress ( <i>MPa</i> )
$F$	applied cleavage force ( <i>kN</i> )
$x$	distance along adhesive line ( <i>mm</i> )
$E$	modulus of elasticity ( <i>GPa</i> )
$E_1$	Young's modulus of composite along x-axis ( <i>MPa</i> )
$E_2$	Young's modulus of composite along y-axis ( <i>MPa</i> )
$\nu_{12}$	Poisson's ratio in xy-plane
$G_{12}$	compression modulus of composite in xy-plane ( <i>MPa</i> )
$G_{13}$	compression modulus of composite in xz-plane ( <i>MPa</i> )
$G_{23}$	compression modulus of composite in yz-plane ( <i>MPa</i> )

### *Acknowledgements*

First of all I would like to thank Dr. Safa A. Hashim for his supervision, encouragement and support throughout this study in all academic and non-academic matters. Thanks are also due to the technicians, Alex Torry and Denis Kearns for their assistance in experimental work. I would also like to thank the computing staff, especially Kenneth Stevenson who helped with computing-related problems. Thanks to Jane Livingston for proof-reading this thesis.

This work would never have taken place without funding from the Overseas Research Scheme (ORS) Award and the Faculty of Engineering Scholarship. I thank both of the governing bodies for their financial support. Supports of Ciba Chemicals (now Vantico) and Hexcel Composites in supplying material are also acknowledged.

Support and encouragement from my wife Asma is acknowledged here. Children Shoaib, Afshan and Suhaib have shown a great deal of understanding and patience during this busy time. Thanks are also due to them. Friendship of good friends, Joan and Suman in particular, provided a good friendly environment throughout the study.

Prayers and good wishes from family and friends, especially my mother in Pakistan have been of great help in motivating me throughout this study.

## CHAPTER ONE

### *INTRODUCTION*

#### **1.1 General Introduction**

The concept of adhesive bonding is not new. The use of copper chloride poisoned casein adhesives by Egyptians in fabricating mummy cases is an example of a very early use of adhesive. It is an ancient art that has become highly sophisticated, nevertheless the formulation and use of adhesive still relies largely on empirical findings<sup>2</sup>.

Except for the introduction of rubber and pyroxylin cements a hundred years ago, there was little advance in adhesive technology until the twentieth century. In World War I casein glues were used to bond wooden structures but they had limited moisture and mould growth resistance. In the 1930's, adhesives based on synthetic resins offered solutions to these problems. Phenol formaldehyde was the first synthetic resin of importance to adhesive bonding. In the 1950's, epoxies, one of the most important structural adhesives, were introduced. Since then, adhesive bonding has grown very rapidly replacing other joining technologies in many structural and non-structural applications. Hart-Smith<sup>3</sup> has given a good summary of the historical background of adhesive bonding, with particular reference to its applications in the aerospace industry.

The rapid expansion<sup>2</sup> in the use of adhesives is due to the continually improving range of properties offered as well as the increasing recognition of their advantages over conventional joining techniques. A number of references highlight the advantages and disadvantages of adhesive bonding<sup>2,4,5,6,7,8,9,10</sup>. Depending on the nature of the adhesive, substrates, bonding procedure, the design of the joint, and the intended end use, adhesive bonding may offer one or more of the following advantages:

- simplified design
- distortion-free joining
- unaffected microstructure of adherends
- dissimilar material and materials difficult to join by conventional methods can be joined (e.g. glass, ceramics and china; wood, rubber and plastics; concrete and stone)
- prevention of cathodic corrosion i.e. ability to join galvanically problematic metals
- weight reduction
- possibility of providing a more uniform stress distribution (Figure 1.1) in comparison with other joining methods. This allows use of thin gauge materials and hence results in weight reduction and cost savings
- increased fatigue life at low loading regime
- ability to join and seal simultaneously
- ability to join shock-sensitive substrates
- potential to join very thin and small parts that would otherwise be difficult to join using other joining techniques
- minimal finishing cost
- complex shapes may be fabricated
- can be combined with other fastening methods
- vibration damping
- large areas and large number of parts can be bonded in one operation
- electrically insulating
- automation
- less expensive than other joining methods
- smoother surface finish due to absence of fastener heads, weld runs etc.

Like any other technology adhesive bonding has limitations including:

- influence of time on process properties
- sensitivity to surface preparation. Careful preparation of the substrate surfaces are needed
- difficult to dismantle and limited repair possibilities

- poor short-term handling in general
- sensitive to elevated service temperatures when compared with other fastening methods
- need for safety precautions in handling adhesives due to toxicity and flammability problems
- lack of reliable non-destructive methods for in-field evaluation of bond properties
- change of properties of joint with time (ageing of adhesive layer etc.)
- bond durability depends strongly on bonding conditions
- special curing conditions such as UV, high temperature may be needed
- can be more expensive than other joining methods
- low peel strength and high creep sensitivity
- complicated strength calculations
- residual stresses may be created due to difference in coefficients of thermal expansion.

Because of the advantages, adhesive bonding is rapidly replacing or complementing other joining techniques in primary structural applications ranging from household items to highly sophisticated fighter planes and space shuttles. The ability of adhesive bonding to join dissimilar adherends with minimal stress concentrations has allowed designers to use composite materials in conjunction with conventional metals. The composite materials offer distinct advantages of corrosion resistance and high stiffness to weight ratios over their metallic counterparts. Such bonded hybrid structures are finding an increasing range of applications in civil, marine, automotive and aerospace industries<sup>11,12</sup>. For example, composite drive shafts are currently being used to reduce weight in military aircraft; to eliminate the lateral critical speed in automotive applications; to span long distances in cooling tower drives; and many other applications. Probably the most challenging and often most overlooked problem is the end fitting attachment method<sup>13</sup>.

In a number of applications involving hybrid composite/steel structures where the adherends are relatively thick, joints are prone to generate cleavage rather than peel failures. Cleavage stresses can be detrimental to the integrity of the load bearing joint

and normally cause failure at lower loads than in other modes. In a number of references it is, therefore, recommended that peel and cleavage loading should be avoided whenever possible<sup>2,10,14</sup>.

An example of cleavage failure in a load bearing joint is shown in Figure 1.1, where despite design measures being taken to reduce cleavage stresses at the end of the stiffeners, failure is taking place. Therefore it is important to understand cleavage strength at a local level, and a good starting point for this is to examine the behaviour of a small standard joint specimen. Despite the critical importance of the cleavage mode, very little work has so far been done on cleavage joints, with practically no work on hybrid steel/composite cleavage joints. In the available references, most of the cited data are for simple lap shear joints, and cleavage strength is very rarely quoted<sup>2</sup>.

## **1.2 Aims and Objectives**

The study is mainly concerned with thick adherend applications and the underlying aims of the research are: (i) to improve the understanding of local cleavage strength and failure of adhesive joints, between steel and composite, (ii) to develop a suitable experimental technique for evaluating the mechanical adhesion mechanism between steel and composite and, (iii) to establish simplified theoretical models to assess critical stresses in cleavage joints, with reference to various bonding parameters. The study is largely based on experimental techniques with numerical and analytical aspects. The detailed objectives of the research programme are:

- to select suitable model materials for cleavage specimens, including epoxy adhesive, steel and polymeric composite
- to modify an existing standard cleavage specimen to suit the mechanical testing of cleavage strength between steel and composite adherends, and to validate the modification
- to design a jig for the in-house production of composite laminates from the prepregs, with well controlled moulding parameters

- to carry out experiments to study the surface preparation methods of composites
- to study the effect of surface roughness and polishing of steel and composite on the strength of steel/steel and steel/composite cleavage joints
- to study the effect of natural oxidation on the initial strength of the steel/steel cleavage strength
- to study the effect of fibre directions of composites on the strength of hybrid cleavage specimens
- to carry out a parametric study based on numerical analyses, on the effect of various surface parameters on the cleavage strength of standard cleavage specimens
- to compare stress results from experiments with those found by finite element analysis
- to partially model the cleavage joint and numerically analyse the effect of surface roughness and laminate insertion on the strength of cleavage joint
- to develop design equations for the calculation of cleavage stresses in the cleavage joints.

### **1.3 Adhesion and Adhesives**

Adhesion is defined as the state in which two surfaces are held together by interfacial forces which may consist of valence forces, interlocking surfaces, or both<sup>15</sup>. Practically, it is the phenomenon by which the adhesive takes up the stress from the adherend<sup>4</sup>. The measured physical strength of an adhesive bond is known as practical adhesion. Bond strength (or adherence) is defined as the load required to break an adhesive assembly with failure occurring in or near the plane of the bond<sup>15</sup>.

An adhesive is needed to generate adhesion. It is a substance capable of holding materials together by surface attachment<sup>15</sup>. A structural adhesive is a bonding agent used for transferring loads between adherends exposed to service environments for the structure involved<sup>15</sup>. Practical adhesive bond strengths are typically in excess of 6.9MPa (1000psi) at room temperature when tests are performed in accordance with ASTM standards for lap shear joints.

Adhesive joining is the process of joining parts using an adhesive which undergoes a physical or chemical hardening reaction causing the parts to join together through surface adherence (adhesion) and internal strength (cohesion). The resultant assembly is an adhesive joint or an adhesive bond<sup>4</sup>.

An adhesive joint is a location at which two adherends are held together by a layer of adhesive<sup>15</sup>. Adhesive joints are composite systems whose strength depends on both the geometrical design and loading type as well as on the individual strengths of the components to be joined, the adhesive and the interface layer. The overall strength of a joint is limited by the weakest member.

A great many types of adhesives are currently in use and there is no adequate single system of classification for all products<sup>16</sup>. Several authors have discussed classification of adhesives in detail<sup>4,16,17</sup>. Adhesive materials may be classified in terms of origin, end use, physical form, chemical composition, methods of application, various processing factors (e.g. setting action) and suitability for particular service requirements or environments. Some common classification methods of adhesives are given below:

- *based on origin*; such as natural products (starch, dextrin, natural rubber), semi-synthetic (cellulose nitrate, castor oil-based polyurethane) or synthetic products, made by various polymerisation techniques, such as epoxies, polyurethane, polysulphide rubber
- *based on end use*; such as metal-to-metal adhesives, wood adhesives, general purpose adhesives, paper and packaging adhesives
- *based on solubility or fusibility of the final glue line*; soluble or fusible adhesives include starch derivatives, asphalt and thermoplastics like vinyl and acrylics. Insoluble or thermosetting include cements, epoxies, polyurethane and vulcanised natural and synthetic rubbers
- *based on chemistry*; adhesives may be classified into two major classes of organic and inorganic. Inorganic adhesives include Portland cement and solder. Organic adhesives are polymers. They normally have lower specific gravity than inorganic adhesives or most adherends. Thus assemblies produced by polymer-based adhesives weigh less than those produced by

inorganic adhesives, a major advantage in the aerospace industry where lightweight structures are of paramount importance<sup>4</sup>.

Organic adhesives can be classified:

- *based on functional group*; such as phenolics, epoxies, proteins, acrylics etc.
- *based on physical form*; such as film adhesives, paste adhesives, liquid adhesives and solid adhesives (hot melts). Film adhesives are the highest performing and most expensive structural adhesives commonly available. Adhesive thickness control is easier in these adhesives. They often require low temperature storage, heat curing and specialised handling. They are single component systems and may be based on phenolics, epoxide, polyimide or any other chemical class. Paste adhesives may be one- or two-part materials. One-part adhesives contain both resin and hardener, and therefore need low-temperature storage. They normally require heat or another form of energy for curing. Two-part adhesives contain a curing agent in one-part and a cross-linkable resin in the other part. They can be stored at room temperature and can normally be cured at room temperature. Liquid adhesives are available as one-component adhesives like cyanoacrylates, which cure by absorbing moisture from the air, or as two-component adhesives in which one component acts as the initiator. They are usually acrylic in nature. Some water-based phenolic adhesives are also available in liquid form. They are used for bonding wood. Hot-melt adhesives are solid compounds that are used as adhesives. They must melt at a much higher temperature than the service temperature.

Some important types of adhesives are detailed below:

*Phenolics:* They are made by the reaction of phenol and formaldehyde. When formaldehyde is kept in excess and a basic catalyst such as NaOH is used, the reaction product is called resole phenolic resin. They are self-curing and water-soluble. When phenol is kept in excess and an acid catalyst is used, the reaction product is a novolac phenolic resin. They need an external curing agent. The most common curing agent is hexamethylene tetra-amine. Phenolic based hot-bonded

systems cure by condensation reaction which means that water vapour is generated during the cure. High pressure is, therefore, needed to be applied across the joint during the reaction period. The difference in peel strength between phenolic resins and modern modified epoxide resins has been one of the reasons why phenolic systems have been replaced in many applications by epoxide resins<sup>18</sup>.

*Urethane resins:* They are reaction products of a polyester-, polyether- or polybutadiene-based polyol and an isocyanate in the presence of a suitable catalyst. They can be formulated to cure at room temperature or at elevated temperature. Both one- and two-component urethane adhesives are available. Single component adhesives cure by reacting with moisture from air. Examples of such adhesives include adhesives used to bond windshield to the main body in automotive applications. Urethane adhesives usually give a rapid cure.

*Acrylics:* Acrylic adhesives are well known for their fast curing characteristics. They are, therefore, very good for automated application in fast assembly lines. Acrylic adhesive can be either a redox-activated or cyanoacrylate type. Redox-activated types undergo a free radical polymerisation. Anaerobic adhesives used in thread locking and many two-part initiator activated acrylics belong to this class. Cyanoacrylate adhesives react by an anionic addition polymerisation. "Super Glue" is a very common example of this type of acrylic adhesive. Cyanoacrylate adhesives are thermoplastic in nature and therefore undergo creep at high temperatures and are susceptible to attack by moisture.

*Epoxy resins:* Resins having oxirane rings as their functional groups are known as epoxy resins. They constitute the largest group of structural adhesives. DGEBA (diglycidal ether of bis-phenol A), the common type of epoxy resin is made by the reaction of epichlorohydrin and bis-phenol A. If bis-phenol F is used in place of bis-phenol A, the epoxy is called DGEBPF. This has a higher crystallisation resistance and a lower viscosity.

One reason for the wide use of epoxy resins in structural adhesives is that they can be cured with a range of hardeners including, but not limited to, aliphatic amines, amides, anhydrides, mercaptanes, aromatic amines, dicyandiamine etc. They can be

modified with a range of fillers and modifiers such as clay, carbon, rubber, glass fibres etc. With an unlimited combination of curing agents, modifiers, catalysts and fillers, a system of required viscosity, pot life, colour, physical and chemical resistance and curing condition can be formulated.

Unmodified, cured epoxy resins are inherently brittle and inextensible materials. Rigidity in cured epoxy resins can be reduced to obtain energy absorption by two methods, flexibilisation and toughening by phase separation. In the flexibilisation method, an elastomer is added to the resin which is soluble before and after the cure. The cured, formulated, flexibilised adhesive has a single glass transition temperature which is lower than that obtained with the unmodified epoxy resin. It also has a lower modulus of elasticity compared to the unmodified resin.

In the second method, an elastomer is added to the resin system which is soluble in the uncured resin but insoluble in the cured epoxy resin. Such an elastomer separates from the resin as the latter starts curing. In a properly chosen elastomer/epoxy system, the elastomer disperses uniformly in the epoxy matrix as discrete balls of about 0.2-2 microns in diameter. The dispersed particles act as a dead-end to stop propagation of a crack. Schematically it is represented in Figure 1.3. A toughened epoxy shows two glass transition temperatures; one for the cured epoxy resin and the other for the phase-separated elastomer. Compared to the flexibilised epoxy adhesive, the toughened epoxy adhesive shows only a moderate increase in extensibility. Since the continuous phase (resin) is left essentially unchanged, its stiffness, high load-bearing capability, creep resistance and thermal stability are preserved<sup>19</sup>. Elastomeric additives increase the fracture energy of the epoxy by an order of magnitude<sup>20</sup>.

#### **1.4 Composites**

A composite material may be defined as a physical mixture of two or more different materials with properties generally better (in relation to defined criteria) than those of any constituents<sup>21</sup>. Polymeric composite materials represent about 90% of all composites<sup>22</sup>.

Resin systems such as epoxies and polyesters have a limited use for the manufacture of structures on their own, since their mechanical properties are not very high compared to most metals. It is when the resin systems are combined with reinforcing fibres such as glass, carbon and aramid that exceptional properties can be obtained. The resin matrix spreads the load applied to the composite between each of the individual fibres and also protects the fibres from damage caused by abrasion and impact. High strength and stiffness, ease of moulding into complex shapes and high environmental resistance, all coupled with low densities, make the resultant composite superior to metals for many structural and non-structural applications. Higher specific strength and stiffness properties are particularly important in applications which involve movement, such as cars, trains and aircraft, since lighter structures play a significant part in making these applications more efficient.

It is however, unrealistic to believe that composites have no disadvantages compared to conventional materials. The principal barriers to their rapid growth are their higher cost, less well-defined and optimised fabrication processes, lack of design and engineering database (which would enable producers to employ advanced composites with acceptable risk) and often lower impact strength.

Mechanical joints are limited by the bearing strength of their substrates. In the case when one or both of the substrates are composites, resin failure at fastener holes and the difference in stiffness properties between the fastener and composite substrate, create bearing stresses and affect the structural integrity at the joint. Therefore, joining techniques used for metals, such as bolting and riveting, are not very suitable for joining composites, and adhesive bonding is often used, which enables designers to take full advantage of their properties.

Composites based on epoxy or polyester resin give a polar surface with high surface energy and therefore lead to good wetting and adhesion via the adsorption mechanism. Thermoplastic composites, on the other hand, have very low surface energies and are difficult to bond without sophisticated surface treatment.

Polymeric composites are divided into two main groups. *Advanced composites*, which are made of very long, very high performance reinforcements and high

performance resins. They are typically used in aerospace, high performance sporting goods and specialised civil applications. *Engineering composites* on the other hand utilise fibres of shorter and lower mechanical properties with lower performance resins. Examples of this type include boat hulls, storage tanks, bath tubs, etc.

The primary role of reinforcement in a composite material is to increase the mechanical properties of the neat resin system. Since the mechanical properties of most reinforcing fibres are considerably higher than those of unreinforced resin systems, the mechanical properties of the fibre/resin composite are, therefore, dominated by the contribution of the fibre to the composite. The four main factors that govern the fibre's contribution are:

- the basic mechanical properties of the fibre itself
- the surface interaction of fibre and resin (the 'interface')
- the amount of fibre in the composite ('Fibre Volume Fraction')
- the orientation of the fibres in the composite.

Only in a few processes, such as hot pressing and filament winding, can individual fibre or fibre bundles be used on their own. For most other applications, the fibres need to be arranged into some form of sheet, known as a fabric, to make handling possible. Owing to the number of ways and orientations in which fibres can be assembled into sheets, a great many varieties of fabrics can be made, each having their own characteristics, which in turn affect the end properties of the end composite. Fabric types are categorised by the orientation of the fibres used, and by the various construction methods used to hold the fibres together. The four main fibre orientation categories are unidirectional, 0/90, multiaxial, and others/random.

To keep the fibres in place, especially in the case of unidirectional fibres, and to ensure that the proper amount of resin is used, the fibres are often impregnated with a pre-catalysed resin system in a separate step to make a sheet. These sheets are called *prepregs*. The resin system in these prepregs is largely latent at ambient temperatures giving rise to working times ranging from many days to several months. The prepreg resins can only be fully cured by heating them to the prescribed cure temperature.

Furthermore, this technology allows the use of very tough and strong resin systems that would be too high in viscosity to be impregnated by hand.

The end properties of a composite are not only a function of the individual properties of the resin matrix and fibres, but are also a function of the way in which the materials themselves are designed into the part and also the way in which they are processed. Some manufacturing methods give precise control over the direction, overlap, and other placement parameters of the reinforcement fibres while the others are more flexible. Accordingly, the fibre directions and hence the end properties of the resultant composites are more random. The common manufacturing processes for composites are spray-up, hand lay-up, filament winding, pultrusion, resin transfer moulding, vacuum bagging and hot press moulding. Each process has its own advantages and disadvantages.

Selection of an appropriate manufacturing process is not only important from the viewpoint of the desired strength and geometric properties of the resulting composite, but it is also important from the point of view of its intended use, especially if the composite is going to be adhesively bonded. Wrong choice of a mould release agent and a thick layer of resin at the composite surface may lead to poor bonded joints. Internal mould release agents, such as those used in pultrusion and other processes, generally give poor adhesion. Thick resin layers formed during hand lay-up and spray-up processes also make the composites weaker for adhesive bonding.

### **1.5 Adhesive Bonding: Process and Applications**

Optimum results from adhesive bonding can only be obtained when attention is given to each step of the bonding process i.e. designing of the joint, selection of the adhesive, selection of the surface pre-treatment method, fabrication of the assembly, process control and the testing procedure (to ensure reliability and durability of the adhesive bond). Most of these factors are inter-related. For example joint stresses, type and size, together with the overall strength requirements, will dominate the selection of a suitable adhesive.

Common processing problems, inconsistencies in surface treatment, misalignment of the parts to be bonded, variation in bond line thickness, inaccuracy in mix ratio, non-uniform mixing, variation in clamp pressure and curing schedule can all drastically affect the end results.

The overall performance of an adhesive metal joint is characterised by the measure to which it is able to withstand loads without any appreciable changes in its original strength values. The specific properties of the adhesive joint are a result of the strengths obtained due to the geometrical and material design.

Three basic requirements for good adhesion, as given by Brewis<sup>23</sup>, are:

- good contact between the adhesive and the substrate i.e. good wetting
- absence of weak boundary layer
- avoidance of stress concentration which could lead to disbonding.

The above requirements are related to a number of factors including (but not limited to) topography of substrate, weak boundary layer, chemistry of adhesive and adherend, pre-treatments, primers, bonding conditions, ageing conditions and stresses in the bonded structures. The combined action of the influencing factors and their parameters are the basis for the production of an optimal adhesive joint, and govern its attainable strength.

Modern adhesives have found extensive usage in a great variety of industries, for example, aerospace, automotive, marine, civil, sports, dental, etc. Almost every industrial and commercial sector benefits from the use of adhesives. Adhesive applications may be classified into two broad categories: non-structural and structural. Examples of non-structural applications include gap-filling and decorative bonding. Structural applications are found in primary load bearing structures, for example, bonding in honeycomb structures, bonding of stiffeners to the bonnet in an automobile, bonded repairs in aerospace and civil applications<sup>24</sup>, etc. Figure 1.4 shows the application of adhesive bonding in honeycomb structures that are used in aerospace, automotive, civil and marine applications for their excellent stiffness and strength-to-weight ratio.

In today's vehicles, metal structural components are usually bolted or welded together. But because tomorrow's more fuel-efficient vehicles will require a variety of lightweight materials, different methods of joining structural pieces together are needed. Structural adhesive bonding is a key technology for joining and assembling advanced, lightweight materials, both critical factors in meeting the goal of developing a car capable of up to 80 mpg that maintains current levels of consumer acceptability for cost, comfort, performance, utility and safety<sup>25</sup>.

In the automotive industry, it is not only weight benefit which is increasing the usage of composite and adhesive bonding, but also their ability to be formed into stylish, aerodynamic shapes and to combine several parts into one, giving better aesthetics and better acoustic and thermal insulation. Examples of composite structures and adhesive bonding in the automotive industry include adhesive bonded stiffeners, windshields, drive shafts, springs for heavy trucks and trailers, air intake manifolds, car hoods, suspension links, cross-vehicle beams, luggage racks and a rivet-free intermodal shipping container. Figure 1.5 shows the locations in a typical automobile where adhesive bonding is used. Figures 1.6-1.8 also show some of the applications of adhesive bonding and/or composite applications in the automotive/locomotive field.

The aerospace industry pioneered the application of adhesives in structural bonding, as well as many other technological innovations. Today, adhesives are used to bond and repair critical components in commercial and military aircraft, helicopters and spacecraft. Figure 1.9 shows the locations where composite structure, and hence adhesive bonding, is applied in a B-2 bomber and a Fokker 100 plane.

US Army UH-60A Black Hawk and US Navy SH-60 Sea Hawk helicopters use lightweight composite floor panels. Composite components (adhesively and non adhesively joined) in the "Velocity" aircraft include the canard and wings, spar sections, fuel/wing strakes, fuselage, main landing gear, fairings, seat backs and bottoms, center console and instrument panel, ducts and covers. In the Bell Helicopter Model 430, the blades and the yoke which holds the blade are made of glass fibre hybrid composite. The bearing-free design improves quality and reduces part count and maintenance (Figure 1.10).

The reduced weight, increased durability and extremely high strength properties achievable with composite products, and their imperviousness to corrosion and attack by marine organisms or degradation, has resulted in many emerging applications in the civil engineering and infrastructure areas as replacements for steel and concrete. A number of these applications also include the application of adhesive bonding. Typical infrastructure/civil/marine engineering applications include decks for both pedestrian and vehicle bridges across waterways, railways and roadways, marine piles and fenders, pier decking, railings, pipes and pontoons. Composite reinforcing bars may be used to replace steel in conventional reinforced concrete in order to prevent "concrete cancer", a problem resulting from internal corrosion of the reinforcement.

Composite power and lighting poles and high voltage electrical transmission towers constructed from pultruded composites are finding increased applications for both performance and environmental reasons.

Composite plates using carbon fibre reinforcement are successfully used to repair masonry beams, columns, buildings and other structures damaged/weakened by impact, earthquake or subsidence, and can usually be bonded in place by hand without the need for heavy lifting equipment. Such repairs can be carried out much more rapidly than by traditional techniques (Figure 1.11).

Several boats, scuba tanks, personal watercrafts and sports items such as golf clubs and tennis rackets are also made from composite materials, and often use adhesive bonding for their assembly (Figure 1.12).

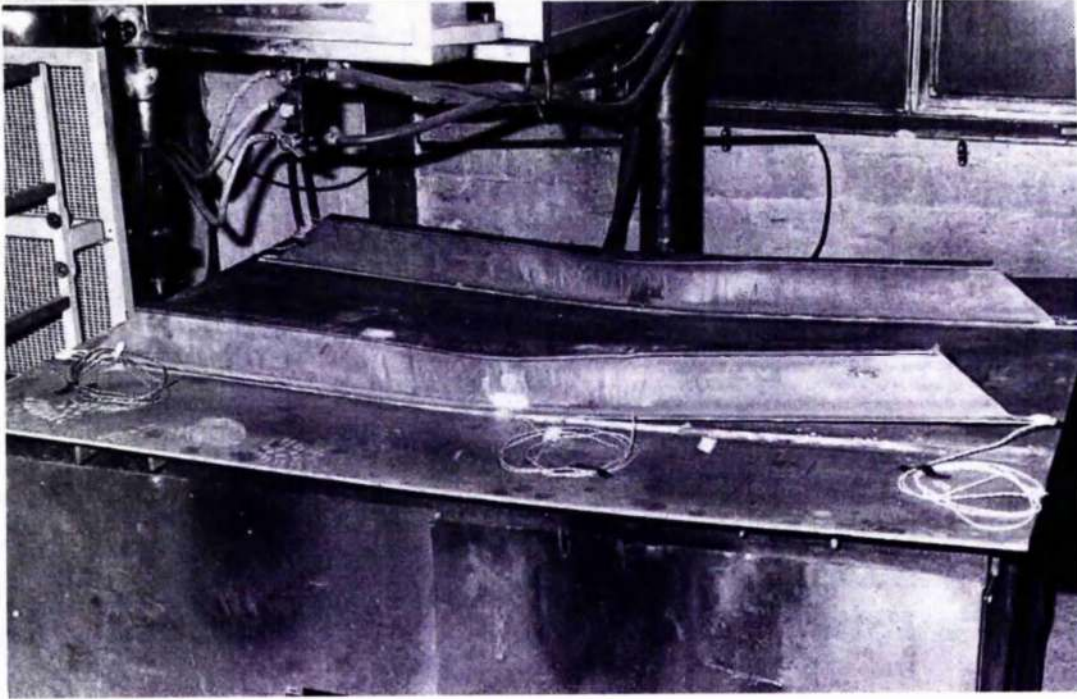


Figure 1.1 Cleavage failure in an adhesively bonded panel (1.2 m x 1.2 m x 8mm)

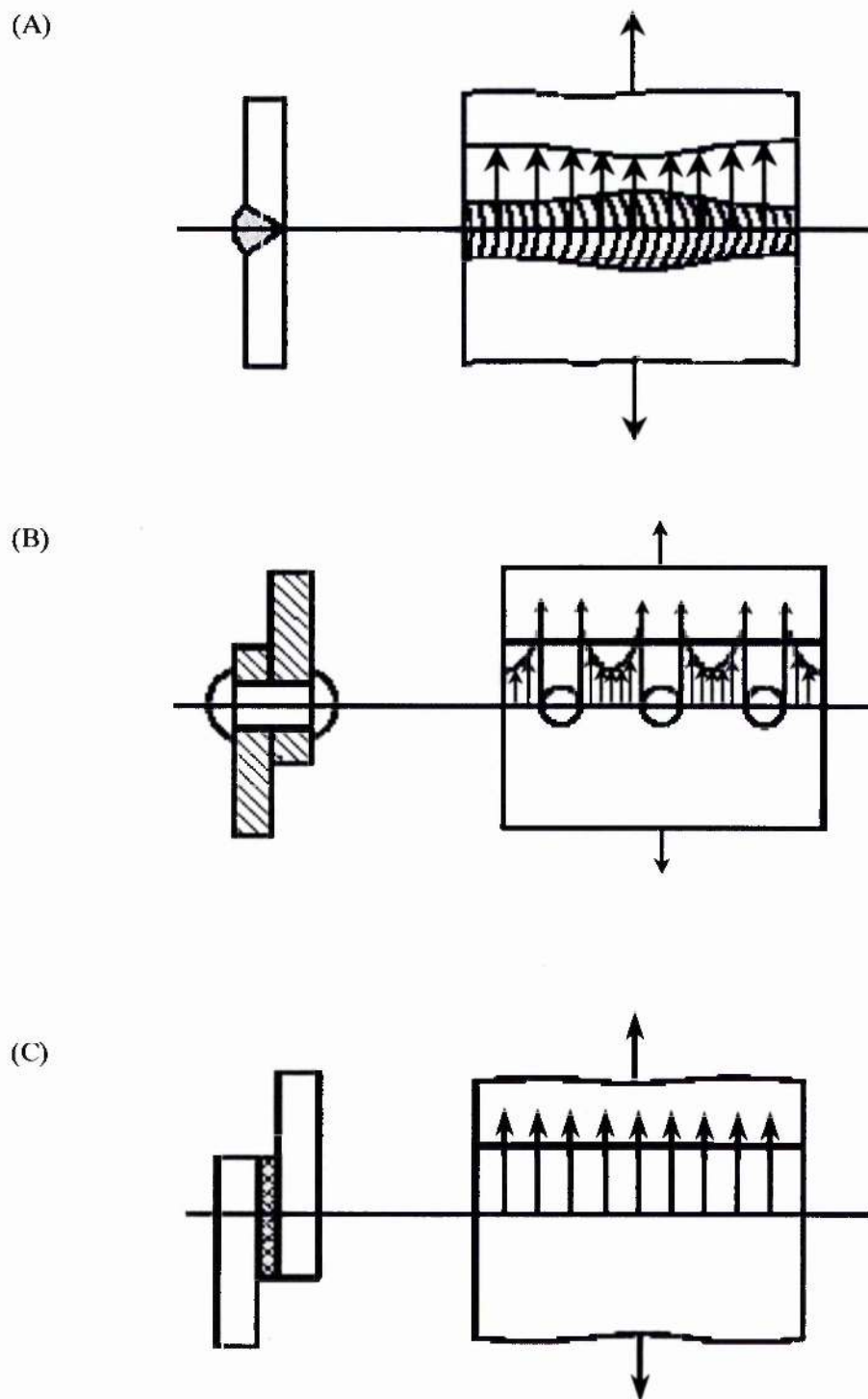


Figure 1.2 Load distribution in different joints: (a) a welded joint; (b) a riveted joint; (c) an adhesive joint

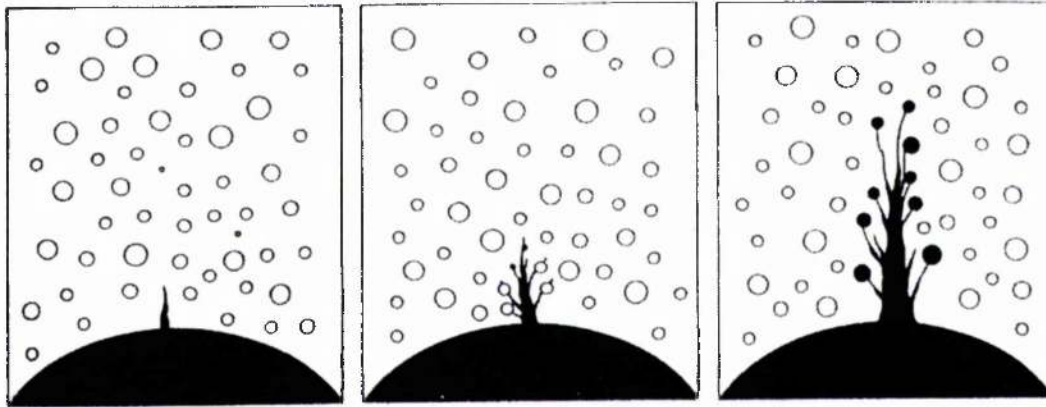
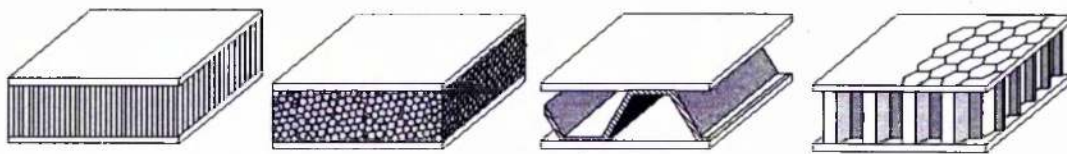
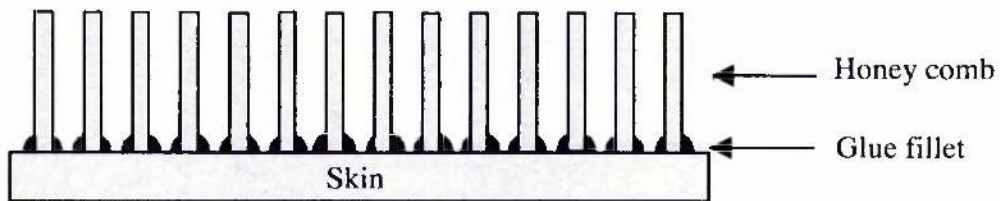
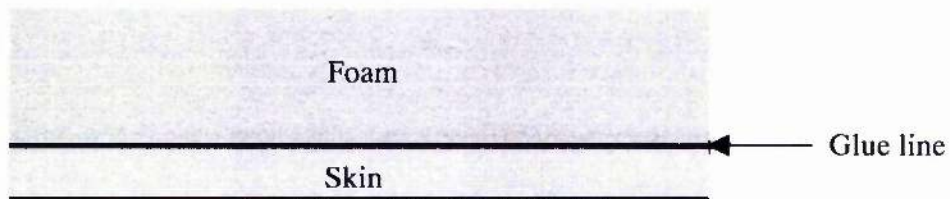


Figure 1.3 Schematic representation of the function of elastomeric spheres<sup>5</sup>



(a)



(b)

Figure 1.4 (a) Supported core sandwich constructions; (b) Core/laminate bonds for foams and honeycombs

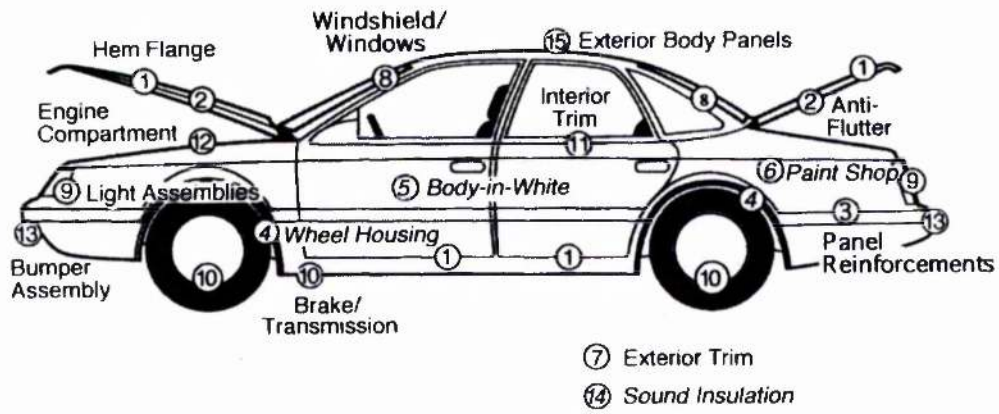


Figure 1.5 Applications of adhesive and sealant in a modern car<sup>4</sup>



Figure 1.6 Suspension link with composite shaft and aluminium ends

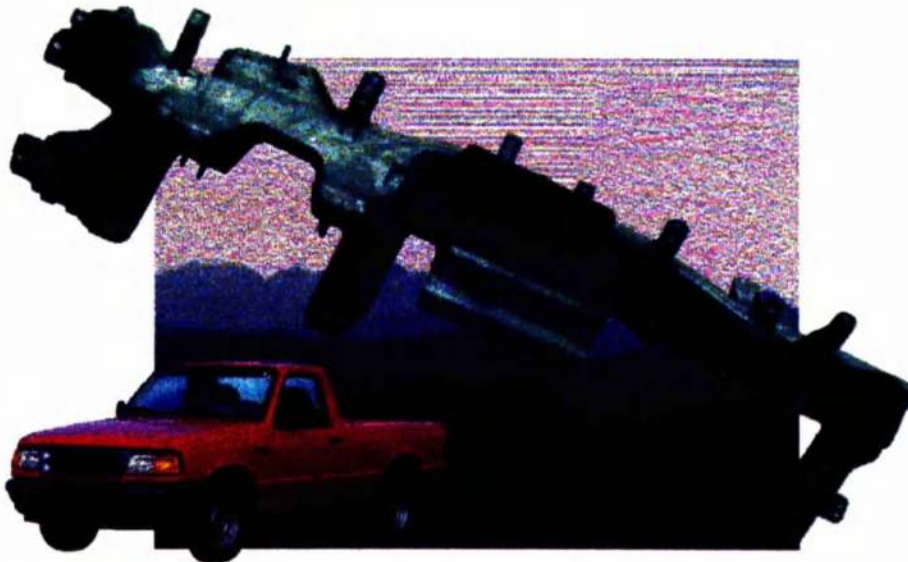
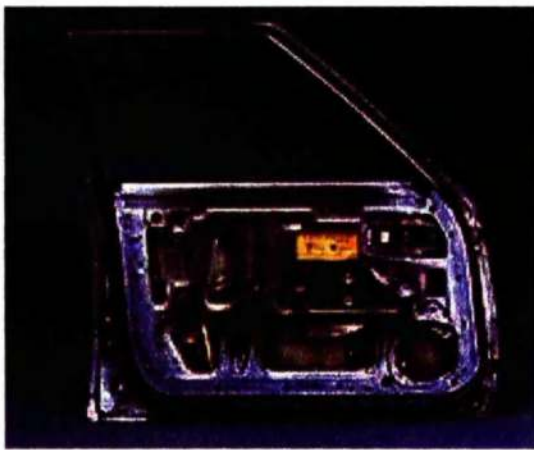
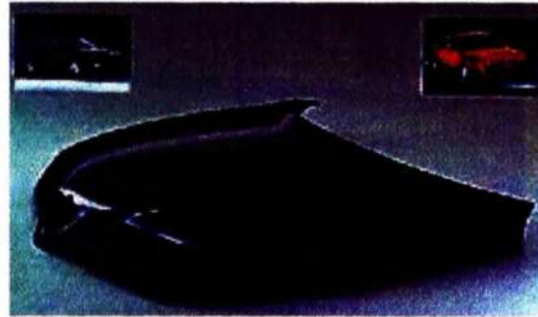


Figure 1.7 Ford Ranger/Explorer cross wheel beam (two component moulded and bonded composite)



(a)



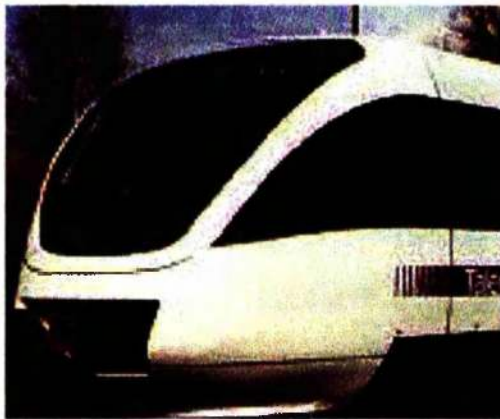
(b)



(c)



(d)

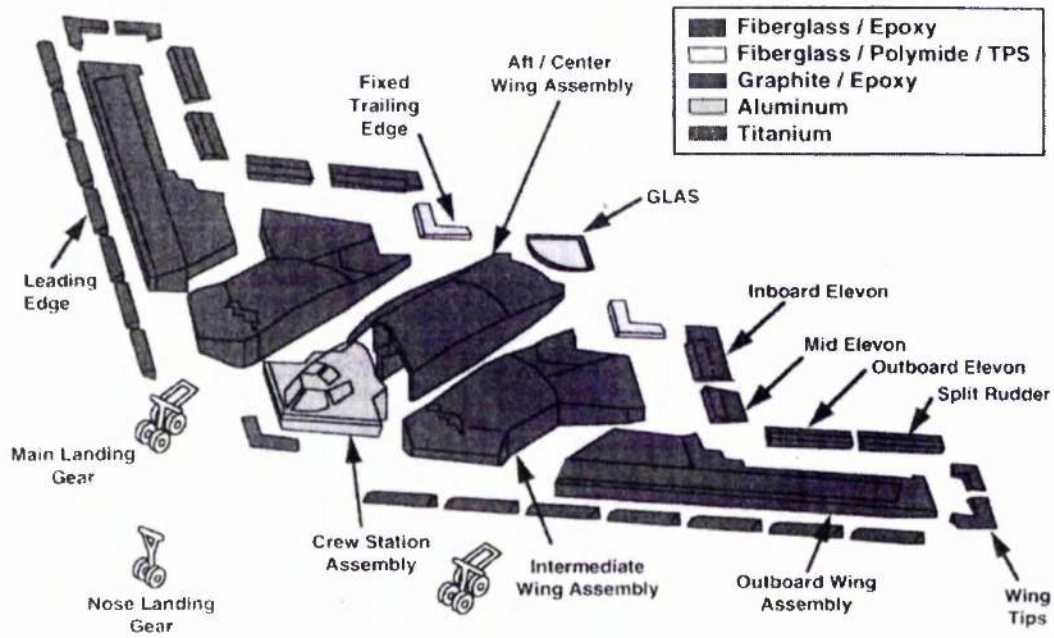


(e)



(f)

Figure 1.8 (a) Police car door (composite ballistic armour); (b) Composite hood of Alfa Romeo; (c) Delphi SuperPlug<sup>®</sup> door modular consolidated sixty parts to one module; (d) Rivet-less composite container; (e) Composite rail car; (f) A composite cycle fork



**Fokker 100**

- Adhesively bonded laminate and stringers
- Adhesively bonded laminate
- Adhesively bonded metal sandwich
- Composites

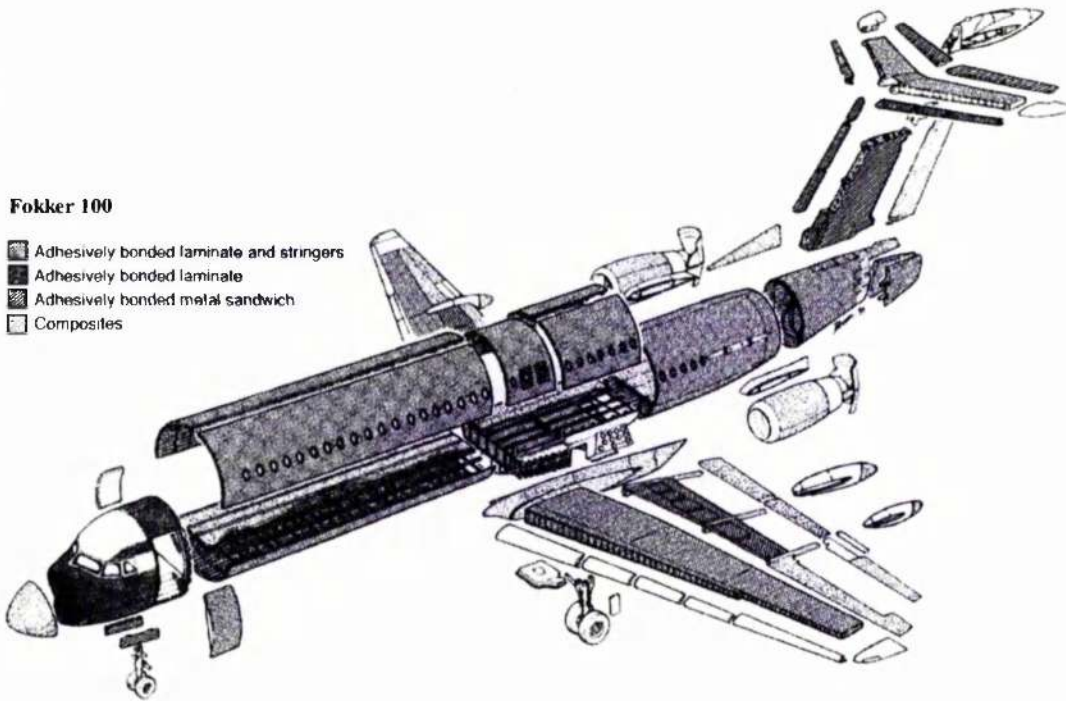
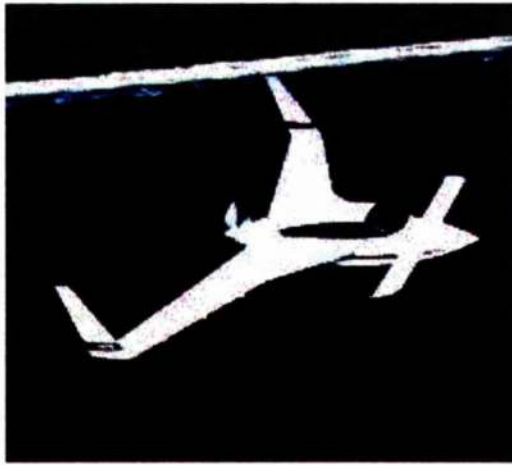


Figure 1.9 Utilisation of composite and/or adhesive technology in the structures of B-2 bomber (top) and Fokker 100 (bottom)<sup>4</sup>



(a)



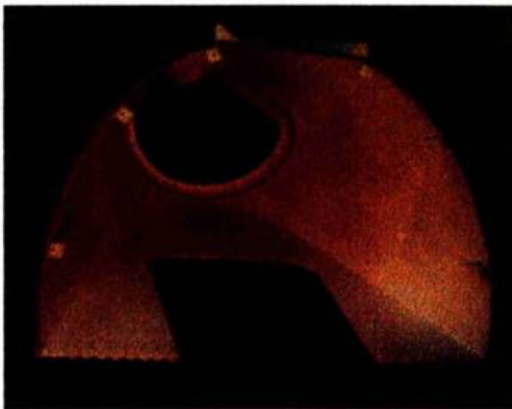
(b)



(c)



(d)



(e)



(f)

Figure 1.10 a) Velocity aircraft; (b) Floor panel of Sea Hawk helicopter; (c) Bearing-free composite blade and yoke in Bell helicopter 430; (d) Floor panel of Black Hawk helicopter; (e) C-141 Tail Cone with aluminium honeycomb core and composite skins; (f) Spoiler made of honeycomb core with formed aluminium skin

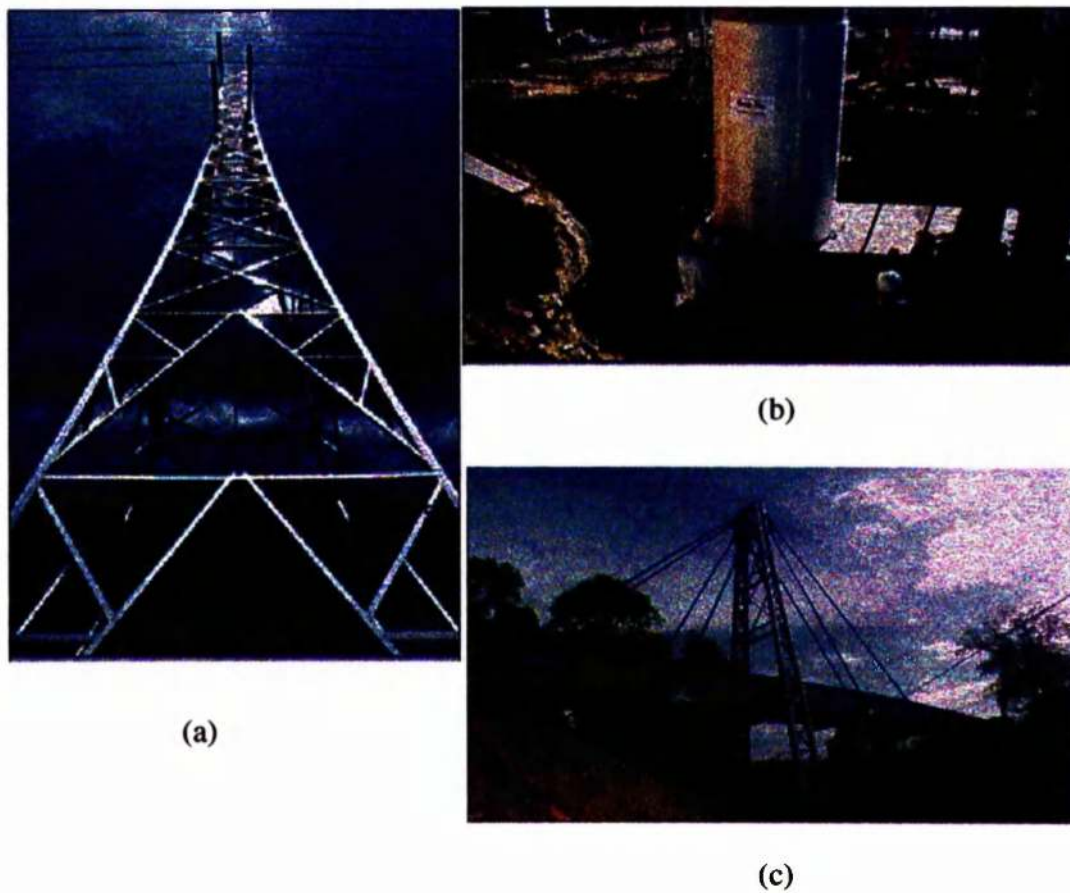


Figure 1.11 (a) A composite electrical transmission tower; (b) Jacketing of free way columns using adhesively bonded composite sheets; (c) A composite bridge

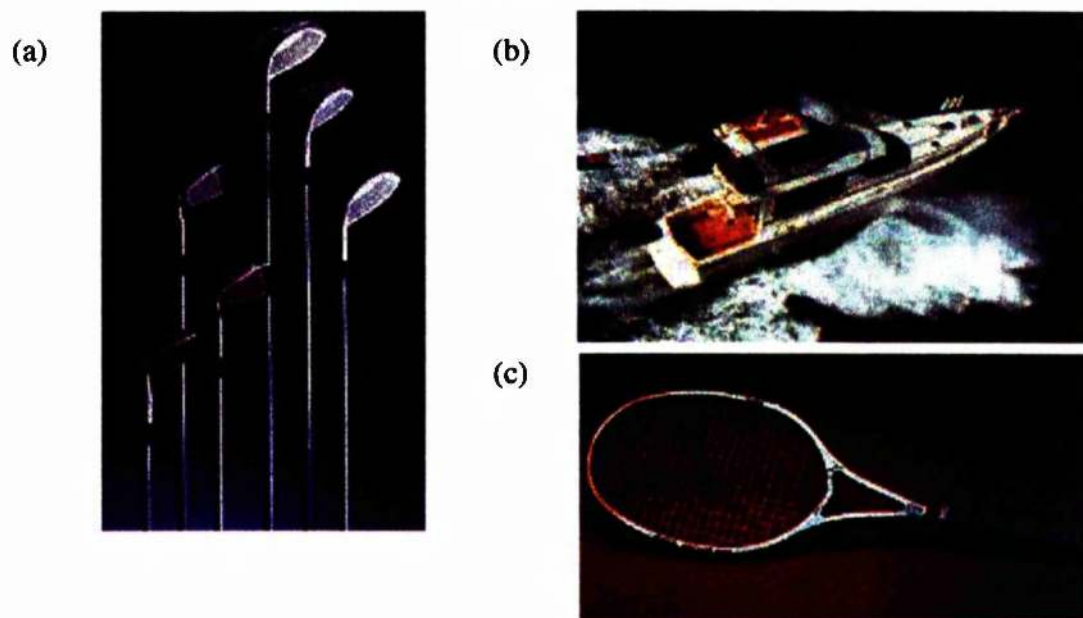


Figure 1.12 (a) Composite golf clubs; (b) A composite leisure boat; (c) A composite tennis racket

## CHAPTER TWO

### *THEORETICAL ASPECTS AND LITERATURE REVIEW*

#### **2.1 General Review**

Achieving the level of strength, reliability and durability in adhesive joints that can match or surpass those of other joining methods is the ultimate target of adhesive bonding technology. Achievement of this target is only possible if we fully understand the actual mechanism of adhesion and the way different parameters affect the bond strength and its durability. Several researchers have made their valuable contribution towards increasing our understanding of the subject. However, very little work has so far been done on cleavage joints, and therefore a general literature review relating to adhesive bonding is presented here.

Total adhesion is a combination of specific adhesion (the adhesion between surfaces which are held together by valence forces of the same type as those which give rise to cohesion<sup>15</sup>) and mechanical adhesion (caused by interlocking of the adhesive on surface irregularities). Both of these adhesion types are important for understanding adhesion improvement by surface pre-treatment.

Ely and Tabor<sup>26</sup> calculated that physical forces (e.g. van der Waals' forces) alone are sufficient to give a strong adhesive bond. The discrepancy between the actual and theoretical strength is because of deviation from the ideal behaviour considered during the calculations. Of various factors that affect the adhesive strength, the most important is the existence of flaws within and at the interface of adhesive and adherends that reduce the joint strength, either by facilitating yielding or initiating crack propagation.

## 2.2 Adhesion Mechanisms and Theories of Adhesion

Implicit in the formation of an acceptable adhesive bond is the ability of the adhesive to wet and spread on the adherends being joined. Attainment of such interfacial molecular contact is a necessary first step in the formation of strong and stable adhesive joints. Once the wetting is achieved, intrinsic adhesive forces are generated across the interface through a number of mechanisms. The precise nature of these mechanisms has been the subject of physical and chemical study since at least the 1960s, with the result that a number of theories of adhesion exist.

The various types of intrinsic forces which may operate across the adhesive (or primer)/substrate interface are commonly referred to as the mechanisms of adhesion<sup>27</sup>. There is no unifying theory that can link the basic physio-chemical properties of materials to the actual strength of an adhesive bond<sup>4</sup>. All different theories and available literature on adhesion address specific phenomena but the actual strength of an adhesive bond is probably a combination of all of these.

Allen<sup>28</sup>, Wake<sup>29</sup>, Kinloch<sup>27</sup>, Hull<sup>30</sup> and Pocius<sup>4</sup> have discussed these theories in detail. Four main mechanisms that can occur at the interface, either in isolation or combination, are detailed below.

### 2.2.1 Adsorption and Wetting

The main mechanism of adhesion is explained by the adsorption theory, which states that substances 'stick' primarily because of intimate intermolecular contact. In adhesive joints this contact is attained by intermolecular or valence forces exerted by molecules on the surface layers of the adhesive and adherend.

When two solids are brought together the surface roughness on micro and atomic scales prevents the surfaces from coming into contact except at isolated points, as shown in Figure 2.1. Even if we assume that the surfaces are free from all contamination and strong adhesion occur at the contact points, the adhesion average over the whole surface will be weak. Therefore, for effective adhesion, the adhesive

must cover every hill and valley of the surface to displace all the air, which in turn requires minimum or no interfacial flaws. A necessary condition for attaining high adhesion forces is the ability of the adhesive to wet the surfaces of the joining parts properly. Therefore, the study of adhesion cannot be separated from the study of wettability and contact angle phenomena.

It has been known that wetting of a surface by liquid is governed by its roughness. Several workers<sup>31,32</sup> have addressed this aspect of wetting behaviour and a number of hypotheses have been proposed to explain the differing wetting characteristics of rough and smooth surfaces. The degree of wetting or spreading can be determined by contact angle measurement.

In contact angle measurement, a drop of liquid is placed on a solid with a condition that the liquid should not swell or interact with the solid. The drop size is in tens of microlitres. The measurements are made by goniometer and dependent upon the direction in which the measurements are made i.e. advancing and receding contact angles. In general, the advancing contact angle is larger than the receding angle. This phenomenon of having different contact angles under receding and advancing condition is called contact angle hysteresis. Non-homogeneous surface chemistry, surface roughness, and possible molecular rearrangement in the solid induced by the liquid and vice versa, are some possible reasons for contact angle hysteresis<sup>31</sup>.

Wetting is considered as an optimal at low contact angles, as shown in Figure 2.2. This can be achieved, in principle, by a suitable surface treatment of the joining parts and by choosing an appropriate viscosity for the adhesive. Pocius<sup>4</sup> and Mittal<sup>33</sup> have discussed in detail the relationship between wetting and adhesion.

Assuming that the surface roughness of the substrate is negligible compared to the dimensions of the drop, and its effect is only an increase in surface area, using a thermodynamic approach, Wenzel<sup>32</sup> arrived at the following equation:

$$\cos \theta_R = W_R \cos \theta_0 \quad (1)$$

where  $W_R$  is the roughness area ratio (true area/nominal area, also called Wenzel's roughness factor) and  $\theta_R$  and  $\theta_0$  are the contact angles of sessile drops on the rough and smooth horizontal surfaces respectively.

In contrast, Shuttleworth and Bailey<sup>34</sup> considered asperity of rough surfaces as a barrier to the spreading of a liquid drop and derived the following relationship, by assuming  $\theta_0$  as an inherent material parameter:

$$\theta_R = \theta_0 + \alpha_m \quad (2)$$

where  $\alpha_m$  is the maximum slope of the surface roughness at the liquid periphery.

Later theoretical analyses<sup>35,36,37</sup> considered both treatments as possible effects of surface roughness. Carre and Schultz<sup>38</sup> proposed that a roughness factor could be determined from the contact angles measured on smooth and rough surfaces.

The ability of an adhesive to spontaneously wet a surface depends on the surface energies of both the adhesive and adherend. From the work of Zisman<sup>39</sup> and co-workers, Pocius<sup>4</sup> has deduced that "for spontaneous wetting and good adhesion, choose an adhesive with surface energy less than the critical wetting tension of the surface to which it is applied."

Levinc et al<sup>40</sup> measured the tensile butt strength of adhesive bonds made with plastic adhesive and found that direct relationships exist between strengths and several wetting parameters determined from contact angle measurement. Barbarisi<sup>41</sup> treated polyethylene with chromic acid and found that the contact angle of water with treated polyethylene surface decreases with increasing treatment time, whereas the practical epoxy-adhesive bond strength increases.

Wetting alone does not explain all aspects of the adhesion phenomenon. For example, for both low and high-energy solids and liquids, roughening decreases the wettability<sup>42,43,44,45,46</sup> whereas several researchers have reported an increase in adhesive strength with increasing surface roughness.

### 2.2.2 *Mechanical Adhesion*

Mechanical adhesion is defined as the adhesion between surfaces in which the adhesive holds the parts together by an interlocking action<sup>15</sup>. According to the mechanical theory, the adhesive interlocks around the irregularities or pores of the substrate as shown schematically in Figure 2.3. However, the effects of topography on adhesion are much more complex than this.

McBain and Hopkins<sup>47</sup> suggested that, at least in the case of wood and other porous materials, mechanical embedding of solidified glue in the pores, and irregularities of the bonded surface are a major factor. Maxwell<sup>48</sup>, however, tested and found that the shear strength of Maplewood specimens bonded with urca-formaldehyde resin at 5psi decreases with the increase in surface roughness. The sanding and combing of wood raises fibres that can easily be broken by quite small forces.

Bickerman<sup>49</sup> proposed that adhesion was due to the inherent roughness of all surfaces. He accepted the role of molecular forces in wetting the adherend surface but felt that once this was achieved mechanical coupling between the adhesive and the rough adherend was more than enough to account for bond strength.

Boroff and Wake<sup>50</sup> concluded that the bond strength of rubber and textile depend upon the number of fibres which are embedded in the rubber.

For mechanical adhesion, the adhesive completely wets the surface and follows every detail of the surface. Such adhesion is unlikely to perform very well under tension unless there are a large number of re-entrant angles on the adherend surface. However, the shear strength may be significant.

### 2.2.3 *Electrostatic Theory*

Electrostatic or Coulombic forces occur between atoms and molecules which bear a charge. These forces play a primary role in the formation of ionic bonds and ionic crystals. The energy required to break an ionic bond is very large, usually on the order of 100 kcal/mole or more<sup>4</sup>.

Derjaguin<sup>51</sup> proposed that the strength of the adhesive bond comes from the forces necessary to move the charged surfaces away from one another against the Coulombic forces. In other words adhesion is because of the electrostatic bilayer formed at the interface between electropositive and electronegative materials (Figure 2.4).

The theory uses Paschen's law of electric discharge through a gas, which states that the potential giving rise to a spark discharge is proportional to the quantity of gas between the electrodes i.e. the spark length and gas pressure. One adherend plus the adhesive are considered to be one plate of a capacitor and the second adherend is considered to be the second plate then, as they are separated, discharge may occur. The result of Derjaguin's theory may be expressed as:

$$W_B = 2\pi\sigma_0^2 h_B \quad (3)$$

where  $W_B$  is the work to break the adhesive bond;  $\sigma_0$  is the surface charge density; and  $h_B$  is the distance or separation at electrical breakdown. Assuming that the energy stored in the capacitor is equal to  $W_B$ , the surface charge density for the adhesion of polyvinyl chloride to glass was calculated in an atmosphere of argon and found to be constant. Skinner et al<sup>52</sup> were, however, unable to detect surface charges of the magnitude which Dergaguin and co-worker thought were involved.

Huntsberger<sup>53</sup> has pointed out basic errors in the assumptions of  $E_c = W_B$  that the plastic deformation of the adhesive and the adherends, and the non-interfacial part of energy dissipated in the peeling of polyvinyl chloride from glass in an atmosphere of argon, was ignored. The assumption may only be true in cases of completely brittle adhesive and adherends.

Voyutskii<sup>54</sup> and Schonhorn<sup>55</sup> have also criticised the electrostatic theory on different grounds. However, despite the shortcomings of this theory, recent work by Dickinson et al<sup>56</sup> and Smith and Horn<sup>57</sup> each give evidence of the presence of an electrostatic component to adhesion.

Despite such criticism, electrostatic attraction may play an important role in promoting adhesion through the application of coupling agents.

#### *2.2.4 Diffusion Theory*

The fundamental concept is that adhesion arises through the inter-diffusion of the adherend and the adhesive at the interface: thus the interface is no longer a true interface, but rather an interface in which the properties of the adhesive change gradually into the properties of the adherend (Figure 2.5). Diffusive bonding is, therefore, the ultimate in adhesive bonding where the interface does not lead to a stress concentration and there is no discontinuity in the physical properties of the adhesive and adherends. In a "normal" situation, however, there is usually a substantial mismatch between the properties of the adhesive and the adherend, and the contact between the adhesive and adherend acts as a discontinuity providing a stress concentration plane<sup>4</sup>.

Only in limited cases are the adhesive and adherend mutually soluble. This theory has, therefore, principally been applied to joints involving polymeric materials. Two common examples of diffusive bonding are solvent welding and thermal (or ultrasonic) welding of polymers. PVC piping is often assembled with a joining solution containing PVC resin in an appropriate solvent mixture (toluene and tetrahydrofuran).

Voyutskii<sup>54</sup> and Vasenin<sup>58</sup> have obtained results from peeling tests that appear to agree with theoretical treatment. Iyengar and Erickson<sup>59</sup> tested several adhesives used to make peel specimens between sheets of polyethylene terephthalate (PET) and found strong dependence of practical adhesion on the solubility parameter of the adhesive. When the solubility parameter of adhesive and substrate match, the failure changes from apparent adhesive failure to cohesive failure in the substrate.

This theory is mainly criticised because it provides no contribution towards an understanding of the adhesion of polymers to insoluble solids like glass or metal. Also all the evidence presented so far comes only from peel tests.

### 2.2.5 Real Solution

In view of the number of different approaches, each giving some particular insight into the phenomenon of adhesion, Allen<sup>28</sup> has combined them to represent a real solution in the following way:

$$\Psi = \alpha\psi_M + \beta\psi_A + \gamma\psi_D + \delta\psi_E + \dots + \omega\psi_X \quad (4)$$

where  $\psi_M$  is mechanical component of adhesion  
 $\psi_A$  is adsorption            "       "       "  
 $\psi_D$  is diffusion            "       "       "  
 $\psi_E$  is electrical           "       "       "  
 $\alpha, \beta, \gamma, \delta$  are mixing constants.

Except in some particular cases when the contribution of one component is negligibly small,  $\alpha, \beta, \gamma, \delta$  will have real and significant values. Packham adopts a similar approach<sup>60</sup> for peel energy in a 90° peel specimen.

Adhesion is not a two-dimensional (2-D) phenomenon in which the two materials, adhesive and adherend, are observed as not being influenced by each other. The boundary layer is in fact a three-dimensional (3-D), multi-material problem and both the adhesive and adherend affect each other in reaching and retaining bond strength<sup>61</sup>.

### 2.3 Factors Affecting Bond Strength

In considering the performance of adhesive joints, the physical and chemical properties of the adhesive are the most important factors. Also important in determining whether the adhesive joint will perform adequately are the types of adherend (that is, the components being joined *e.g.*, metal alloy, plastic, composite material) and the nature of the surface pre-treatment or primer. These three factors: adhesive, adherend and surface, have an impact on the service life of the bonded

structure. Table 2.1 summarises the chemical, physical and geometric factors that affect the ultimate strength of an adhesive joint.

Bonding parameters also appeared to affect the joint strength, for example, increasing applied pressure during curing increases the average joint strength and reduces its standard deviation in lap shear joints of aluminium adherend, bonded with supported epoxy adhesive<sup>62</sup>.

In the formation of an adhesive bond, a transitional zone arises in the interface between adherend and adhesive. In this zone, called the interphase, the chemical and physical properties of the adhesive may be considerably different from those in the noncontact portions. It is generally believed that the interphase composition controls the durability and strength of an adhesive joint and is primarily responsible for the transference of stress from one adherend to another. The interphase region is frequently the site of environmental attack, leading to joint failure.

### *2.3.1 Effect of Adherend Surface Pre-treatment*

Some form of substrate pre-treatment is almost always necessary to achieve a satisfactory level of bond strength. A number of references are available emphasising the dependence of bond strength on surface preparation of adherends<sup>11,61</sup>. Two main reasons for surface pre-treatment before bonding are reproducibility and durability. Depending on the type of adherend and the nature of treatment, a surface pre-treatment serves one or more of the following purposes:

- to remove a weak boundary layer
- to increase surface roughness
- to alter surface chemistry
- to increase surface energy
- to introduce polar groups etc.

An unpre-treated metal surface may be covered with oxide or mill scale of chemical characteristics not suitable for good adhesion, adsorbed organic molecules, water and

gases, as shown in Figure 2.6. Due to these contaminations, a high-energy surface (metal) may behave as a low energy surface and must be cleaned for maximum adhesion<sup>63,64</sup>. It has however, been shown that epoxy/amidoamine adhesives, modified with an epoxy-functional silane, provide strong, durable bonds to oil-contaminated steel substrates as long as the amine number of the curing agent is relatively low<sup>65</sup>.

In the case of polymeric materials, compounding materials such as plasticisers, antioxidants, mould release agents etc. may be a source of contamination. Lower molecular weight materials may be exuded at the surface of the polymer thus making a weak boundary layer. For thermoplastic surfaces, corona discharge treatment, flame treatment, plasma treatment, UV radiation treatment, ion beam etching and radio-frequency sputter etching are common physical pre-treatment methods. Chemical treatments of plastics include treatment with strong oxidising agents such as chromic acid and application of various primers. Thermoset composites are generally characterised by relatively high surface energy, polar surfaces, and are free from corrosion or oxide layers<sup>14</sup>. Due to these properties surface treatment is usually meant to remove contaminants such as mould release agent or dust and other contaminants. Brewis and Briggs<sup>66</sup> and Pocius<sup>4</sup> have given detailed accounts of these methods.

Selection of the pre-treatment process depends on the nature of adherend, adhesive and working environment in which the joint is expected to perform well in the long term (durability). Table 2.2 outlines the pre-treatment options that may be adopted, alone or in combination, for adhesive bonding.

Surface treatment methods may be classified as chemical, mechanical, thermal, electrical etc. (Table 2.3). Some methods are restricted to plastics or metals only whereas others may be applied to both. With some exceptions, surface preparations do bring about surface chemical changes, whatever the method is<sup>4</sup>.

There is more literature available on the treatment of aluminium than on any other metal. Kozma and Olefjord<sup>67</sup> have reviewed in detail the different surface

preparation techniques used for the adhesive joining of steel adherends and their influence upon the strength and durability of the adhesive joints.

In the case of metal joints, pre-treatment of adherends before bonding is more important from a durability point of view, and may have little effect on the initial bond strength of the joints. On the other hand, in the case of fibre-reinforced epoxy resin adherends, the initial strength is related to the presence of contaminants on the adherend surface and is, therefore, directly related to the pre-treatment of adherends<sup>12</sup>. A better joint performance has been observed when stainless steel surfaces were grit-blasted and degreased compared to 'ultra-clean' surfaces produced by argon ion etching in high vacuum<sup>68</sup>.

Although the majority of the procedures used in preparation for adhesive bonding recommend solvent degreasing, washing with aqueous solutions of alkali and detergent is also effective, but obviously thorough immediate drying is necessary.

No well-evaluated method exists for determining the cleanliness of surfaces to be bonded. In the case of metal adherends, however, the Franklin Research Institute has proposed a method involving observation of the spreading tendency of a water drop on a cleaned surface<sup>69</sup>.

Wingfield<sup>11</sup> has discussed various pre-treatment methods for adhesive bonding of composite surfaces. Commonly used pre-treatment techniques for a FRP (fibre reinforced plastic) surface are:

- dry clean rag wipe. This is good for dust only but may smear grease and oil and transfer them to the next part
- solvent wipe. This is better than dry cleaning but can still transfer oil and grease to the next part
- abrasion with emery paper
- grinding and grit-blasting
- flame, corona, laser, plasma and other treatment. Usually only for low surface energy thermoplastics

- peel ply.

In the peel ply method, a ply of fabric, such as woven polyethylene terephthalate, is applied on the bonding surface of the laminate during manufacturing. The peel ply is then removed just before bonding to ensure a clean surface. It may, however, be noted that in many cases it is not possible to achieve a contamination-free surface with the peel ply because it leaves behind the chemicals, such as the sizing agent, used during its manufacturing.

The effectiveness of a pre-treatment method for composite adherends depends on the chemical nature of the composite and the adhesive. Guha and Epel<sup>70</sup> tested a range of adhesives for bonding graphite composites in single lap-shear joints. They found that a primer wipe on one or both surfaces was satisfactory for acrylic and urethane adhesives, but either scuff sanding or flame treatment of surfaces was required for good bonding with epoxy adhesives.

#### **2.3.1.1 Effect of Surface Roughness**

Several researchers have studied the effect of surface roughness on the strength and durability of the adhesive joint using various adherends and adhesives<sup>71,72,73,74,75,76</sup>. Venables<sup>77</sup> has defined a micro-rough surface as one having fine structures with dimensions of 0.1 $\mu$ m or less. The relationship between the roughness and adhesion is not very simple. An optimum surface profile varies from one adhesive to another, and depends upon the type of stresses applied<sup>78</sup>. Figure 2.7 shows the variation of adhesive joint strength with surface roughness.

Almost all surface treatment methods bring some degree of changes in surface roughness, but grit-blasting is usually considered as one of the most effective methods in bringing the desired level of surface roughness. Variables in grit-blasting include the size of grit, the blast pressure, the treatment time, the blast angle and the distance from the blast nozzle to the surface<sup>11</sup>. Small particle (grit) size apparently leaves a greater percentage of contaminant residues on the surface<sup>71</sup>.

Harris et al<sup>71</sup> found that different shapes of grit do not affect the generated surface roughness. They also found that the grit-blasting process not only removes weak boundary layers but can also alter the surface chemistry of the adherend. They concluded that surface roughness depends more on size than on the type of alumina grit, and that with some alumina grit, higher surface roughness leads to lower surface energy. This may be the reason for a better joint performance when stainless steel surfaces were grit-blasted and degreased compared to 'ultra-clean' surfaces produced by argon ion etching in high vacuum<sup>68</sup>. The roughness of real surfaces is very variable depending upon how they have been prepared. Some possible positive effects of surface roughness are<sup>4,78,79,80</sup>:

- increased surface area (means more intermolecular bonds)
- availability of keying for mechanical bonding
- diversion of failure path away from the interface into the bulk of the adhesive, as shown in Figure 2.8.

The actual microscopic distribution of stress at a rough interface will be very complex. Kalnins et al<sup>81</sup> found that the initial joint strength of a polyethylene-steel adhesive joint increases with the growth of the specific surface area of a chemically treated substrate.

Some possible disadvantages of surface roughness are that certain surface profiles will lead to trapping of air beneath the adhesive and will result in poor filling of crevices. These voids may lead to stress concentrations and hence a lower joint strength<sup>82</sup>. Depending on the nature of the roughness and the adhesive (surface tension and viscosity) a surface may not be wetted properly, and adhesive may even start setting before going deeper into the pore (Figure 2.9). Hitchcock et al<sup>46</sup> report that the increasing roughness usually reduces the wettability of the surface with the exception of very wetting liquids and very rough surfaces (Figure 2.10).

Pocius<sup>4</sup> has reported the work of Arrowsmith<sup>83</sup>, who electroformed the surface of a copper foil to produce a surface of varying roughness, and measured the peel strength of the same epoxy adhesive to the copper. He observed that an increase in

the peel strength with increasing surface roughness might be due to an increase in the plastic deformation of the adhesive in the interphase region (Table 2.4).

Bullet et al<sup>84</sup> tested mild steel specimens prepared by grinding with coarse emery paper then with successively finer papers, and finally with diamond paste. They found that the polished surface gave the best results, whereas the finer abrasive gave better adhesion than the coarser one. In the case of stainless steel, however, sand blasted substrates showed better joint strength compared to the polished ones.

Janarthanan et al<sup>85</sup> found adhesion enhancement in a bilayer construct through the introduction of macroscopic roughness, and controlled through the orientation and morphological features of the roughness.

Using AFM (atomic force microscopy) Zhang and Spinks<sup>86</sup> studied the effect of surface roughness on the lap shear strength and fracture energy of adhesively bonded aluminium. They found that the lap shear strength does correlate with the surface roughness at the sub-micrometer scale and that the fracture energy is directly proportional to the percentage of etched area on the adherend surface.

Garnish and Haskins<sup>87</sup> tested lap shear specimens of aluminium and steel using one-part, hot curing, epoxy adhesive, and found a higher strength in the shot-blasted specimens than in those degreased only. Gilibert et al<sup>74</sup> investigated the effect of surface roughness on the strength of mild steel, tensile lap shear specimens. They found that a finer grinding produces better mechanical properties than a coarser one. Also the deviation in ultimate strength was higher for non-grit-blasted surfaces than for grit-blasted surfaces. Harris and Beever<sup>73</sup> investigated single lap shear and tensile butt specimens of mild steel and aluminium alloy. They prepared the surface with different grit sizes to produce a varying surface roughness. Higher adhesive joint strength was observed compared to "as-rolled" steel surfaces. They also found that treated mild steel substrates produced higher surface energies than aluminium alloys and that surface energies of both aluminium and mild steel decrease with the increase in surface roughness, which is in line with other findings<sup>44,46</sup>. They also found that the initial joint strength of mild steel joints (both lap shear and tensile butt) were

independent of grit type. They have concluded that changes in surface energy might be attributed to changes in surface composition.

Sargent<sup>76</sup> investigated Redux<sup>®</sup> 775 (a modified phenolic adhesive) bonding of aluminium peel test specimens, and found a distinct correlation between increasing peel strength and increasing surface roughness. However, he found no correlation with any features of the oxide or interfacial region. Bijlmer<sup>88</sup> also found that a fine etch pit structure within coarser etch pits was the most desirable structure for high peel strengths.

Brockmann<sup>18</sup> found that when shot blasted, mild steel specimens were exposed to room temperature and 60% R.H. (relative humidity) for a varying length of time before bonding, initial and residual shear strength increase at first with the increasing 'open time' of the surfaces up to 24hrs, and remain at a high level until a storage time of 150hrs. He concluded that adhesives need not to be applied immediately after mechanical treatment of steel.

Loss in adhesive strength of a joint with immersion in water depends on the chemical characteristics of the adherend, adhesive and joint geometry. For example, no significant change in joint strengths was observed with degreased only, aluminium lap shear joints, when immersed for up to 211 days using Araldite<sup>®</sup> 2007<sup>72</sup>. However, Kinloch et al<sup>89</sup> found that an adherend formed from high magnesium aluminium alloys performed poorly in durability when tested in butt joint configuration.

The effect of surface roughness also depends on the type of adhesive used and its temperature during the application to adherends. For example, at higher temperature or with low-modulus adhesive, where plastic or viscous flow is possible and flaws are less important to the strength of the joints, roughness would be expected to have a minor effect<sup>75</sup>. Thus, a low Young's modulus nylon epoxy film adhesive (Metlbond<sup>®</sup> 1301) did not show a difference in joint strength between polished and grit-blasted specimens<sup>75</sup>.

### 2.3.1.2 Effect of Adhesive Thickness

At least for certain types of adhesive joints, thickness of the adhesive layer has an effect on bond strength<sup>90</sup>. Dependence of bond strength on adhesive thickness is not straightforward. It depends on a number of factors including, but not limited to, the nature and properties of substrate and adhesive, surface treatment of adherends and the geometry of the joint.

In the case of butt joints loaded in tension, Gardon<sup>91</sup> and Williams<sup>92</sup> found an increase in joint strength with a decrease in adhesive thickness. Dukcs and Bryant<sup>93</sup> tested circular and tubular butt joints with a wide range of adhesive thicknesses and found that joint strength increases in proportion to the log of decrease in adhesive thickness.

Minnetyan et al<sup>94</sup> tested the effect of adhesive thickness on a stiffened composite joint under different loading conditions. They found that under compressive loading, there is a critical thickness of the adhesive bond. If the adhesive is made thicker than this critical value, both damage initiation load and the structural resistance to damage propagation are lowered. Under lateral pressure loading, the difference in damage propagation was not significant for adhesive thicknesses of 0.132mm or 0.265mm. However, failure propagation was slower in the case of the thicker adhesive joints. Under tensile loading, a thicker adhesive bond was found to improve the structural resistance to damage propagation, even though the damage initiation load was lowered.

An increase in bond line thickness generally results in reduction in bond strength. This effect may be more prominent with adhesive thicknesses from 0.1mm to 0.5mm. For adhesive thicknesses more than 0.5mm, the cohesion forces in the bulk adhesive may determine bond strength<sup>2</sup>. For adhesive (epoxies, urethanes and acrylics) bonded graphite composites in single lap shear configuration, Cuha and Epe<sup>70</sup>, found a small decrease in lap shear strength for bond thicknesses up to 1mm. In the case of single lap shear joints the effect of bond thickness is more pronounced with short overlaps, thick adherends, and stiff adhesives<sup>95</sup>.

Lees<sup>5</sup> reports that, in the case of a T-peel joint bonded with toughened epoxy, the adhesive peel strength increases with the increase in adhesive thickness. Although this effect is not directly proportional, it is significant. However, Adams et al<sup>96</sup> carried out a range of tests on lap shear joints in three point bending and T-peel joints in tension over a range of adhesive thicknesses between 0.1mm to 3.0mm. In the case of lap joints, they found that the failure load decreases almost linearly with the increase in adhesive thickness. However, in the case of T-peel joints, the failure load decreased slightly when increasing the adhesive thickness. This contradiction in these findings may be due to the difference in the adhesives and adherends used in these T-joints.

Matsui<sup>97</sup> reports an almost linear increase in the theoretical and experimental strengths of standard cleavage specimens for adhesive thickness from 0.1mm to approximately 1.5mm. For single and double lap joints he<sup>98</sup> found an initial increase in the ultimate shear strength with increasing adhesive thickness until approximately 0.05mm adhesive thickness. After that, the failure stress remained at about the same level up to about 2mm.

A number of researchers have tried to look into the possibility of differences in the bulk and thin-film adhesive properties which may affect joint strength in relation to change in adhesive thickness. Peretz<sup>99</sup> and Brinson<sup>100</sup> found that adhesive materials have different mechanical properties when tested in thin-film and bulk form. X-ray photoelectron spectroscopy (ESCA) results showed a difference in the chemical properties between the remaining polymer residues on the metal surface and the bulk polymer<sup>101</sup>. Dolcv et al<sup>102</sup>, Peterz<sup>99</sup> and Brinson<sup>100</sup> also found that the mechanical properties of an adhesive depend on its thickness. However, Lilleheden<sup>103</sup>, Jcandreau<sup>104,105</sup> and Adams et al<sup>106</sup> found a good agreement between thin-film and bulk properties. Gali et al<sup>107</sup> found that the bulk adhesive properties obtained by uniaxial tests, such as tension, compression and torsion, can be related to the properties of an 'in-situ' adhesive layer in shear by a combined stress law that follows a modified von Mises failure criterion.

Baker<sup>68</sup> also considered the possibility that the orientation of the polymer at a metal/polymer interface may alter its modulus close to the surface.

### 2.3.2 *Effects of Geometric Parameters*

A number of geometric factors such as overlapping, thickness of adherend, presence and geometry of fillet etc. also affect the ultimate joint strength. For example, the strength of a narrow overlapped joint is limited by the adhesion and cohesion forces in the adhesive layer. In overlapping lengths exceeding a certain amount, stress peaks occurring at the overlap ends may cause a reduction in joint strength. The overall effect depends on the geometry of the joint, strength of adherends and the flexibility of the adhesive layer. Stress peaks arising at the overlap ends are lower for thick adherend joints than for thin ones. The higher rigidity of the thick adherends allows the adhesive layer to accommodate a larger part of the load.

Spew fillet is the excess of adhesive squeezed out from the overlap area. The size and geometry of the spew fillet also affect the strength of the adhesive joints. Adams and Peppiatt<sup>108</sup>, Crocombe and Adams<sup>109</sup>, Rispler et al<sup>110</sup> and several others have studied the effect of the size and shape of spew fillets on stress distribution. These researchers show that the presence of a spew fillet helps in reducing the peak peel and shear stresses in the adhesive layer, and therefore can improve the joint strength. In experiments with a coach joint (similar to a T-peel joint), Hadavinia et al<sup>111</sup> found that for sheet thickness of 1mm and adhesive thickness of 0.2mm a five-fold increase in strength and stiffness took place when the fillet was increased from zero to 100% for a given size and shape. This would only be a very small increase in the case of thick adherend joints<sup>112</sup>.

## 2.4 **Adhesive Joints**

Joints are sources of stress concentrations, which compromise the overall efficiency of a structure. In strength-critical components it becomes imperative to reduce the stress concentration factors so as to increase structural efficiency.

An ideally made adhesive joint is expected to have a uniform stress distribution throughout the joint, to acquire strengths comparable to those achieved by other joining methods, and to retain this joint strength during its entire operational life. In

practice, however, as mentioned earlier, a number of factors affect the performance of an adhesive joint, and its performance depends on the type of joint and its mechanical behaviour.

#### **2.4.1 Type of Joints**

However complex, all bonded joints can be reduced to four basic types<sup>16</sup>, as shown in Figure 2.11.

After basic selection of the joint type, detailed design should be made with the consideration of directions of all the applied loads and forces that the joint has to withstand in service. Whenever possible an adhesive joint should be designed in such a way that it is under compressive or shear load or a combination of both.

#### **2.4.2 Mechanical Behaviour**

The mechanical behaviour of the bonded structure is influenced by the details of the joint design and by the way in which the applied loads are transferred from one adherend to the other. Stresses occurring within the adhesive layer of a loaded joint are highly complex. There are four types of stress in an adhesive bonded joint. These are normal stresses, shear stresses, cleavage stresses and peel stresses. Normal stresses are further divided into tensile and compressive stresses. Graphical representation of these stresses in the form of a stress distribution curve along the adhesive length is shown in Figure 2.12.

Shear loading distributes the stress over the whole bonded area and therefore gives an economical joint. In general, toughened structural adhesives can carry loads about 100 times greater in shear mode than that they can in peel<sup>5</sup>. In tension, the stress is again distributed over the entire area, but due to difficulty in applying a uniform load, a cleavage stress may be generated that may initiate failure at a far lower load.

Unlike normal and shear stresses, in cleavage mode a localised loading occurs on one side of the joint while the other side is virtually unloaded. This type of load should,

therefore, be avoided in the design of joints<sup>2</sup>. Anderson et al<sup>113</sup> have concluded that in many standard lap shear specimens failure initiation is primarily because of the induced cleavage stresses which can be reduced using thicker adherends. Peel stresses are similar to cleavage in nature, with the difference that for peel stress to occur, one or both of the adherends should be flexible.

In practice a joint can be subjected to a combination of the different stresses mentioned above. As local stresses in an adhesive layer in a joint are generally non-linear, it is impossible to predict proper stress and strain relationships without recourse to finite element analysis.

In the case of composite materials, orientation of the fibres in a composite is also important since fibres have their highest mechanical properties along their lengths, rather than across their widths. This leads to the highly anisotropic properties of composites, where, unlike metals, the mechanical properties of the composite are likely to be very different when tested in different directions. This means that it is very important when considering the use of composites to understand at the design stage, both the magnitude and the direction of the applied loads. When correctly accounted for, these anisotropic properties can be very advantageous since it is only necessary to put material where loads will be applied, and thus redundant material may be avoided.

### ***2.4.3 Mechanical Testing***

The strength of adhesive bonds is usually determined by destructive tests, which measure the average stresses set up at the point or line of fracture of the test piece. The primary ways of testing the physical properties of adhesive and the adhesive bonds are<sup>4</sup> in tension, shear, cleavage and peel. A number of test methods are described in the literature of the American Society of Testing Materials (ASTM)<sup>114</sup> and British Standard Institutions (BSI)<sup>115</sup>. These tests are carried out over a wide range of temperatures and under various environmental conditions. An alternate method of characterising an adhesive joint is by determining the energy expended in cleaving apart a unit area of the interphase. The conclusions derived from such

energy calculations are, in principle, completely equivalent to those derived from stress analysis.

Although a few non-destructive tests based on acoustic, electrical, thermal and radiation techniques are available, the disadvantage of all non-destructive tests is that although they may allow the measurement of non-uniformity and defects in the adhesive line, they do not measure the quality and level of adhesion.

Of the various different test methods, lap shear and cleavage testing are of particular importance in the case of thick adherends. Lap shear tests measure the shear strength of the cured resin system by bonding two thick, overlapping steel blocks together and pulling them apart. It is carried out to the British Standard BS 5350:Part C5:1990. This is one of the most severe shear tests that can be applied to an adhesive, since the steel blocks do not flex at all, and so cannot provide any stress relief to the joint. This is in contrast to the thin aluminium plates often used for adhesive testing, where the flexibility of the aluminium can sometimes enable artificially high shear strengths to be obtained.

The cleavage strength test is carried out to BS 5350:Part C1:1986<sup>1</sup>. In this test two steel blocks are bonded together and pulled apart by loading in a mode which will cause cleavage of the adhesive joint. This is a mode in which most adhesives are poor, and is generally avoided in design. However it gives a useful indication of the toughness of an adhesive and its resistance to cracking. It gives a load in kN to failure for a 25x25mm<sup>2</sup> bond area.

In the testing of adhesive joints, it is not only the adhesive material which is evaluated but also the bonding techniques which include preparation of the surface, application of the adhesive, and curing of the adhesive. The standard test methods utilise specimens of standard dimensions, shape and design prepared specifically for the purpose. Therefore, the resulting data are important in establishing the comparative characteristics of adhesives. However, using these data, it is difficult to predict the performance of adhesives when subjected to varying stresses and environmental conditions in the real world.

Due to the anisotropic nature of fibreglass composite materials, standard test methods available for the testing of metals are often not directly applicable to them. Although some standard test methods are available for the testing of bonded composites, such as ASTM D 3165-95<sup>116</sup> and ASTM D5041-93b<sup>117</sup>, the need for standard test methods for the testing of bonded metal/composite adherends to depict a real-life situation, is still there.

Mechanical testing of adhesive joints and structures is important for assessing the overall integrity of the structure. A clear understanding of the mechanical behaviour of the bonded components may permit idealisation and simulation of the overall joint into a small standard shape specimen to save the testing cost. For example, a large tubular joint may be idealised into lap shear joints, cutting cost while giving tangible results (Figure 2.13).

Mittal<sup>33</sup> used the term practical adhesion for the stress necessary to break the adhesive bond. It is primarily determined by the mechanical (physical) properties of the adherends and the adhesive<sup>4</sup>.

#### ***2.4.4 Modes of Failure***

The mode of failure is the locus in the adhesive bond or adherend through which the failure propagates. Cohesive failure, or failure in cohesion, is the type of failure where the adhesive can be seen on both sides of the specimen. Adhesive failure, or failure in adhesion, is usually an apparent adhesive failure, meaning that it is only visually an adhesion failure and a thin cohesive layer of adhesive may still be on the adherend surface. Such a failure may be confirmed by the use of instruments like a scanning electron microscope. An apparent mixed mode failure also occurs in many adhesive joints (Figure 2.14). Failure in cohesion is the preferred mode of failure because it shows that the strength of the bond was limited by the physical properties of the adhesive and not adhesion<sup>4</sup>. An adhesion failure indicates that the surfaces of the parts to be joined had not been properly treated.

ASTM D 5573-94<sup>118</sup> characterises failure modes in FRP joints into seven different modes as follows:

- *adhesive failure (interfacial failure)*, rupture of the adhesively bonded joint such that separation appears to be at the adhesive-adherend interface
- *cohesive failure*, rupture of the adhesively bonded joint such that separation is within the adhesive
- *thin-layer cohesive failure (interphase failure)*, failure similar to cohesive failure except that the failure is very close to the adhesive-adherend interface
- *fibre-tear failure*, failure occurring exclusively with the FRP matrix characterised by the appearance of reinforcing fibres on both ruptured surfaces
- *light-fibre-tear failure*, failure occurring within the FRP adherend characterised by a thin layer of the FRP resin matrix visible on the adhesive with few or no glass fibres transferred from the adherend to the adhesive
- *stock-break failure*, when an FRP adherend breaks outside the adhesively bonded-joint region
- *mixed failure*, when any combination of two more of the above take place.

The above classification of modes of failure for bonded composite joints is more suited to writing product specifications or contracts. For most practical purposes, however, classification of failure into cohesive, adhesive, adherend and mixed modes is considered sufficient (Figure 2.14).

Most brittle adhesives fail by a flaw-initiated crack mechanism. Cohesive failure in the polymer does not imply that it fails at the bulk strength of the polymer. The ultimate cohesive stress can vary with the adherend, its metallurgical state, and surface preparation<sup>75</sup>. Joint strengths higher than the corresponding reported bulk polymer strength have been reported<sup>75,119,120</sup>. This may be due to several factors such as:

- lateral constraint offered by the higher modulus adherend. In the case of adhesives this effect may be more prominent at a higher temperature where adhesive is more ductile
- nature of polymer formed in the joint i.e. change in polymer surface morphology due to the adherend
- the type, number and distribution of flaws.

## 2.5 Failure Analysis

Failure analysis is an extremely complex subject and may involve several specialities in the areas of mechanics, physics, chemistry and electrochemistry, manufacturing processes, stress analysis, design analysis, fracture mechanics, etc.

The sequence of stages in the investigation and analysis of failure is as follows<sup>121</sup>:

- collection of background data and selection of samples
- preliminary examination of the failed part (visual examination)
- non-destructive testing
- mechanical testing
- selection, identification, preservation and/or cleaning of specimens
- macroscopic examination and analysis and photographic documentation
- microscopic examination and analysis
- selection and preparation of metallographic sections
- examination and analysis of metallographic sections
- determination of failure mechanism
- chemical analysis
- analysis of fracture mechanics
- testing under simulated service conditions
- analysis of all the evidence, formulation of conclusions, and writing the report.

Bonded structures, or their components, fail because of a fracture or an excessive deformation. In attempting to prevent such a failure, the designer estimates how

much stress (load per unit area) can be anticipated, and specifies materials or designs that can withstand these expected stresses. A stress analysis, accomplished either experimentally or by means of a mathematical model, indicates the expected areas of high stress in an adhesively bonded structure. Stress analysis techniques can generally be classified into two major categories, analytical analysis and finite element analysis. In analytical analysis, stresses and strains in the joints are expressed in the form of differential equations which are then solved to obtain close form solutions. Finite element analysis is a numerical method. In this method the joint is divided into a number of small discrete portions having compatible force and displacement continuum across the boundaries of each adjacent element. Boundary conditions are applied and loading is simulated. Obtained equations of state are then solved numerically. Due to the huge number of equations to be solved, this method needs a digital computer. Several researchers have performed linear, non-linear, and elasto-plastic finite element analyses. In practice, both analytical and finite element methods complement each other.

Some bonded joints such as double lap, butt and thick adherend joints, undergo a small deformation and can be analysed with reasonably good accuracy using a small deformation formulation<sup>10</sup>.

Besides the stress and strain limitations of an adhesive, inherent damage may be the cause of joint weaknesses. Air bubbles trapped during the bonding process may create voids in the adhesive. Debonding due to improper surface pre-treatment or defective bonding may also cause areas of stress concentration. Hart-Smith<sup>122</sup> performed elastic-plastic shear stress analysis of bonded joints with debonds and discontinuities and found the effect of such defects on adhesive stresses and strains. Rossetos and Zang<sup>123</sup> studied the effect of adhesive voids in the overlap on the stress distribution in a bonded joint. Ignoring peel stresses, they found that a central void does not affect peak shear stresses, but a void close to either end causes a noticeable increase in peak stress. Heslehurst<sup>124</sup> used holographic interferometry to study the structural response of bondline defects, debonds and weak bonds. He observed that these defects reduce the peel strength and stiffness of the bondline.

With a fracture energy approach, Papini et al<sup>125</sup> carried out a parametric study on varying geometric parameters such as adherend lengths and thicknesses and adhesive terminus conditions on the strength of single lap, cracked lap shear and double strap joints.

### 2.5.1 *Classical Mechanics (Analytical) Analysis*

Volkersen<sup>126</sup> carried out the earliest analysis on a single lap shear joint under tension. Assuming a linear elastic adhesive and a stiff adherend, he analysed the shear stress distribution in the adhesive layer and found that the stresses are at their maximum at both ends of the overlap. Volkersen did not consider the peel stresses in the bond line due to bending moment in the joint caused by non-collinear applied forces, and rotation in the joint due to bending of the adherend which in turn makes the problem geometrically non-linear. Goland and Reissner<sup>127</sup> considered the shortcomings in Volkersen's analysis. They incorporated the bending effects of the adherends. They assumed a very thin layer of adhesive compared to adherend, so that its effect on the flexibility of the joint is negligible, and the flexibility of the joint arises mainly from the adhesive. They considered the adhesive layer as a system of infinitesimal springs placed between the two adherends. Plane strain conditions were assumed in solving the differential equations. The shear deformations and tensile stresses across the adherend and in the adhesive layer were neglected.

Sneddon<sup>128</sup> pointed out the inconsistency of signs in Goland and Reissner's formulation and obtained an amended expression. Adams and Peppiatt<sup>108</sup> also reported that the expression given by Goland and Reissner for the normal stresses in the adhesive was incorrect and gave the amended solution. They have also shown<sup>129</sup> analytically and using finite element analysis, that Poisson's ratio, strain related, transverse shear stresses exist in the adhesive layer of a lap shear joint, even when bending is prevented. However, Carpenter<sup>130</sup> argued and concluded that small errors found in the equations of Goland and Reissner's paper<sup>127</sup> occurred during the manuscript preparation and the final equations are correct. Tsai and Morton<sup>131</sup> also support the correctness of the original expression for peel stress developed by

Goland and Reissner. They pointed out that the first mistake in the signs was neutralised by a second mistake and that the end results are correct.

Allman<sup>132</sup>, Chen and Cheng<sup>133</sup> and Adams and Mallick<sup>134</sup> included the variations in the shear and normal stresses throughout the thickness of the adherend and adhesive layer, which were originally ignored by Goland and Reissner. Renton and Vinson<sup>135</sup> only considered the variation of stresses in the adherends but not in the adhesive. Hart-Smith<sup>136</sup> included the effect of adhesive shear and peel stresses in determining the edge bending moment. His analysis simultaneously determines the edge bending moment and the adhesive stresses, and takes into account the effect of large deflection of the free adherends, but ignores the large deflection effect in the joint overlap. Oplinger<sup>137</sup> took into account the large deflection effect in the overlap and presented a more detailed analysis.

Using reflective photoelastic analysis of a lap joint, Hahn<sup>138</sup> showed that the shear stresses in the adhesive are not uniform across the width but are highest at the corners. Adams et al<sup>139</sup> analysed single and double lap joints made of hard rubber adherends and soft rubber adhesive and found good agreement between the experimental and theoretical results. They concluded that this kind of joint gives an accurate representation of the shear stresses existing in lap joints and provides a simpler means of strain analysis than the photoelastic technique.

Ojalvo and Eidinoff<sup>95</sup> studied the effect of adhesive thickness on lap joints by considering linear variation in shear stress in the adhesive layer and constant peel stresses.

In earlier analyses, adherends and adhesives were considered elastic materials whereas ductile adhesives inevitably exhibit nonlinear material behaviour and can undergo inelastic and plastic deformation. This nonlinearity may affect stresses and strain in the adhesive and adherends. Under the PABST (Primary Adhesively Bonded Structure Technology) programme, Hart-Smith<sup>136,140,141,142</sup> carried out detailed analysis of single lap, double lap, scarf and stepped lap shear joints. He<sup>122,143</sup> also included elastic-plastic characteristics of the adhesive in the closed form analysis and found that under shear loading, the stress concentration decreases

significantly with a plastic adhesive. The Engineering Science Data Unit (ESDU) also carried out elastic and elastic-plastic analysis of double lap joints<sup>144</sup> and stepped lap joints<sup>145</sup>.

Roberts<sup>146</sup> developed a two-stage analytical procedure for determining the distribution of shear and peel stresses in various adhesive joints. He assumed a linear adhesive behaviour. Bigwood and Crocombe<sup>147</sup> presented elastic analysis and engineering design formulae for bonded joints. Wang and Rose<sup>148</sup> presented an analytical solution for the triaxial stresses in bonded joints.

Using analytical and finite element analysis supported with experiments, Adams et al<sup>149</sup> concluded that thermal effects, whether due to mismatch of the adherends or to adhesive contraction by temperature or cure, lead to significant changes in the stress state of lap joints. They recommended that adhesive should be used in the temperature range for which it is made.

Several researchers have developed analytical solutions for joint configurations other than for the single lap joint. Volkersen<sup>150</sup> gave a closed form solution for the shear and tensile stresses in the adhesive layer of a double-lap joint. Hart-Smith<sup>140</sup> performed elasto-plastic analysis of the adhesive bonded double-lap joint, and derived formulae for calculating the bond shear strength and the plastic zone length. Tong<sup>151</sup> studied double lap joints with non-linear shear stress-strain behaviour.

Lubkin<sup>152</sup> calculated the elastic stresses in scarf joints. By allowing adherends to undergo longitudinal deformations only and modelling the adhesive layer as pure shear springs, Erdogan and Ratwani<sup>153</sup> calculated the stress distribution in the adhesive layer and axial stresses in the adherends in scarf and stepped joints. Hart-Smith<sup>141</sup> studied an elasto-plastic adhesive model of scarf and stepped lap joints. Chang et al<sup>154</sup>, Gent and Hamed<sup>155</sup>, and Kim and Aravas<sup>156</sup> carried out elasto-plastic analyses of the peel test.

Lubkin and Reissner<sup>157</sup> investigated the distribution of stress in the adhesive lap joints between two thin circular cylindrical tubes subjected to tensile axial load. They modelled adhesive consisting of an infinite number of tensile and shear springs.

Shear and normal stresses in adherends were assumed negligible in comparison with those in the adhesive. Shear and normal stresses were found at their maximum at the end of the adhesive layer. Volkersen<sup>150</sup> gave a closed form solution for the shear stress in the adhesive layer of a tubular joint subjected to torsional loading. Kukovyakin and Skory<sup>158</sup> set up differential equations for the stresses in the tubular lap joints considering the effect of adherend bending. Alwar and Najaraja<sup>159</sup> calculated the stress distribution in the viscoelastic adhesive of a tubular joint subjected to axial loading. Shi and Cheng<sup>160</sup> reported analysis of an axially loaded cylindrical lap adhesive joint. Ikegami et al<sup>161</sup> looked into the effect of the spew fillet on a coupled cylindrical joint. Chon<sup>162</sup> considered a composite tubular lap joint in torsion and derived a closed form solution for the stress distribution. Zhou and Rao<sup>163</sup> treated an adhesive bonded tubular joint under tension with a viscoelastic option.

Matsui<sup>98</sup> looked into the effects of the geometric size and mechanical properties of both adherends and adhesive on the average ultimate shear stress of the bonded rectangular and tubular lap joints. He derived four formulae, one each for cohesive failure in the adherend, interfacial failure at the adherend/adhesive interface, cohesive failure in the adhesive layer and adhesive failure. Failure loads were then calculated with varying geometric sizes and mechanical properties in single lap, double lap and tubular lap joints and compared with experimental results. The effect of surface roughness was also modelled using triangular roughness profiles. Good agreement was found between the theoretical and experimental results. In a similar fashion he<sup>97</sup> also considered the effects of adherend sizes on the nominal ultimate tensile stresses of adhesive bonded circular and rectangular joints under bending and peeling load. This time he considered circular butt, rectangular butt and rectangular lap joints and T-type peel and cleavage specimens, and presented model equations for calculating the nominal ultimate tensile stresses and failure criteria. Among other results it was found that peel and cleavage strengths increase with the increase in adhesive thickness up to about 1.5mm in the case of a cleavage specimen, and then start decreasing. Again, good agreement was found between the experimental and theoretical results.

Sargent<sup>76</sup> analysed the expected contribution from increased the surface area and departure from flatness (surface roughness) by considering the force distribution at an idealised surface consisting of spherical depressions.

Sawa and Uchida<sup>164</sup> analysed the stresses in band adhesive butt joints (a term used by the authors for a recessed butt joint) using the 2-D theory of elasticity (plane stress). They replaced the adherends and adhesive bonds by finite strips and analysed the effect of the ratio of Young's modulus of the adherends to that of the adhesive, the adhesive thickness, the adhesive region and its application and the tensile load distribution on the stress distribution at the interfaces. They found that the interface stress at the edge decreases with the increasing ratio of the modulus of the adherends to the adhesive and with decreasing adhesive thickness.

Using the 2-D theory of elasticity, Nakano et al<sup>165</sup> examined the stress distribution in an adhesively bonded butt joint between dissimilar materials subjected to cleavage loads. They studied the effects of the ratio of Young's modulus of the adherends to that of the adhesive and of the thickness of the adhesive on the stress distributions, and found that the maximum normal stress increases with a decrease in the thickness of the adhesive bond. They also made a quantitative evaluation of the stress singularity near the edge of the interface for both the plane stress and plane strain conditions, and found it more severe in the latter case.

### ***2.5.2 Numerical (Finite Element) Analysis***

The finite element method is one of the most important, versatile and powerful numerical analysis techniques. By this method, the response of a structure subject to a variety of boundary and loading conditions may be assessed. It, therefore, helps in analysing and optimising an adhesive joint configuration. Depending on available computing power, complex geometric and non-linear material properties can be modelled.

The existing analytical solutions have been derived with certain simplifying assumptions used in formulating the problems. With finite element analysis, on the

other hand, it is possible to treat all three materials (i.e. the two adherends and the adhesive) as elastic continua.

Wooley and Carver<sup>166</sup> performed finite element analysis of a single lap joint to study the effect of the adhesive modulus, overlap length and adhesive thickness, and found good agreement between the analytical and numerical results. Barker and Hatt<sup>167</sup> applied finite element analysis to study the single-lap and smoothly tapered joint between aluminium and boron-epoxy composite and steel. They modelled the adhesive layer with a joint element which behaved as a combined shear and tension spring whose stiffness properties vary with thickness. They found lower stresses in the smoothly tapered joints. Carpenter<sup>168</sup> proposed a finite element idealisation of the adhesive of a lap joint, which treats the adhesive element as an axial spring. He later<sup>169</sup> showed that his original finite element formulation was inadequate except for the case of zero adhesive thickness. He proposed a new formulation based on the assumptions common to the theories of Goland and Reissner<sup>127</sup> and Ojalvo and Eidinoff<sup>95</sup>, which can idealise a finite thickness of adhesive.

Richardson et al<sup>170</sup> have compared the 2- and 3-D finite element analyses of an adhesive joint similar to the standard cleavage joint defined by ASTM D1062-78 (the cleavage strength of metal to metal adhesive bonds). They found that with appropriate correction, a 2-D finite element analysis could reproduce the conditions at various positions across the width of 3-D joints.

Delale et al<sup>171</sup> carried out a closed form analysis of the general plane strain problem of adhesively bonded structures consisting of two different orthotropic adherends in single lap and stiffened plate configurations. They assumed that the thicknesses of the adherends, treated as plates, are constant and small compared to the lateral dimensions of the bonded region. They also assumed a thin adhesive without considering the through thickness variation of stresses in the adhesive. They found that the results of their analytical analysis are in line with those of the finite element analysis.

Crocombe and Adams<sup>109,172</sup> presented elasto-plastic analysis of a peel test. They<sup>173</sup> demonstrated that in a peel test, principal tensile stress drives the crack towards the thinner flexible adherend.

Stress concentrations can occur at the end of the interface between the adherends and adhesive layer. These stresses are shown to be mesh dependent in the absence of adhesive fillets<sup>10</sup>. This mesh dependency also exists even when non-linear analysis is considered<sup>174</sup>. Adams and Peppiatt<sup>108</sup> used FE analysis to look into the effect of the spew fillet on lap joints. A linear elastic behaviour was assumed for the adhesive and adherends. They found a good agreement between the theoretical and FE results. Using finite element analysis, Adams et al<sup>175</sup> showed that the presence of a spew fillet causes shear concentration in an adhesive butt joint subject to torsion whereas in the case of tension, the shear concentration at the adherend edge decreases due to the presence of the spew fillet. Crocombe and Adams<sup>109</sup>, Adams and Harris<sup>176</sup>, Adams et al<sup>177</sup> also studied the effect of spew fillets on adhesive joints and found that spew fillets can improve joint strength by reducing peak shear and peel stresses.

Crocombe et al<sup>178</sup> discussed different approaches for analysing an adhesive joint design including finite element analysis. They analysed cleavage and compressive shear joints both numerically and experimentally and found that for joints made with two component, room-temperature curing, epoxy adhesive, the maximum principal stresses give a good indication of joint strength for any kind of loading. However, for toughened single component epoxy adhesive, it is only true in cleavage or mode I loading. They also found that adherend thickness has a more dominant effect in the cleavage than in the compressive shear test. Increasing the adherend thickness increases the failure load.

Hashim and Cowling<sup>179</sup> performed a numerical analysis of cleavage specimen and found no stress concentration towards the interface. They concluded that the failure could be cohesive unless the surface preparation is not ideal.

Li<sup>180</sup> carried out stress, stiffness and non-linear analysis of adhesive bonded Tee joints using the finite element method, and found good agreement between the experimental and finite element results.

The finite element method has been widely used to predict the behaviour of adhesively bonded joints. Geometric and material discontinuities at the adhesive/adherend interface in the joints make it difficult to predict joint failure. Such discontinuities may cause a stress or strain concentration or even a stress or strain singularity, which cannot be eliminated in a full non-linear elastic-plastic analysis<sup>10</sup>. Hatori<sup>181</sup> and Groth<sup>182</sup> predicted joint failure based on stress singularity. Tong and Steven<sup>10</sup> believe that a true singularity point does not exist at the end of the joint due to the presence of some spew fillet and zones of local damage such as voids, local crazing or local cracking. Lang and Mallick<sup>183</sup> used a linear, 2-D, plane-strain, finite element model of a single-lap joint with spew fillet to analyse stresses in a recessed bond. They found that in recessed joints, like continuous single-lap joints, maximum stresses occur near the adhesive spew terminus, and increase only slightly with the increased level of recessing.

Katona and Batterman<sup>184</sup> performed a parametric finite element analysis of stresses generated by adherend surface roughness in lap and butt joints. Roughness asperities were idealised as having a round shape.

### **Modelling of Composites:**

Several researchers have attempted the modelling of composite materials using classical and finite element approaches. Probably the first analytical model for the laminated composites was that of Smith<sup>185</sup>. His work later evolved into classical laminate theory. The work of Pyror and Barker<sup>186</sup> is one of the first attempts to perform finite element analysis of laminated composites.

Liu et al<sup>187</sup> calculated stress distribution of single-lap adhesive joints of dissimilar adherends subjected to external bending moments. They used the 2-D theory of elasticity (plane strain). They replaced the adherends and adhesive bonds by finite strips and analysed the effect of the ratio of Young's moduli of the adherends, the adherend thickness ratio and the adherend length ratio on the stress distribution at the interfaces. They found the presence of a stress singularity at the end of the interface of the adherend, higher for thinner and low modulus adherends. A good agreement was found between the analytical and finite element results.

Surace and Brusa<sup>188</sup> carried out a parametric study of single lap adhesive joints, with metal and composite adherends, using numerical analysis. They considered the effect of adhesive and adherend thicknesses, joint width, elastic properties of material and angle ply orientation of composites.

Tong and Steven<sup>10</sup> carried out 1-D analytical and 2-D non-linear plane strain finite element analysis of a double lap joint with composite adherends (unidirectional graphite/epoxy). Figure 2.15 shows a comparison of the results calculated using finite element analysis and a 1-D analytical procedure. It can be seen that comparable values of maximum peel stresses are obtained by the two methods.

Pickett and Hollaway<sup>189</sup> analysed elastic-plastic adhesive stresses in lap joints in FRP structures. Herakovich<sup>190</sup> found that the interlaminar shear stresses and interlaminar normal stresses are the dominant stresses initiating delamination failures.

Ripling et al<sup>191</sup> used uniform double cantilever beam (UDCB) and width tapered beam (WTB) specimens to study the fracture of composite-adhesive-composite systems, and found that in a well-made joint cracks appeared to initiate and propagate between the plies near the adhesive. This fracture behaviour was also observed by Han et al<sup>192</sup> for adhesives using a glass fibre reinforced polyester composite. Williams<sup>193</sup> applied elastic beam analysis to study the fracture mechanics of a delamination test in mode I loading.

Kairouz and Matthews<sup>194</sup> conducted a parametric study of the effect of the stacking sequence on the peak stresses within the adhesive and composites in a single lap joint. They performed a linear elastic, small displacement and plane stress finite element analysis and found a good correlation between the observed position of failure with stress maxima from the finite element analysis. They concluded that a non-linear effect should be included in the analysis for prediction of the laminate failure. They also concluded<sup>195</sup> that the stacking sequence does not strongly influence the strength but it does influence the failure mechanism that is dominated by bending stresses.

Pradhan et al<sup>196</sup> studied the effect of parameters such as stacking sequence in the lay-ups, locations of crack initiations, bond lengths, bond thicknesses and modulus of adhesive on the bond strength. They used finite element analysis to calculate the strain energy release rate to indicate possible debonding. They found that the strain energy release rate is sensitive to fibre orientation. They have recommended low moduli ratio (adherends to the adhesive), low overlap ratio (total length to overlap length) and high thickness ratio (adherend thickness to adhesive thickness) for a stronger double lap joint.

Ratwani and Kan<sup>197</sup> investigated the effect of stacking sequence on damage propagation and failure modes in graphite epoxy composites under a compression fatigue test. They found a dependence of the direction of damage propagation on the stacking sequence. The location of delamination and matrix cracking for the different laminates appeared to coincide with the positions of highest interlaminar shear or normal stress predicted by an approximate finite element analysis.

Lu et al<sup>198</sup> studied the relationship between the burst strength of fibre-wound pressure vessels and resin properties. The interlaminar shear strength of the resin matrix was found to be an important resin property in controlling the failure pattern. Talreja<sup>199</sup> has reviewed the mechanisms and modelling of damage and its development in composite materials subjected to mechanical loads. Both micromechanics and continuum damage modelling approaches were discussed.

Lin et al<sup>200</sup> proposed a method for elasto-plastic analysis of unidirectional composites. They assumed high modulus, high strength fibres in a low modulus, low strength matrix. Using plane-strain finite element analysis and a Prandtl-Reuss incremental plasticity relationship, they derived a relationship between composite behaviour and the material properties of the fibre and matrix.

Lakshminarayana and Viswanath<sup>201</sup> have demonstrated the accuracy of finite-element modelling employing a quadratic strain triangular finite element for the stress analysis of composite material laminates. They found good agreement among finite element, analytical and experimental results.

Naik<sup>202</sup> reviewed in detail the work done on modelling of composites and presented a 2-D woven fabric composite stiffness model for the prediction of the thermoelastic properties of 2-D orthogonal plain weave fabric laminates. Three idealised laminate configurations (one quasi-symmetric lay-up and two symmetric lay-ups) were considered, and good correlation was observed between the analytical and experimental results.

Based on beam theory, Ducept et al<sup>203</sup> developed a mixed-mode initiation failure criterion for the delamination of unidirectional glass/epoxy composite and its composite/composite bonded joint. Fracture energies were found to be higher for the joints than for the composite specimens.

Rispler et al<sup>110</sup> used the evolutionary, structural optimisation, finite element method to optimise the shape of adhesive fillets in double lap shear joints with Carbon fibre reinforced plastic (CFRP) as the central adherend. Two cases of upper adherend were considered: a CFRP adherend and a titanium adherend. Different adhesive properties were also considered. The analysis was performed with plane strain assumption and orthotropic material properties.

Yamada and Okumura<sup>204</sup> considered 3-D finite element analysis to look into non-uniform distribution of stresses in composite materials. They found this method useful in incorporating anisotropic material properties and singularity transformation.

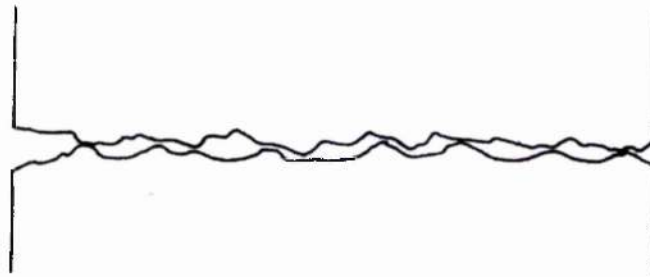


Figure 2.1 Isolated contact points leading to weak adhesion between two rigid rough surfaces<sup>30</sup>

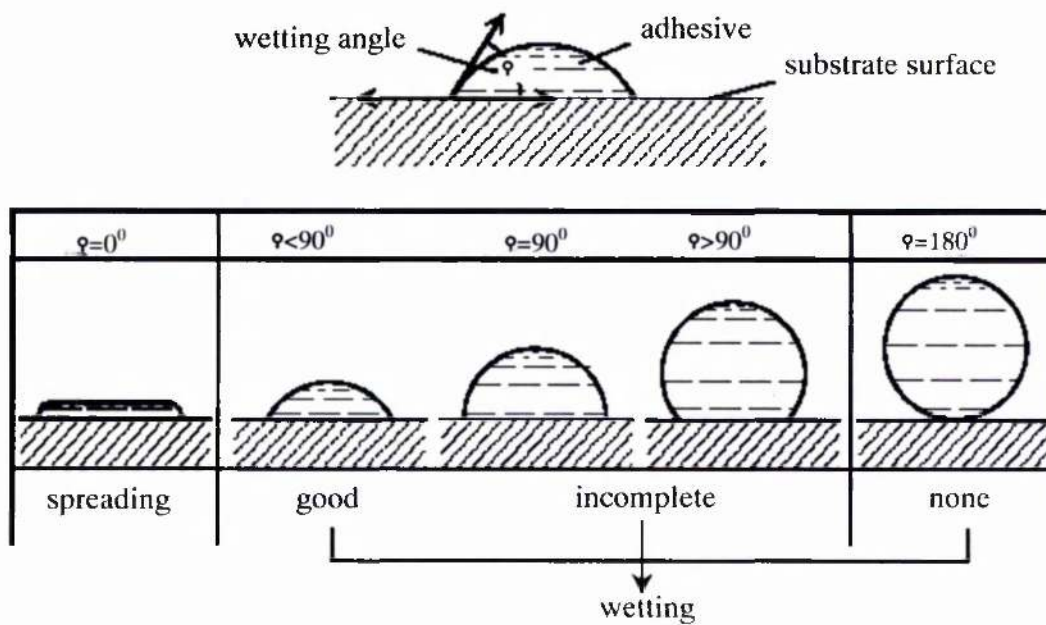


Figure 2.2 Correlation between wetting angle and behaviour of adhesives<sup>205</sup>

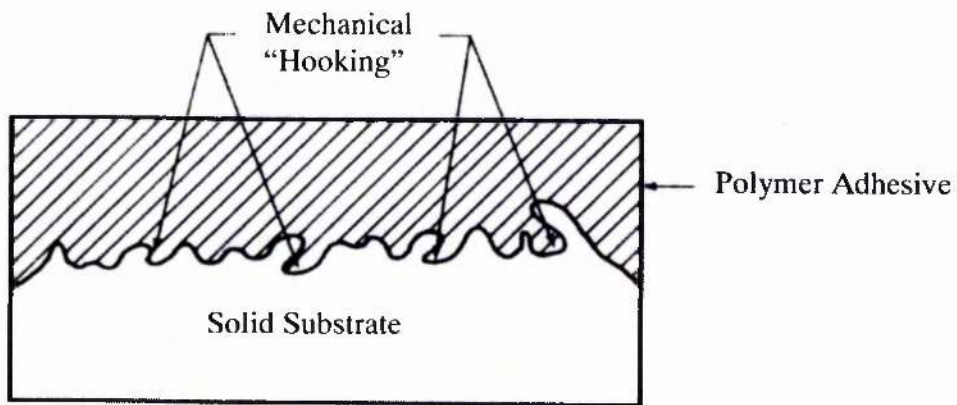


Figure 2.3 Schematic representation of mechanical hooking<sup>206</sup>

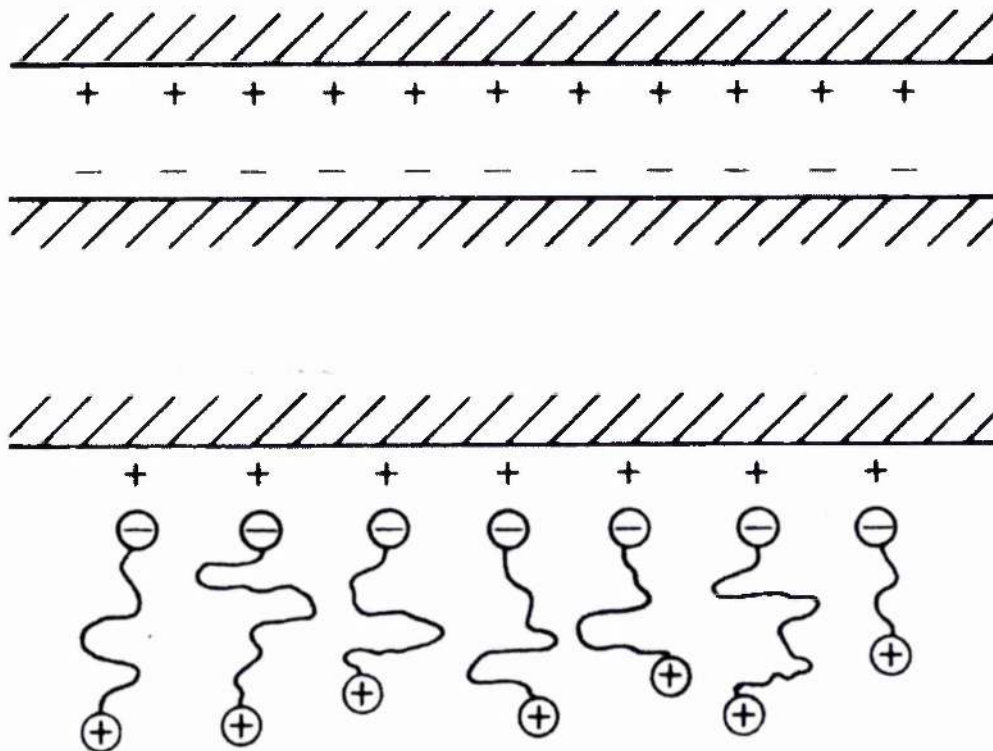


Figure 2.4 Schematic representation of bond formation by electrostatic attraction<sup>30</sup>

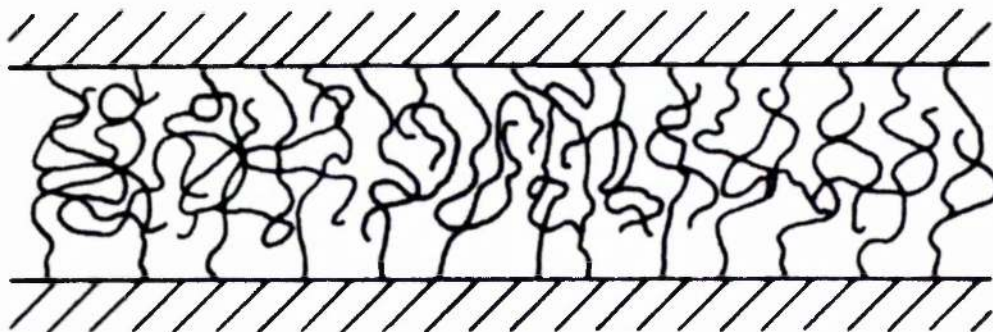


Figure 2.5 Schematic representation of bond formation by molecular entanglement<sup>30</sup>

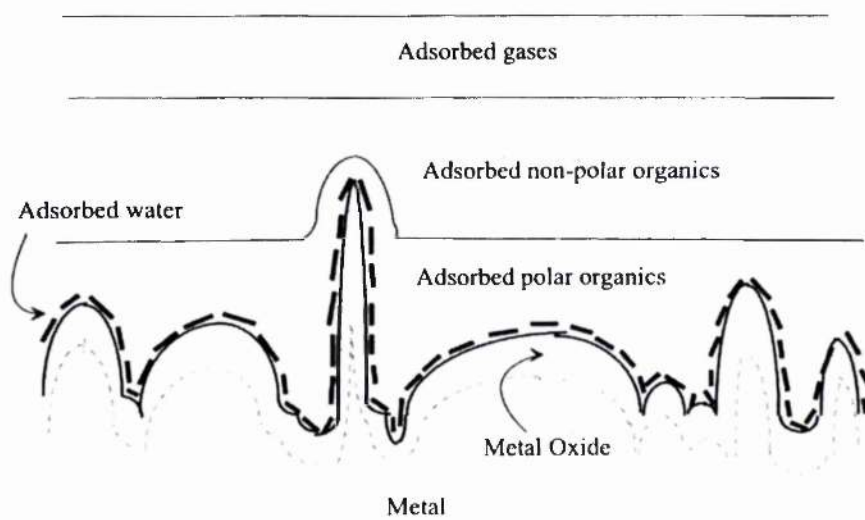


Figure 2.6 Schematic representation of various impurities present on an untreated metallic surface<sup>4</sup>

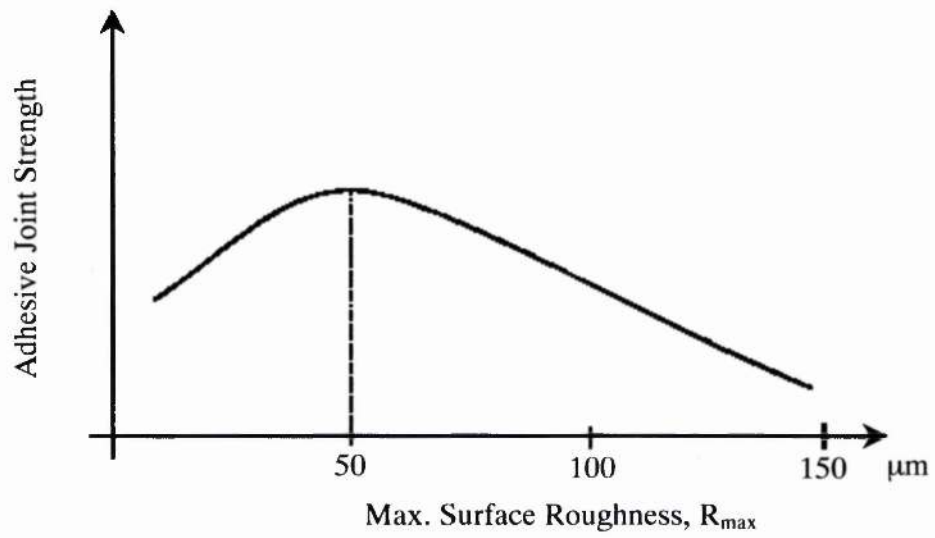


Figure 2.7 Correlation between adhesive strength and surface roughness<sup>205</sup>

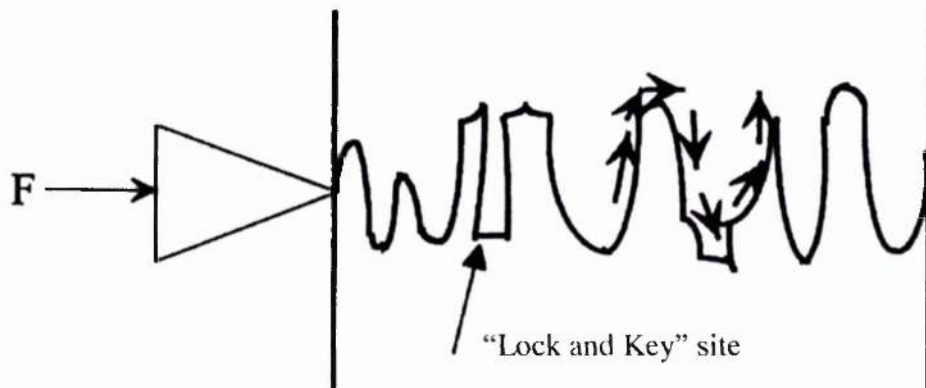


Figure 2.8 Diversion of stresses- lock and key effect<sup>4</sup>

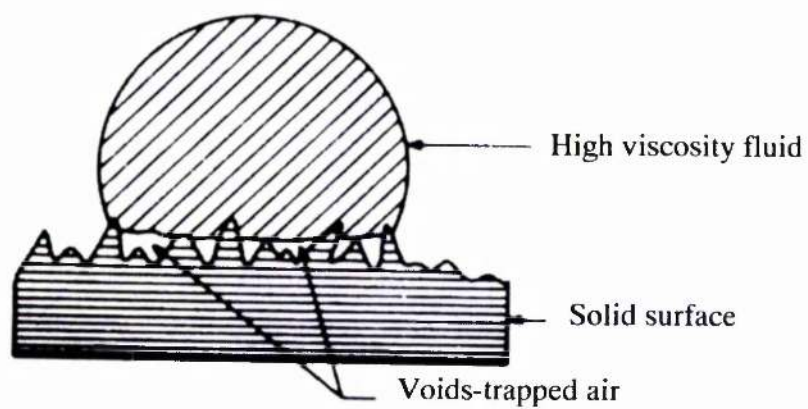


Figure 2.9 Schematic representation of trapped air under the adhesive<sup>206</sup>

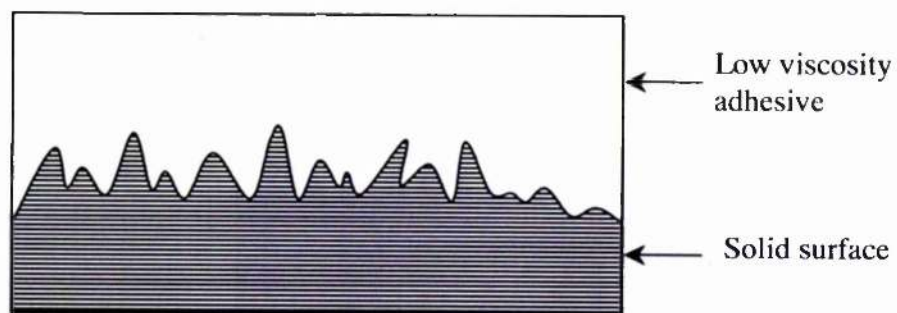


Figure 2.10 Void-free ideal interfacial contact with a low viscosity adhesive

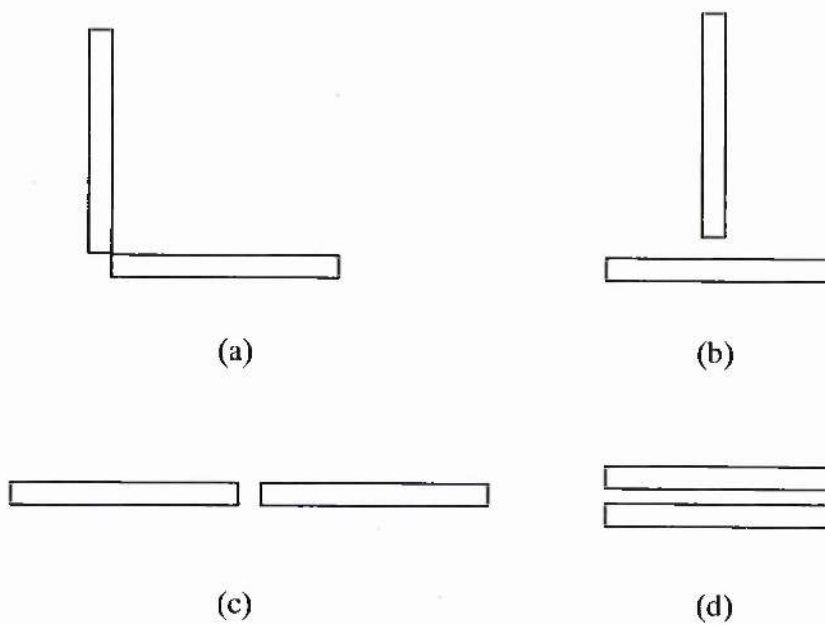


Figure 2.11 Four basic types of joints: (a) angle; (b) tee; (c) butt; (d) surface<sup>16</sup>

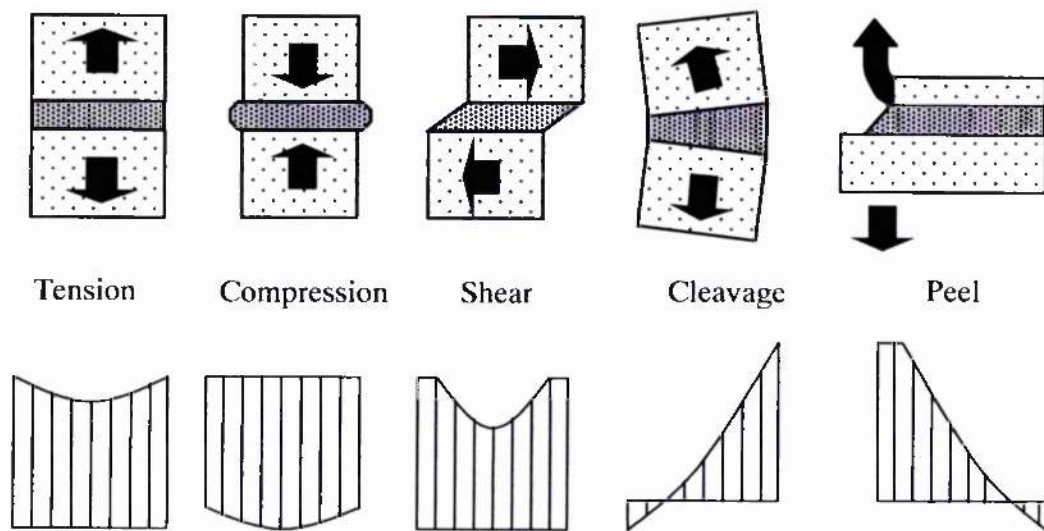


Figure 2.12 Stresses in adhesively bonded joints

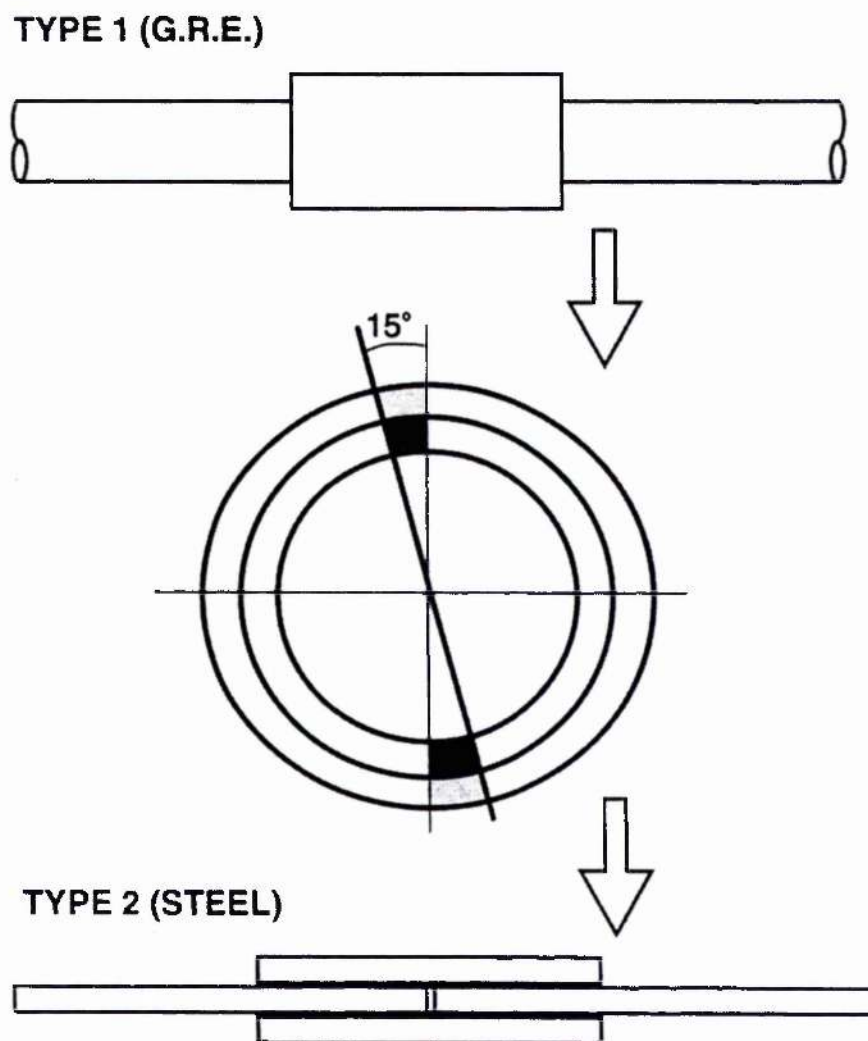


Figure 2.13 Idealisation of a tubular joint into a lap shear joint<sup>207</sup>

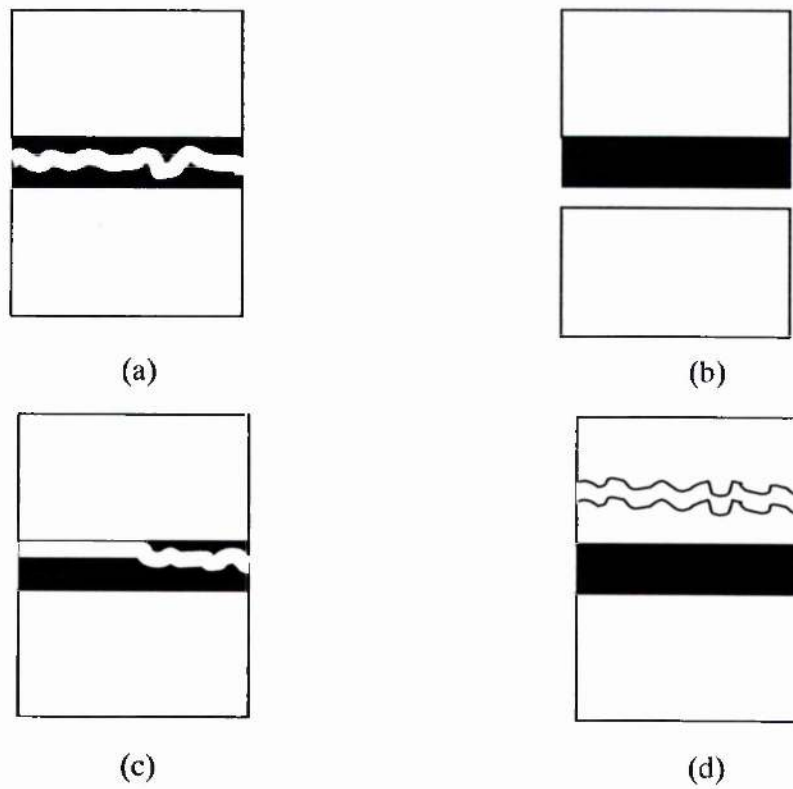


Figure 2.14 Failure modes in adhesive joint: (a) cohesion; (b) adhesion; (c) mixed mode; (d) adherend

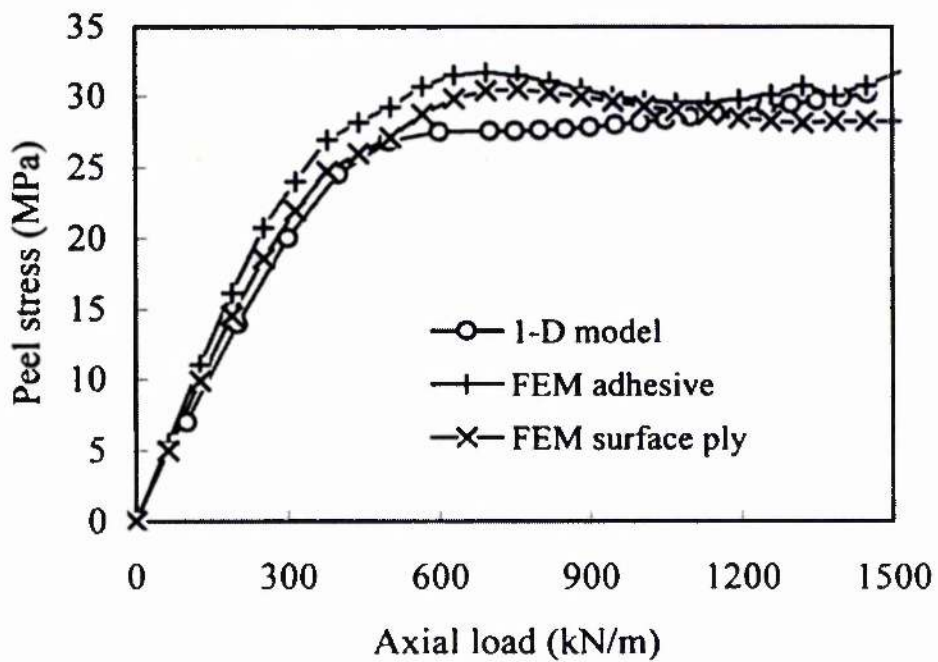


Figure 2.15 Comparison between analytical and finite element results for a double lap joint with composite adherends<sup>10</sup>

Table 2.1 Parameters influencing the strength of adhesive joints

<i>Adhesive layer</i>	<i>Joining material</i>	<i>Geometric design</i>	<i>Stress type</i>
Modulus of elasticity	Modulus of elasticity	Overlap length	Mechanical
Shear modulus	Tensile strength	Overlap width	Physical
Poisson's ratio	Yield strength	Joining part thickness	Chemical
Stress-shearing behaviour	0.2% Offset yield strength	Adhesive layer thickness	Complex mech., phy., chem., time-dependent
	Poisson's contraction		

Table 2.2 Typical surface pre-treatment processes

<i>Surface preparation</i>	<i>Surface pre-treatment</i>	<i>Surface post-treatment</i>
Cleaning	Mechanical processes	Conditioning
Degreasing	Chemical processes	Priming
Fitting	Electrochemical processes	
	Others (plasma etc.)	

Table 2.3 Various surface pre-treatment methods

<i>Mechanical</i>	<i>Chemical</i>	<i>Thermal</i>	<i>Electrical</i>	<i>Others</i>
Grinding	Solvent cleaning	Flaming	Corona	Electrochemical
Brushing	Chemical oxidation	Thermal oxidation	Plasma	UV radiations
Blasting	Gas cleaning	Silicoater	Ion beam etching	Radio frequency

Table 2.4 Effect of surface topography on peel load<sup>83</sup>

Surface topography of copper foil		Mean peel load lb/in
	Diagrammatic representation	
3 $\mu$ high angle pyramids		3.75
Flat		3.8
Flat + 0.3 $\mu$ dendrites		4.4
Flat + 0.3 $\mu$ dendrites + oxide		5.9
3 $\mu$ pyramids (high angle)		7.3
2 $\mu$ low angle pyramids + 0.3 $\mu$ dendrites		8.8
2 $\mu$ low angle pyramids + 0.2 $\mu$ dendrites + oxide		13.5
3 $\mu$ high angle pyramids + 0.2 $\mu$ dendrites + oxide		

## CHAPTER THREE

***PROPERTIES OF THE MATERIALS*****3.1 Introduction**

Successful stress analysis of an adhesive joint depends on the correct evaluation of the constitutive properties of the participating materials i.e. adherends and adhesive. Adhesives may be characterised as either bulk adhesive or an adhesive layer in a bonded assembly. Jeandrau<sup>208</sup> has discussed these methods and appears to agree that if the adhesive characteristics in one loading direction (compression, tension or shear) are known, using the von Mises strength criterion, one can find the mechanical behaviour of adhesive up to its elastic limit in any complex state of stress.

Several factors affect the measurement of the mechanical properties of a material, including the test method and testing conditions such as temperature, moisture, loading rate, etc. Although there are many standard test methods for measuring adhesive properties, adhesive manufacturers do not currently supply the mechanical properties that are directly useful to stress analysis<sup>10</sup>.

This chapter describes the model materials used in the experimental programme, the considerations used in selecting the adhesive, the experimental details for finding its mechanical properties, a procedure for making the composite and the relevant mechanical properties of the materials used.

**3.2 Model Materials**

The model materials used in the fabrication of specimens were mild steel to British Standard BS4360 grade 43A, glass reinforced epoxy (GRE) composite, and a structural epoxy adhesive.

GRE laminates were produced from Fibredux<sup>®</sup> 913G/37%/7781 and Fibredux 913G/30%/E5 prepregs from Hexcel Composites, UK. For verification purposes, a finished GRE, Tufnol<sup>®</sup>, was also tested along with Fibredux. An epoxy adhesive, Araldite<sup>®</sup> 420A/B (Redux<sup>®</sup> 420A/B), from Ciba Speciality Chemicals (UK) Ltd. (now Vantico Ltd.) was used for all adhesive bonding needs. In addition, a glass reinforced polyester (GRP) composite was also used in some testing. This was produced by hand lay-up moulding by Vosper Thornycraft Ltd.

### 3.3 Adhesive Selection

A modified room-temperature curing two-part toughened epoxy adhesive, Araldite 420 A/B was selected for all adhesive bonding needs in this research. Its choice was based on the following considerations:

- it is made specifically for bonding composite materials and used by many end users for bonding epoxy fibreglass composite to itself and other adherends. Therefore, the data generated during this research will not only be of academic interest but also of direct use to the end users
- it has good overall strength, toughness and temperature resistance properties
- an earlier comparative study<sup>209</sup> on six selected adhesives showed that Redux 410 (superseded by Redux 420) exhibits good overall mechanical properties for bonding GRP composites in shear, tensile and cleavage loading
- it has a good shelf life and can be stored at room temperature
- it can either be cured at room temperature or at elevated temperature.

### 3.4 Production and Testing of Bulk Adhesive

Mechanical properties required for the finite element analysis, such as tensile strength and Young's modulus, were provided by the resin supplier, Ciba Chemicals. Poisson's ratio was determined in the departmental laboratory by casting the bulk adhesive into dog-bone specimens and testing them after mounting strain gauges (as explained later). The Young's modulus of elasticity supplied by Ciba Chemicals was found to be in line with the values derived from these tests.

The dimensions of the bulk adhesive specimens were similar to those of British Standard BS18: 1987 for testing steel (Figure 3.1). They were produced using the aluminium mould shown in Figure 3.2. This mould was first sprayed with PTFE mould release spray to allow easy removal of cured specimens. The resin mixture of Araldite<sup>®</sup> 420 A/B was poured into the mould using a manual gun and mixing nozzle MC 06-24. The filled moulds were then covered with a heavy flat metal plate to ensure uniform thickness and smooth surfaces, and placed in a preheated electrical convection oven at 70°C for curing. This cure schedule was selected by keeping in view the production constraints and considering adhesive tensile strength values as quoted at various curing temperatures in the product data sheet. In addition, as our main target was to compare various strength values, a curing temperature was selected that can be applied for all specimens, including hybrid cleavage joints. After two hours of curing, the mould was taken out of the oven and allowed to reach room temperature before removing the cured dog bone specimens. These specimens were then cleaned of any extrusions beyond their expected dimensions. The actual dimensions of the specimen was then measured using a micrometer.

Rosette type strain gauges (EA-06-060RZ-120 of Measurement Group Inc.) were used for the strain measurements. Before bonding a strain gauge, the surface of the specimen was roughened with fine emery paper to remove the remains of PTFE. It was then cleaned with recommended primers and bonded with the supplier's recommended strain gauge adhesive, M-BOND 200. The specimens were left for one day before testing. A strain gauge mounted dog-bone specimen is shown in Figure 3.3.

Of the five specimens made, the best one (void free) was carefully tested on a Lloyd 10000L tensile testing machine at a constant cross-head speed of 0.5mm/min at ambient temperature (Figures 3.4 and 3.5). A Solaritron Schlumberger 3531D data acquisition system was used for data logging. The load input from the tensile tester was recorded by the data logger in terms of voltage (10V=5kN). With the application of load, the length of strain gauge arms changes, producing strains that were recorded by the data logger on three selected channels. Output from the data logger in the form of a .dat file was converted to a .dif file, which was then read and analysed with an Excel spreadsheet.

The ratio of the strains measured normal and parallel to the load directions was taken as Poisson's ratio (Appendix 1).

### 3.5 Production of Laminates

Glass reinforced epoxy laminates were produced largely from woven fabric preregs, Fibredux<sup>®</sup> 913G/37%/7781, by hot press moulding. To study the effect of unidirectional fabric, a unidirectional prepeg, Fibredux 913G/30%/E5, was stacked on both surfaces of the woven fabric to produce laminates with a unidirectional surface ply.

For the production of laminates, a special steel frame mould was designed and manufactured with removable edges. The mould allows a batch production of 125mmx125mm laminates with the required thickness. It also makes the removal of the finished product easy (Figure 3.6).

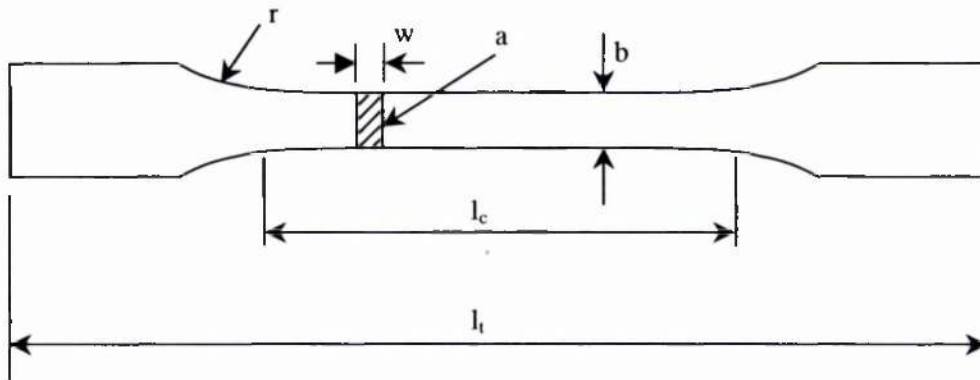
A number of the laminates were produced by varying the number of the plies and the applied moulding pressure to give the optimum quality. The best results, both in terms of minimum resin loss and surface finish, were obtained when 8 plies of woven roving prepreg (or 4 plies of the woven roving with 7 plies of the unidirectional prepreg) were moulded at an initial pressure of 2MPa. Figure 3.7 shows the surface finishes for a poor and a good laminate. Various options for mould release methods were considered. These included using Mylar<sup>®</sup> D polyester film, the supplier's recommended peel ply (N2019 of Carrington Performance Fabrics, UK) and a PTFE spray. It was not possible to remove the Mylar film from the cured laminate surface without damaging it. The peel ply method was found suitable from a production viewpoint but it did not give good results as initially expected. The probable reason for such a poor performance is the presence of chemicals used in the production of the peel ply itself. This was later confirmed by the supplier. Further discussion regarding this is presented in Chapter 8. The PTFE spray was the easiest to apply and gave good surface finishes. Removal of the PTFE from the moulded laminates was, however, a little inconvenient and unreliable.

The appropriate number of plies were cut into 125x125mm pieces and stacked in the required sequence in the PTFE sprayed mould. The mould was then closed and placed between the heated platens of the press for 20min at 150°C under 2MPa pressure (Figure 3.8). After curing, the moulded laminates were de-moulded, trimmed along each side and then cut into nine equal square pieces using a manual hacksaw. The edges of each piece were then finished to remove loose fibres to make them safe for handling. An appropriate surface pre-treatment operation was then performed before the bonding process as detailed in Chapter 6.

### 3.6 Properties of the Materials

For the composite materials, the three properties of principal interest are those associated with uniaxial tensile, uniaxial compressive and in-plane shear loadings. Since composites are typically orthotropic i.e. they have two identifiable in-plane principal directions, it is necessary to measure the tensile and compressive properties in both directions. Thus, a total of five different tests are required to fully characterise the orthotropic composite, i.e., axial and transverse tension, axial and transverse compression, and longitudinal (in-plane) shear. It is usually most difficult to test unidirectionally reinforced, continuous fibre composites because these materials exhibit the highest degree of material anisotropy.

For lack of in-house facilities to fully characterise the composites, attempts were made to get the composite properties from the supplier, but having no response from them, typical properties of similar materials were then obtained from the available literature<sup>202,210,211</sup>. The mechanical properties of a typical laminate, the adhesive, and the steel, are summarised in Tables 3.1–3.3



<i>Dimensions</i>					
$l_t$	$l_c$	$r$	$a$	$b$	$w$
(mm)	(mm)	(mm)	(mm <sup>2</sup> )	(mm)	(mm)
179	62	25	38	11.2	3.4

Figure 3.1 Sketch of bulk adhesive tensile test specimen and dimensions



Figure 3.2 Production of dog-bone specimens

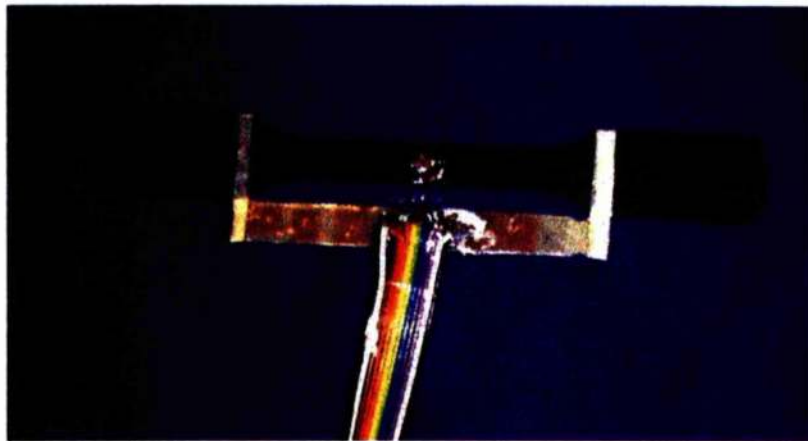


Figure 3.3 Strain gauge mounted dog-bone specimen.

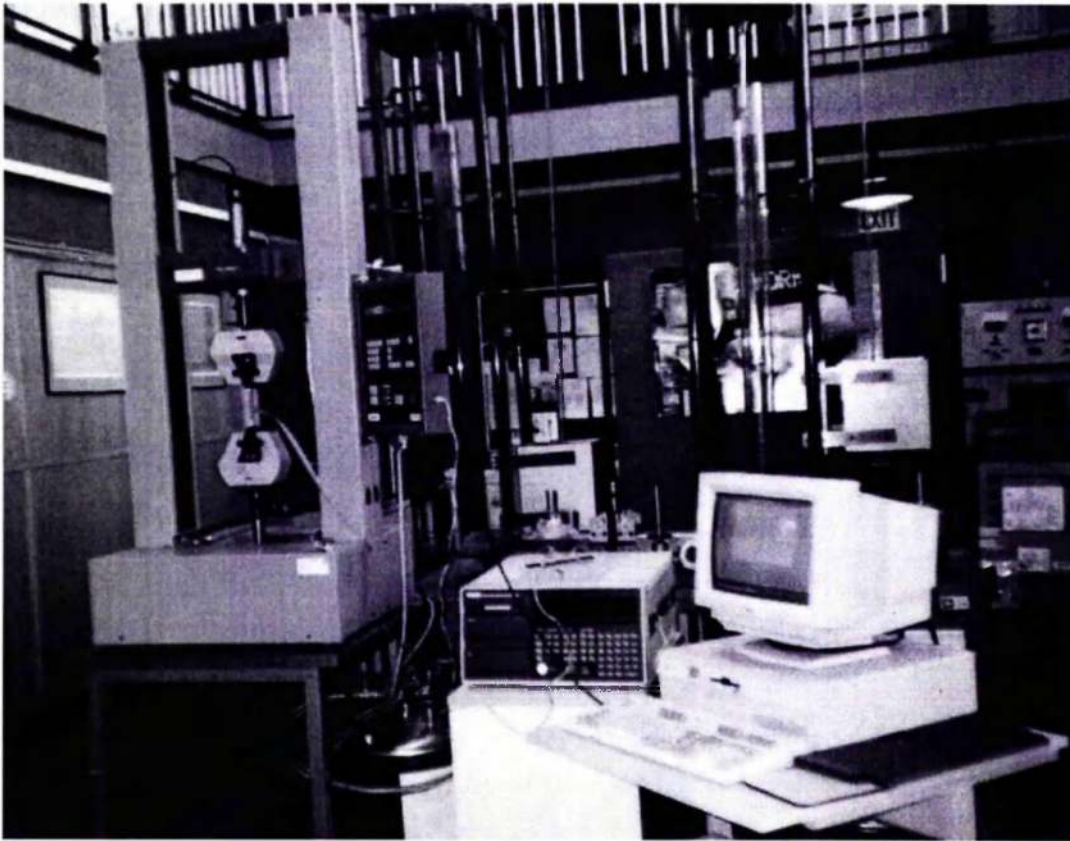


Figure 3.4 Experimental set-up for testing dog-bone specimen

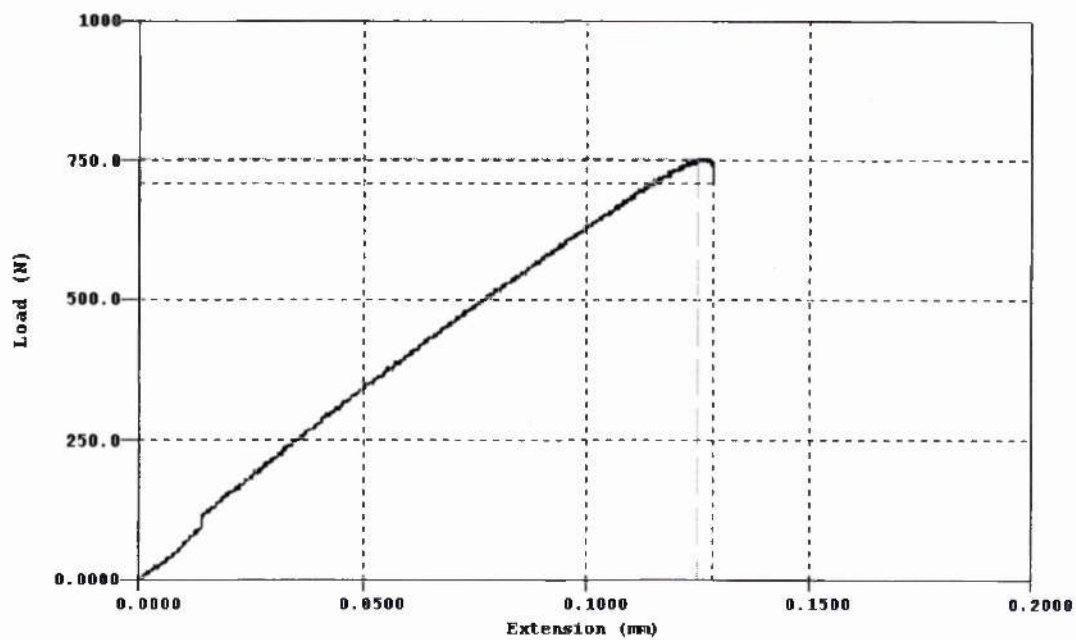


Figure 3.5 Load extension graph from the testing of a bulk adhesive specimen

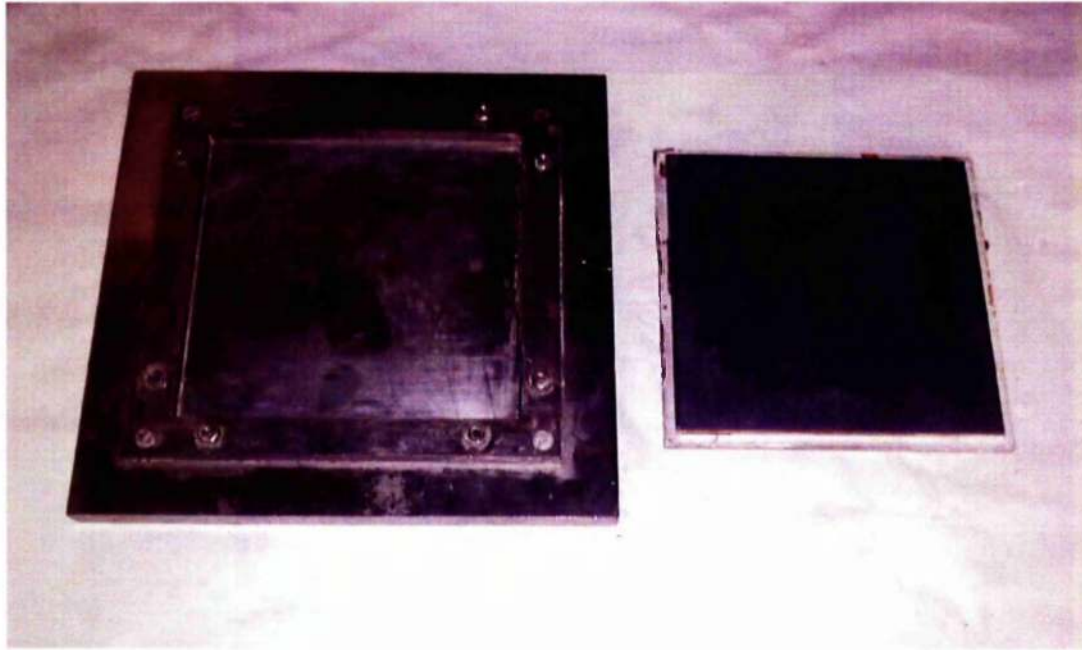
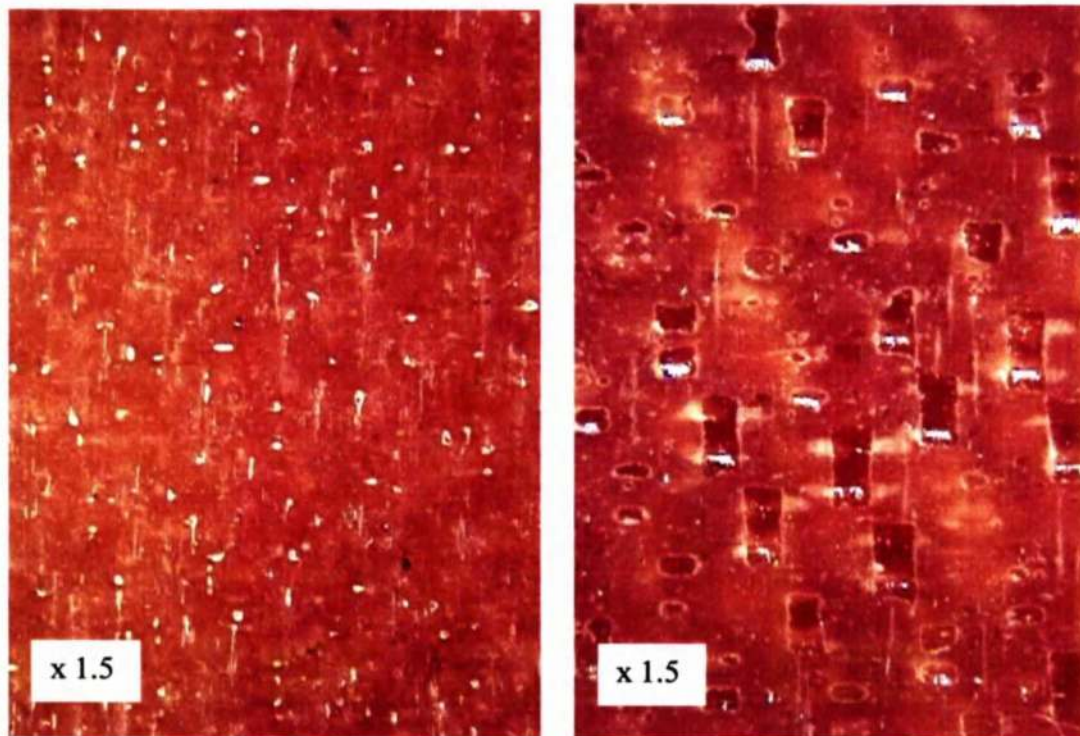


Figure 3.6 Mould for the production of laminates



(a)

(b)

Figure 3.7 Micrograph showing (a) a good laminate; (b) a bad laminate

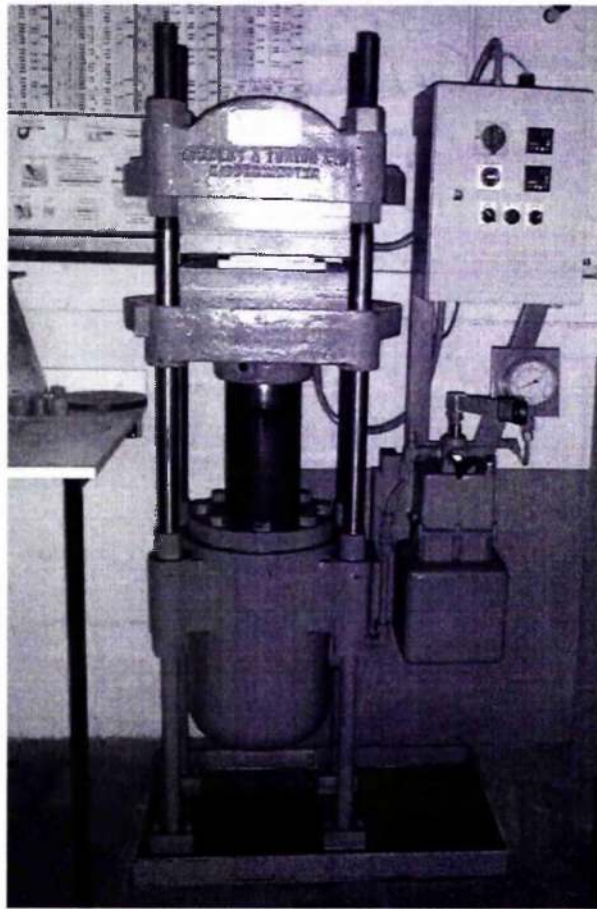


Figure 3.8 Hydraulic heated platen used for moulding laminates

Table 3.1 Properties of bulk adhesive (Araldite 420A/B)

<i>Parameter</i>	<i>Value</i>	<i>Standard deviation</i>
Tensile strength (MPa)	40.29	2.94
Young's modulus (MPa)	2268	203.5
Poisson's ratio	0.40	-

Table 3.2 Properties of laminate in warp direction<sup>210</sup>

<i>Parameter</i>	<i>Fibredux 913G/30%/E-5</i>	<i>Fibredux 913G/37%/7781</i>
	<i>(unidirectional)</i>	<i>(woven roving)</i>
Nominal fibre volume (%)	60	46
Tensile strength (MPa)	1310	440
Young's modulus (GPa)	42	23
Flexural strength (MPa)	1847	550
Flexural modulus (GPa)	48	24
Compressive strength (MPa)	750	468

Table 3.3 Properties of mild steel<sup>212</sup>

<i>Parameter</i>	<i>Value</i>
Young's modulus (GPa)	210
Poisson's ratio	0.29

## CHAPTER FOUR

***SURFACE PROFILOMETRY*****4.1 Introduction**

Profilometry is a general term given to the techniques used for measuring and analysing surface irregularities. Real surfaces are never ideally smooth and contain ups and downs of varying dimensions, depending on the methods by which they are prepared. Each roughness measuring instrument has its own merits and limitations in terms of ease of use, range of measurement and accuracy.

In this chapter, different profilometric techniques used for the measurement of surface roughness are described, namely: Talysurf surface profilometry, Atomic forces microscopy and Michelson's interferometry. Where possible, more than one technique was utilised for roughness measurement to verify the results. Brief descriptions of various roughness parameters are also given here.

**4.2 Roughness Parameters**

Solid surfaces, irrespective of the method of formation, contain surface irregularities or deviations from the prescribed geometrical form. Characterising surface roughness is important for predicting and understanding the tribological properties of solids in contact.

No single parameter could be used to fully describe all features of surface roughness. Therefore, a series of parameters is used to accurately express the complexities of the surfaces. In general, profile parameters fall into three groups:

*Amplitude parameters*, which are determined solely by the peak or valley heights, or both, and are irrespective of horizontal spacing (e.g.  $R_a$ , average roughness).

*Spacing parameters*, which are determined solely by the spacing of irregularities along the surface (e.g.  $S_m$ , mean spacing).

*Hybrid parameters*, which are determined by both the amplitude and spacing of irregularities (e.g. average wavelength).

The following parameters are used in this study:

**average roughness ( $R_a$ ):** is the most commonly used parameter which is also known as Centre Line Average (CLA) or Arithmetic Average (AA) roughness. Taking  $Y$  as the height coordinate and  $X$  as the horizontal coordinate, for a length  $L$ , mathematically it is represented as<sup>213</sup>,

$$R_a = \frac{1}{L} \int_0^L |Y| dx \quad (4.1)$$

Graphically,  $R_a$  is the average roughness is the area between the roughness profile and its centre line divided by the evaluation length (Figure 4.1).

**root mean square roughness ( $R_q$ ):** is the standard deviation of surface heights, which is the square root of the arithmetic average of squares of the vertical deviation of a surface profile from its mean plane<sup>214</sup>. Mathematically,

$$R_q = \sqrt{\frac{1}{L} \int_0^L Y^2 dx} \quad (4.2)$$

**maximum peak to valley height ( $R_t$  or  $R_{y_{max}}$ ):** is the vertical height between the highest and the lowest point of the profile within the evaluation length i.e. the sum of the highest peak and the lowest valley in the evaluation length. Graphically it is represented as shown in Figure 4.2.

**linear profile length ( $R_{l_0}$ ):** is defined in ISO 4287 1984 para 6.7. It is the measured length of the profile surface within the evaluation length i.e. the length obtained if

the profile, within the evaluation length, was to be drawn out into a straight line<sup>215</sup>. Mathematically it is represented as follows:

$$R_{1\sigma} = \int_0^{\ln} \sqrt{1 + \left(\frac{dy}{dx}\right)^2} dx \quad (4.3)$$

Graphically, this is explained in Figure 4.3.

**root mean square slope ( $R_{dq}$ ):** is defined in ISO 4287 1997 para 4.4.1. It is the root mean square value of the ordinate slope  $dz/dx$  within the sampling length. The mathematical representation for this parameter is,

$$R_{dq} = \sqrt{\frac{1}{L} \int_0^L (\theta(X) - \bar{\theta})^2 dx} \quad (4.4)$$

where  $\theta$  is the slope of the profile at any given point and

$$\bar{\theta} = \frac{1}{\ln} \int_0^{\ln} \theta(X) dx$$

Graphically, this is explained in Figure 4.4.

Due to the multiscale nature of surfaces, roughness parameters depend strongly on the resolution of the roughness-measuring instrument or any other form of filter, and hence are not unique for a surface<sup>217</sup>. Therefore, a rough surface should be characterised in such a way that the structural information of roughness at all scales is retained.

The measured roughness profile is dependent on the lateral and normal resolutions of the measuring instrument. Instruments with different lateral resolutions measure features with different scale lengths. Bhushan<sup>214</sup> has therefore concluded that a surface is composed of a large number of length scales of roughness that are superimposed on each other.

### 4.3 Talysurf

Taylor and Hobson's Form Talysurf Series 2 *50i* surface profiler, shown in Figure 4.5, was used to measure the surface roughness of metallic and composite adherends. It is provided with a 50mm traverse unit with motorised column and a universal worktable to ensure horizontal measurements. It provides a resolution of 16nm @1mm range. Taylor and Hobson's software "Ultra" was used for measurements and analysis.

#### 4.3.1 Basic Principle

In principle, the majority of surface measuring instruments use the same technique. A very sharp stylus traverses the surface at a constant speed for a set distance and the gauge converts its vertical movement into an electrical signal which is amplified to produce a much enlarged vertical magnification. The signals are displayed on graphical and/or screen outputs. The values of the roughness parameter are calculated using an appropriate filter. The general principal behind the operation of Form Talysurf is shown in Figure 4.6.

The stylus is the only active part of the instrument that comes into contact with the surface to be analysed. The shape and dimensions of the tip are therefore very important for accurate measurement of the surface profile.

The gauge functions to convert the vertical movement of the stylus into usable electrical signals. The gauge resolution is the sensitivity of the gauge in responding to a stylus movement, typically of the order of 10nm. The type of transducer used determines the gauge range i.e. analogue or digital. Analogue transducers can be further divided into position-sensitive or motion-sensitive types. Among digital transducers, two commonly used are laser interferometric and phase grating interferometric gauges. Some non-contact gauges are also available which can measure a fragile surface without touching it.

In a typical variable inductance gauge, shown in Figure 4.7., the stylus is mounted at one end of a beam pivoted on a knife edge in the middle, linked to an armature at the other end, which moves between two coils, changing their relative inductance. The coils are connected in an a-c bridge circuit such that when the armature is central between the bridge it is balanced and gives no output. Movement of the armature unbalances the bridge and produces an output proportional to the displacement. In modern instruments like the Form Talysurf Series, knife-edge pivots are replaced by more precise pivot bearing for higher resolution<sup>216</sup>. The Form Talysurf Series 2 50i surface profiler uses a position-sensitive transducer which can give a range to resolution ratio of over 65000.

#### ***4.3.2 Measurements of Specimens***

After necessary pre-treatment, the surface roughness of adherends was measured. An ISO-2CR filter was used with a cut-off limit of 0.8mm. A sampling length of 15mm was taken in each case. The surface roughnesses of the grit-blasted and the polished steel and composites were measured with this instrument. The roughness of the grit-blasted composite was not measured to avoid any potential damage of the sensitive stylus. At least five specimens of each type were measured at various locations.

#### ***4.3.3 Results***

The results of the measured average surface roughness parameters and their standard deviation values are given in Table 4.1. The measured values of the roughness parameters are in line with the other findings<sup>71,74</sup>. It can be seen from the results that the diamond finish of steel surfaces are much smoother (about four-times in terms of the average roughness) compared to those of the woven roving composites polished to the same level. Standard deviation values are typically very high for the polished surfaces, reflecting the difficulties in achieving a uniformly polished surface. Further discussion about the roughness measurement results is given in Chapter 8. Some representative graphs and surface profiles are shown in Figures 4.8-4.12.

## 4.4 Atomic Force Microscope

Atomic force microscopic (AFM) techniques are increasingly being used for tribological studies of engineering surfaces at scales ranging from atomic and molecular to micro-scales. These techniques have been used to study surface roughness, adhesion, friction, scratching/wear, indentation, detection of material transfer and boundary lubrication and for nanofabrication/nanomachining purposes. These micro/nanotribological studies are needed to analyse and develop a fundamental understanding of interfacial phenomena on a small scale<sup>214</sup>.

An Explorer<sup>®</sup> AFM from ThermoMicroscopes with “Topometrix<sup>®</sup>” software was used in the present study in contact and constant force modes.

### 4.4.1 Basic Principle

The atomic force microscope (AFM), or scanning force microscope (SFM) was invented by Binnig, Quate and Gerber in 1986<sup>217</sup>. It is a *tactile* instrument<sup>218</sup> that is employed to image surface structures and to measure surface forces. AFM measures ultra-small forces (less than 1nN) present between the AFM tip surface and a sample surface. Like all other scanning probe microscopes, the AFM probes the surface of a sample with a sharp tip, a couple of microns long, ranging from 10 to 100nm in diameter, located at the free end of a light and very flexible cantilever beam, 100 to 200 $\mu$ m long. The movement of the tip or sample is performed by an extremely precise positioning device constructed from piezo-electric ceramics, most often in the form of a tube scanner. The scanner is capable of sub-angstrom resolution in x-, y- and z-directions. The z-axis is conventionally perpendicular to the sample (Figures 4.13 and 4.14).

While scanning, the topographic features of the sample cause the tip to deflect in the vertical direction. This tip deflection changes the direction of the reflected laser beam and hence the intensity difference between the top and bottom photodetectors (AFM signal). Normal and frictional forces at the tip-sample interface are measured using a laser beam deflection technique. A laser beam from a diode laser is directed by a

prism onto the back of a cantilever near its free end, tilted downward at about  $10^\circ$  with respect to a horizontal plane. The reflected beam from the vertex of the cantilever is directed through a mirror on to a quad photodetector (split photodetector with four quadrants). The differential signals from the top and bottom photodiodes provide the AFM signals, which is a sensitive measure of the cantilever vertical deflection. The deflection can be measured up to 0.02nm. So, for a typical cantilever with a force constant of 10N/m, a force as low as 0.2nN can be detected. The measured cantilever deflections allow a computer to generate a map of surface topography. The first AFM used a scanning tunnelling microscope at the end of the cantilever to detect the bending of the lever, but now most AFMs employ an optical lever technique.

AFM can generate sets of topographic data by operating in one of the two modes: *constant-height mode* (without feedback control) or *constant-force mode* (with feedback control).

In *constant force* or *height mode*, the positioning piezo, which moves the sample up and down, responds to any change detected in a pre-determined value of the force and restores it by altering the tip-sample separation. This mode is generally preferred for most of the applications.

*The Constant height or deflection mode* is useful for imaging very flat sample surfaces at high resolution or for changing surfaces where high scan speed is essential.

Image contrast can be obtained in many ways. The three main classes of interaction are: *contact mode*, *tapping mode* and *non-contact mode*.

**Contact mode** is the most common method of operation. In this mode, an AFM tip makes soft "physical contact" with the sample surface and is held less than a few angstroms from it. The interatomic force between the cantilever and the sample is repulsive. As the tip travels across the sample, the contact force causes the cantilever to bend and accommodate changes in topography. In addition to the repulsive van der Waal's forces, two other forces are generally present during this mode of

operation: the force exerted by the cantilever and a capillary force exerted by a thin water layer often present in an ambient environment, whose magnitude depends upon the tip-to-sample separation. The force exerted by the cantilever is like the force of a compressed spring. The magnitude and sign (repulsive or attractive) of the cantilever force depends upon the deflection of the cantilever and its spring constant. An exemplary force curve is shown in Figure 4.15.

A major drawback of the contact mode is the existence of large lateral forces due to dragging of the tip over the specimen surfaces. It may therefore not be suitable for soft samples.

In **Tapping mode** the cantilever is oscillated at its resonant frequency (often hundreds of kilohertz) and positioned above the sample surface so that it only touches the surface for a very small fraction of its oscillation period. As the contact time is much less than that in contact mode, the lateral forces are dramatically reduced as the tip scans over the surface. This mode is suitable for imaging poorly immobilised or soft samples.

**Non-contact mode** is a method of operation in which the cantilever is held from the sample surface on the order of tens to hundreds of angstroms and the interatomic forces between the cantilever and the sample surface are attractive (largely as a result of the long-range van der Waal's interactions). This is a very difficult mode to operate in an ambient condition because the thin layer of water vapours that exist on the surfaces of the samples will invariably form a small capillary bridge between the tip and the sample and will cause the tip to "jump-to-contact".

Atomic force microscopy is capable of investigating the surfaces of both conductors and insulators on an atomic scale. It can also be used in a liquid environment. This is important not only for biological systems, but also for investigating adsorption from solutions and other such applications. For such applications, the cantilever block is mounted inside a quartz glass holder so that the space between glass and sample can be filled with the desired solvent (e.g. water) as shown in Figure 4.16.

#### **4.4.2 Measurements of Specimens**

Before measuring surface roughnesses with AFM, acetone cleaned steel and composite specimens were first diamond polished, as detailed in Chapter 5, followed by acetone pot-cleaning and hot air drying. Because of protruding glass fibres, attempts at measuring surface roughness of the grit-blasted composite specimens were not successful. Since measurements were made using the AFM available in the Department of Mechanical and Chemical Engineering, Heriot Watt University, Edinburgh, only one specimen of each type was measured at different locations on the surface.

#### **4.4.3 Results**

The average values of the surface roughness parameters measured by the AFM and their standard deviations are given in Table 4.2. The average  $R_a$  and RMS values for the polished steel surfaces, measured by the AFM, are approximately 26% higher than those measured by the Talysurf. On the other hand, these parameters measured for the polished composites are lower than the corresponding Talysurf values. This difference is perhaps due to the anisotropic nature of the composite surfaces, the higher sensitivity of the instrument and a very small valuation length in the case of AFM measurements. Representative AFM surface profiles are shown in Figures 4.17 and 4.18.

#### **4.5 Michelson's Interferometer**

A Michelson double-beam interference microscope, OPTIPHOT<sup>®</sup> 100 from Nikon Corporation, was used to measure roughnesses of polished steel surfaces (Figure 4.19). It is fitted with a M Plan 2.5 TI double beam interference system and has the facility to use an on-line camera and computer. Micromap<sup>®</sup> software from the Micromap Corporation was used to measure and analyse the surface patterns.

### 4.5.1 Basic Principle

In a double beam interference microscope, an emitted light source is divided into two beams. One beam is used as the reference beam while the other is reflected off the specimen surface. The two beams are superimposed at the point of observation and their differences are observed as interference fringes. By this method, variations in specimen surface can be observed directly.

As shown in Figure 4.20, the light passing through the objective is divided into two beams by the half-reflecting prism (G). The transmitted portion of the beam reflects off the specimen (P), and the reflected portion reflects off the reference mirror (R). These two beams are then superimposed on the half-reflecting prism (G), where they interfere to create the characteristic fringe patterns of interferometry. The direction and spacing of the interference fringes are adjusted at the interference mirror (R).

Difference in step height or surface variations are measured with reference to the pitch ( $\lambda / 2$ ) of the observed interference fringes, where  $\lambda$  is the wavelength of the light source.

Surface variations show up as a disturbance in the fringe pattern, which are then measured with a filar micrometer eyepiece or using an appropriate software system. By assigning the value  $A$  to the fringe pitch ( $\lambda / 2$ ) and the value  $B$  to the amount of fringe disturbance ( $y$ ) detected, surface variations can be calculated using the following formula (Figure 4.21):

$$N = \lambda / 2 \times \frac{B}{A} \quad (4.5)$$

When the interference filter is being used, a wavelength value of 546nm can be assigned to  $\lambda$ . In this study, the Micromap<sup>®</sup> software performed these calculations.

#### **4.5.2 Measurements of Specimens**

Because of very high sensitivity and the limited roughness measurement range of this instrument, roughnesses of only polished steel specimens were measured. Specimens were acetone-cleaned and dried before the measurements. Approximately 20 specimens were measured with at least three measurements taken on each surface.

#### **4.5.3 Results**

The average values of the surface roughness parameters measured for the polished steel surfaces and their standard deviations are presented in Table 4.3. A typical surface profile, as seen by the interferometer, is shown in Figure 4.22. The measured values of the roughness parameters,  $R_a$ , RMS and  $R_{y_{max}}$ , are of the same order as those measured by the Talysurf.

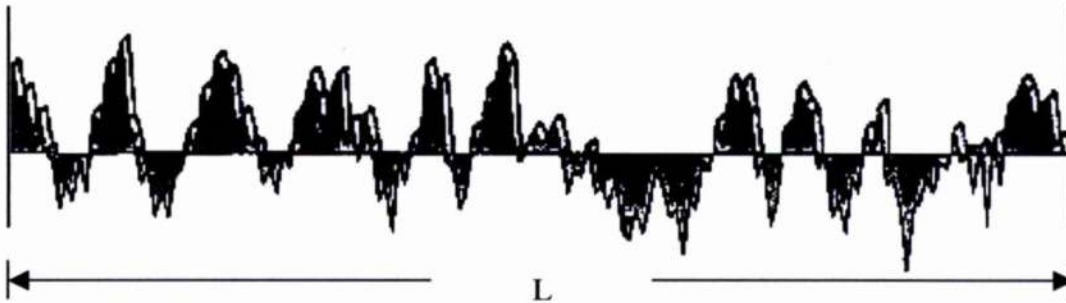


Figure 4.1 Graphical representation of  $R_s$

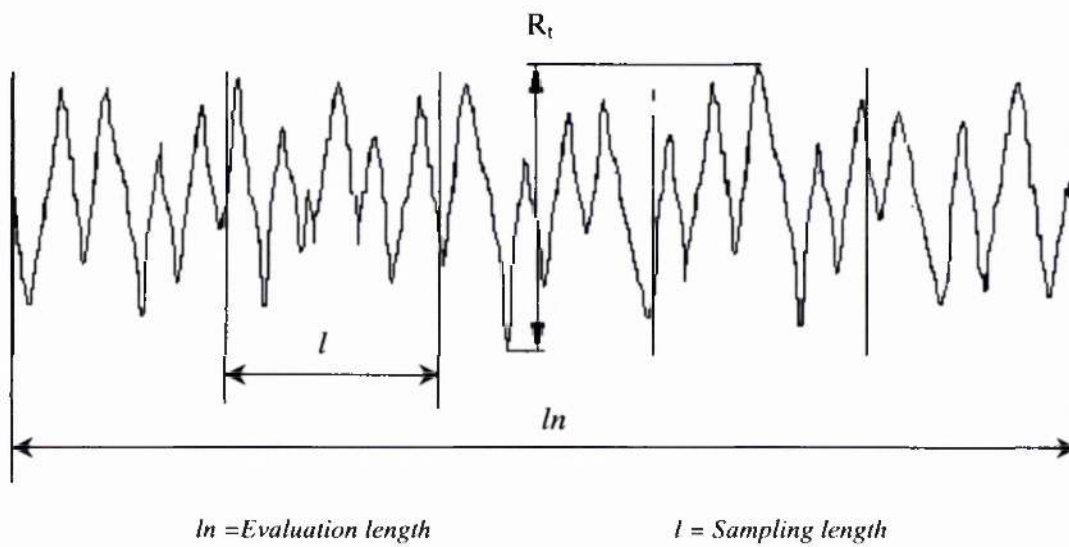


Figure 4.2 Graphical representation of  $R_t$

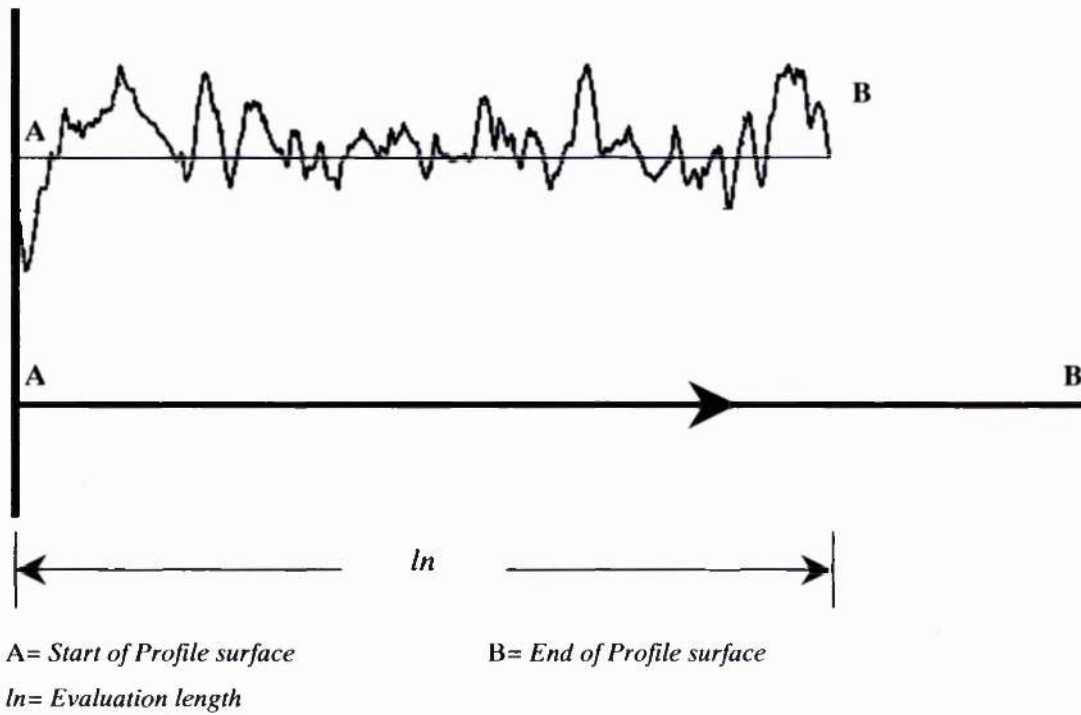


Figure 4.3 Graphical representation of linear profile length,  $R_{l_0}^{215}$

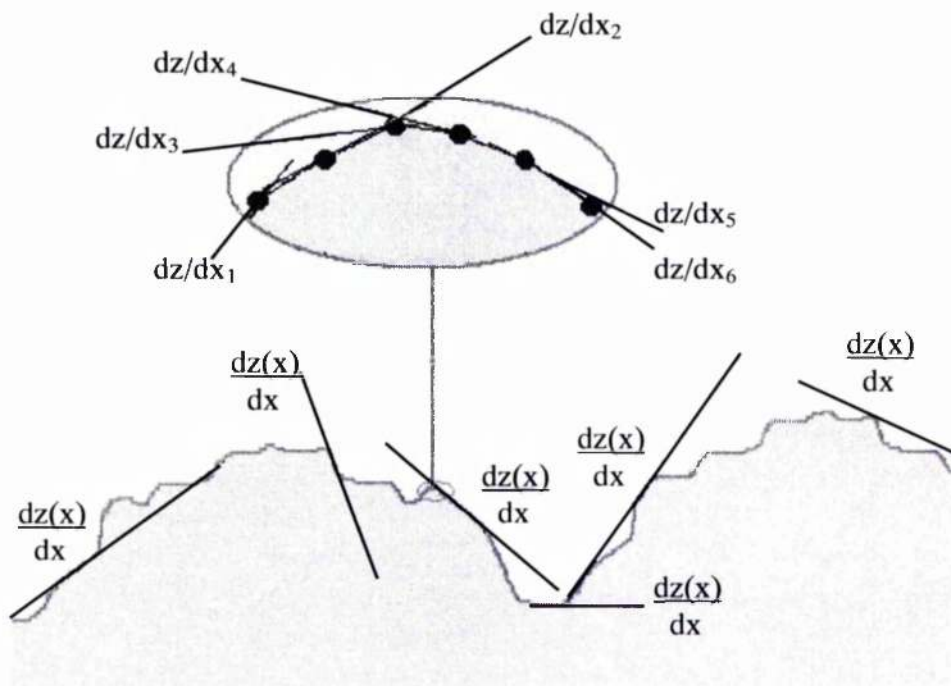


Figure 4.4 Graphical representation of  $R_{dq}^{215}$

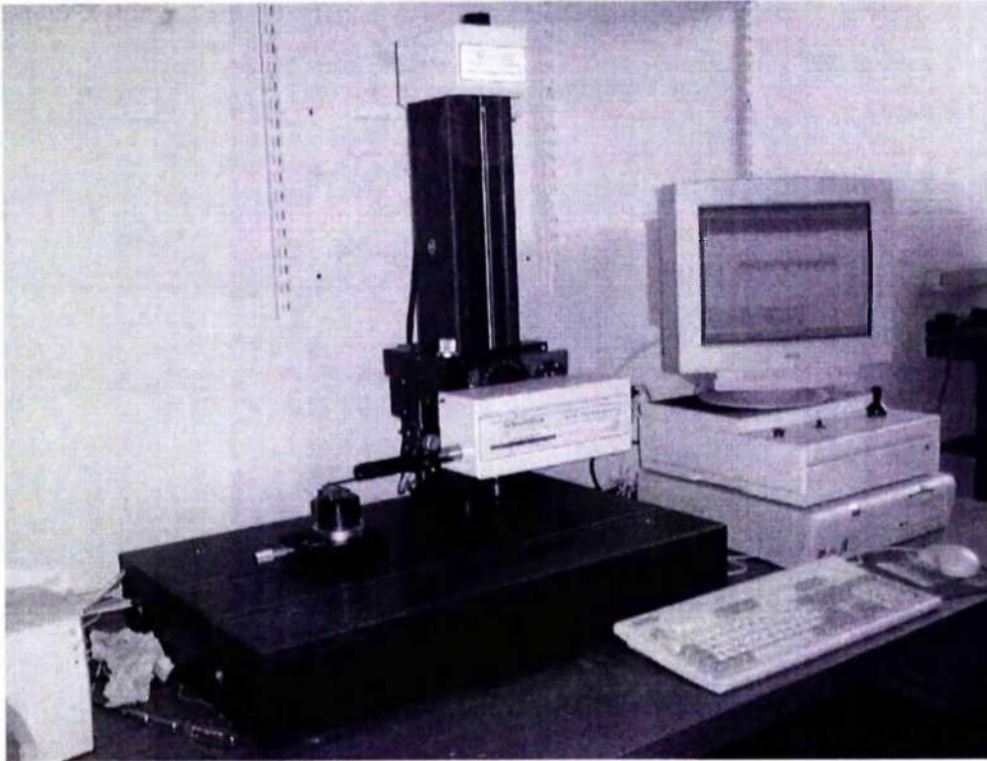


Figure 4.5 Taylor and Hobson's Talysurf Series 2 50i surface profiler

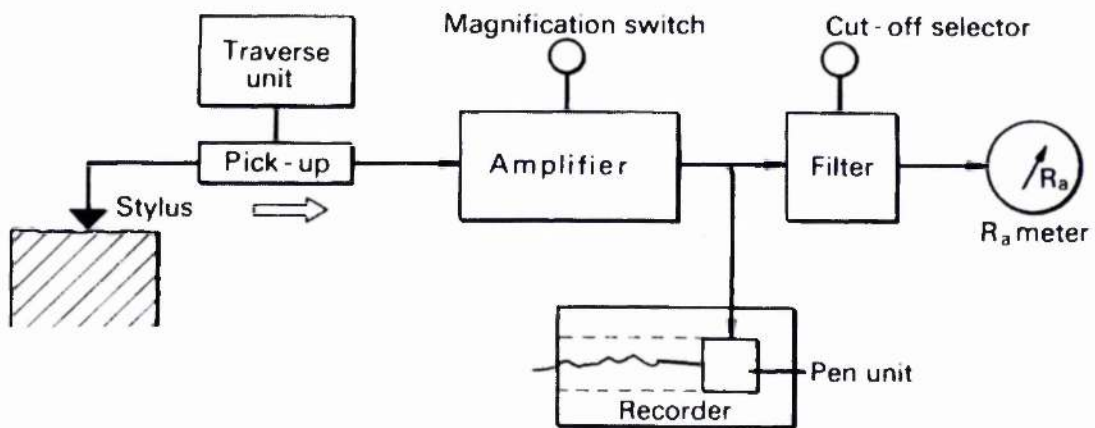


Figure 4.6 Schematic layout of a typical Talysurf instrument<sup>216</sup>

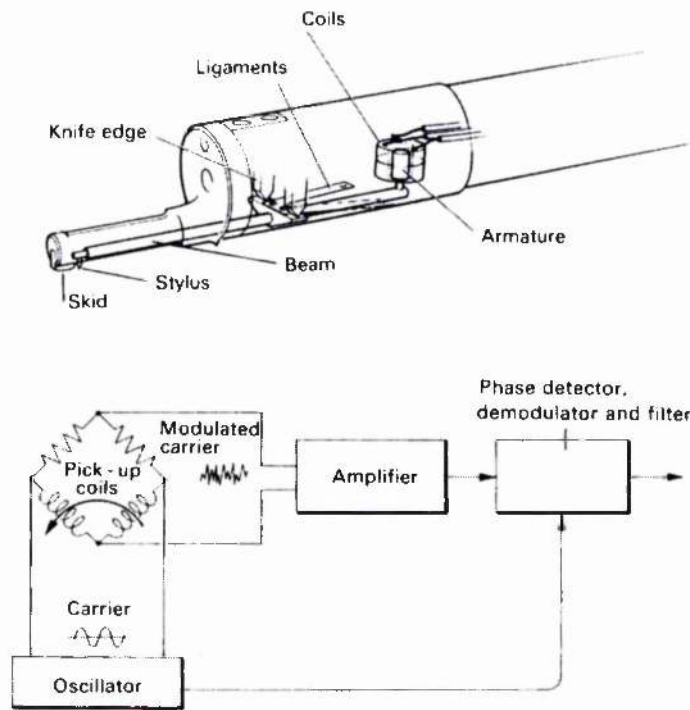


Figure 4.7 A typical inductive gauge and its working principle<sup>216</sup>

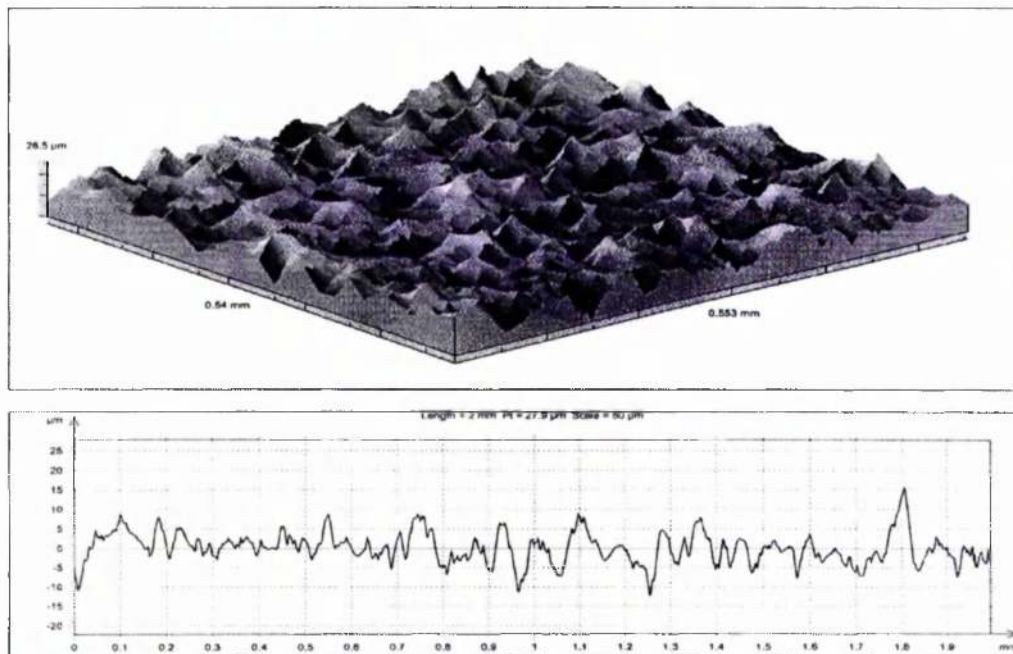


Figure 4.8 A 3D surface profile of grit-blasted (40/60) steel as characterised by Talysurf

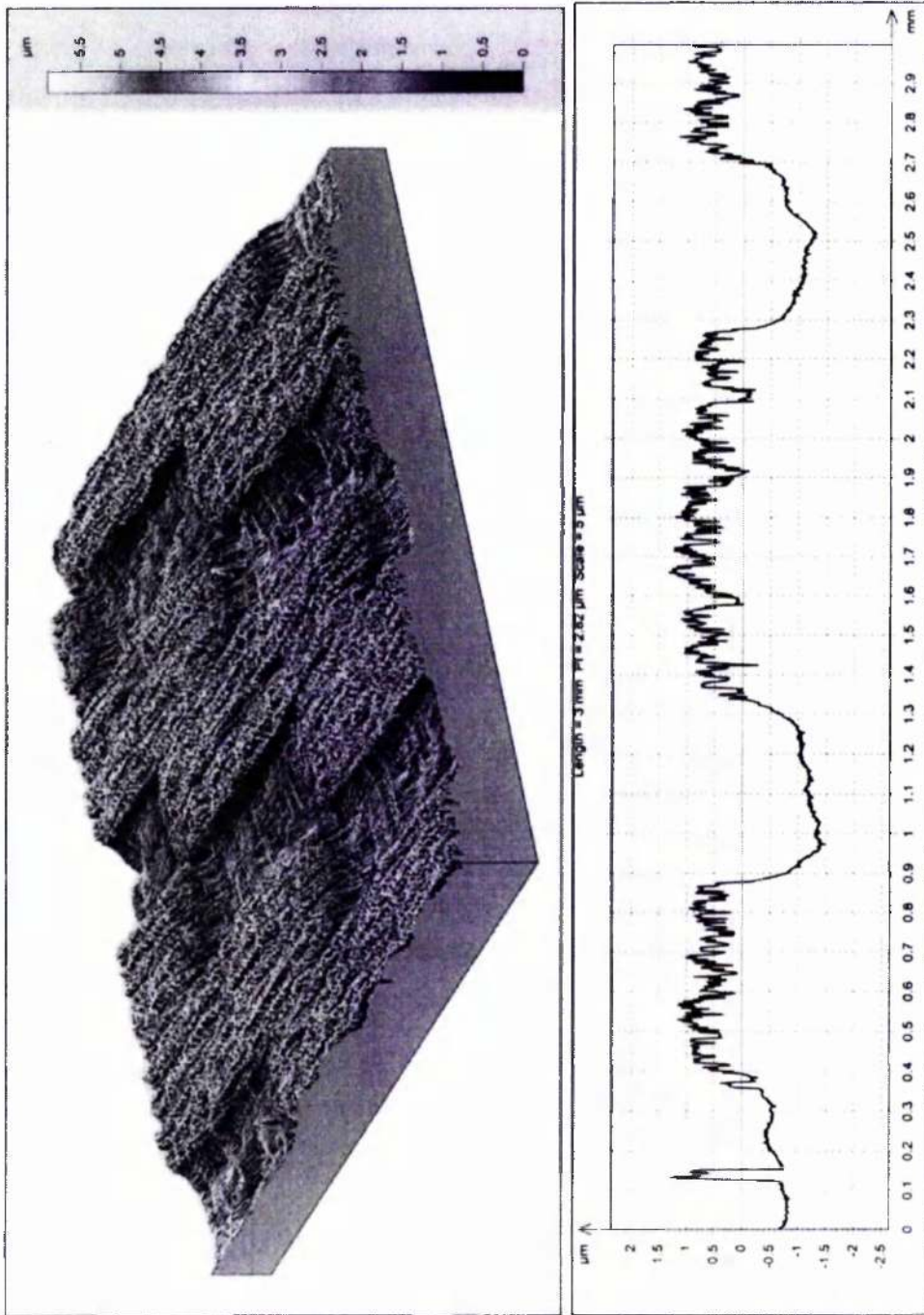


Figure 4.9 A 3D surface profile of polished Fibredux (WR) surface as characterised by Talysurf

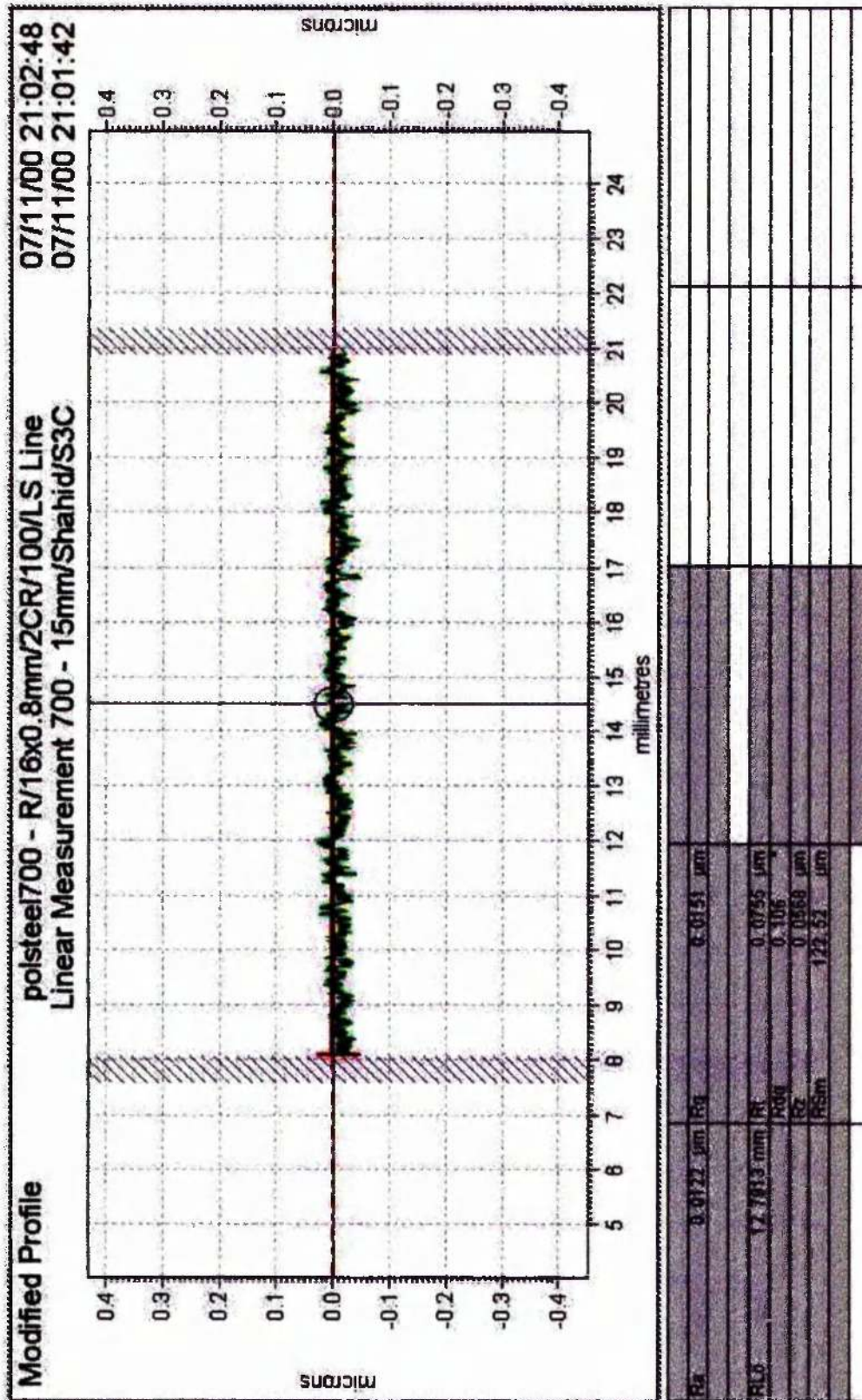


Figure 4.10 Roughness profile of polished steel surface

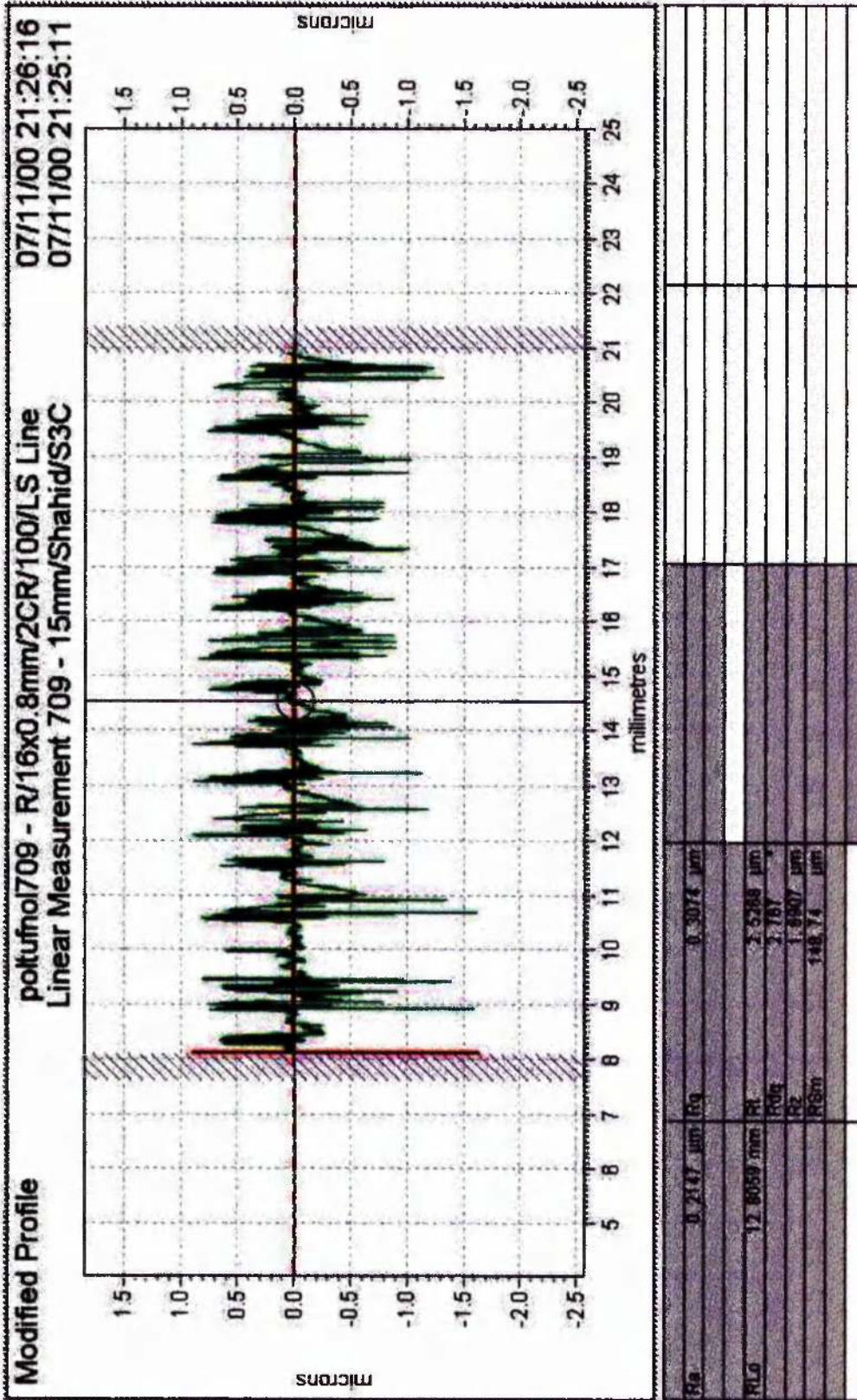


Figure 4.11 Roughness profile of polished Tufnol surface

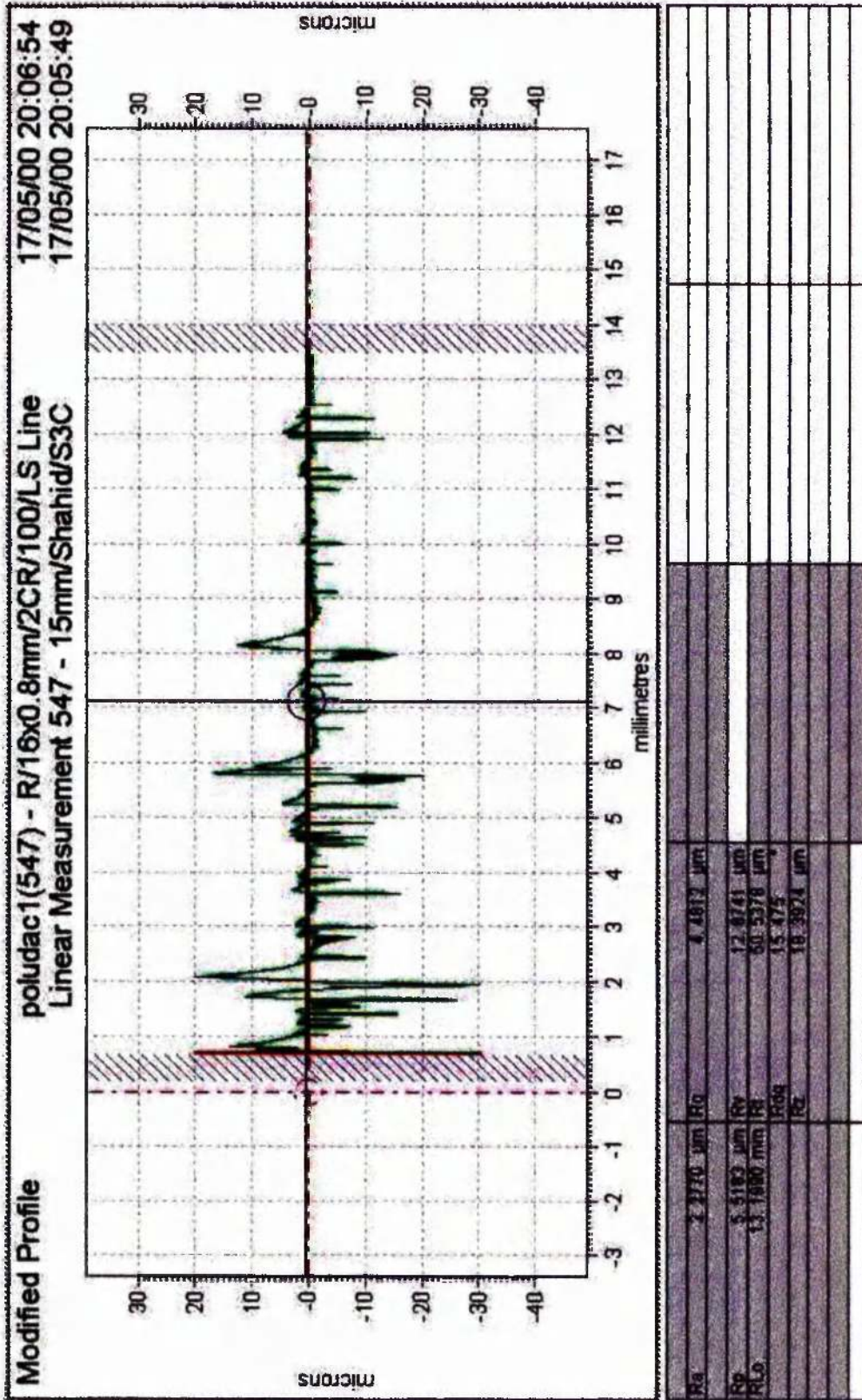


Figure 4.12 Roughness profile of polished Fibredux (UD) surface

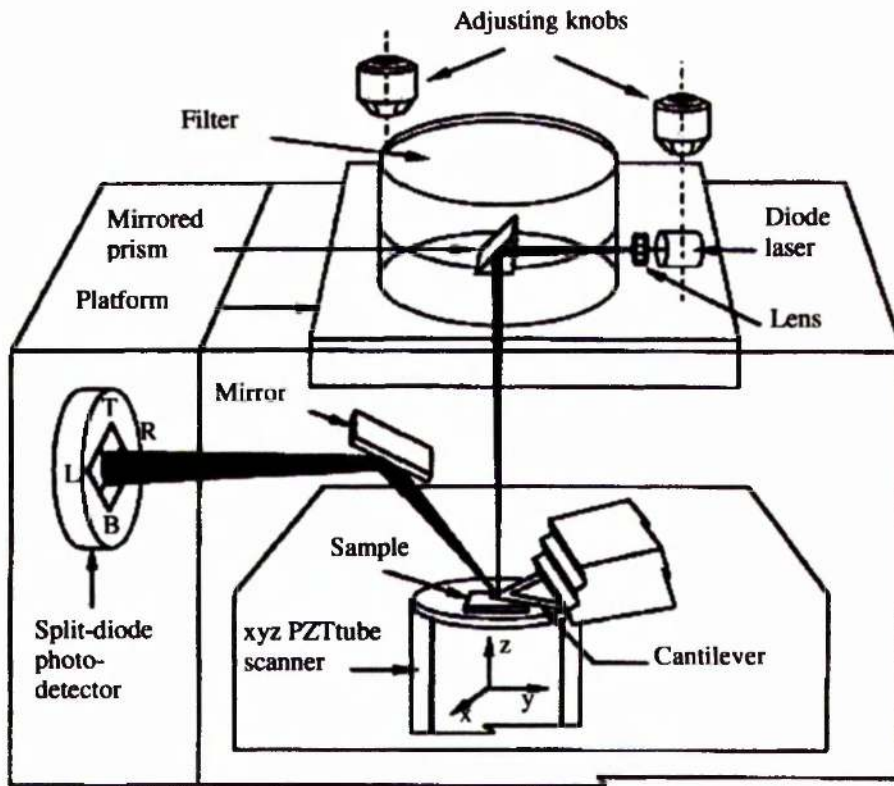


Figure 4.13 Schematic diagram of the overall operation of a typical AFM<sup>217</sup>

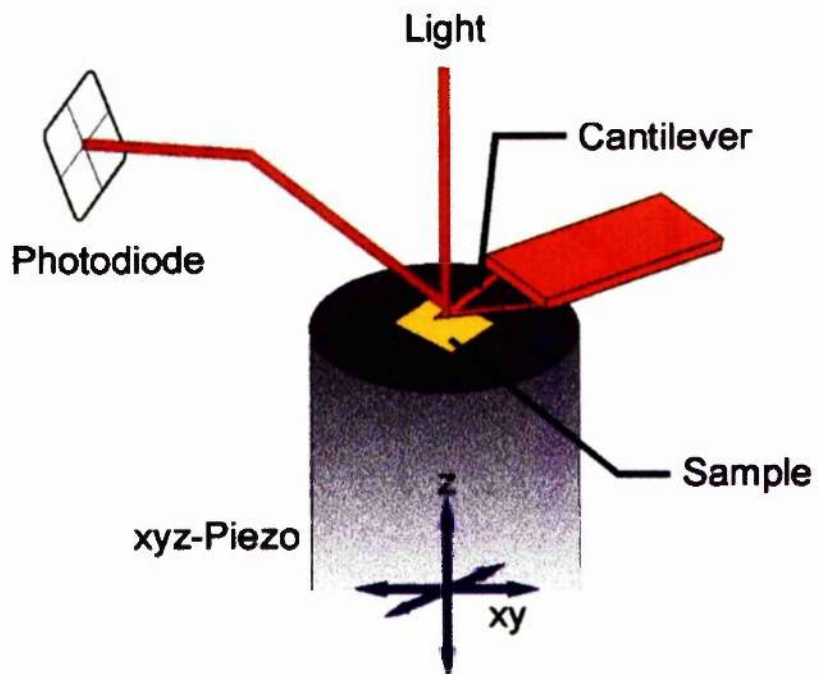


Figure 4.14 The beam-bounce detection scheme<sup>218</sup>

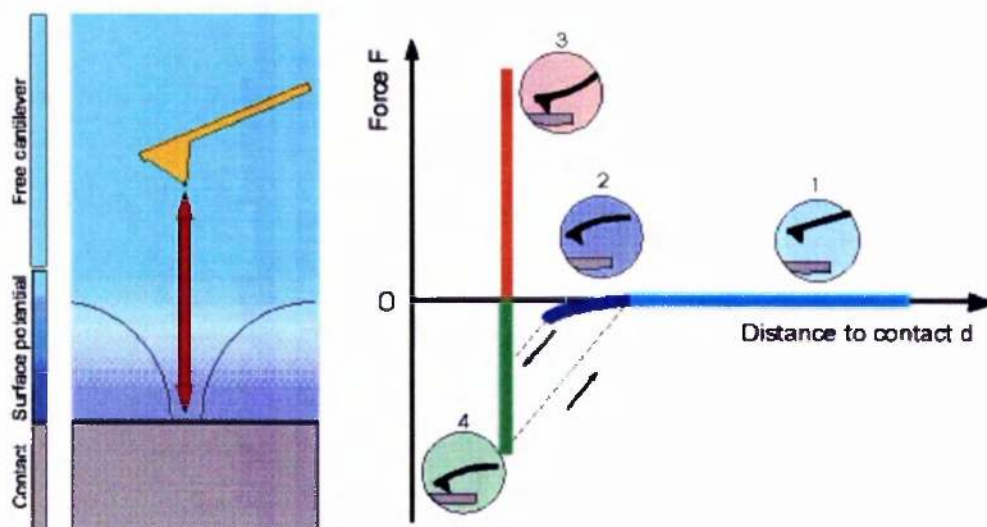


Figure 4.15 The working cycle of AFM <sup>218</sup>

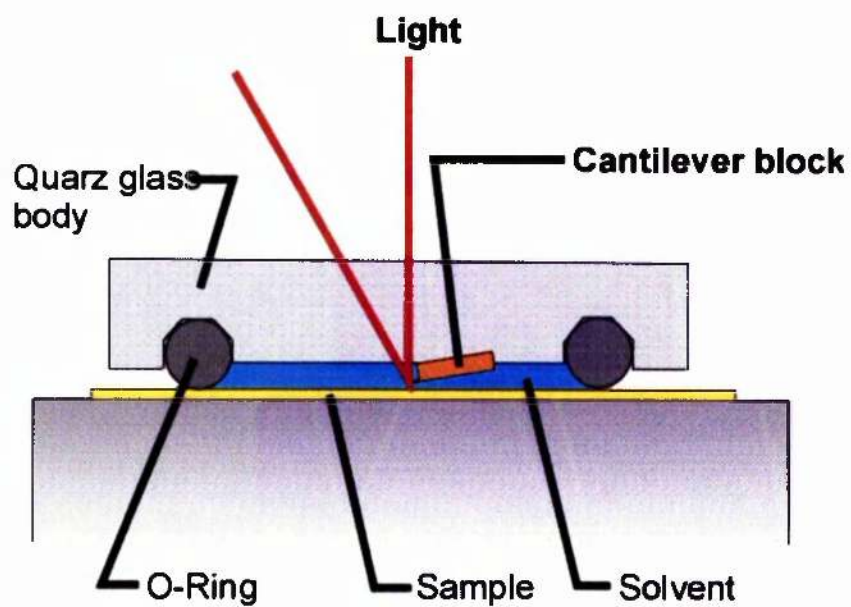


Figure 4.16 AFM set-up for operation in liquid environment

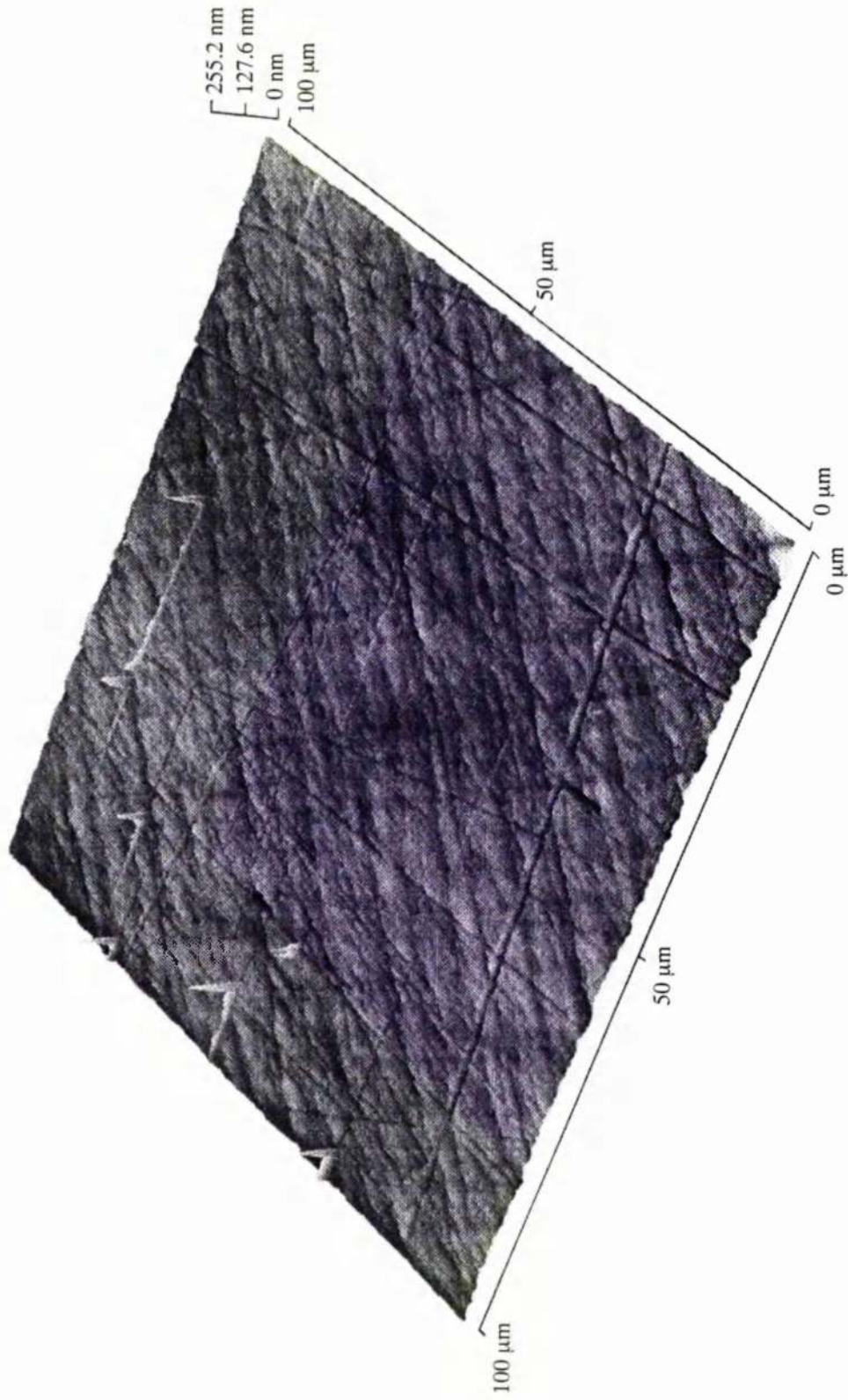


Figure 4.17 AFM profile of a polished steel surface

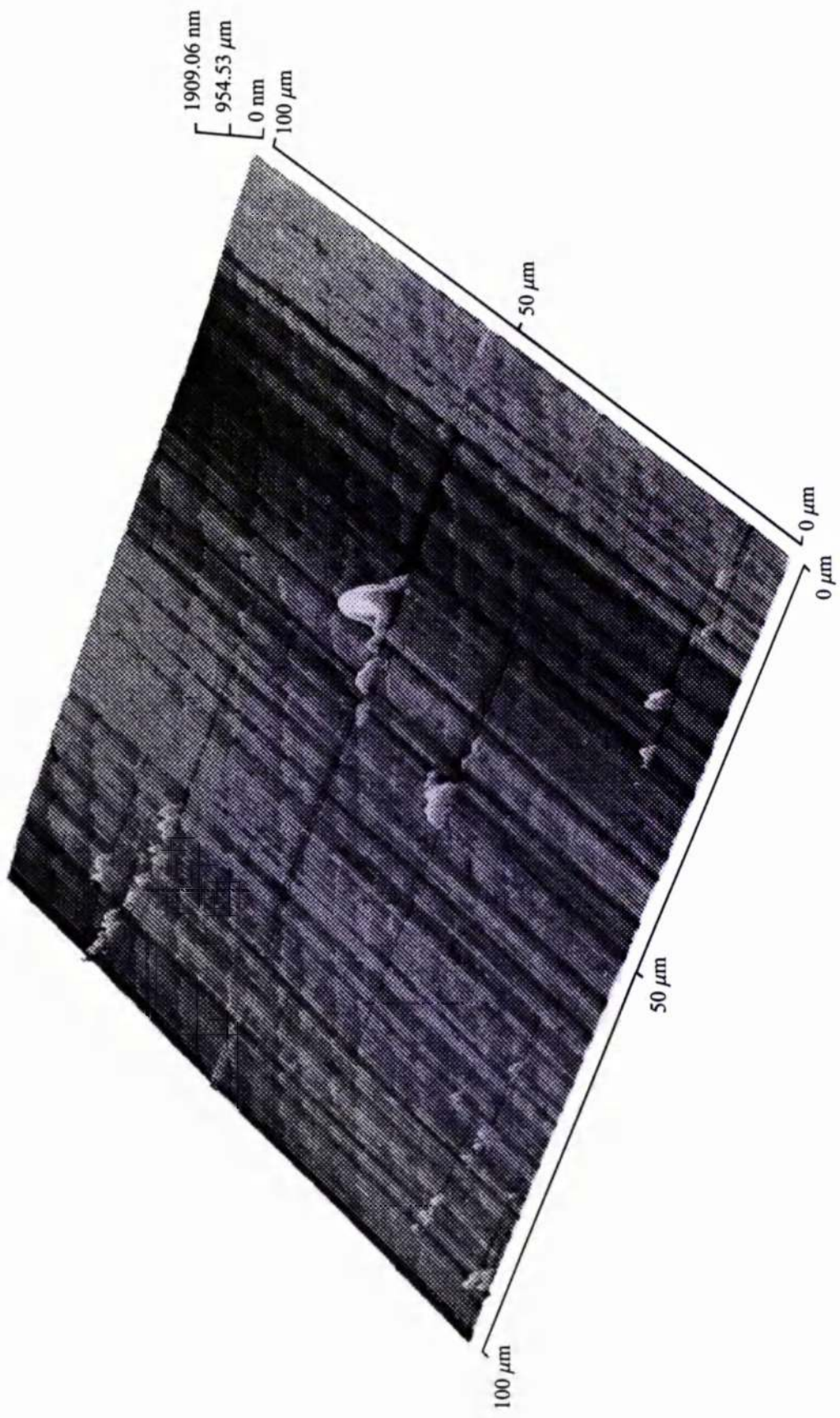


Figure 4.18 AFM profile of a polished Fibredux (WR) surface

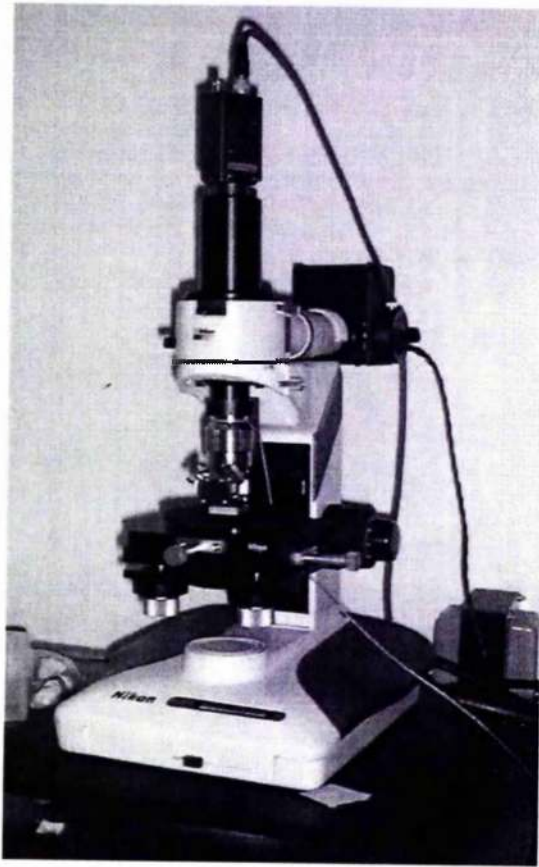


Figure 4.19 Nikon Corporation's OPTIPHOT interference microscope

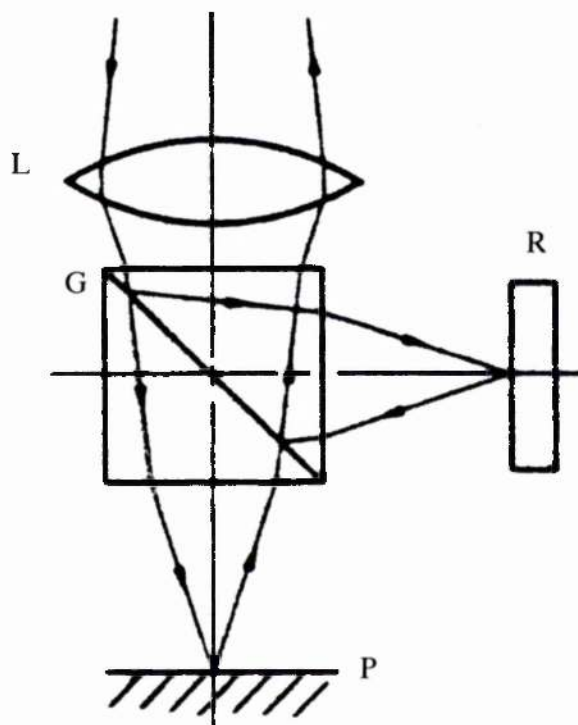


Figure 4.20 Working principle of a double-beam interference microscope<sup>219</sup>

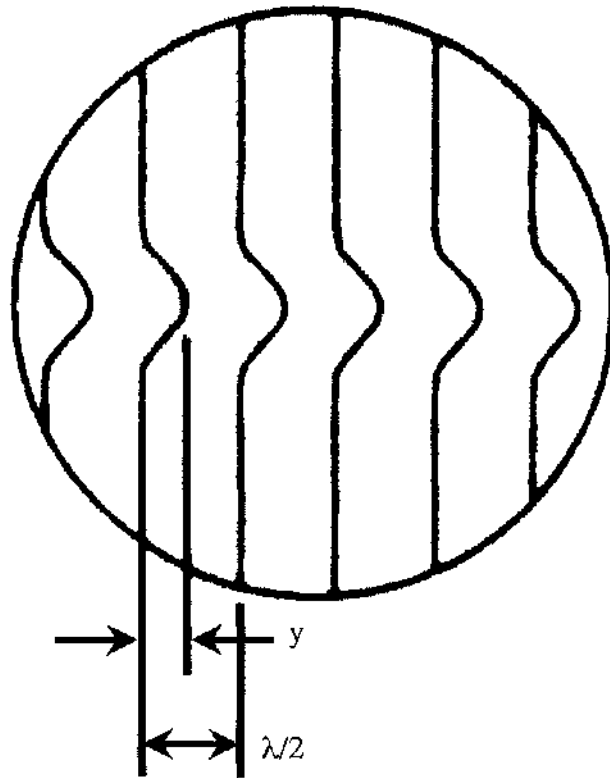


Figure 4.21 Disturbance fringes<sup>219</sup>

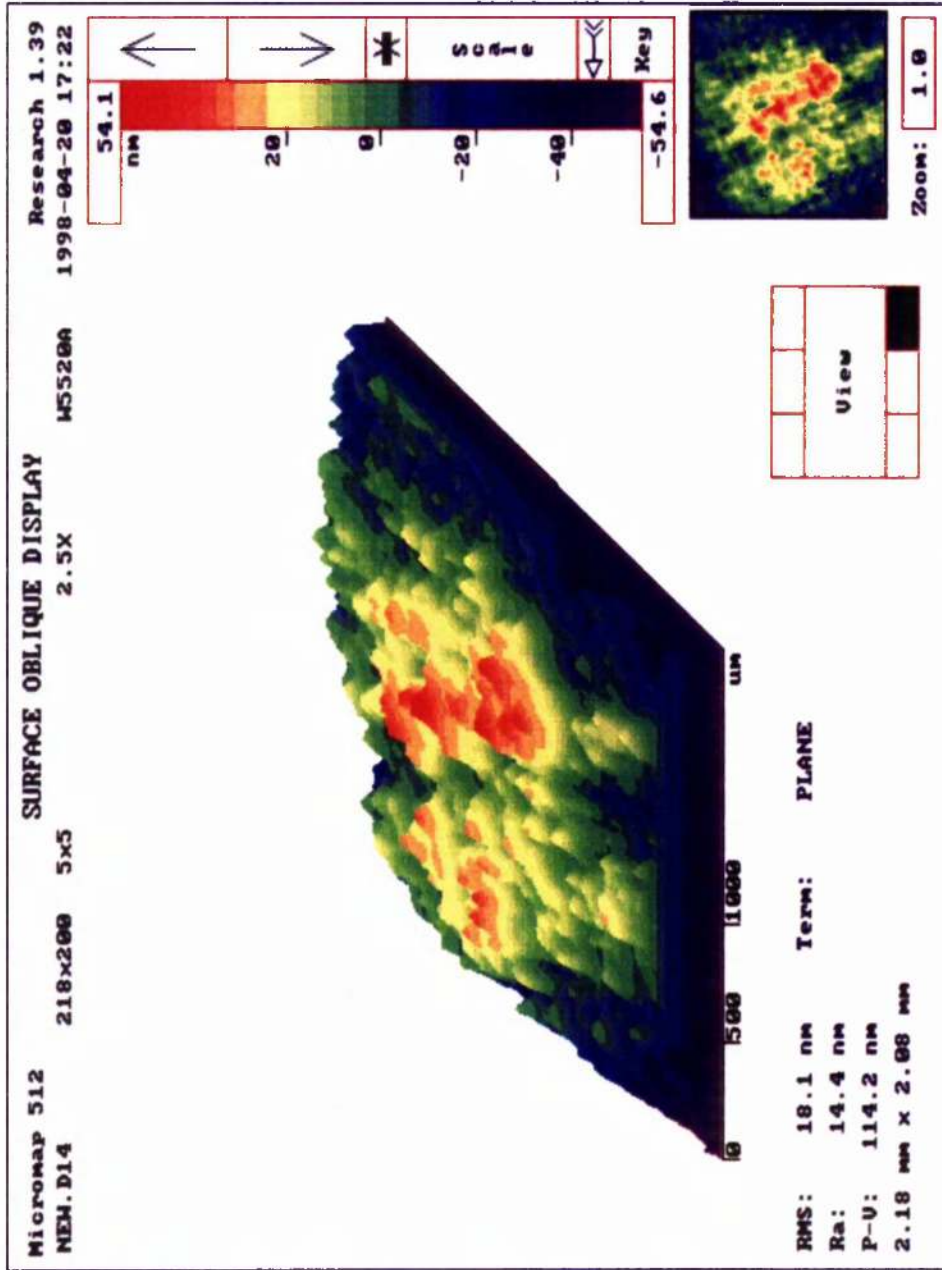


Figure 4.22 Interferometric profile of a polished steel surface

Table 4.1 Surface roughness of adherends measured by Talysurf

<i>Surface finish</i>	<i>R<sub>a</sub></i> ( $\mu\text{m}$ )	<i>Average roughness square roughness</i> ( $\mu\text{m}$ )	<i>Average root mean square roughness</i> ( $\mu\text{m}$ )	<i>Average maximum peak to valley height</i> ( $\mu\text{m}$ )	<i>Average profile length</i> ( $\mu\text{m}$ )	<i>Average root mean square slope</i> ( $^{\circ}$ )
	<i>R<sub>a</sub></i>	<i>RMS</i>	<i>R<sub>y</sub>max</i>	<i>R<sub>10</sub></i>	<i>R<sub>dq</sub></i>	
Grit-blasted						
Steel 40/60	2.97±0.18	3.77±0.32	17.98±7.84	13.69±0.04	22.70±0.56	
Steel 24/30	6.31±0.28	8.17±0.68	64.72±14.00	13.95±0.07	25.96±0.82	
Polished						
Steel	0.043±0.021	0.055±0.020	0.379±0.310	12.79±0.01	0.13±0.02	
Fibredux (WR)	0.208±0.061	0.270±0.084	2.74±0.54	12.80±0.01	1.04±0.58	
Tufinol (WR)	0.187±0.047	0.280±0.053	2.93±0.68	12.81±0.01	2.87±0.92	
Fibredux (UD)	0.944±0.72	1.95±1.38	25.56±16.00	12.92±0.15	7.60±4.74	

Table 4.2 Surface roughness of adherends measured by AFM

	<i>Average roughness</i> ( $\mu\text{m}$ )	<i>Average root mean square roughness</i> ( $\mu\text{m}$ )	<i>Average maximum peak to valley height</i> ( $\mu\text{m}$ )
<i>Surface finish</i>	$R_a$	$RMS$	$R_{y\text{max}}$
Polished			
Steel	0.053±0.001	0.072±0.001	0.307±0.060
Fibredux (WR)	0.071±0.041	0.090±0.040	1.44±0.54
Tufnol (WR)	0.153±0.080	0.222±0.124	2.64±0.84

Table 4.3 Surface roughness of adherends measured by Interferometer

	<i>Average roughness</i> ( $\mu\text{m}$ )	<i>Average root mean square roughness</i> ( $\mu\text{m}$ )	<i>Average maximum peak to valley height</i> ( $\mu\text{m}$ )
<i>Surface finish</i>	$R_a$	$RMS$	$R_{y\text{max}}$
Polished steel	0.044±0.019	0.056±0.026	0.361±0.159

## CHAPTER FIVE

***TESTING OF STEEL/STEEL CLEAVAGE SPECIMENS*****5.1 Introduction**

In order to understand the behaviour of steel/composite cleavage joints, it is necessary to first look into the effects of various surface and geometric parameters on the strength of standard steel/steel cleavage specimens. In view of the unlimited possible combinations of options, only a few common factors were considered. This chapter details the experimentation and findings of a number of experiments executed in this regard.

**5.2 Specifications of Specimens**

The mild steel cleavage specimens were made to British Standard BS 5350:Part C1:1986<sup>1</sup>. These were bonded with Araldite<sup>®</sup> 420A/B (Redux<sup>®</sup> 420A/B) at controlled adhesive thicknesses of 0.1mm and 0.5mm. Configuration of the standard cleavage joint is shown in Figure 5.1. The bond area for this specimen was 25x25mm<sup>2</sup>.

To obtain tangible results, a limited number of thick steel adherend, lap-shear specimens, modified from ASTM D5656, were also tested. The dimensions of the modified specimens are shown in Figure 5.2. The bond area for this specimen was 15x25mm<sup>2</sup>.

**5.3 Experimental Programme**

Experiments were carried out to study the effects of the following surface and geometric conditions on the strength of standard cleavage specimens:

- grit-blasting of adherends using two different grit sizes

- diamond polishing of the adherends (steel)
- rusting (natural oxidation) of the adherends
- bonding with different adhesive thicknesses
- bonding with different bond areas (partial bonding)
- over-curing of the adhesive.

#### **5.4 Grit-blasting of Adherends**

Grit-blasting, where applicable, was performed on acetone cleaned specimens using Saftigrit<sup>®</sup> alumina grits from Guyson Corporation. Two grit sizes, 40/60 mesh and 24/30 mesh, were used to produce different levels of surface roughnesses. Grit-blasting was performed at a pressure of approximately 550kPa, at right angles to the surface of the adherends and at a distance of about 5cm from the nozzle. To produce stable parameters of surface roughness<sup>74</sup>, a grit-blasting time of at least 30sec was considered. After grit-blasting, specimens were blown free of remaining grit and cleaned again with acetone just before bonding. A typical grit-blasted steel surface is shown in Figure 5.3.

#### **5.5 Polishing of Adherends**

Polishing, where applicable, was performed first by manual abrasion using coarse waterproof silicon carbide paper (Grit P240), followed by finer papers (up to Grit P1200 of Buehler Krautkramer, UK). This was followed by diamond polishing using oil-wetted 1-micron diamond paste (METADI<sup>®</sup> II diamond paste from Buehler Krautkramer, UK). After polishing, the specimens were washed with soap and water and then with acetone. They were finally dried with hot air. A typical polished surface is shown in Figure 5.4.

After necessary pre-treatments, the surface roughness of these adherends was measured (as detailed in Chapter 4) using Taylor Hobson's Form Talysurf Series 2 50i surface profiler and, where possible, with the atomic force microscope and Michelson's interferometer.

## 5.6 Natural Oxidation of Adherends

Three specimens each of the polished and grit-blasted type, prepared as mentioned in sections 5.4 and 5.5, were allowed to rust in a natural environment for 17 days at an average temperature of 6°C and relative humidity of 85%. This was aimed at producing results for the effect of corrosion on the bonding process and subsequent joint strength.

## 5.7 Control of Adhesive Thickness

Two different methods were tried for controlling adhesive thicknesses in the bonded joints. Initially, an attempt was made to control adhesive thicknesses by placing specially machined spacers in the frontal portion of the specimens, but this resulted in obtaining non-uniform thicknesses. Consequently, the strength results were also inconsistent, especially in the case of the 0.1mm adhesive thickness. Later, wire spacers of diameter equivalent to the required adhesive thicknesses were tried. This approach gave a more uniform adhesive thickness with more consistent strength results.

## 5.8 Bonding of Specimens

Carefully machined steel cleavage specimens were cleaned with acetone before being treated to an appropriate pre-treatment i.e. polishing, grit-blasting or rusting. After the pre-treatment, the two wire spacers were attached to the metallic adherends near the front and rear ends (Figure 5.5). The specimens were cleaned again with acetone and dried with hot air just before bonding. In the case of the grit-blasted specimens, the bonding was carried out approximately 24hrs after the grit-blasting, to ensure a consistent bond strength<sup>18</sup>. A manual dispensing/mixing gun was used with an appropriate mixing nozzle (MC 06-24) to dispense the adhesive in the correct ratio (Figure 5.6). The adhesive was applied and spread onto the bonding surfaces with a spatula and the specimens were clamped using the jig shown in Figure 5.7. All the specimens were cured at 70°C for 2hrs. The cured specimens were removed from

the jig and the adhesive fillets were manually removed by scraping with a razor blade.

For partial bonding of the specimens, PTFE sprayed spacers were inserted at the rear portions of the specimens to give a 25%, 50% and 75% area of bonding (Figure 5.8).

## 5.9 Testing of Specimens

The specimens were mechanically tested to destruction on a Lloyd tensile testing machine using standard clamps and fixtures (Figure 5.9). All the tests were carried out under monotonic loading at room temperature and with a cross-head speed of 0.5mm/min. With the exception of the rusted specimens, a minimum of five specimens of each type were tested to obtain an average result. Three specimens were tested in the case of the rusted specimens due to production limitations. After each test, the failure load was recorded and the fractured surfaces were examined visually to determine whether the failure was adhesion or cohesion. In the cases where no clear pattern was apparent, the failure is referred to as adhesion/cohesion.

## 5.10 Results

Results from mechanical testing of the steel/steel cleavage specimens are presented in Tables 5.1-5.6 including individual failure loads and average strength values. The average strengths, calculated by dividing the failure load by the bond area, are presented for comparison. The coefficient of variation (COV) is calculated by using the following formula:

$$\text{COV} = \frac{\text{Std. deviation}}{\text{Average strength}} \times 100 \quad (1)$$

### 5.10.1 Influence of Adhesive Thickness

The test results presented in Tables 5.1-5.3 show the effects of adhesive thicknesses on the strength of the standard cleavage and lap-shear specimens. From the results in

Table 5.1 it appears that in the case of the grit-blasted cleavage specimens, only a 4% increase in joint strength takes place as a result of decreasing the adhesive thickness from 0.5mm to 0.1mm. However, the specimens bonded with 0.5mm adhesive thickness appear to show a smaller coefficient of variation. This small increase in strength may be due to the effects of triaxial constraint, adhesive defects and thermal shrinkage. These effects are perhaps more pronounced in the case of the thinner adhesive layer. In the case of the corroded (after grit-blasting) cleavage specimens, the increase is approximately 8%. On the other hand, in the cases of the polished cleavage specimens (both clean and corroded) the joint strength decreases by approximately 11% for the same decrease in the adhesive thickness. A possible reason for this decrease may be due to poor wetting of the polished steel surfaces in the case of the 0.1mm adhesive thickness as shown in Figure 5.10. Further discussion is presented in Chapter 8.

In the case of the lap-shear specimens (Table 5.2), the reduction in shear strength with a increase in adhesive thickness, is approximately 22%. Therefore, it appears that shear strength is more dependent on adhesive thicknesses than cleavage strength (Table 5.1).

In view of the reduced dependence of cleavage strength on adhesive thicknesses in the above range, and the low coefficient of variation associated with the 0.5mm adhesive thickness, all of the following experimentation will be based on the 0.5mm.

Microscopic examination of the fractured surfaces (both adhesive thicknesses), shows that failure is apparently of a mixed mode type (adhesion/cohesion) for grit-blasted specimens. For the polished specimens, failure appears to be of an adhesive type (adhesion). For the grit-blasted lap-shear specimens however, marks of adhesive shearing are more prominent. Figures 5.11-5.16 show various fractured surfaces.

### ***5.10.2 Influence of Natural Oxidation***

Table 5.3 shows the test results for the corroded specimens. The polished specimens, in particular, appear to show a considerable drop in strength when compared with the

equivalent uncorroded ones (Table 5.1). With both adhesive thicknesses (0.1mm and 0.5mm), the strengths in the case of the uncorroded specimens are higher by approximately 600% and 280% for polished and the grit-blasted specimens, respectively. These results are only comparative and perhaps indicate the combined effect of surface roughness and corrosion. However, practically, the steel adherends may never be exposed to such an environment before bonding.

From visual examination of the fractured surfaces it is apparent that failure initiated at the adherend's weak oxide layer (Figure 5.17). The expected high scatter in these results (Table 5.3) is obvious due to the uncontrolled nature of exposure.

### ***5.10.3 Influence of Bonding Area***

It can be seen from the results given in Table 5.4 that the average failure load decreases steadily with the decrease in bonding area. It can also be seen that the reduction in the failure load is slightly more significant in the case of the polished specimens. For example, a reduction of 25% in the bonding area gives approximately a 23% and 17% reduction in the failure loads for polished and grit-blasted specimens respectively. This trend may be attributed to the limited resistance offered by the polished surfaces to detachment propagation.

A visual and light microscopic examination of the fractured surfaces revealed that the nature of joint failure in these cases is similar to those in the cases of fully (100%) bonded specimens i.e. an adhesion failure in the case of polished specimens and a mixed mode failure in the case of grit-blasted specimens (Figure 5.18).

### ***5.10.4 Influence of Surface Roughness***

Table 5.5 shows the test results of the cleavage specimens with different surface finishes. This shows that the finer the grit size, the stronger the joint. Upon visual and light microscopic examination, the fractured surfaces prepared with coarser grit showed a significantly higher crazing (stress whitening zones) in the initial areas of the joint compared to those prepared with finer grit (Figure 5.19). In both cases,

however, the failure took place near the adherend/adhesive interface region and was apparently of a mixed adhesion/cohesion mode. From the intensity of whitening it appears that the failure initiated from one of the corners of the adherend (Figure 5.20). This is in line with findings by Crocombe et al<sup>178</sup>. In the case of polished specimens, on the other hand, the fractured surfaces of the joints showed an apparent adhesion failure with no signs of crazing and with visible bare steel and adhesive regions (Figure 5.14). It was, however, not possible to confirm this without using a more sophisticated technique such as an electron microscopy or x-ray diffraction. Such a technique will help to establish whether or not the bare portions of the fractured surfaces were completely free from adhesive residues.

#### 5.10.4.1 Effect of $R_a$

Figure 5.21 shows the relationship between the average cleavage strength and the  $R_a$  value of the adherend surfaces. It can be seen that the cleavage strength increases with the increase in  $R_a$  values. The increase in cleavage strength may be attributed to both the increased bond surface area and the diversion of failure path (thus giving mini scarf joints on the adherend surfaces at micro level). These findings are in line with those of Sargent<sup>76</sup> who reports an increase in the peel strength of aluminium test specimens with increasing surface roughnesses (without reporting the level of increase). However, he did not find any correlation between peel strength and any features of the oxide or interfacial region.

#### 5.10.4.2 Effect of $R_{i_0}^2$

$R_{i_0}^2$  was considered as a comparative measure of the effective surface area available for bonding, and this parameter was noted in each case by keeping the same evaluation length, filter etc. These values were then compared with cleavage strengths as shown in Figure 5.22. It can be seen that the experimental cleavage strength increases with the increase in the effective surface area. It is however realistic to believe that such an increase will be limited by bulk adhesive strength i.e. until failure becomes cohesive within the adhesive.

Due to the concentrated loading at one end of the cleavage joint and the complex geometry of the surfaces, consisting of hills and valleys of various shapes, it is very difficult to look into the contribution of different portions of the surface towards the overall strength. This is especially important because the initial few millimetres of the adherend's surface contribute greatly towards the total joint strength.

#### *5.10.5 Influence of Over-curing*

In order to investigate the sensitivity of cleavage strengths of steel specimens towards over-curing, five steel cleavage specimens with adhesive thicknesses of 0.1mm and 0.5mm were cured for three hours at 70°C, instead of two hours as in the other cases.

The test results are presented in Table 5.6. It can be seen that the results obtained with curing for 3hrs (50% higher over-curing) are within 1% of those obtained with curing for 2hrs. It may therefore be concluded that the adhesive, Araldite<sup>®</sup> 420, is not very sensitive to over-curing within a reasonable limit.

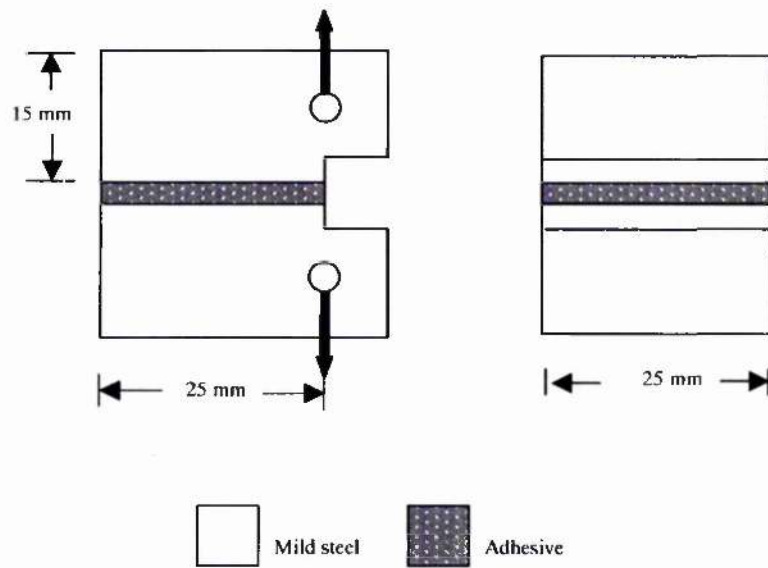


Figure 5.1 Standard cleavage test specimen

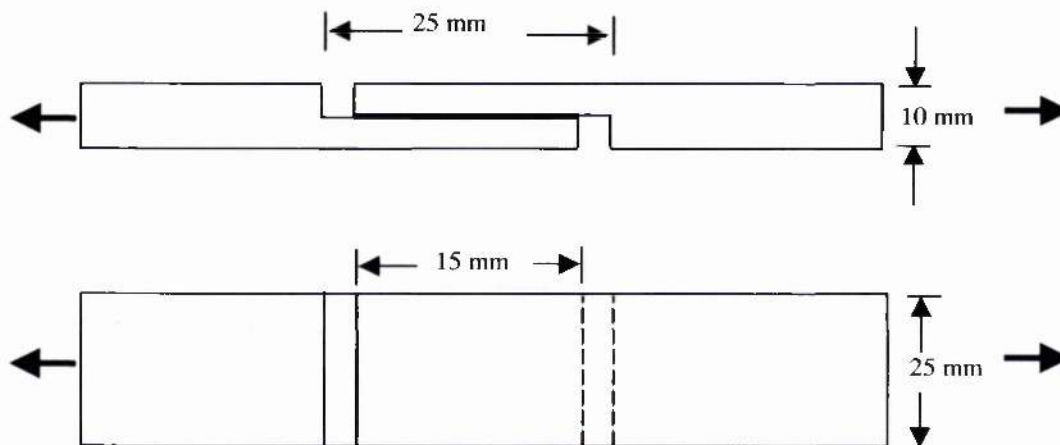


Figure 5.2 Thick adherend lap-shear specimen



Figure 5.3 Typical grit-blasted steel surface

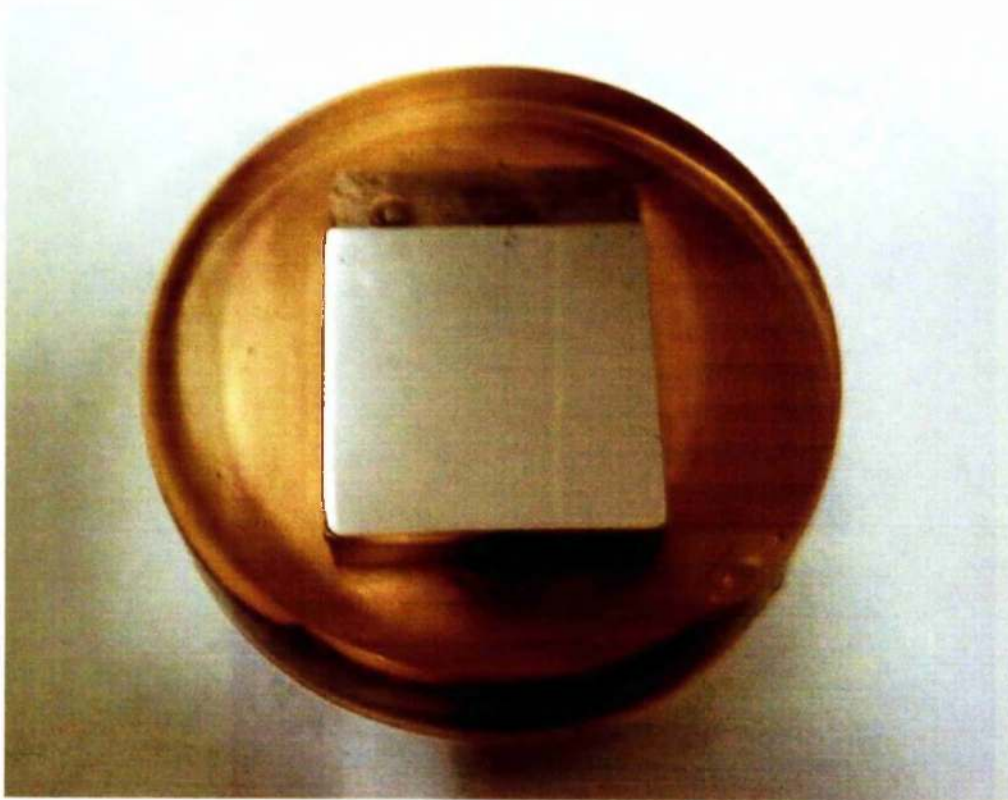


Figure 5.4 Typical polished steel surface

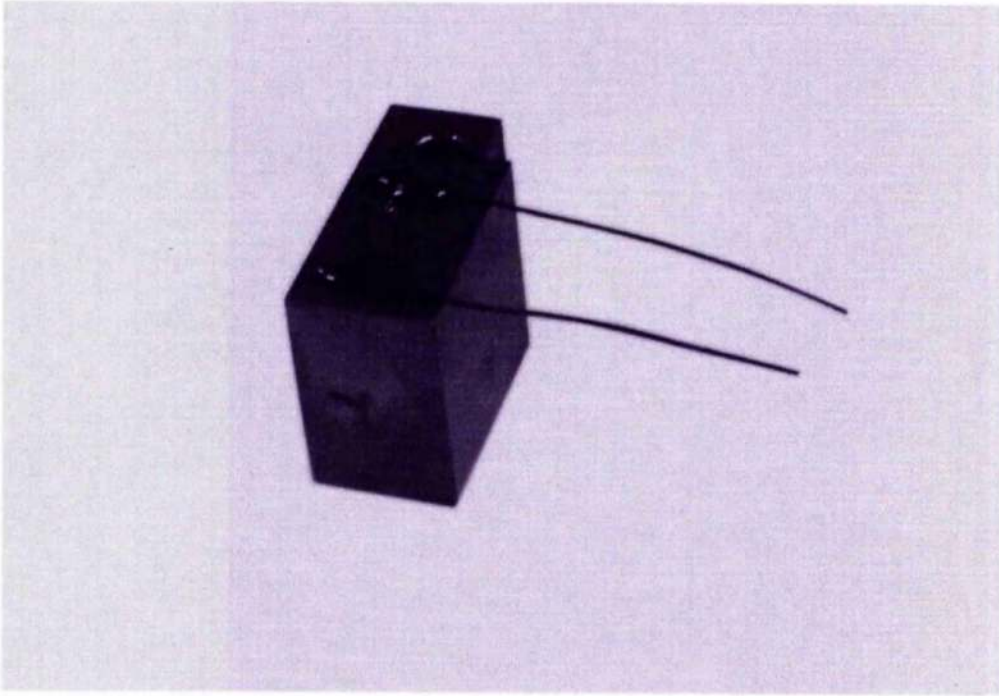


Figure 5.5 Specimen with attached wire spacers

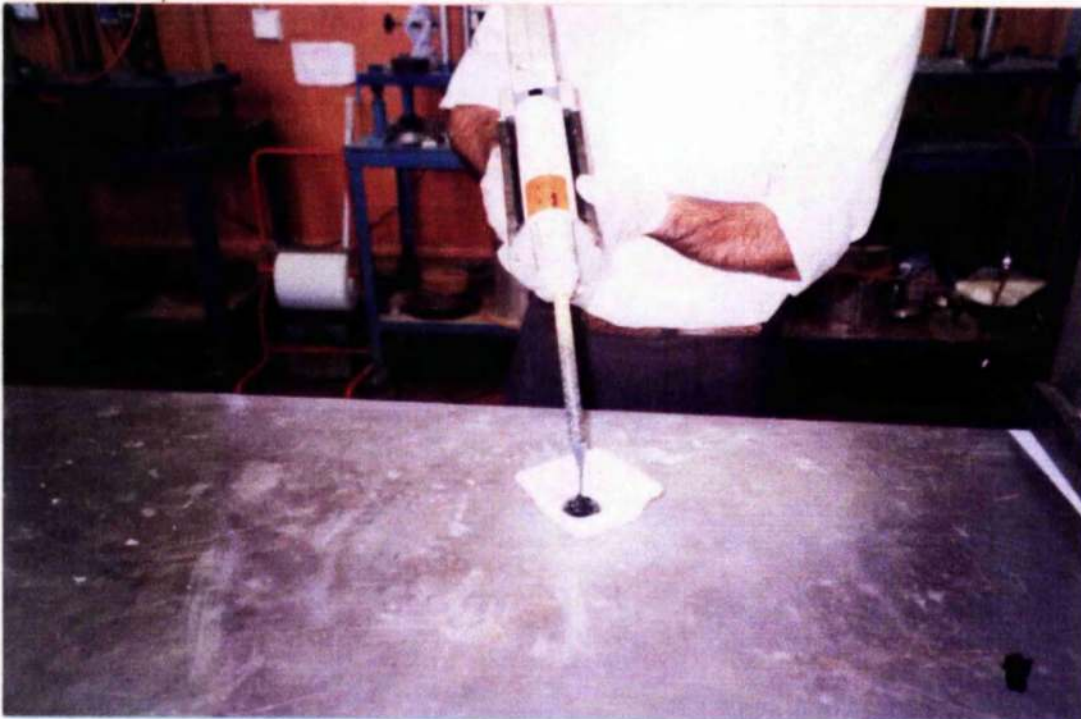


Figure 5.6 Mixing of adhesive by manual mixing gun



Figure 5.7 Jig used for bonding cleavage specimens

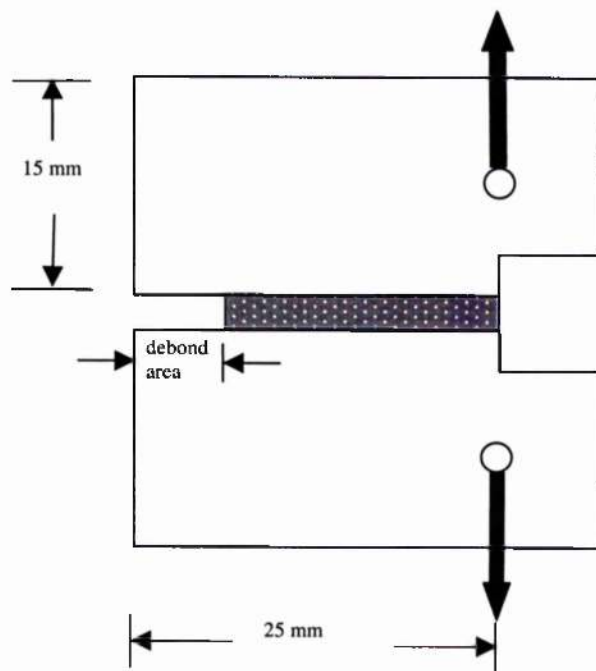


Figure 5.8 Partially bonded cleavage specimen with debond at the rear end



Figure 5.9 Testing of cleavage specimens

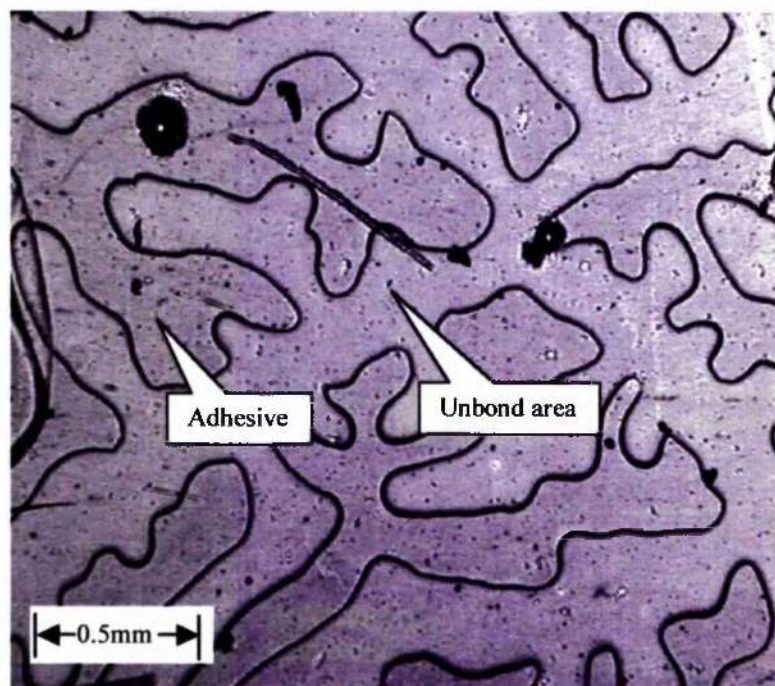


Figure 5.10 Fractured surface of polished steel joint showing unbonds

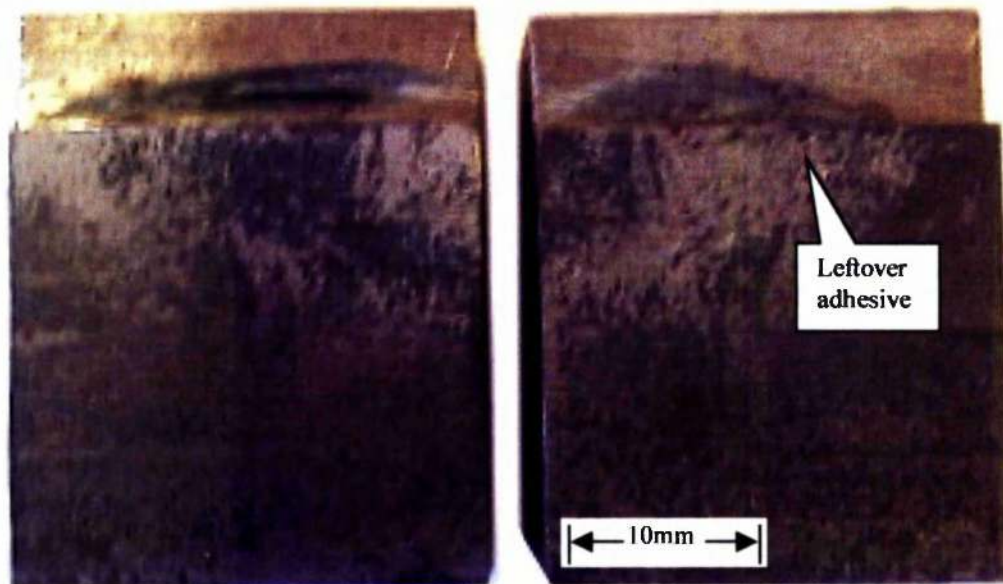


Figure 5.11 Fractured surfaces of grit-blasted cleavage specimen showing mixed mode failure (0.1mm adhesive)

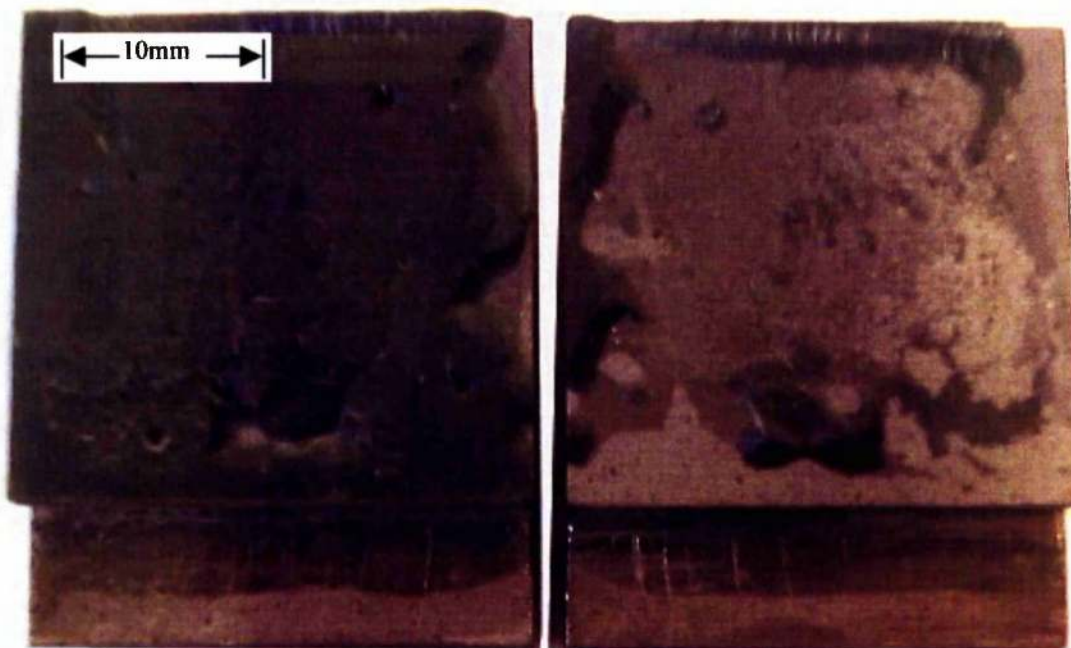


Figure 5.12 Fractured surfaces of grit-blasted cleavage specimen showing mixed mode failure (0.5mm adhesive)

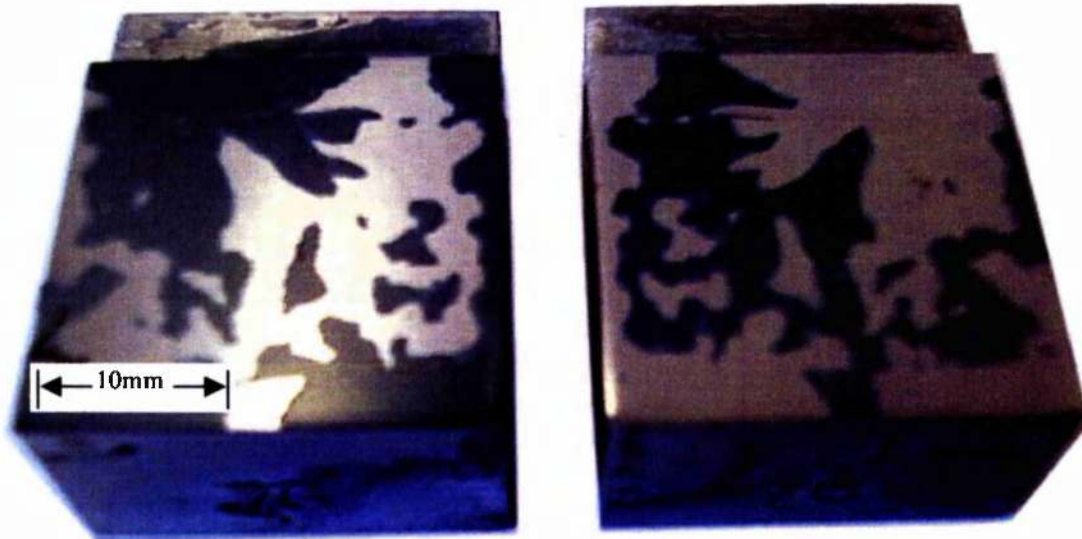


Figure 5.13 Fractured surfaces of polished cleavage specimen showing adhesion failure (0.1mm adhesive)

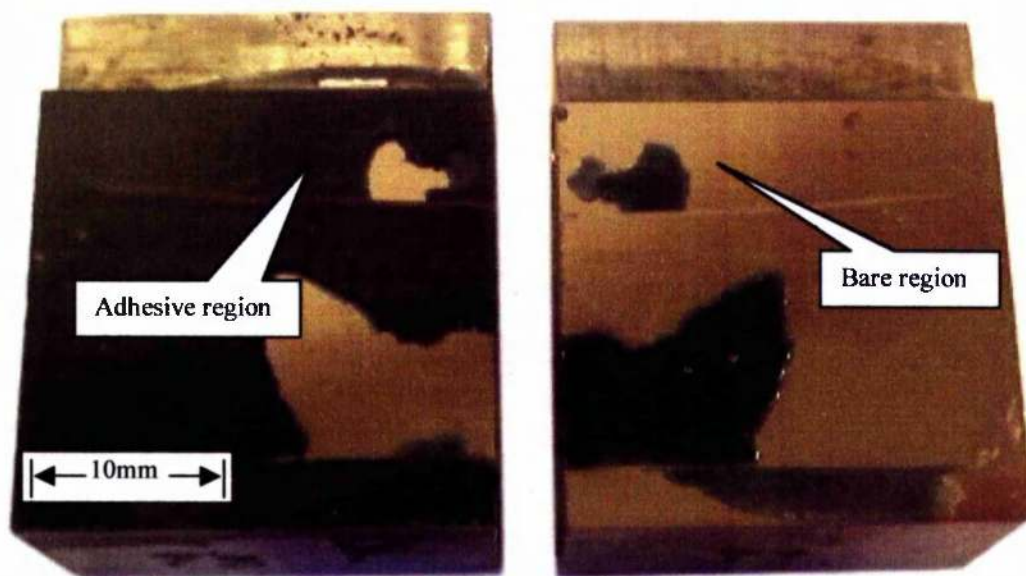


Figure 5.14 Fractured surfaces of polished cleavage specimen showing adhesion failure (0.5mm adhesive)

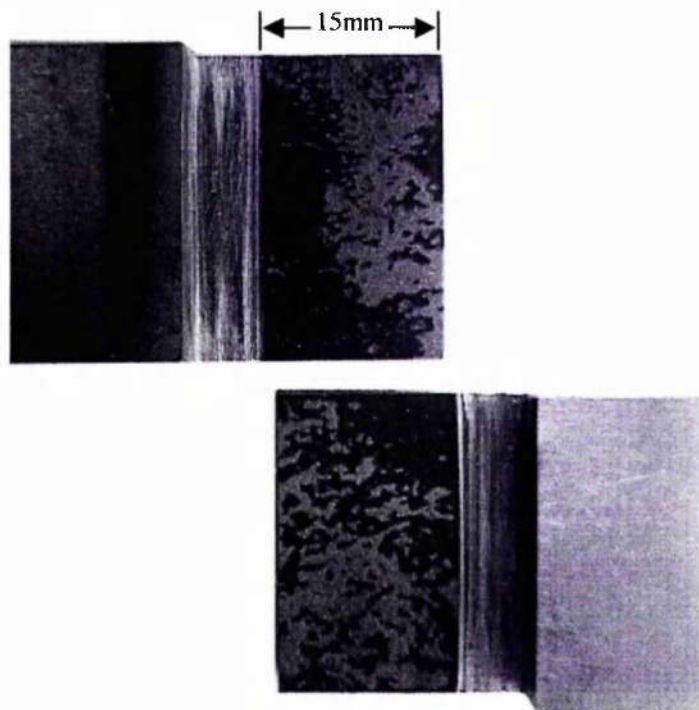


Figure 5.15 Fractured surfaces of a lap-shear specimen showing mixed mode failure (0.1mm adhesive)

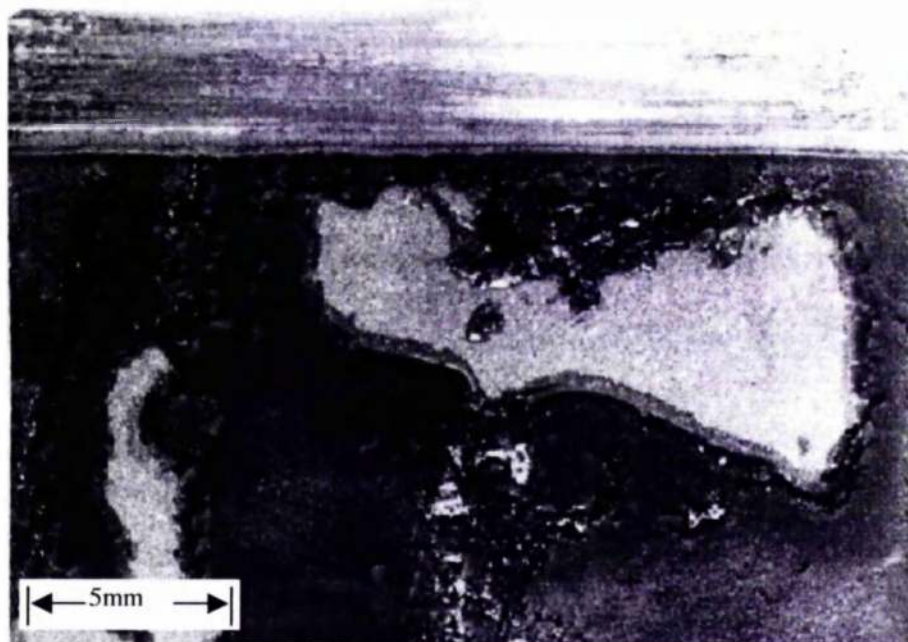
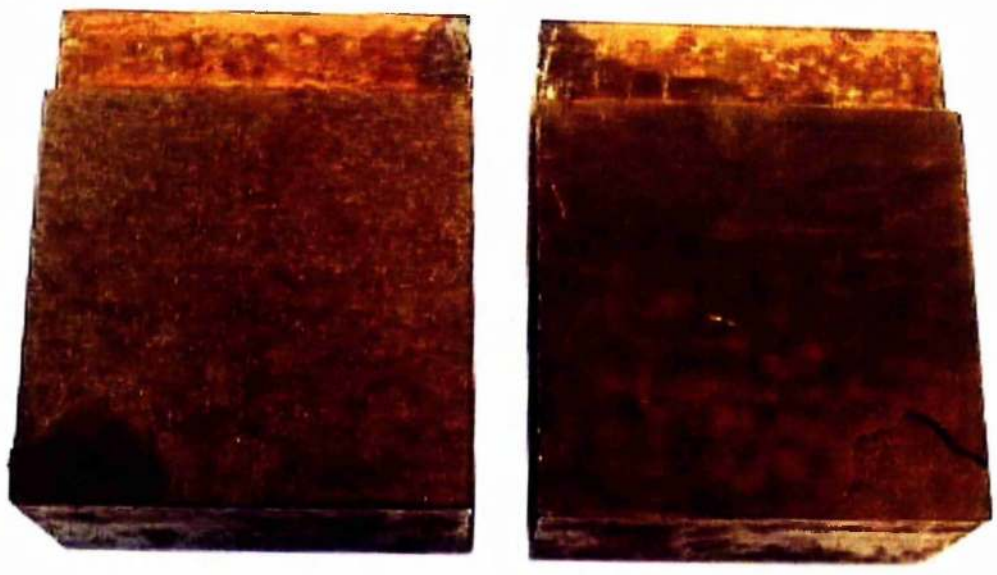


Figure 5.16 Fractured surface of a lap-shear specimen showing adhesive shearing (0.5mm adhesive)

a



b

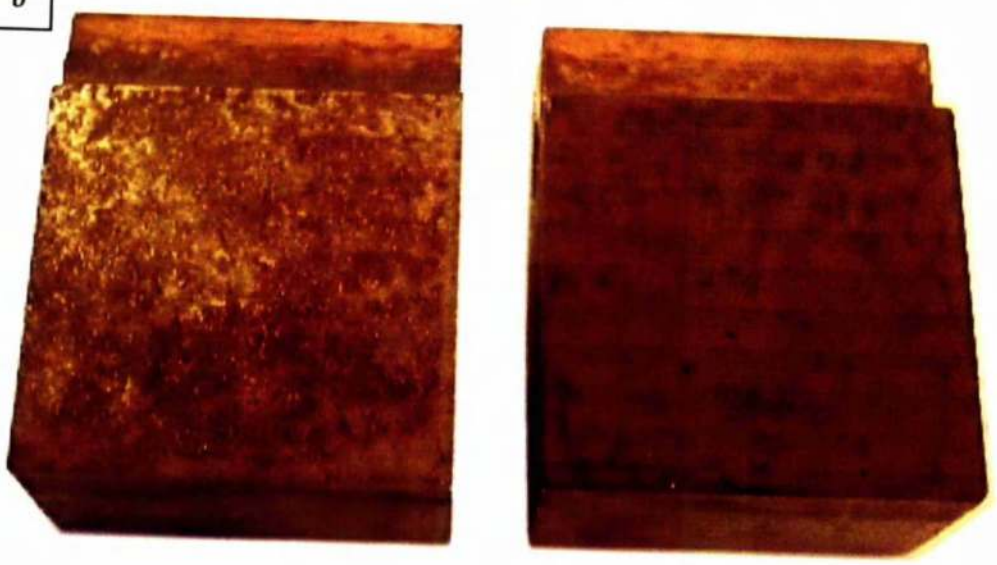
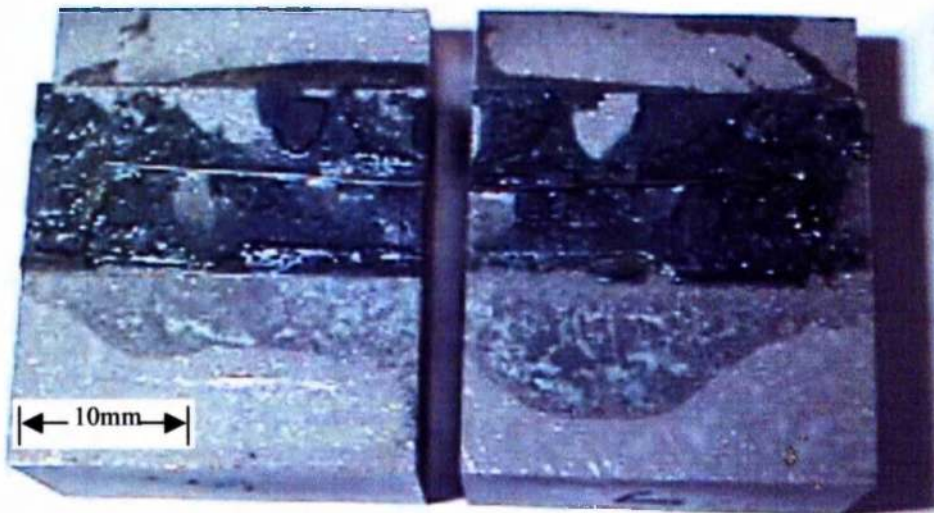


Figure 5.17 Fractured surfaces of rusted steel cleavage specimen (a) grit-blasted; (b) polished

a



b

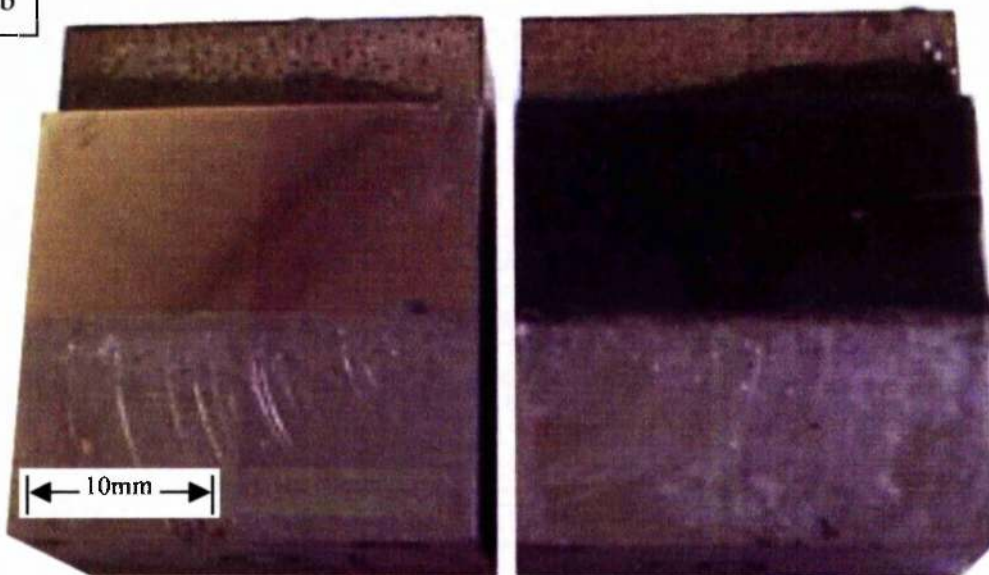


Figure 5.18 Fractured surfaces of partially bonded (50%) steel cleavage specimen (a) grit-blasted; (b) polished

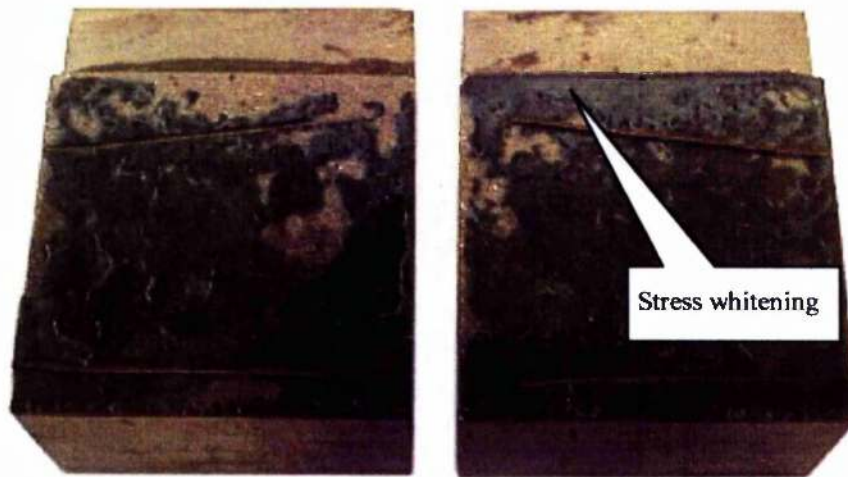


Figure 5.19 Fractured surface of grit-blasted cleavage joint showing stress whitening in the initial joint region

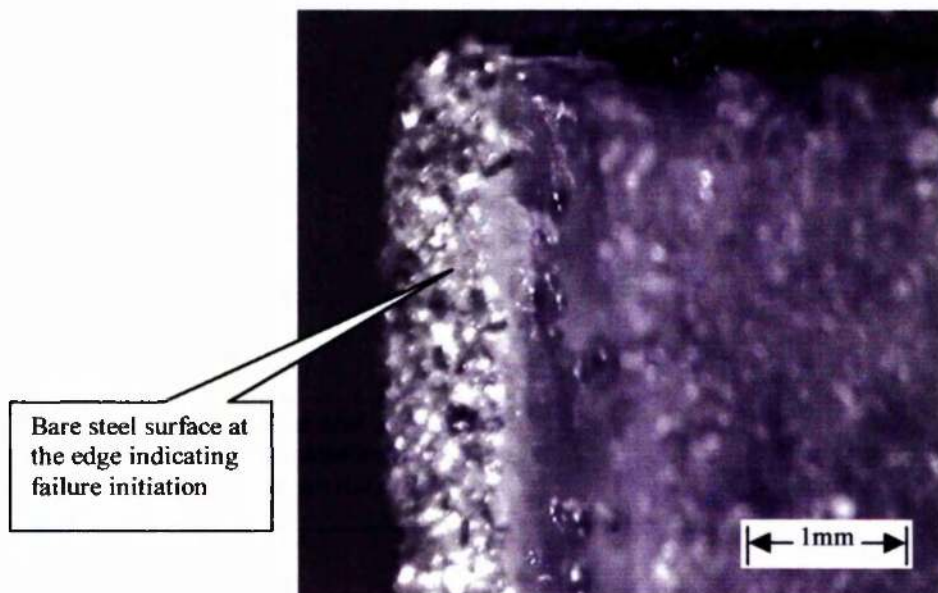


Figure 5.20 Fractured surface of grit-blasted steel cleavage specimen showing failure initiation from the edge

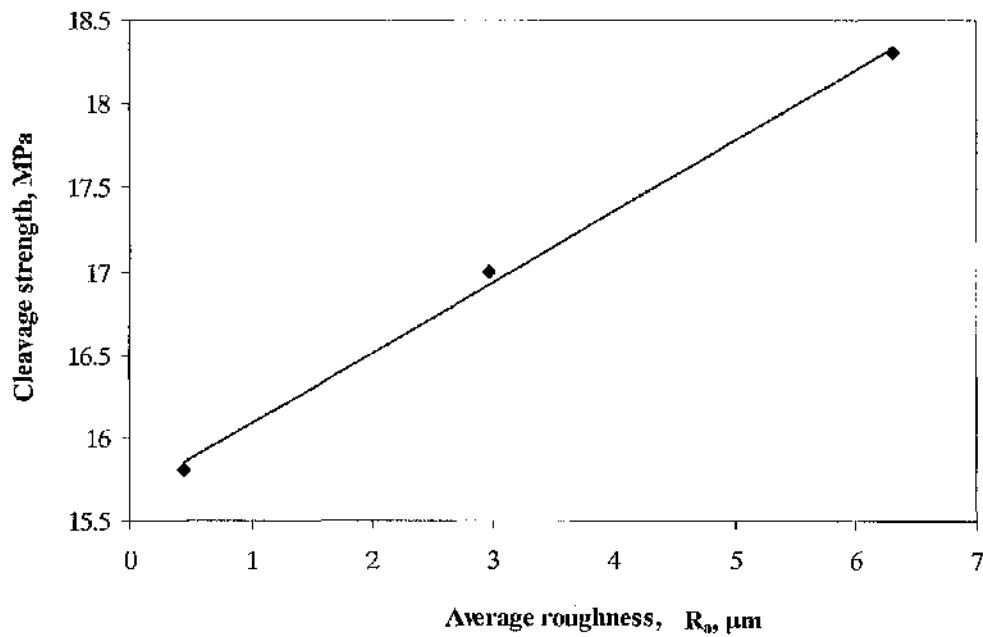


Figure 5.21 Variation of cleavage strength with average roughness,  $R_a$

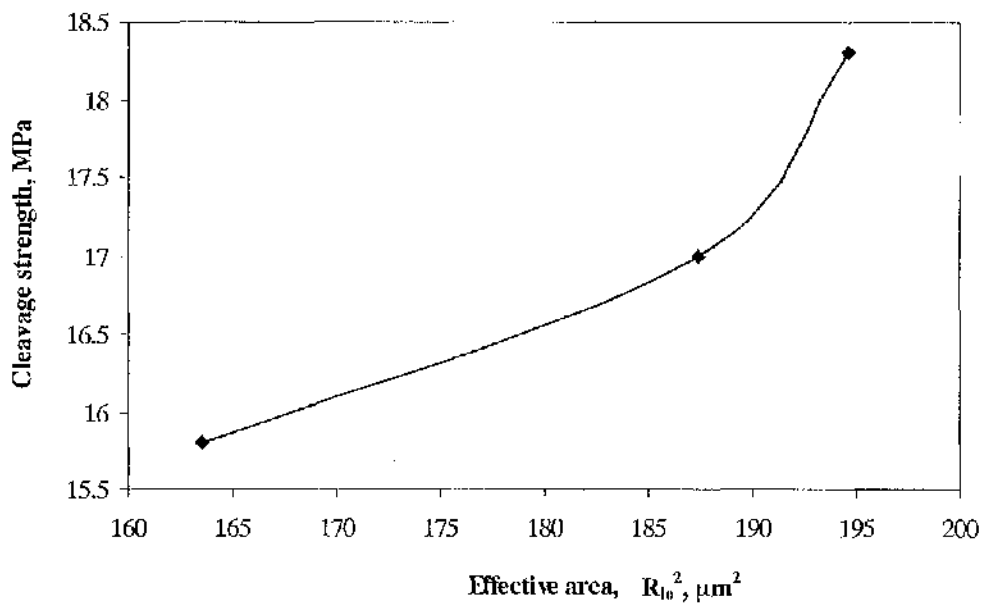


Figure 5.22 Variation of cleavage strength with effective area of bonding (experimental results)

Table 5.1 Effect of adhesive thickness on cleavage strength of steel specimens

Surface finish	Adhesive thickness (mm)	Failure load (kN)					Average strength (MPa)	Coefficient of variation (%)	Possible failure initiation
		1	2	3	4	5			
Polished	0.1	8.10	6.73	10.86	8.39	9.79	14.0	18.2	Adhesion
	0.5	9.61	9.92	10.03	9.58	10.25	15.8	2.9	Adhesion
Grit-blasted	0.1	11.78	10.25	11.34	9.85	12.18	17.7	9.0	Adhesion/Cohesion
	0.5	10.13	10.59	10.63	10.66	11.10	17.0	3.2	Adhesion/Cohesion

Table 5.2 Effect of adhesive thickness on lap-shear strength of steel specimens

Surface finish	Adhesive thickness (mm)	Failure load (kN)					Average strength (MPa)	Coefficient of variation (%)	Possible failure initiation
		1	2	3	4	5			
Grit-blasted	0.1	9.32	8.47	8.59	9.78	7.37	23.2	10.6	Adhesion/Cohesion
	0.5	6.29	6.87	7.36	6.64	6.98	18.2	5.9	Adhesion/Cohesion

Table 5.3 Effect of corrosion on cleavage strength of steel specimens

<i>Surface finish</i>	<i>Adhesive thickness (mm)</i>	<i>Failure load (kN)</i>			<i>Average strength (MPa)</i>	<i>Coefficient of variation (%)</i>	<i>Possible failure initiation</i>
		<i>1</i>	<i>2</i>	<i>3</i>			
Rusted after Polishing	0.1	1.84	1.48	1.00	2.3	29.1	Adherend (oxide)
	0.5	1.58	1.83	1.43	2.6	12.4	Adherend (oxide)
Rusted after grit-blasting	0.1	3.94	4.24	4.08	6.5	3.8	Adherend (oxide)
	0.5	4.29	4.52	2.45	6.0	30.2	Adherend (oxide)

Table 5.4 Effect of variable bonding area on cleavage strength of steel specimens

<i>Surface finish</i>	<i>Bonding area (%)/(mm<sup>2</sup>)</i>	<i>Failure load (kN)</i>					<i>Average failure load (kN)</i>	<i>Coefficient of variation (%)</i>	<i>Possible failure initiation</i>
		<i>1</i>	<i>2</i>	<i>3</i>	<i>4</i>	<i>5</i>			
Polished	100/625	9.61	9.92	10.03	9.58	10.25	9.88	2.9	Adhesion
	75/468.75	8.37	7.33	7.14	8.30	7.01	7.63	8.6	Adhesion
	50/312.50	4.17	5.05	4.48	4.14	5.00	4.57	9.6	Adhesion
	25/156.25	2.38	2.05	2.26	2.06	2.40	2.23	7.6	Adhesion
Grit-blasted (40/60 grit)	100/625	10.13	10.59	10.63	10.66	11.10	10.62	3.2	Adhesion/Cohesion
	75/468.75	8.72	8.60	8.49	8.84	9.35	8.80	3.8	Adhesion/Cohesion
	50/312.50	6.10	5.73	5.86	5.37	5.48	5.71	5.1	Adhesion/Cohesion
	25/156.25	2.80	3.06	2.86	2.88	3.08	2.94	4.3	Adhesion/Cohesion

Table 5.5 Cleavage strength with different surface finishes of steel

Surface finish	Adhesive thickness (mm)	Failure load (kN)					Average strength (MPa)	Coefficient of variation (%)	Possible failure initiation
		1	2	3	4	5			
Polished	0.5	9.61	9.92	10.03	9.58	10.25	15.8	2.9	Adhesion
Grit-blasted									
40/60	0.5	10.13	10.59	10.63	10.66	11.10	17.0	3.2	Adhesion/Cohesion
24/30	0.5	11.58	11.56	11.38	11.22	11.38	18.3	1.3	Adhesion/Cohesion

Table 5.6 Effect of over-curing on cleavage strength of steel specimens

Surface finish	Adhesive thickness (mm)	Failure load (kN)					Average strength (MPa)	Coefficient of variation (%)	Possible failure initiation
		1	2	3	4	5			
Grit-blasted	0.1	11.67	10.28	11.59	10.06	11.44	17.6	7.0	Adhesion/Cohesion
	0.5	10.48	10.84	10.96	10.39	10.88	17.14	2.4	Adhesion/Cohesion

## CHAPTER SIX

***TESTING OF STEEL/COMPOSITE CLEAVAGE SPECIMENS*****6.1 Introduction**

Because of the anisotropic strength properties of fibreglass composite materials, testing of steel/composite cleavage specimens is not possible in a configuration similar to that of steel/steel cleavage specimens (Chapter 5). Standard cleavage specimens were therefore modified and a layer of laminate was inserted in between the metallic adherends to achieve cleavage joints between steel and composite adherends.

In this chapter details of testing of steel/composite/steel specimens are given. Several surface pre-treatment schemes for the composite adherends were considered, including diamond polishing. Two different fibre orientations, i.e. woven roving and unidirectional, were also considered.

**6.2 Specification of Specimens**

The steel/composite/steel cleavage specimens were made by modifying the standard cleavage specimens specified in British Standard BS 5350:Part C1:1986<sup>1</sup>. Approximately 40mmx40mm pieces of laminate were inserted between the mild steel adherends and bonded with Araldite<sup>®</sup> 420A/B (Redux<sup>®</sup> 420 A/B) adhesive at the controlled adhesive thickness. The configuration of modified cleavage joint is shown in Figure 6.1. The bonded area for each of the modified specimens was 25x25mm<sup>2</sup>.

**6.3 Experimental Details**

Experiments were carried out to look into the effect of the following laminate surface conditions on the strength of modified steel/composite/steel cleavage specimens:

- as moulded
- acetone cleaned
- diamond polished
- grit-blasted with 40/60 mesh alumina grit
- manually roughened with silicon carbide paper
- peel ply
- unidirectional surface ply.

In all cases, steel adherends were grit-blasted with 40/60 mesh alumina grit. To verify the findings in the case of lab-made epoxy fibreglass laminates, tests were also conducted on Tufnol<sup>®</sup>, a commercially available finished woven roving laminate. In addition, woven roving glass/polyester laminates were also tested to check on the effect of matrix strength i.e. polyester resin.

#### **6.4 Pre-treatment of Adherends**

The grit-blasting of both steel and composite adherends was performed on acetone cleaned specimens in a way similar to that mentioned in Chapter 5 for steel adherends. Only one grade (40/60 mesh) of alumina grit was used. After grit-blasting, the specimens were blown free from the remains of grit and cleaned again with acetone just before bonding. A typical grit-blasted surface of GRE laminate is shown in Figure 6.2.

For polishing, the GRE laminates were first abraded with sandpapers (of decreasing roughnesses) and then polished with oil-wetted 1-micron diamond paste. Following the polishing, the specimens were washed with soap and water, acetone and then dried in hot air. A typical diamond polished GRE surface is shown in Figure 6.3.

For manual roughening, the laminates were first cleaned with acetone and then abraded with a fine emery paper (Grit P1200 of Buchler Krautkramer, UK) to remove the remains of PTFE. They were then roughened with Naylobon<sup>®</sup> P60 waterproof emery paper (three times width wise and twenty four times length wise). Care was taken in avoiding damage to the fibres, as much as possible. Remains of

grit from the emery paper were blown free with air and the surfaces were finally cleaned with acetone and dried in hot air.

After the necessary pre-treatment, the surface roughnesses of adherends were measured (as detailed in Chapter 4) using Taylor Hobson's Form Talysurf Series 2 50i surface profiler and, where possible, with an atomic force microscope.

### **6.5 Bonding of Specimens**

Two wire spacers of 0.5mm diameter were attached to both pre-treated metallic adherends near the frontal and rear ends to control the adhesive thicknesses between the metallic and the composite adherends. For the comparison of test results with those from steel/steel cleavage specimens, the hybrid specimens were also bonded approximately 24hrs after the grit-blasting. A manual dispensing/mixing gun was used with an appropriate mixing nozzle (MC 06-24) to dispense adhesive in the correct ratio. Adhesive was applied and spread onto the bonding surfaces with a spatula and the specimens were clamped using a specifically designed jig that allowed bonding of hybrid cleavage specimens (Figure 6.4). As much as possible, excessive adhesive was cleaned from the specimens using metallic strips. All specimens were cured for 2hrs at 70°C, and following this the cured specimens were removed from the jig and adhesive fillets, if any, were removed manually by scraping away with a razor blade.

### **6.6 Testing**

The specimens were tested to failure on a Lloyd tensile testing machine using standard clamps and fixtures. All tests were carried out under monotonic loading at room temperature and with a cross-head speed of 0.5mm/min. A minimum of five specimens of each type was tested to achieve an average result. After each test, the failure load was recorded and the fractured surfaces were examined to determine whether the failure was adhesion, cohesion or within the composite adherends. In the cases when no clear pattern was apparent, the failure is referred to as adhesion/cohesion.

## 6.7 Results

The effects of various composite surface treatments were studied by keeping other variables constant i.e. surface treatment of metallic adherends, adhesive bond thickness and curing conditions. Results of mechanical testing are presented in Tables 6.1-6.3. For the purpose of comparison, average strength values obtained by dividing the failure load by the bond area are presented.

### 6.7.1 *No Surface Pre-treatment (as moulded)*

Composite adherends bonded without any pre-treatment, on one or both surfaces, produced joints of very low strength, approximately 3% of the maximum strength obtained with such joints. In addition, the coefficients of variation were very high because of the good adhesion properties of PTFE. Examination of the fractured surfaces clearly indicates that these failures are completely of the adhesion type with no visible traces of the adhesive present on the fractured surfaces.

### 6.7.2 *Acetone Cleaning*

Composite adherends, cleaned with acetone on both the surfaces, gave a much better performance than their uncleaned counterparts. Although there is an increase of about 900% in the joint strength, it is still only about 25% of the best average strength obtained with these kind of laminates. Moreover, the coefficient of variation has reduced to about 25%, which is not very low, but can well be expected with such pre-treatment methods, where it is very difficult to control the consistency in the quality of surfaces produced.

The fracture pattern was again of the adhesive type with no apparent residues of resin present on the laminate surfaces (Figure 6.5).

### 6.7.3 *Roughening with Emery Paper*

The manual roughening was performed to evaluate the effectiveness of the combined action of acetone cleaning and surface roughening. It can be seen from the test results given in Table 6.1 that with this method about 90% of the maximum average strength value can be achieved. The coefficient of variation is also within a reasonable limit.

Examination of the fracture surfaces revealed a mixed mode failure (Figure 6.6) and this will be discussed in Chapter 8.

### 6.7.4 *Grit-blasting*

For many adherends including composites, grit-blasting is generally considered as one of the most satisfactory methods of surface pre-treatment. It was therefore imperative to study this parameter with reference to the hybrid cleavage specimens.

The hybrid cleavage specimens produced by grit-blasting of composite (woven roving composite) and steel adherends appear to produce approximately 18% lower joint strength values than the steel specimens (Table 6.1 and Table 5.1). From visual and light microscopic examinations, it appears that the failure initiates in the composite adherends (Figure 6.7). This may be due to damages of the fibres and resin during the grit-blasting process. A similar failure pattern can also be seen in the case of a finished composite laminate type woven fabric-Tufnol<sup>®</sup>, obtained from a commercial manufacturer (Figure 6.8).

It may be noted that the coefficient of variations is high (>10%) in both cases, i.e. the laboratory moulded and commercially produced laminates (Table 6.1). This may again be due to damage to the glass fibres and resin during the grit-blasting. Such damage may also result in poor wetting and the development of stress concentrations at the broken ends of the exposed fibres.

### **6.7.5 Influence of Polishing**

The joint strength of the diamond polished composite adherends outperformed all other surface conditions. Specimens made with polished epoxy fibreglass composites failed at about the same average load as those made with all grit-blasted (40/60 mesh) steel adherends (Table 5.1). This is not only true for the laboratory made composites, but also for the finished Tufnol® composites (Table 6.1). In all the specimens, failure appears to initiate at the metal-adhesive interface, shifting later into the composite adherend (Figure 6.9). Possible reasons for this increased strength may include a total removal of any mould release agent and the limited damages to the fibres and resin during the polishing operation in comparison with grit-blasting and manual roughening.

### **6.7.6 Influence of Peel Ply**

Joints made of laminates produced with the supplier's recommended peel ply appear not to perform as well as the grit-blasted and diamond polished ones. The reduction in strength, as a result of using peel ply, is approximately 31% and 42% compared to the grit-blasted and polished laminate joints respectively. The failure in this case is apparently an adhesion type failure (Figure 6.10) indicating the presence of some contamination that might have transferred from the peel ply sheets during the moulding operation. Later correspondence with the peel ply manufacturer did confirm this suspicion.

In the case of polyester laminate, on the other hand, peel ply appears to perform satisfactorily, and in all the cases failure initiated within the weak composite laminate (Figure 6.11). This will be discussed further in Chapter 8.

### **6.7.7 Influence of Fibre Directions**

Lower cleavage strength was obtained in the case of grit-blasted laminate with 90° unidirectional surface ply compared to the 0° unidirectional and woven roving laminates (Table 6.1). 0° unidirectional laminates produced higher strength than

woven roving and  $90^0$  unidirectional laminates. These increases are 4% and 11% respectively. This may be attributed to the higher stiffness of the glass fibre reinforcements along the loading direction compared to the epoxy matrix. The results also show a higher coefficient of variation in the case of  $0^0$  unidirectional laminate, which reduces the significance of this higher strength value.

A typical fractured surface for  $90^0$  unidirectional laminate is shown in Figure 6.12 with cohesive type failure within the composite adherend.

### ***6.7.8 Influence of Matrix Material***

From comparing the results presented in Tables 6.1 and 6.2, it can be seen that the composites made with epoxy-based matrices produce three-times stronger cleavage joints than those made with a polyester-base matrix. Therefore, it appears that the selection of the matrix material is very important in achieving higher cleavage strengths. For the laminates made with a low strength matrix material, simple surface pre-treatments may be sufficient to give strength values that are limited by the strength of the laminates rather than the adhesive strength of the adhesive. On the other hand, for high strength laminates, a more elaborate surface pre-treatment such as diamond polishing is necessary to achieve optimum cleavage strength.

### ***6.7.9 Influence of Insert on Joint Strength***

In order to validate the method adopted for the testing of hybrid cleavage specimens and to look into its influence on the boundary conditions and strengths, tests were conducted by inserting a rectangular piece of steel between the two steel adherends. The results obtained in this testing also gave an idea of the possible effect of changing the insert's Young's modulus on the joint strength.

From the test results given in Table 6.3, it can be seen that the hybrid specimens with steel inserts show approximately 7% higher strength compared to those without any inserts (Table 5.1). This difference in strength may be due to additional toughness induced by a second adhesive layer which allows more flexibility to the joint.

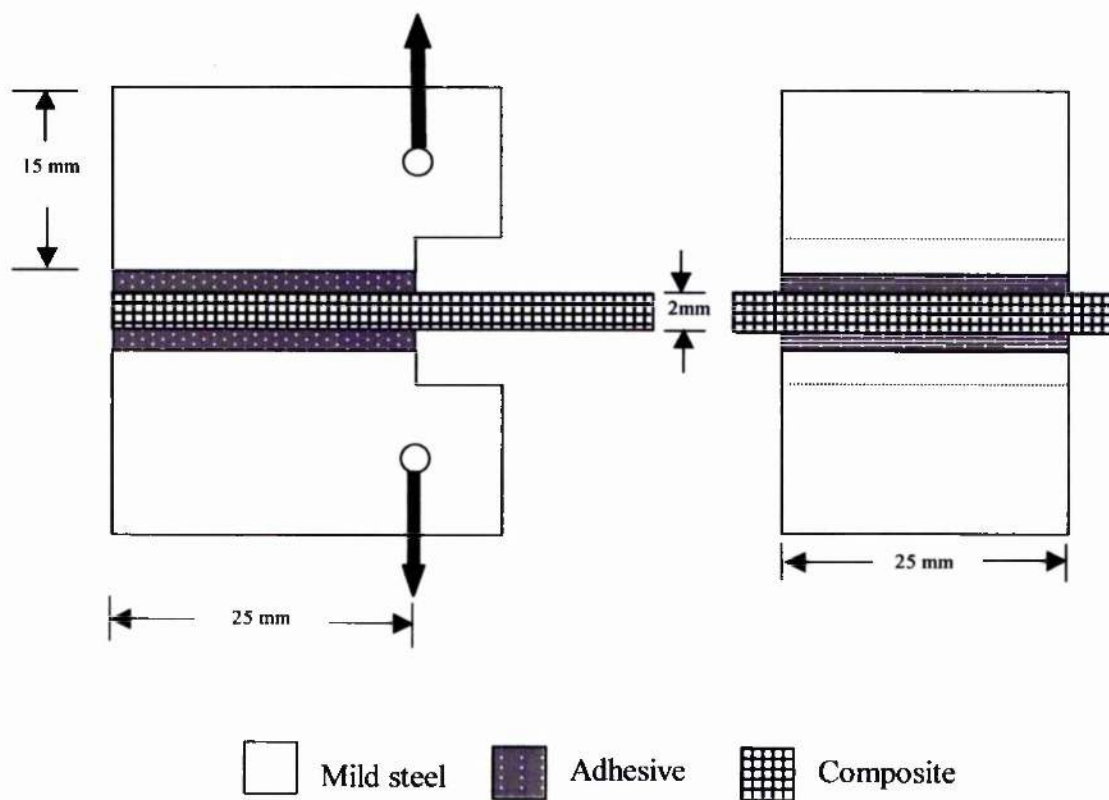


Figure 6.1 Configuration of modified cleavage specimens



Figure 6.2 Typical grit blasted surface of a GRE laminate



Figure 6.3 Typical polished GRE surface

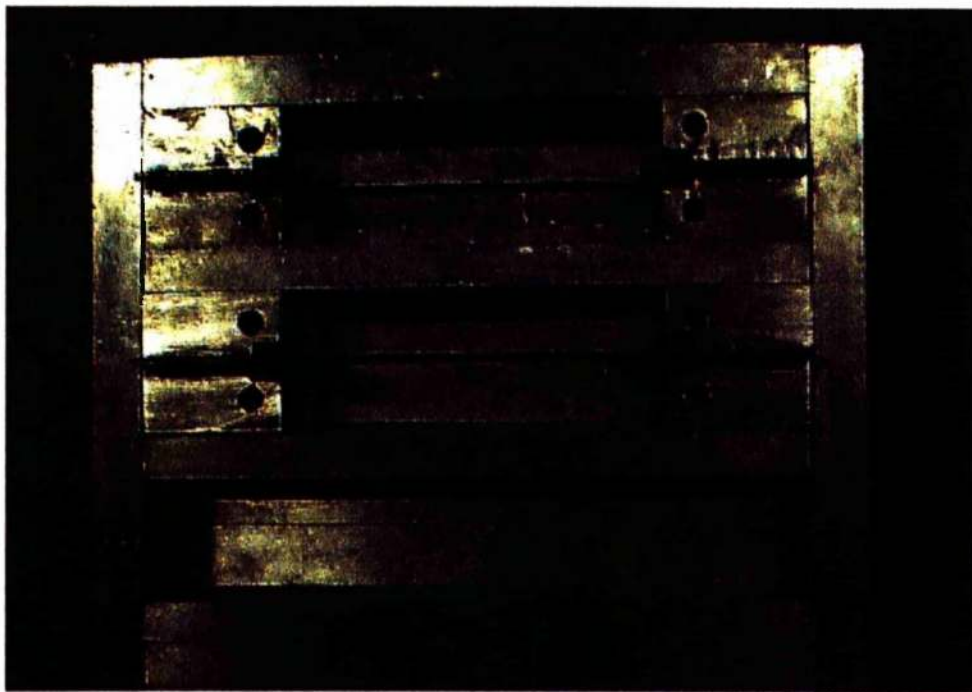


Figure 6.4 Jig for the bonding of hybrid cleavage specimens

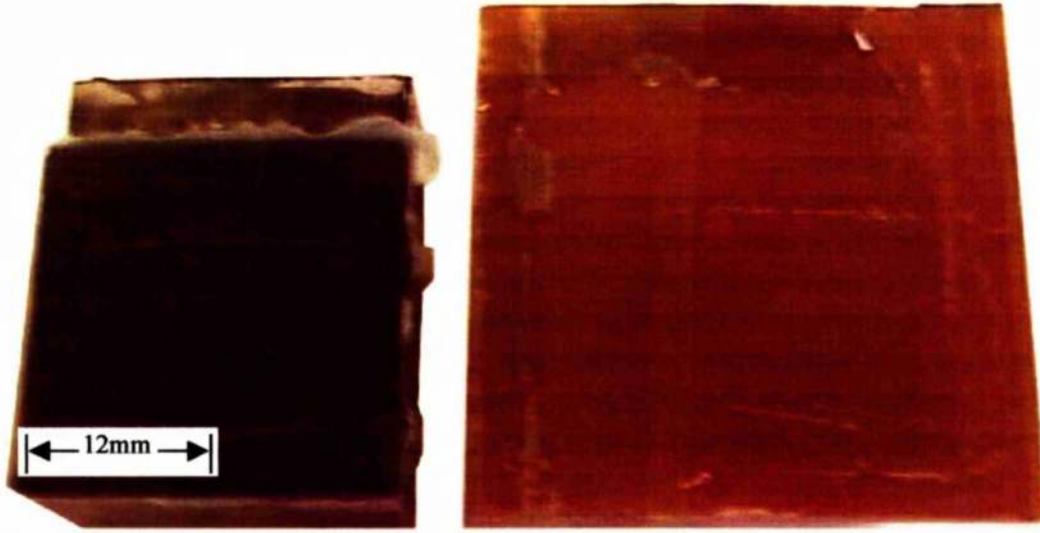


Figure 6.5 Fractured surfaces of a hybrid joint made with solvent cleaned laminate showing adhesion failure

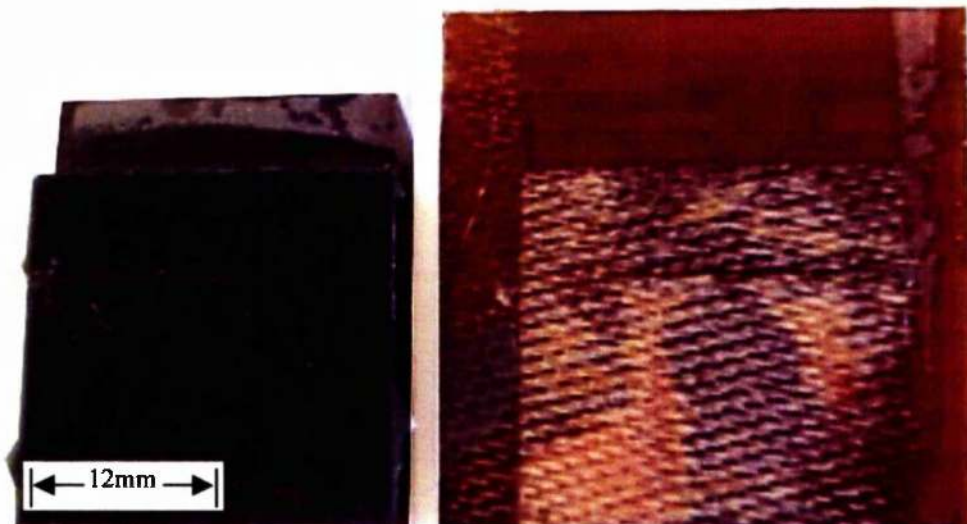


Figure 6.6 Fractured surfaces of a hybrid joint made with emery paper roughened laminate

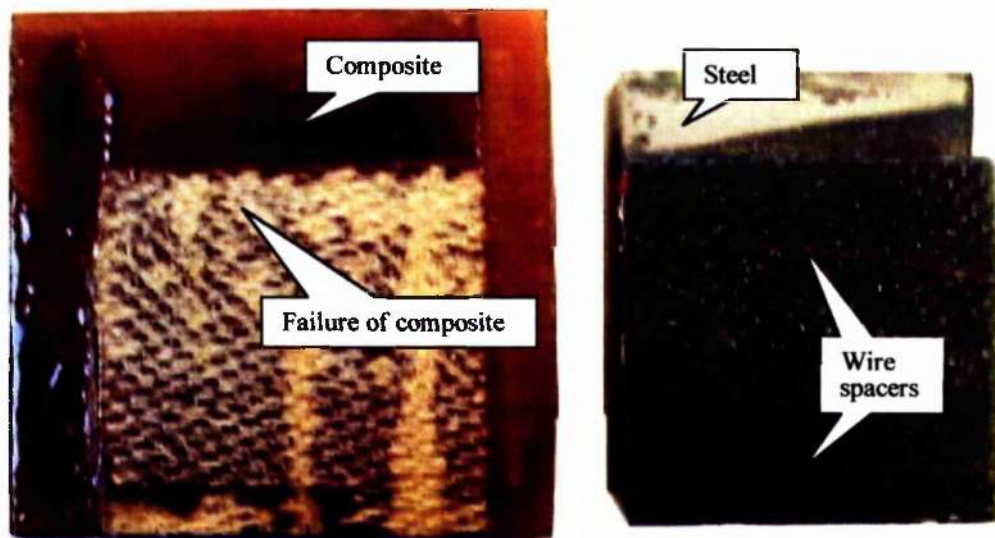


Figure 6.7 Fractured surfaces of a hybrid joint made with grit-blasted Fibredux laminate showing failure initiation at the composite surface



Figure 6.8 Fractured surfaces of a hybrid joint made with grit-blasted Tufnol laminate showing failure initiation at the composite surface

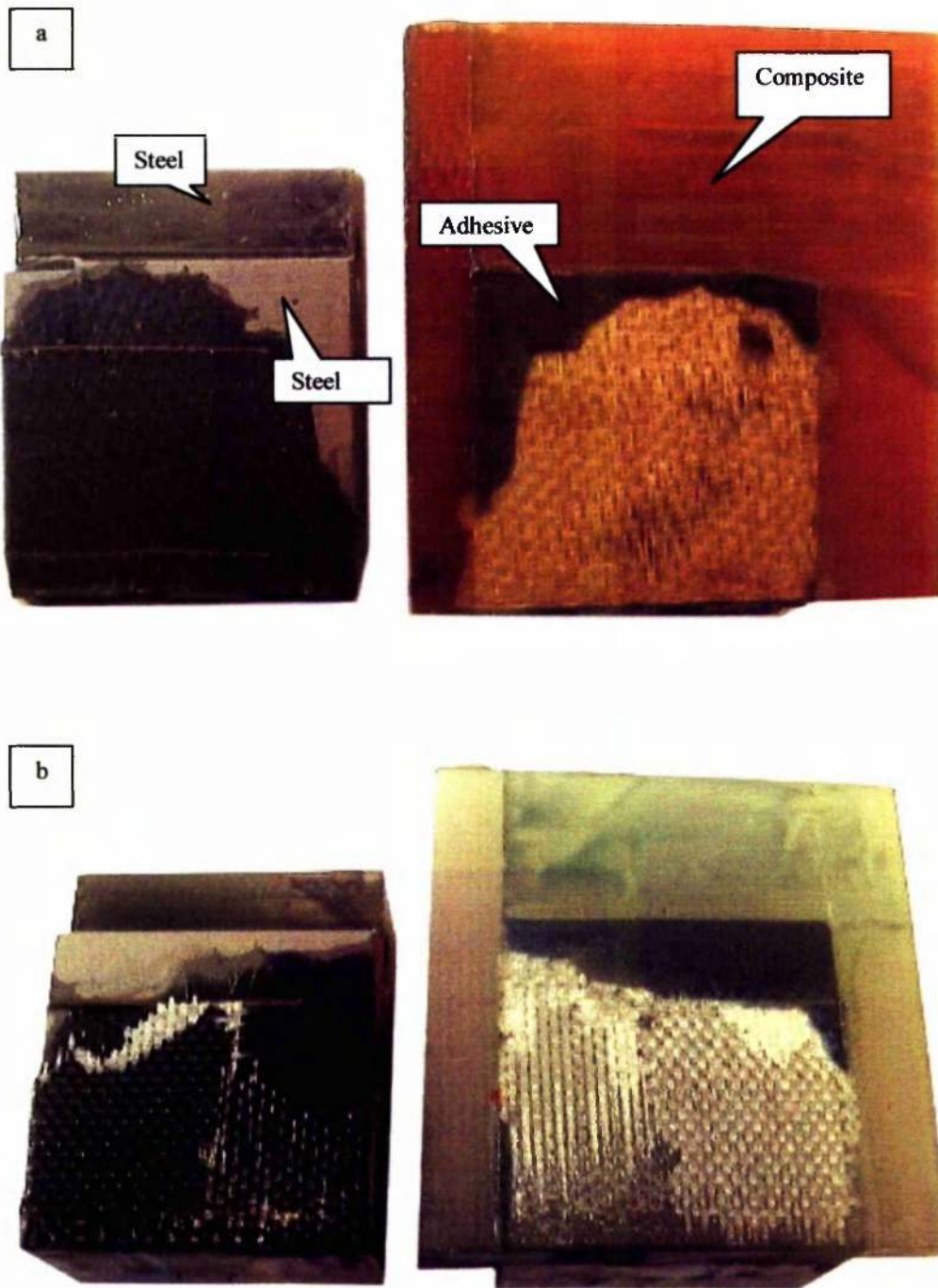


Figure 6.9 Fractured surfaces of a hybrid joint made with polished composite showing failure initiation at the steel surface (a) with Fibredux laminate; (b) with Tufnol laminate

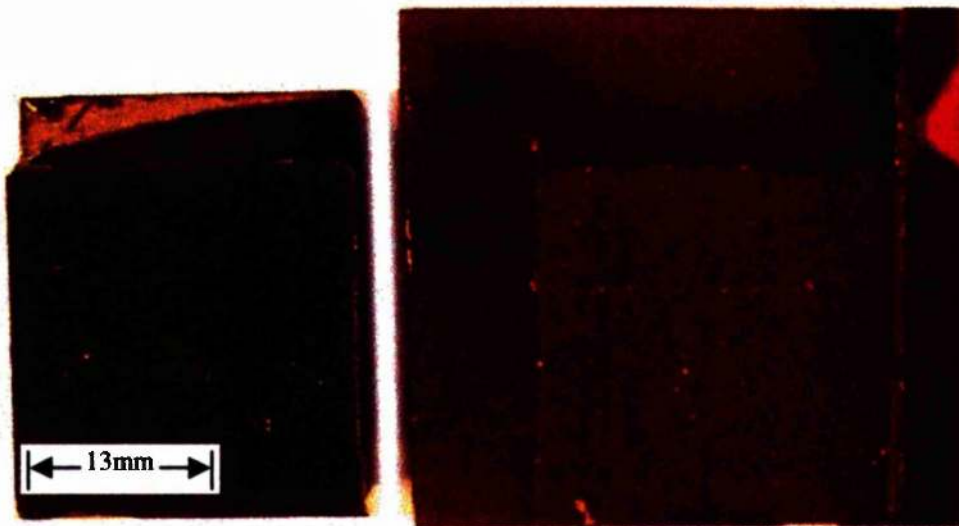


Figure 6.10 Fractured surface of a hybrid joint using Fibredux composite made with peel ply

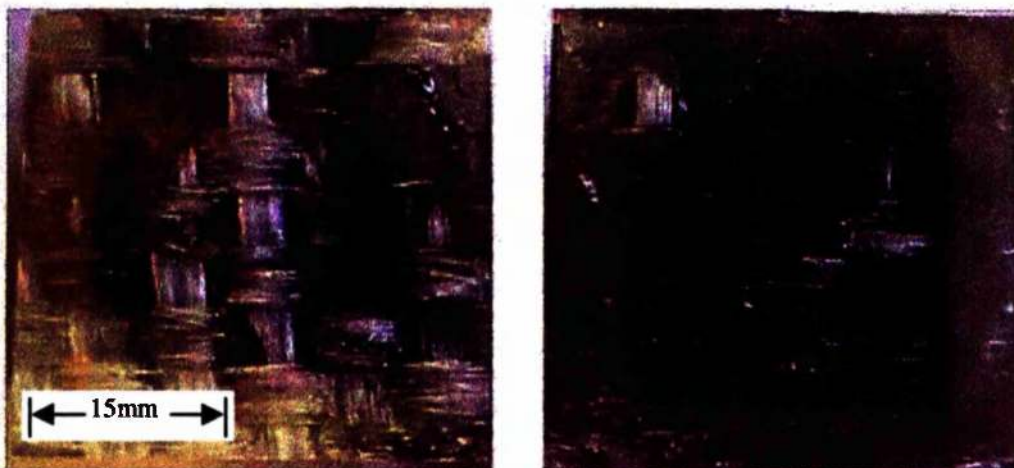


Figure 6.11 Fractured surface of a hybrid joint made with polyester laminate showing interlaminar failure

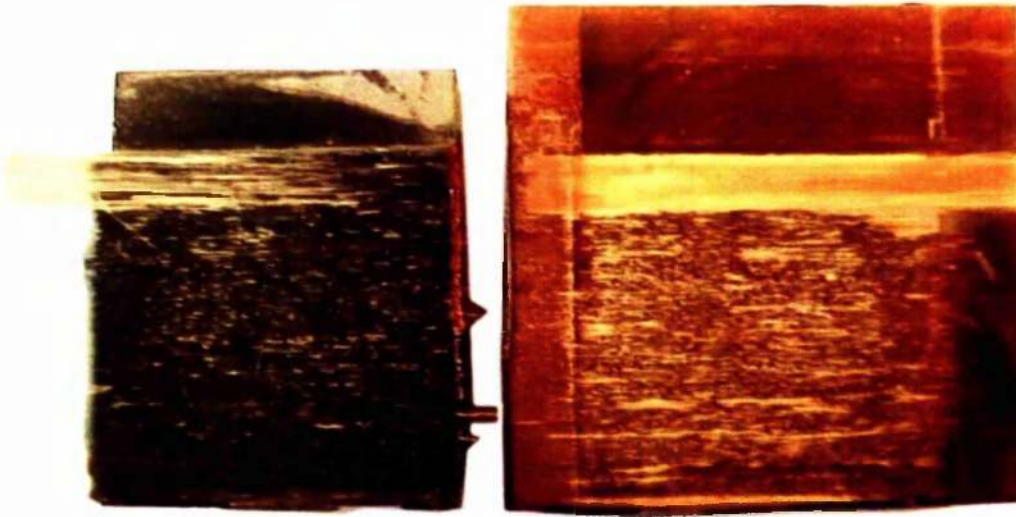


Figure 6.12 Fractured surfaces of a hybrid joint made with  $90^{\circ}$  unidirectional Fibredux laminate

Table 6.1 Effect of surface treatment of GFR laminates on cleavage strength of hybrid specimens

Surface finish	Failure load (kN)					Average strength (MPa)	Coefficient of variation (%)	Possible failure initiation
	1	2	3	4	5			
As moulded	0.13	0.49	0*	0.38	0.20	0.4	82.0	Adhesion
One side acetone cleaned	0.44	0.15	0.07	0.30	0.19	0.4	63.2	Adhesion
Both sides acetone cleaned	2.24	3.21	2.90	1.81	3.45	4.4	25.0	Adhesion
Peel ply	6.69	5.70	6.06	5.61	6.59	9.8	8.1	Adhesion
Manually roughened	9.11	8.85	10.37	9.56	10.03	15.3	6.6	Adhesion/Cohesion
Grit-blasted								
Woven fabric-Fibredux	9.44	7.41	9.76	9.00	7.80	13.9	11.8	Adhesion/Cohesion
Woven fabric-Tufnol	9.14	7.49	7.63	8.20	9.39	13.4	14.1	Adhesion/Cohesion
Unidirectional 0° Fibredux	9.20	9.11	8.85	9.12	9.10	14.5	1.5	Adhesion/Cohesion
Unidirectional 90° Fibredux	7.75	9.59	7.57	7.51	8.36	13.1	10.7	Adhesion/Cohesion

\* Failed during handling.

Contd.

Contd. Table 6.1

Surface finish	Failure load (kN)					Average strength (MPa)	Coefficient of variation (%)	Possible failure initiation
	1	2	3	4	5			
Polished								
Woven fabric-Fibredux	10.79	10.56	10.61	10.99	10.04	17.0	3.3	Adhesion/Cohesion
Woven fabric-Tufnol	11.18	10.50	10.05	10.81	10.19	16.9	4.4	Adhesion/Cohesion
Unidirectional 0° Fibredux	4.06	4.86	4.54	4.41	3.48	6.8**	12.3	Adherend (composite resin)
Unidirectional 90° Fibredux	5.56	5.00	4.94	4.24	4.61	7.8**	10.1	Adherend (composite resin)

\*\* Material expired during storage.

Table 6.2 Cleavage strength of hybrid specimens with GRP laminate

	Failure load [kN]					Average strength [MPa]	Coefficient of variation [%]	Possible failure initiation
	1	2	3	4	5			
Composite								
GRP laminate	3.61	3.33	3.75	2.80	3.97	5.6	13.0	Adherent (composite resin)

Table 6.3 Cleavage strength of hybrid specimens with steel insert

	Failure load [kN]					Average strength [MPa]	Coefficient of variation [%]	Possible failure initiation
	1	2	3	4	5			
Insert								
Steel	10.57	10.46	12.04	11.62	12.05	18.2	6.9	Adhesion/Cohesion

## CHAPTER SEVEN

***STRESS ANALYSES*****7.1 Introduction**

It is often difficult to use simple analytical techniques to determine the detailed behavioural characteristics of bonded cleavage joints. One method of overcoming this problem is using finite element analysis. The finite element method is a numerical analytical technique for obtaining an approximate solution to a wide variety of engineering problems. This method envisages the solution region as built up of many small, interconnected sub-regions or elements. Although originally developed to study stresses in complex airframe structures, it has since been applied to analyse problems of heat transfer, fluid flow, lubrication, electric and magnetic fields, and many others.

A finite element analysis may be divided into the general steps of discretisation of continuum, selecting interpolation functions, finding the element properties, assembling the element properties to obtain the system equations, defining boundary conditions and solving the system equations.

Although the range of possible applications of the finite element method extends to all engineering disciplines, civil, mechanical, and aerospace use it more frequently. Finite element modelling has been successfully used to study and investigate adhesive joints and is now considered as an established technique for analysing and optimising adhesive joint geometry. Like any other method of analysis, finite element modelling also has its own limitations. High stress gradients occur in certain regions of the joint, and therefore these regions have to be modelled very accurately and economically. Owing to the very fine mesh, the number of degrees of freedom in a joint is typically very high, especially in a 3-D model. Availability of the right material data, especially that of the adhesive and its interface with the adherend, may also be problematic.

In this study two approaches were used to carry out stress analyses in cleavage specimens. Firstly, a finite element approach, in which cleavage specimens between similar and dissimilar adherends were modelled using the Patran<sup>220</sup> pre-processor and the Abaqus<sup>221</sup> standard solver to carry out parametric studies. Micro modelling of the joint interfaces has been carried out to study stresses at the interfaces. Attempts have also been made to correlate these finite element results to the experimental findings. In the second approach a simple set of mathematical equations, based on classical mechanics and finite elements, have been developed to find the maximum cleavage stress in an adhesively bonded cleavage specimen. Mathematica<sup>222</sup> software was used to solve the equations.

## 7.2 Software Packages

Owing to the general applicability of finite element methods a number of commercial finite element software packages are available. In this study, the Abaqus finite element program was used as the main processor to simulate the problem with Patran acting as a pre-processor and Abaqus Post as a post-processor.

A complete finite element analysis consists of three distinct stages: pre-processing, simulation and post-processing.

In the pre-processing stage, a model of the physical problem is defined and a suitable finite element mesh and corresponding load and boundary conditions are applied to the model. An input file is created for the simulation processor. This is a very important step because this is where all material properties are defined and the decisions about the selection of elements and the size of the problem are made.

Processing or simulation is the stage in which the processor solves the problem defined in the input file. In stress analysis, element strains are calculated from the nodal degrees of freedom and the element displacement field interpolation, and finally stresses are calculated from the strains. Both linear and non-linear analysis can be carried out.

Post-processing is needed to evaluate the results of the analysis. Abaqus Post reads the binary result files and provides graphical representations of the output. It has a variety of options for displaying the results, including colour contour plots, deformed shape plots and x-y plots. The x-y plot data may also be exported for further processing by Microsoft Excel.

### **7.3 Numerical Analysis**

Numerical analysis based on the elastic properties of the adhesive was used to support experimental results and to extend the understanding of failure initiation at micro level. Various numerical models of both steel/steel and steel/composite/steel, as detailed in the following sections, were considered. In most of the cases 2-D models were made but in some cases 3-D models were also made which will be discussed in Chapter 8. Figure 7.1 summarises the type of models used for numerical analyses in this chapter. Further details for these are given throughout the relevant sections.

Second-order reduced integration 8-noded shell elements (S8R5) were selected in most of the models for their effectiveness in bending. Due to their higher order of interpolation they are also effective at capturing stress concentrations expected at the bond termination. An adhesive thickness of 0.5mm was considered in all models, unless stated otherwise, and was generally modelled with 3 elements through the thickness. A finer mesh of elements was applied to the adhesive region at the loaded edge to account for the high stress gradients. Elastic isotropic properties were assigned to steel and adhesive (Table 7.1).

To avoid mathematical singularity problems at the free tension edge of the joint, stresses at the edge nodes were ignored in all models.

#### **7.3.1 Steel/Steel Cleavage Specimen**

A simplified approach for modelling the standard cleavage specimens was used. The simplified steel/steel model (Model S), made of two rectangular steel adherends with

the dimensions of 25mmx25mmx9mm and bonded with an adhesive of 0.5mm thickness, is shown in Figure 7.2. A 2-D model was generated using the Patran pre-processor. Figure 7.3 shows the details of the numerical model. The experimental boundary conditions for the cleavage specimens were simulated and a nominal load of 2kN was applied. Output from the Patran, in the form of an input file, was then fed to the Abaqus Standard processor for simulation. The results obtained from the analysis were viewed and processed by the Abaqus Post post-processor.

Three possible failure sites within the bond line were considered as shown in Figure 7.4. These are adhesive interfaces with the upper steel adherend (Site 1-1), the lower steel adherend (Site 3-3) and the centre of the adhesive line (Site 2-2). The distribution of stresses  $SP1$ ,  $SP2$ ,  $S_{11}$ ,  $S_{22}$ ,  $S_{12}$  and von Mises along the three sites were assessed from the xy plot of Abaqus Post (Figures 7.5-7.10). Contour plots showing the distribution of normal stress ( $S_{22}$ ) and von Mises stress in the stressed joint are shown in Figures 7.11 and 7.12 respectively.

It can be seen from Figures 7.5-7.10 that, with the exception of  $S_{12}$ , the values of the corresponding stresses at Sites 1-1 and 3-3 are the same. Therefore, for all further modelling of cleavage specimens with similar adherends, only two sites i.e. Site 1-1 and Site 2-2 were considered.

From the stress plots (Figures 7.5-7.10) it may be noticed that the first few millimetres of the joint are of paramount importance and bear most of the high stresses. Among the different stresses mentioned above,  $S_{22}$ ,  $SP2$  and von Mises stresses were found to be significantly higher. However, considering the geometry of the joint, the loading conditions, the results from the FE analysis and the possibility that the failure initiates at the interface between the adherends and the adhesive (where normal tensile stresses play the most significant role), it was decided to take the critical values of the normal tensile stress ( $S_{22}$ ) in the adhesive along the joint edges for the assessment of failure. Perhaps it is more difficult to consider resultant stresses from the maximum principal stress ( $SP2$ ) or von Mises stresses.

From Figure 7.8a, showing the variations of the normal tensile stress along the adhesive line of the Model S, it can be seen that about one millimetre away from the

joint edge, stresses at both Sites 1-1 and 2-2 are of the same value. At the edge, however, stresses are higher at Site 1-1 than at Site 2-2. It may, therefore, be expected that the failure will initiate at the steel interface. This is in line with the experimental findings where examination of the fractured surfaces (Figure 7.13) revealed that in the cases of steel/steel cleavage specimens, both polished and grit-blasted, fracture always initiated at the interface between the adhesive and the steel adherend. Further discussion will be brought up in Chapter 8.

### *7.3.2 Steel/Composite/Steel Hybrid Cleavage Specimen*

For finite element analysis of hybrid steel/composite/steel cleavage joints, a similar approach of simplified joint was used, as mentioned in earlier sections. In this case, a composite laminate of 2mm thickness was inserted between the two steel adherends, as shown in Figure 7.14 (Model H). Model H was generated in the same way as Model S. The GRE laminate insert was modelled with 8 elements through the laminate thickness. Figure 7.15 shows the details of the numerical model. The plies and resin details were not considered for the composite and therefore, isotropic properties were assumed (Table 7.2). Again, a nominal load of 2kN was applied and the experimental boundary conditions were simulated.

Although there is a possibility of interlaminar failure within the composite adherend, the stresses through the GRE laminate were not considered to be critical, especially when the possibility of delamination was largely reduced due to the laminate extension beyond the steel adherends. Three possible failure sites within the bond line were considered as shown in Figure 7.16. These are adhesive interface with the steel adherend (Site 1-1), the composite adherend (Site 3-3) and the centre of the adhesive line (Site 2-2).

Again, the distribution of stresses: SP1, SP2,  $S_{11}$ ,  $S_{22}$ ,  $S_{12}$  and von Mises, along these three sites was assessed. Contour plots showing the distribution of normal stress ( $S_{22}$ ) in a fully stressed joint and the adhesive layer are shown in Figures 7.17 and 7.18 respectively.

For the reasons mentioned in section 7.3.1, the assessment of failure was considered with reference to the critical values of the normal tensile stresses ( $S_{22}$ ) at the joint edge.

Figure 7.19 shows the variation of the normal stress ( $S_{22}$ ) along the three chosen sites in the adhesive layer of Model H. Near the edge, the value of  $S_{22}$  is highest at Site 1-1 than at Sites 2-2 and 3-3. Hence, it may be expected that the failure would initiate at the steel interface. Experimentally, this trend was noticed in the case of hybrid specimens made with polished woven fabric GRE laminates, where the failure initiated at the steel interface (Chapter 6). If we compare the highest values of  $S_{22}$  (excluding those at the edge nodes) in Model HI with those in Model S, we find that the latter is higher by approximately 8%. We may therefore expect that failure in the case of the hybrid specimens would take place at about 8-16% higher loads (depending on surface roughness of the steel adherend). Comparing the failure loads given earlier (Chapters 5 and 6), we see that the hybrid specimen made with polished GRE laminates shows approximately an 8% increase in strength compared with the polished steel/steel specimens. At a distance of about 0.5mm from the edge, the stress at Site 2-2 becomes larger than that at Site 1-1 (adhesive's interface with steel) and hence a shift in the failure path into the adhesive line may be expected, as seen in fractured surfaces shown in Figure 7.20. Shifting of the failure path may not simply be attributed to the values of stresses alone as after initiation of the crack, failure propagation takes place in a dynamic rather than a static condition.

Considering the orthotropic nature of the GRE composites it was felt necessary to perform another analysis on Model H with ELASTIC TYPE "LAMINATE" in the input file and assigning orthotropic properties to the laminate. Attempts were made to get the required laminate properties from the supplier, but failing to do so, approximate properties were assumed (Table 7.3) from the data available in the product leaflets and other literature quoting similar materials (Chapter 3). The variation in  $S_{22}$  along the adhesive layer at the three sites of this model is shown in Figure 7.21. With the exception of some higher stresses at the edge nodes, all the features present in Figure 7.19 are also present here i.e. higher stresses at the steel interface near the edges (this would be more prominent with finer meshing at the

edges) shifting toward the centre of the adhesive line. Further details about other modelling options considered are discussed in Chapter 8.

In order to validate the method adopted for the testing of hybrid cleavage specimens and to look into its influence on the boundary conditions and strengths, tests were conducted by inserting a rectangular piece of steel between the two steel adherends. The results obtained in this testing also gave some idea of the possible effects of changing the insert's Young's modulus on the joint strength and the comparison of stresses between the Models S and H.

To simulate the effect of replacing the laminate with a steel insert, the laminate properties in Model H were replaced by those of steel, and the model was generated and run in the same way as mentioned in section 7.3.2.

Comparing the maximum normal stress ( $S_{22}$ ) in Model S (Figure 7.8) and this model (Figure 7.22), we find that stress in the former is higher by approximately 11%. Hence, the cleavage specimens with inserts are expected to perform better. The experimental results showed approximately 7% higher strength in the joints with steel inserts compared to those without it (Table 5.1 and Table 6.3). The difference in the predicted and the actual strength results may be due to the doubling of the overall adhesive layer thickness in the cases of joints with inserts.

### ***7.3.3 Partial Modelling of Joints***

From the elastic stress distribution in Model S, as shown in Figure 7.8, it was realised that such a stress profile might approximately be represented as a histogram by assuming that a cleavage joint is made of a series of small independent butt joints. To study the effect at a micro-level, each bar in the histogram was then considered as representative of a portion of the joint (Figure 7.23). Micro modelling based on partial butt joints to look into the effects of surface roughness and failure in hybrid specimens was considered, as detailed in the following sections.

### 7.3.3.1 Modelling of Surface Roughness

Due to the uneven geometry of the grit-blasted surfaces, it is very difficult to exactly model the surface roughness with all the true features. A simplified approach was therefore used to represent the roughness in a sub-joint model.

In view of the shape of the actual roughness profile from the grit-blasted specimen (Figure 7.24), roughness of the butt joint was idealised into convex and concave shapes (Models P1 and P2), as shown in Figure 7.25. The surface of the upper adherend was idealised as a flat shape (polished). This was meant to give an easy comparison between the stresses at a polished and a rough surface. It was modelled in 2-D with an adhesive thickness of 0.5mm, modelled with five elements through the thickness. The configuration and meshing of the numerical model is shown in Figure 7.26. A distributed load of 1kN was applied at the top of the butt joint whereas the lower adherend was constrained in the three axes.

Again, three possible failure sites within the adhesive line were considered as shown in Figure 7.27. These are the adhesive interface with the upper flat steel surface (Site 1-1), the centre of the adhesive line (Site 2-2) and the lower triangular steel adherend surface (Site 3-3). The maximum value of normal tensile stress ( $S_{22}$ ) in the adhesive along the joint edges was taken as the failure criterion. In the case of the lower triangular surfaces, the values of  $S_{22}$  were transformed with reference to the slope angle ( $\theta$ ). This was achieved by multiplying the stress along Site 3-3 by  $\text{Cos}^2\theta$  (Figure 7.28). The angle was taken as equal to the average of the root mean square slope ( $R_{dq}$ ) for various specimens, which is 22.7 degrees in the case of 40/60 mesh grit-blasted specimens (Chapter 4).

Figure 7.29 shows the critical failure stresses at the three sites for Models P1 and P2. It can be seen that in both models the stresses at Site 1-1 are higher than the corresponding stresses at Site 3-3. At most places, they are also higher than those at the Site 2-2. As expected, adhesive stresses near the adherends' corners are significantly higher than those at the other locations, causing failure to initiate from the edges. This is also consistent with experimental observations where the failure appears to originate from the edges (Figure 7.31). This will be discussed in Chapter

8. The stresses near the edges are significantly higher in Model P2 than those in Model P1. At the centre of the models, however, an opposite trend may be noticed. This is largely due to the convex and concave shapes of the micro roughnesses. On average, stresses at Site 1-1 are 30% higher than those at Site 3-3, as shown in Table 7.1 (Figure 7.30). The experimental difference in the average cleavage strength between the polished and the rough specimens (24/30 mesh) is about 16% (Table 5.5, Chapter 5). This difference is possibly due to the lack of wetting in the bonded joints. This could play a more critical role in the cases of cleavage joints where the edge stresses are highly concentrated.

#### 7.3.3.2 Hybrid Steel/Composite/Steel Joint

Two different 2-D partial models were made in the same manner as presented in section 7.3.2. The two hybrid partial models are:

Model P3: representing fibres running at an angle of 90-degrees (Figure 7.32)

Model P4: representing fibres running at an angle of 0-degrees (Figure 7.33).

In Model P3, a 0.7mm thick composite laminate model was positioned between two steel adherends ( $5 \times 5 \text{mm}^2$ ) with a 0.5mm thick adhesive layer on either side of the laminate. The GRE laminate was modelled as circular glass cylinders of 0.4mm diameter (representing glass fibres) embedded centrally in 0.7mm thick resin matrix in a direction perpendicular to the plane of the model (Z-direction). A total of nine cylinders, spaced at an interval of 0.1mm, were considered with a distance of 0.3mm from the edges (Figure 7.32).

The adherends, the adhesives, the matrix (resin) and the glass cylinders were all considered to have elastic and isotropic properties (Table 7.1). The steel adherends and the adhesives were modelled with 8-noded reduced integration quadrilateral shell element whereas three noded triangular shell elements were used in the matrix and the cylinders (fibres) to model their curved shapes. Seven elements were used through the adhesive thicknesses in two way biased configurations to capture stress concentrations at the edges. Details of the numerical model are shown in Figure 7.34. Adherend surfaces were considered to be ideally flat (polished). A nominal

distributed load of 1kN was applied at the top of the joint whereas the lower adherend was constrained in the three axes.

Four possible failure sites were considered within the joint (Figure 7.35). These are:

Site 1-1: the adhesive interface with the upper flat steel surface

Site 2-2: the centre of the adhesive line

Site 3-3: the adhesive interface with upper surface of the laminate (matrix)

Site 4-4: the interface between the matrix and the glass cylinder.

Again, the assessment of failure was considered with reference to the maximum values of the normal tensile stress ( $S_{22}$ ) at these sites. Contour plots for the normal stresses ( $S_{22}$ ) in the adhesive line and the laminate matrix are shown in Figures 7.36 and 7.37, respectively.

Figure 7.38 shows the variations of normal stresses along the adhesive line at the three chosen sites within the adhesive of Model P3. Comparing the stresses at the first node away from the edge we find that the stress at Site 1-1 is higher by approximately 33% than that at Site 2-2. It is also higher by approximately 40% than that at Site 3-3. Soon after, the stress at Site 3-3 becomes higher compared to those at the other two sites. It may, therefore, be expected that in an "ideal" hybrid joint, fracture will initiate at the steel interface and will shift towards the laminate, as clearly shown from the experimental findings (Chapter 6). Stress peaks at Site 3-3, corresponding to each underlying glass cylinder, may be noticed due to the thinness of the resin matrix in that area.

The variation of the normal stress ( $S_{22}$ ) at the surface of the glass cylinder (Site 4-4) is shown in Figure 7.39. As expected, it shows a cyclic trend with a maximum value at the top of the fibre. At this point, stress is highest amongst the four sites. It is approximately 4% higher than the maximum value measured at Site 3-3 (the laminate-adhesive interface). However, it would be realistic to believe that failure will not occur at Site 4-4 (fibre-matrix interface) due to the fibre treatment (sizing) and better controlled processing of the prepreg materials. Furthermore, according to

FE analysis, crack initiation starts at Site 1-1. This will be discussed later in more detail in Chapter 8.

In the second model (Model P4) the same dimensions of the adherends, the adhesives and the laminate were used as those for Model P3 with the difference that this time a rectangular glass column of 0.4mmx4.4mm was used to represent fibre strands, in the x-direction (Figure 7.33). The same elastic isotropic material properties, load and boundary conditions were used as those in Model P3. The numerical model is shown in Figure 7.40.

Here again, four possible failure sites were considered within the joint as shown in Figure 7.41. These are:

Site 1-1: the adhesive interface with the upper flat steel surface

Site 2-2: the centre of the adhesive line

Site 3-3: the adhesive interface with upper surface of the laminate (matrix)

Site 4-4: the interface between matrix and the upper surface of the glass strand.

The critical values of the normal stress ( $S_{22}$ ) at the four sites were again considered for the assessment of the failure initiation. A contour plot for the normal stress ( $S_{22}$ ) in the adhesive line is shown in Figure 7.42.

Figure 7.43 shows the variation of normal stresses along the three selected sites in the adhesive layer. Comparing this with that of Model P3 (Figure 7.38) shows that the normal stress ( $S_{22}$ ) has the same trends mentioned in the former case except that there are no sudden peaks in the stresses at Site 3-3. The variation in  $S_{22}$  through the joint thickness (represented by a vertical line joining the first matching nodes at the four sites) is shown in Figure 7.44. It can be seen that the stress at Site 3-3 is higher by approximately 13%, 6% and 3% than those at Sites 1-1, 2-2 and 4-4 respectively. This situation again favours a fracture pattern initiating at the steel interface and shifting towards the laminate surface, a pattern that was observed in the actual fractured surfaces of polished steel/composite/steel specimens. In all such specimens,

the failure appears to initiate at the adhesive-steel interface and shifts towards the adhesive-laminate interface (Figure 7.20).

#### 7.4 Development of Equations for Maximum Cleavage Stress

In engineering practice the average cleavage stress in a cleavage joint, like other types of joints, is calculated by dividing the applied load by the bond area. This approach is not a suitable representation as the load is concentrated at one end while the other end is virtually unloaded. An attempt has, therefore, been made to develop a better calculation method, based on a simple mathematical relationship, with which we can find the maximum stress in a standard cleavage joint.

##### 7.4.1 *Classic Mechanics Approach*

Once again, the analogy of representing the cleavage joint with multiple butt joint elements has been used (section 7.3.3). The tensile forces acting on these butt joints are assumed to follow the pattern of the normal stress ( $S_{22}$ ) distribution along the adhesive line of the cleavage specimens, as shown in Model S (Figure 7.8). Figure 7.45 illustrates the idealised force distribution. Here it can be seen that a cleavage joint of 25mm length can actually be considered as equivalent to a triangular load distribution along a beam (connecting strap) of half the length i.e. 12.5mm whereas the rest of the joint is assumed to take zero loading. Each force ordinate in the triangular distribution represents a tensile force per butt joint element. Assuming that the butt joints are spaced at 1mm intervals along the strap and using static equilibrium conditions for forces and moments i.e. using  $\sum F_y=0$  and  $\sum M_A=0$  produced a number of simultaneous equations, as detailed in Appendix 2. Thirteen simultaneous equations were generated and solved using Mathematica software. Dividing the resultant force acting on each individual butt element, by the element area, gives the tensile stress. The stresses were then plotted against the distance along the adhesive bond line, as shown in Figure 7.46. A regression equation of the trend line based on the reactions of the butt joints spaced at 1mm width was found to be:

$$\sigma = (1.5828x - 21.487)F/2 \quad (1)$$

where  $\sigma$  = Cleavage stress (MPa)  
 $F$  = Applied cleavage force (kN)  
 $x$  = Distance along adhesive line (mm)

Figure 7.47 shows the stress distribution in the first half of Model S calculated using equation (1), the finite element analysis and the average cleavage stress (force divided by area). Comparison of the stresses at the edge reveals that the calculated stress is approximately 3% lower than that found by FE analysis. On the other hand, average stress calculated by dividing the applied load by the total bond area, gives a stress that is approximately 83% lower than the corresponding FE stress. Therefore, using equation (1) it is possible to estimate the maximum cleavage stresses with a reasonable accuracy in the steel (metallic) adherend cleavage joints without using FE analysis. It may also be noticed that the current method of calculating average stress gives a stress value too far from the actual maximum value.

In a similar manner, an equation for the estimation of stresses in the hybrid cleavage joints (Model H) has also been developed. Details of this treatment are shown in the Appendix 3. In this case, the equation for normal stress was found to be:

$$\sigma = (1.0867x - 10.867)F/2 \quad (2)$$

where  $\sigma$  = Cleavage stress (MPa)  
 $F$  = Applied cleavage force (kN)  
 $x$  = Distance along adhesive line (mm)

Figure 7.48 shows the stress distribution in the first 60% of Model S calculated using equation (2), FE analysis and the average cleavage stress. In this case, the stress at the edge calculated from equation (2) is approximately 16% and 5% lower than those at Sites 1-1 (steel interface) and 3-3 (laminated interface) respectively. However, just at 0.2 mm away from the edge, this difference reduces to only about 1%. On the other hand, the average stress, calculated by dividing load by area, is approximately 80% lower compared to that predicted from FE analysis. Hence again, with equation

(2), maximum cleavage stresses can be estimated with reasonable accuracy without involving FE analysis.

#### 7.4.2 *Finite Element Approach*

The results of the finite element modelling were used to develop an equation for calculating the maximum cleavage stress in a standard cleavage specimen bonded with 0.5mm thick adhesive.

The finite element model (Model S), as described in section 7.3.1, was made with different adhesive moduli ranging from 1 to 5GPa and simulated with a load of 2kN. The resultant values of the maximum normal stresses at the edge node were then plotted against the adhesive modulus (Figure 7.49) and the equation of trend line was found to be as follows:

$$\sigma = -0.2119E^2 + 2.3471E + 14.68 \quad (\text{for the edge node}) \quad (3)$$

where

$\sigma$  = Normal stress ( $S_{22}$ ) (MPa)

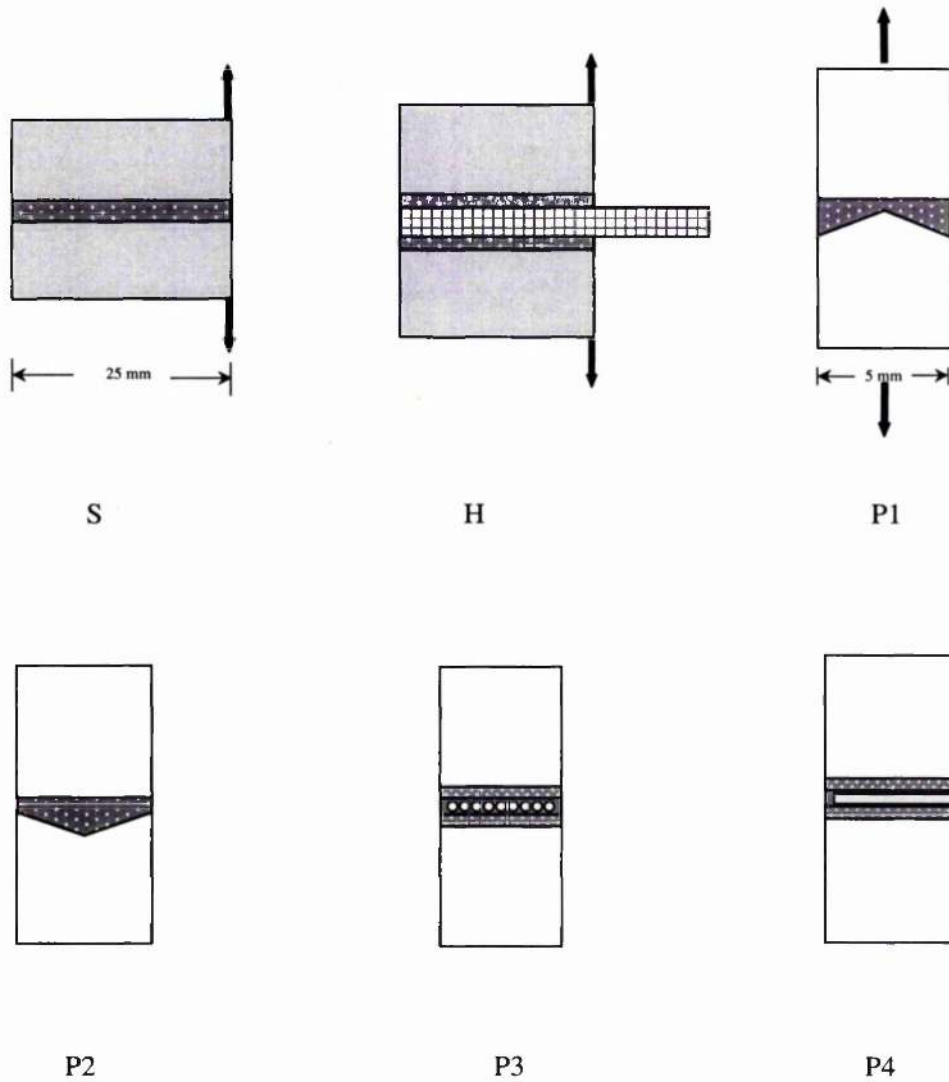
E = Adhesive's modulus of elasticity (GPa)

To verify that the above generated equation is giving results within reasonable limits, the calculated maximum stress for an adhesive of modulus 2.268GPa was compared with that from a finite element model made assuming an adhesive of modulus 2.268GPa. It was found that the calculated result agrees within 2% with that from the finite element analysis.

The above equation is not only valid for a 2kN load but can also be used to calculate maximum cleavage stress at any other load by applying an appropriate correction factor. This was verified by calculating the maximum stress at a load of 10.625kN.

To compare the effect of change in the adhesive modulus in Model S to that in Model H, the latter was generated and reanalysed, as mentioned earlier in section 7.3.2, but with an adhesive of double Young's modulus value (4.536 GPa).

Figure 7.50 shows the variation of the normal stress ( $S_{22}$ ) at the three sites along the adhesive line in Model H (after doubling the adhesive's Young's modulus). It can be seen from the figure that the stress distributions have the same shape and pattern as those in Figure 7.19. However, the stresses at Sites 1-1 and 3-3 are higher by approximately 13% and 16% respectively, due to the doubling of the adhesive's modulus. Similar behaviour resulted from increasing the adhesive's modulus in Model S. Since adhesives of different moduli may fail at different stresses, it is difficult to comment on their expected failure patterns.



Model S: Steel/steel cleavage joint

Model H: Hybrid steel/composite/steel joint (composite insert)

Model P1: Partial steel butt joint with convex macro-roughness

Model P2: Partial steel butt joint with concave macro-roughness

Model P3: Partial steel butt joint with composite insert (UD fibres at 90-degree angle)

Model P4: Partial steel butt joint with composite insert (UD fibres at 0-degree angle)

Figure 7.1 Schematic details of types of numerical models

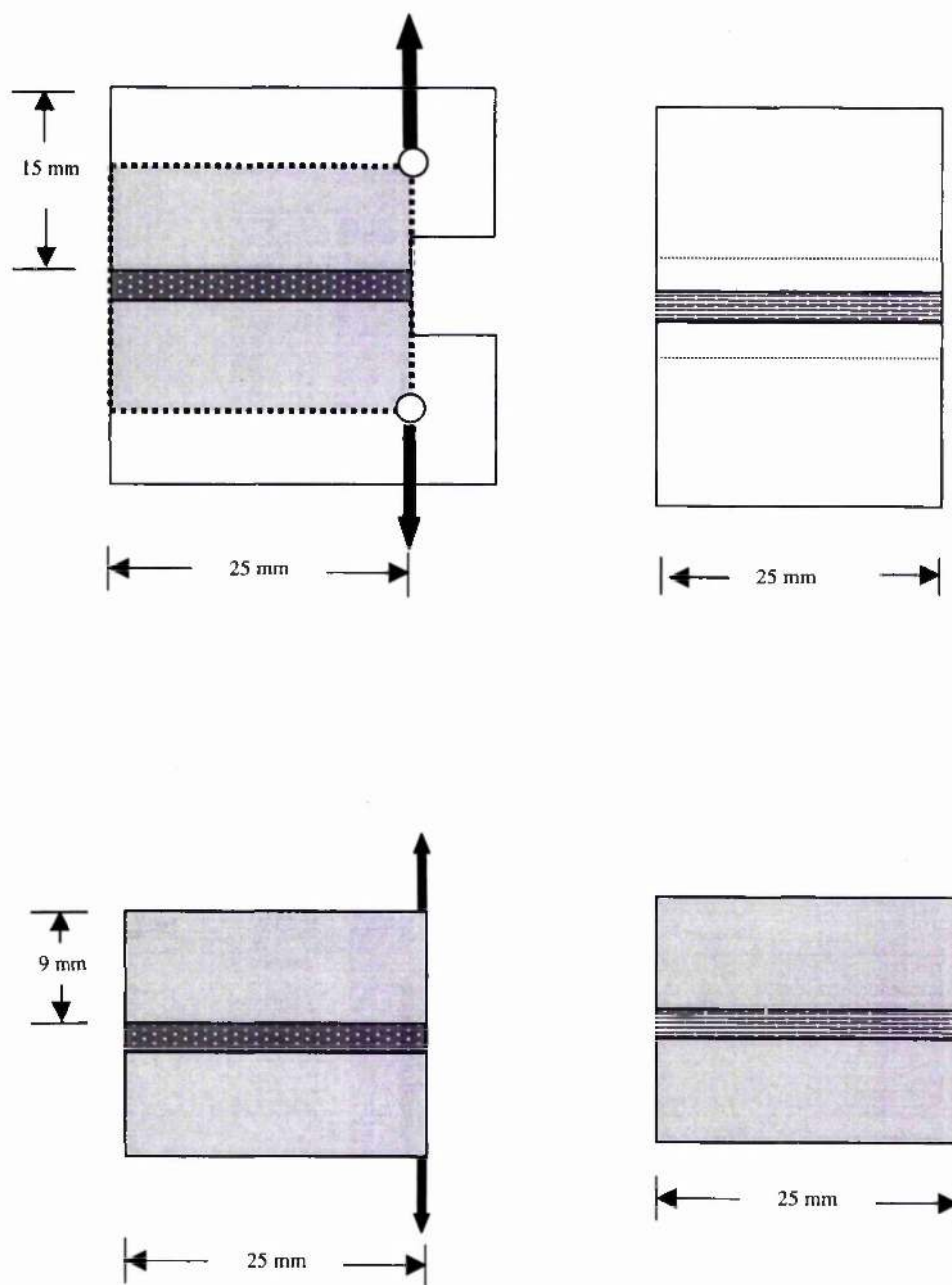


Figure 7.2 Cleavage specimens (a) standard; (b) simplified (Model S)

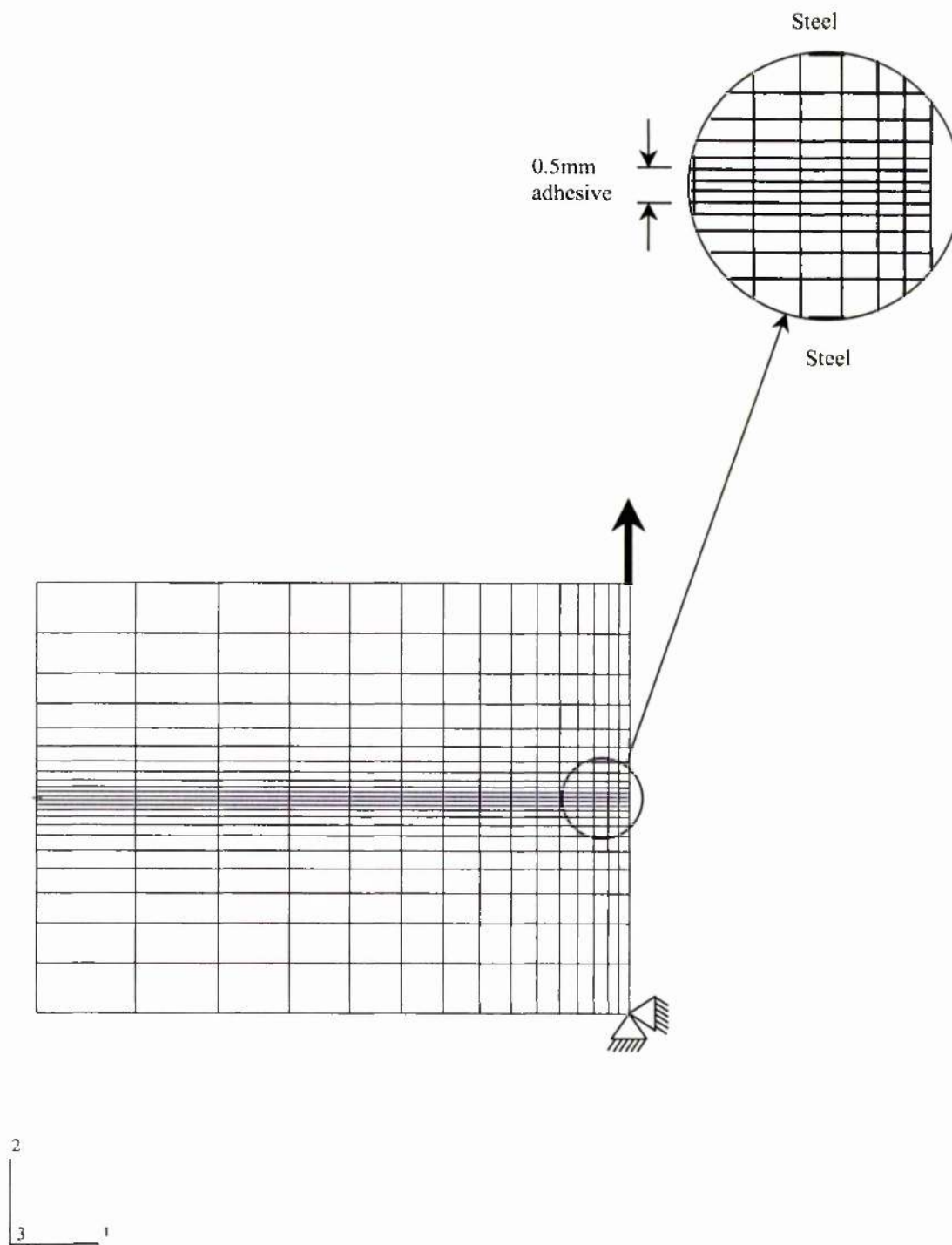


Figure 7.3 Finite element model (Model S)

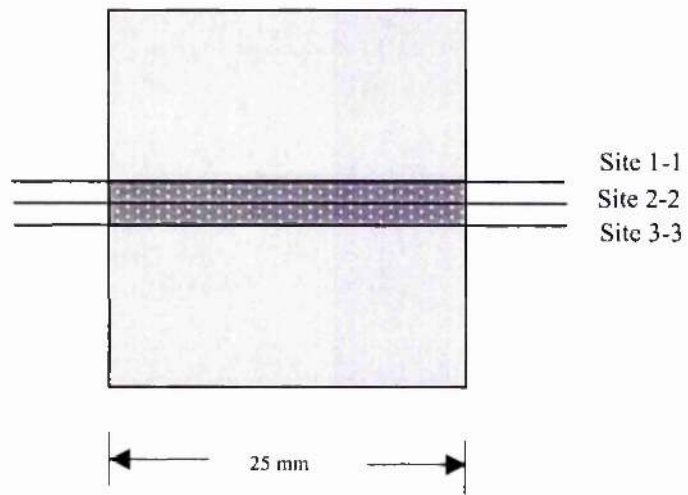


Figure 7.4 Possible failure sites in the adhesive line

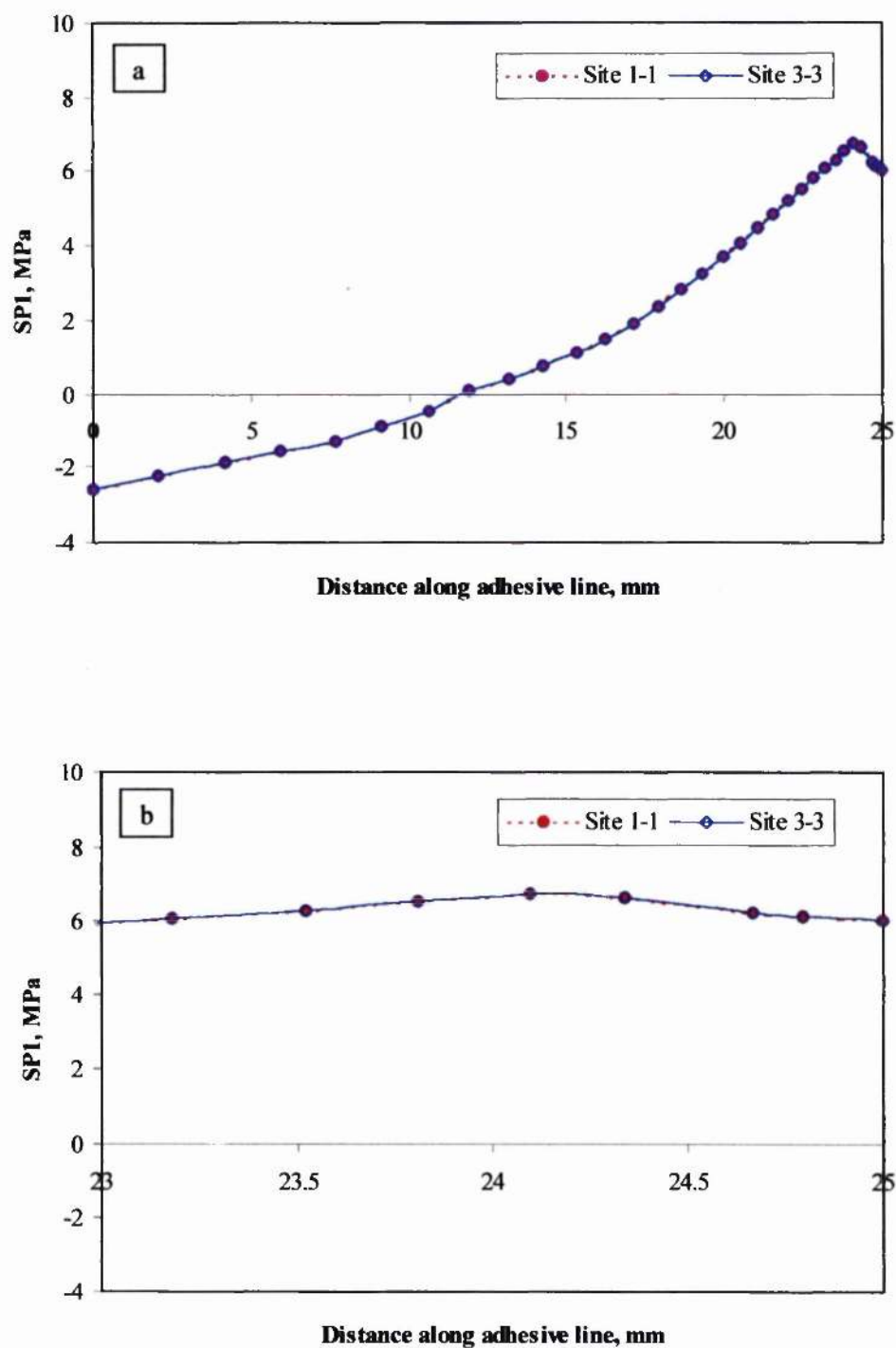


Figure 7.5 Minimum principal stress distribution in adhesive line of Model S (see Fig. 7.4) (a) full length; (b) initial 2mm (due to coinciding points the two sites are hard to distinguish)

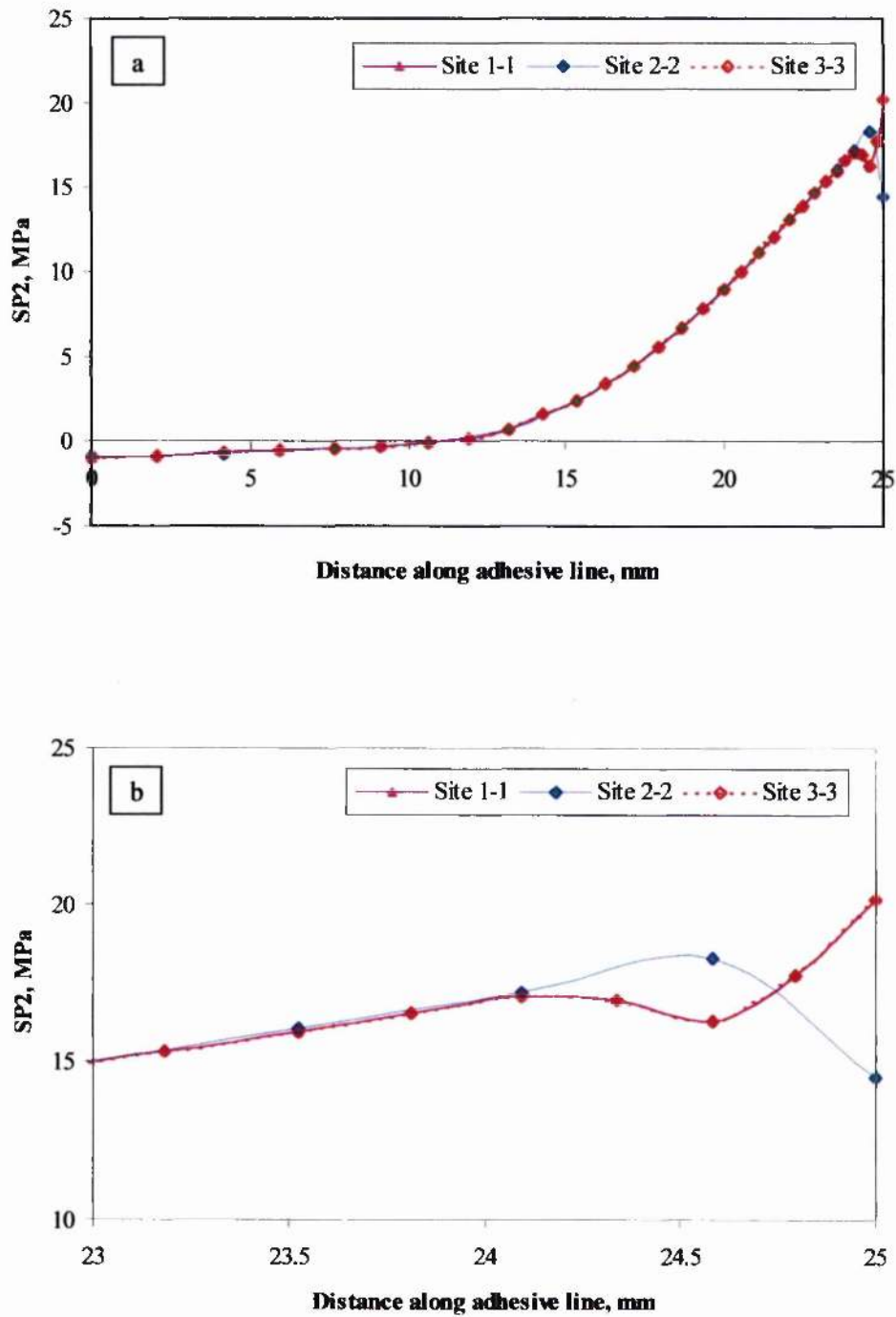


Figure 7.6 Maximum principal stress distribution in adhesive line of Model S (see Fig. 7.4) (a) full length; (b) initial 2mm

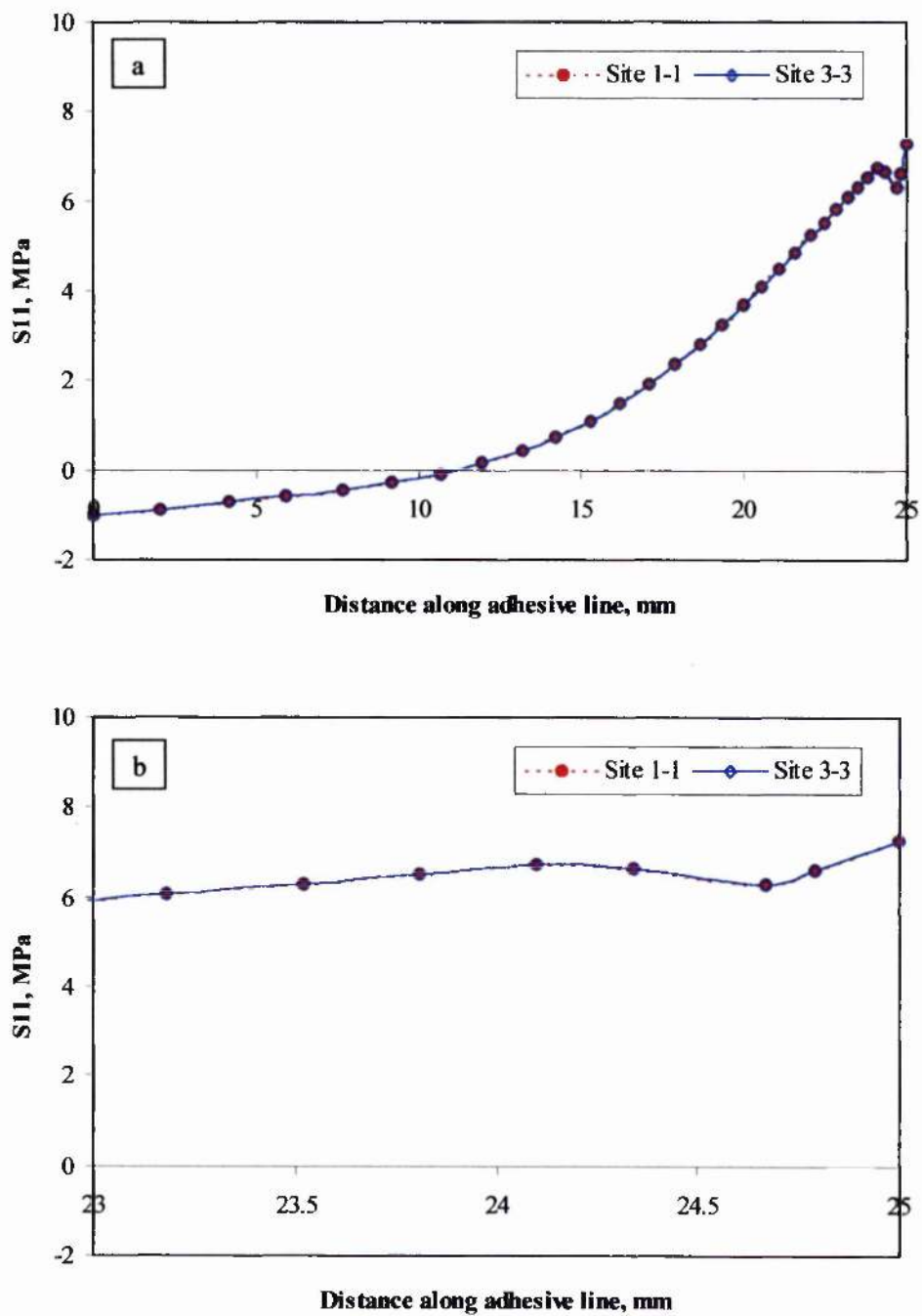


Figure 7.7 Axial stress distribution in adhesive line of Model S (see Fig. 7.4) (a) full length; (b) initial 2mm

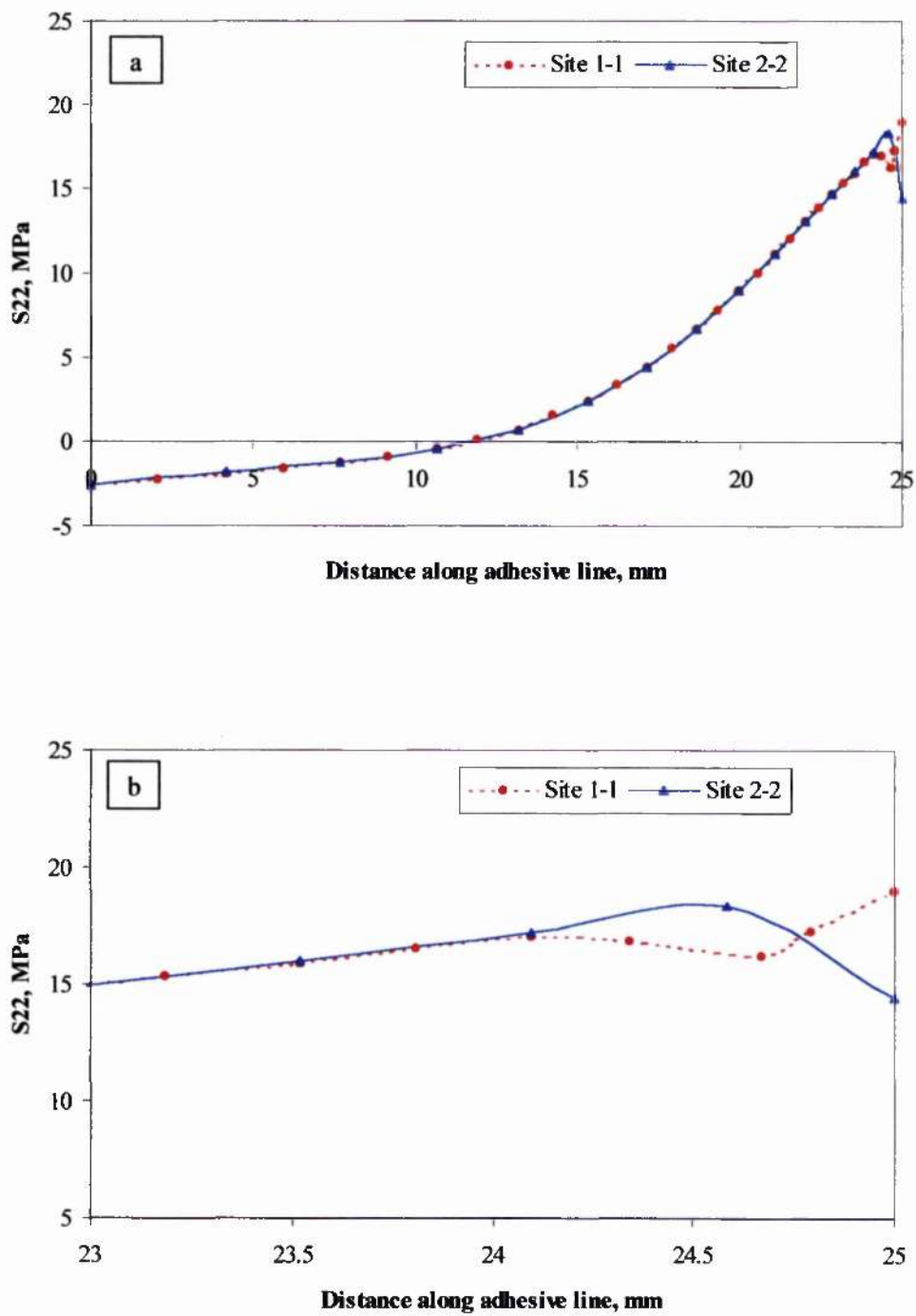


Figure 7.8 Normal tensile stress distribution in adhesive line of Model S (see Fig. 7.4) (a) full length; (b) initial 2mm

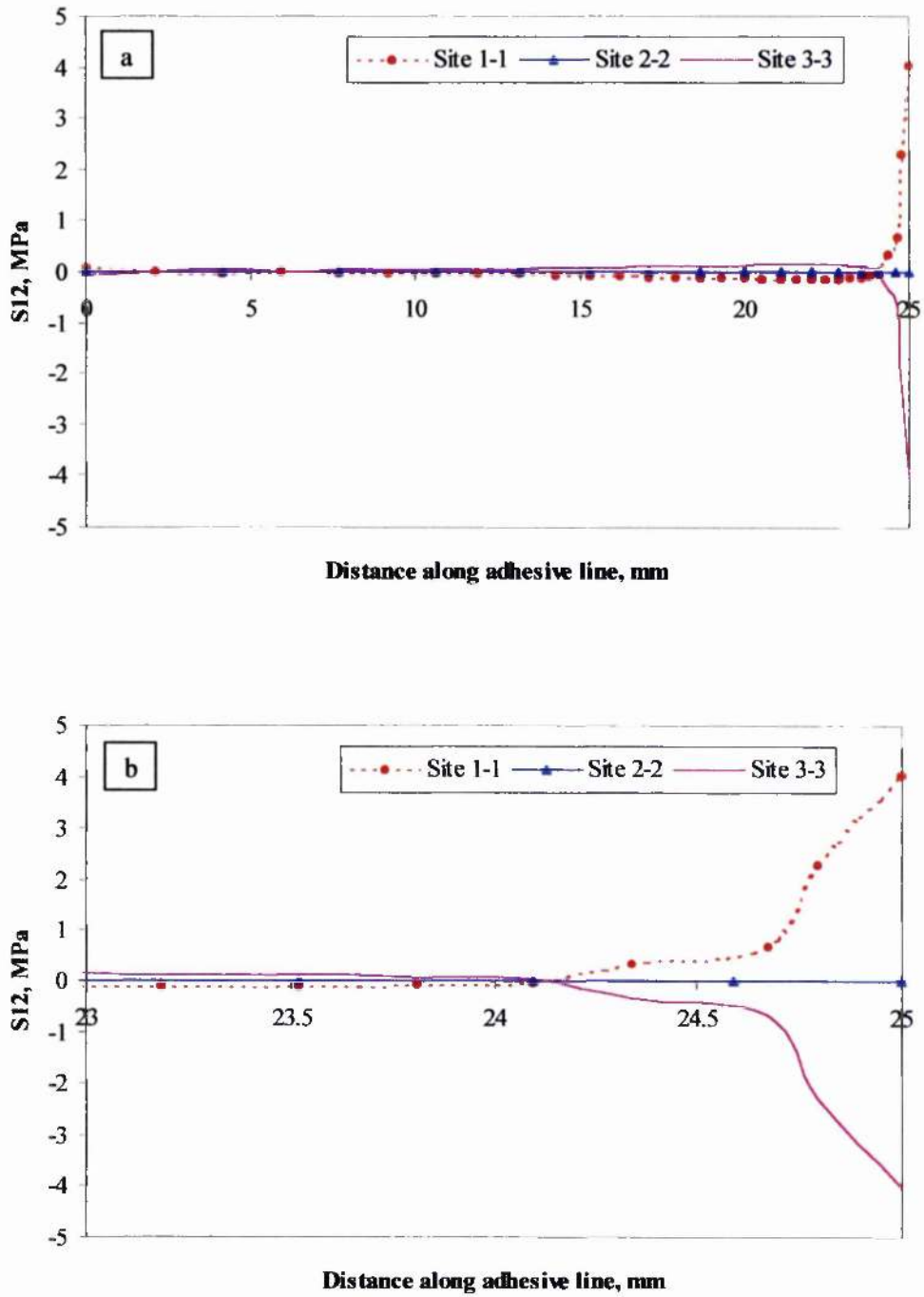


Figure 7.9 Shear stress distribution in adhesive line of Model S (see Fig. 7.4) (a) full length; (b) initial 2mm

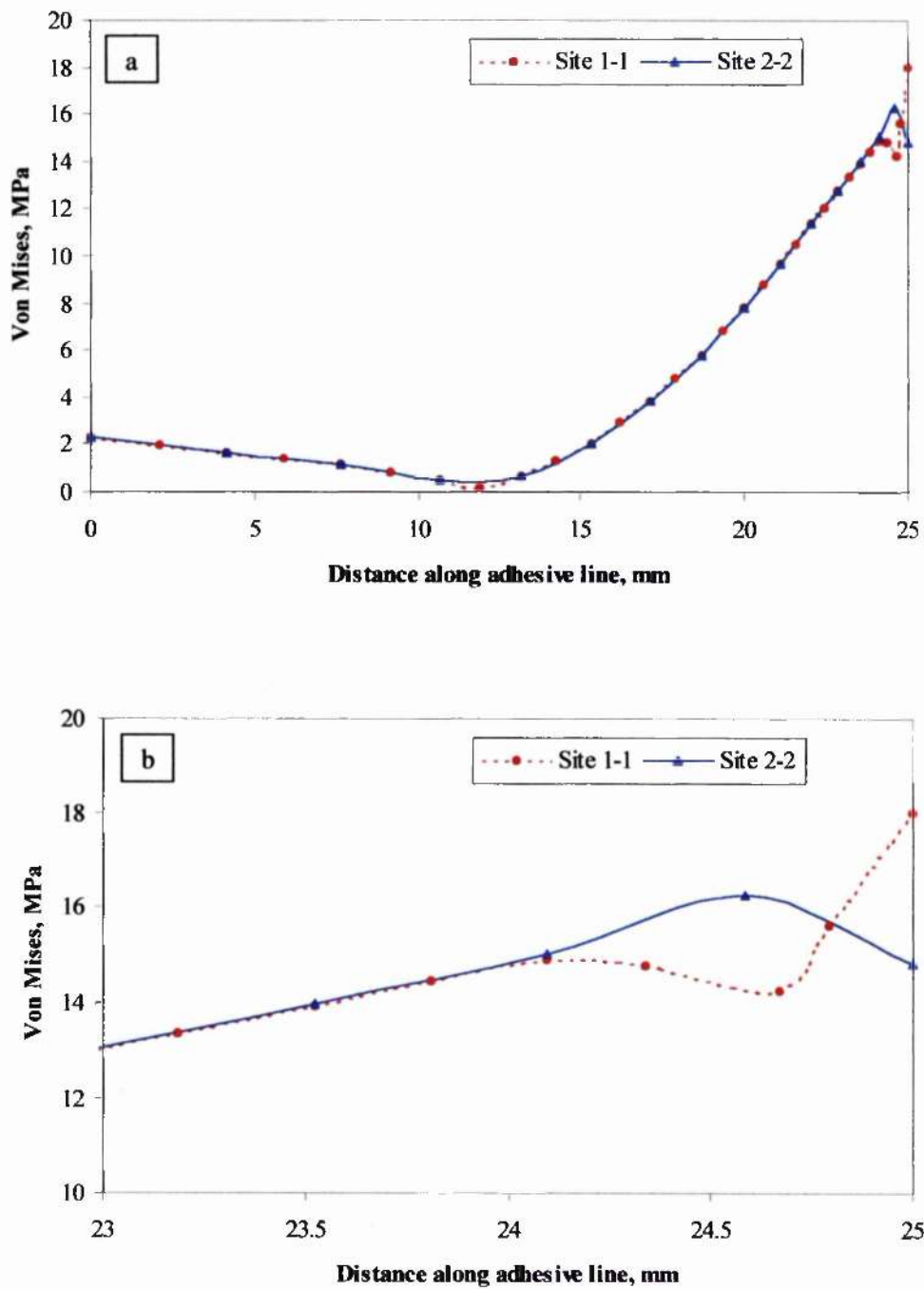


Figure 7.10 Von Mises stress distribution in adhesive line of Model S (see Fig. 7.4) (a) full length; (b) initial 2mm

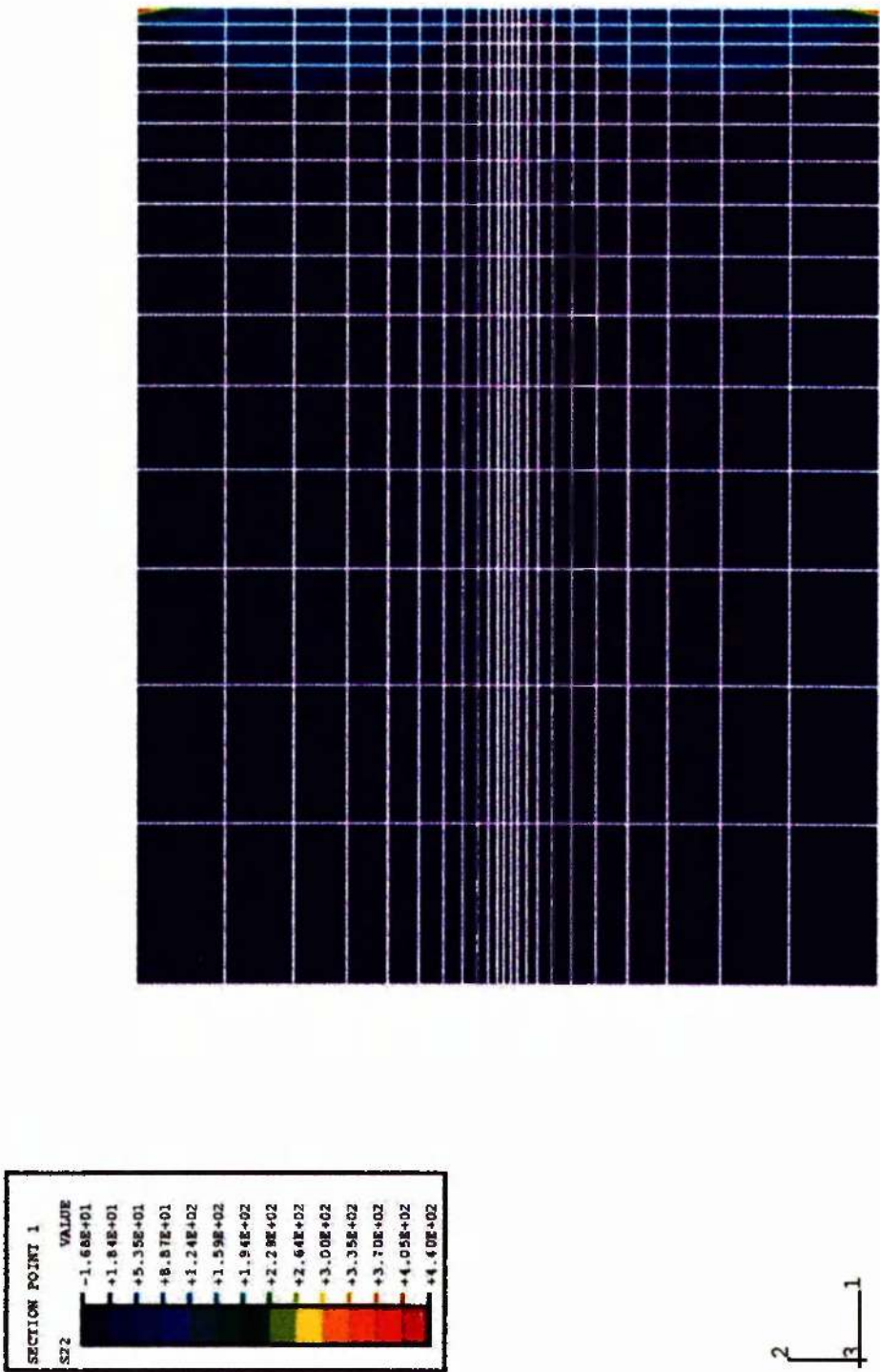


Figure 7.11 Contour plot of normal stress ( $S_{22}$ ) in Model S

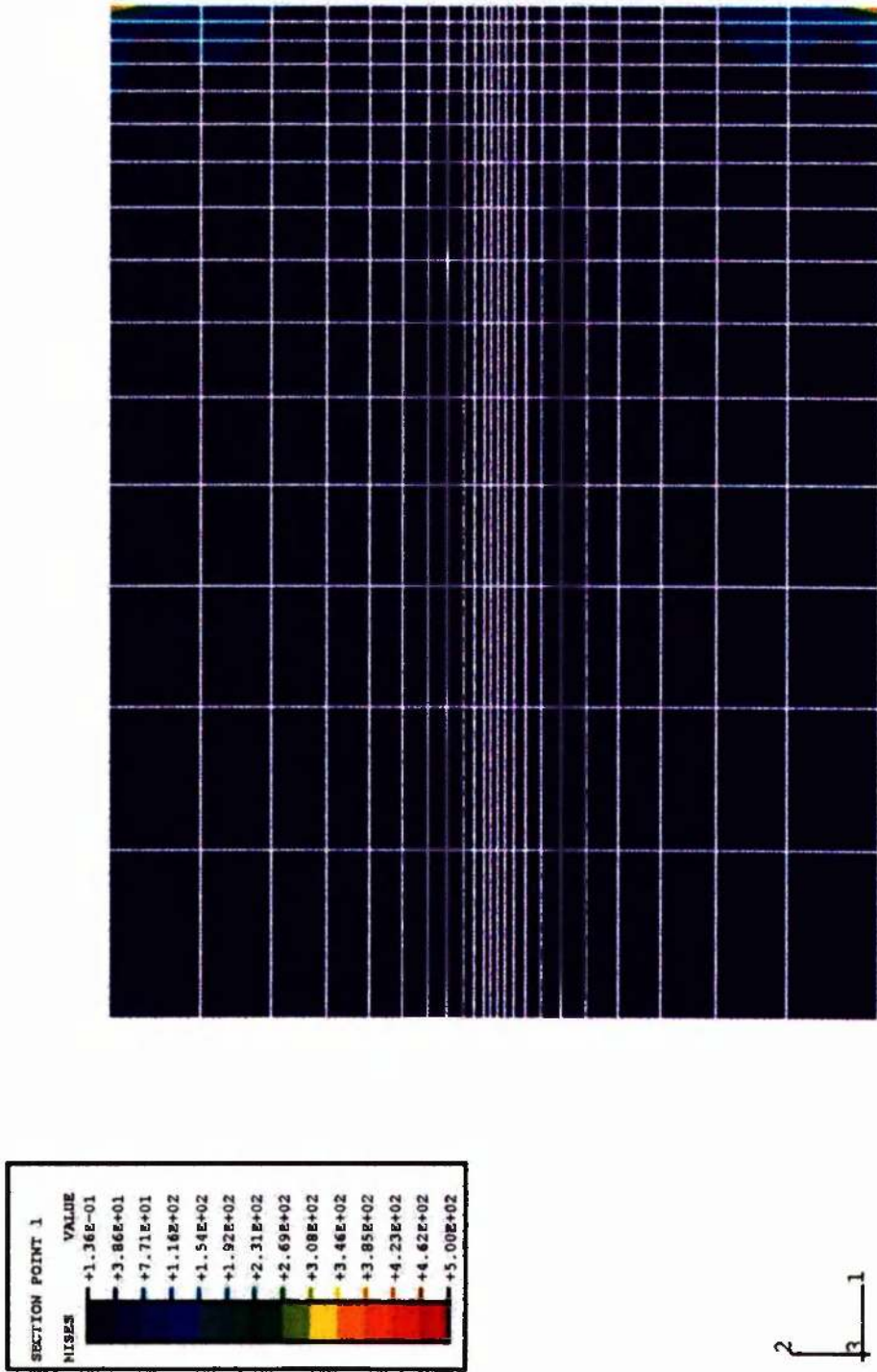


Figure 7.12 Contour plot of von Mises in Model S

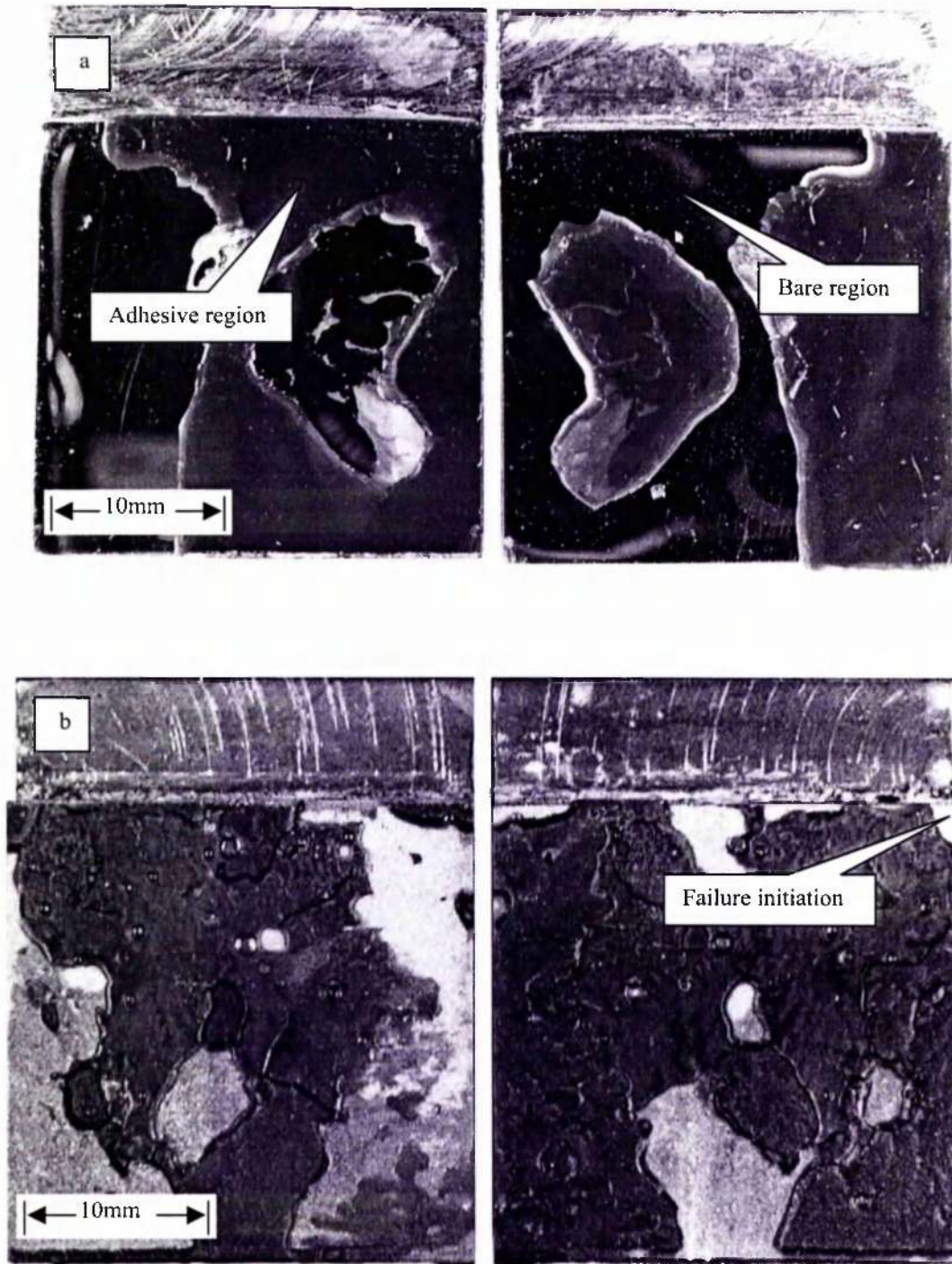


Figure 7.13 Fractured surfaces of steel/steel cleavage specimen showing failure initiation at the surface (a) polished steel; (b) grit blasted steel

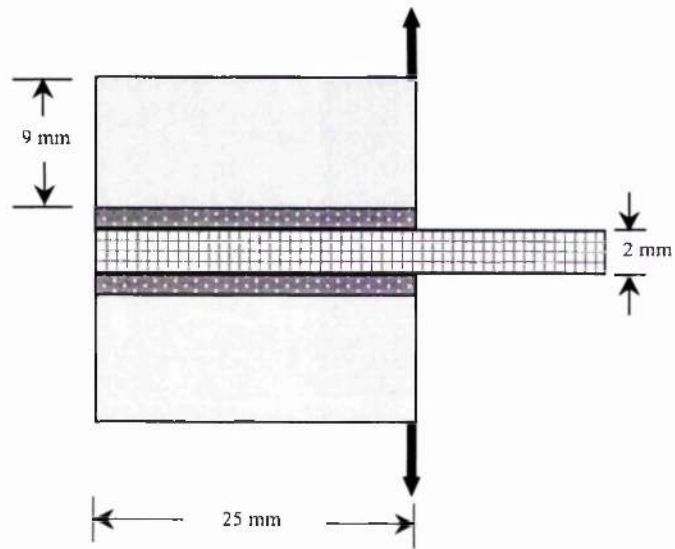


Figure 7.14 Modified hybrid cleavage specimen (Model H)

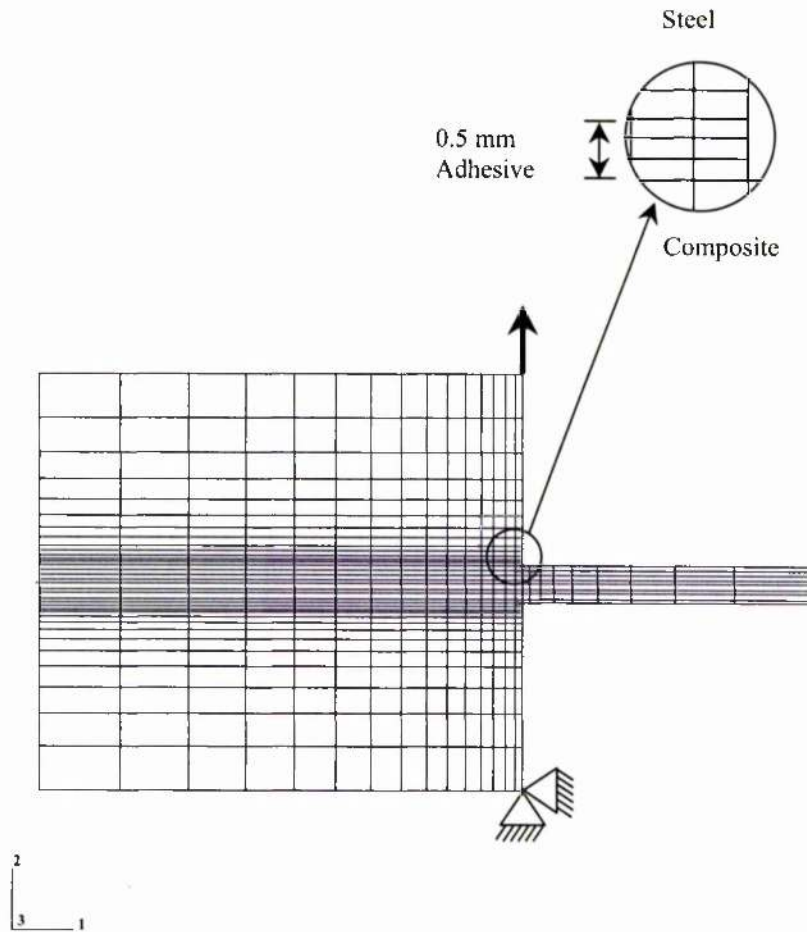


Figure 7.15 Finite element model (Model H)

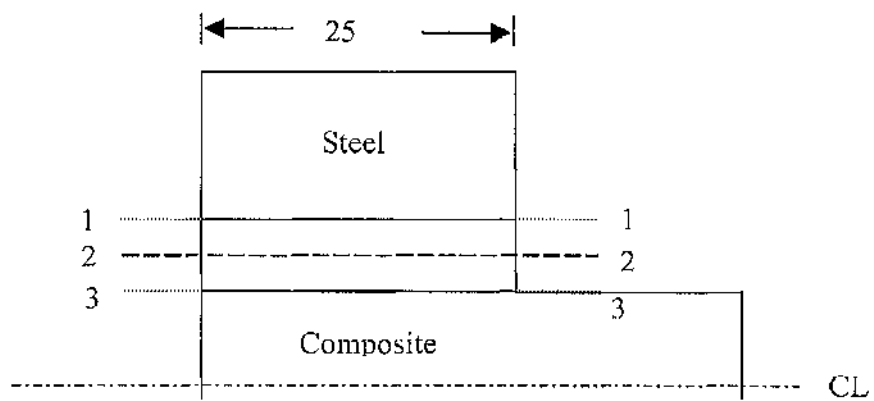


Figure 7.16 Possible failure sites in Model H

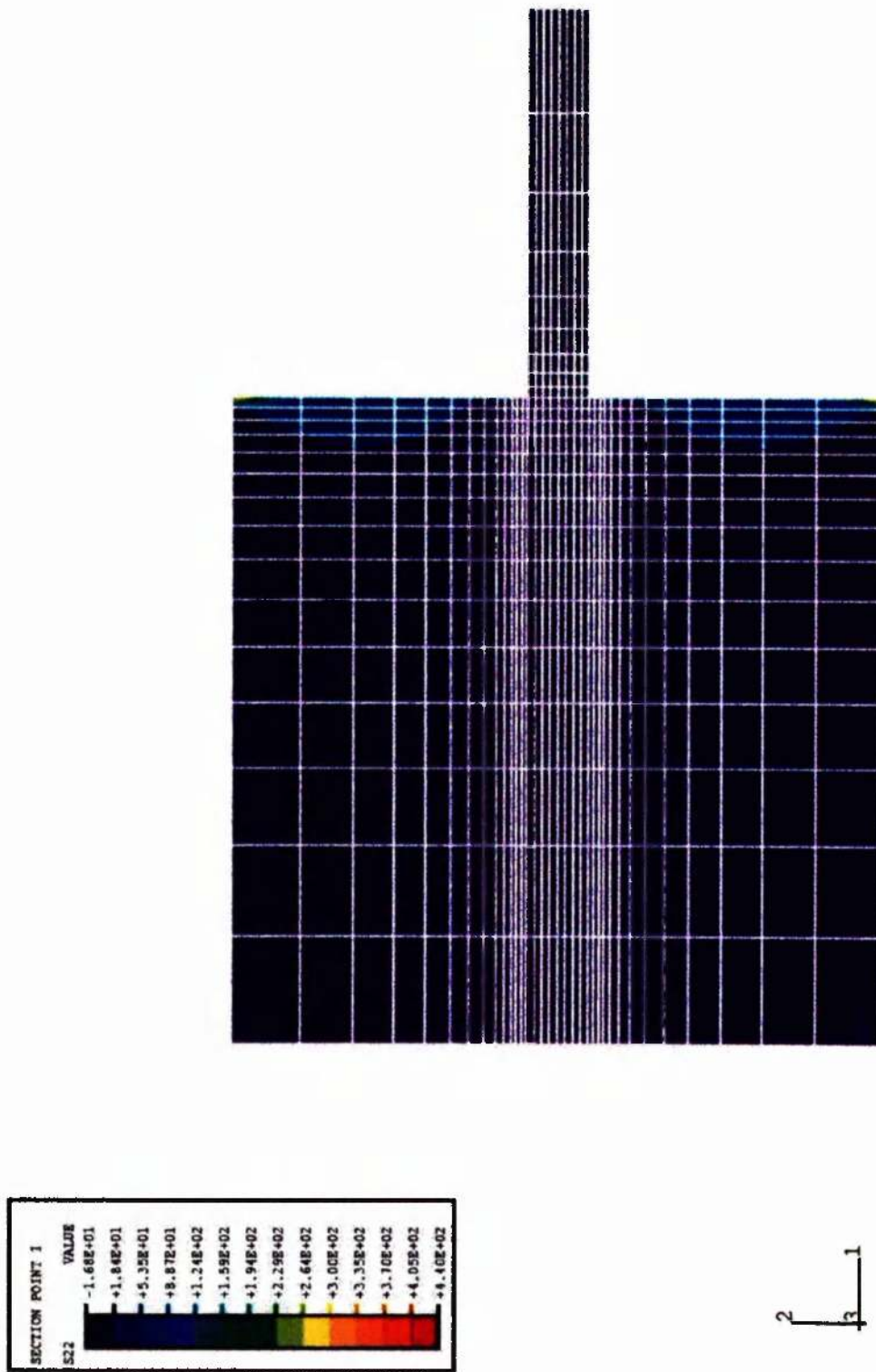


Figure 7.17 Contour plot of normal stress ( $S_{22}$ ) in Model H

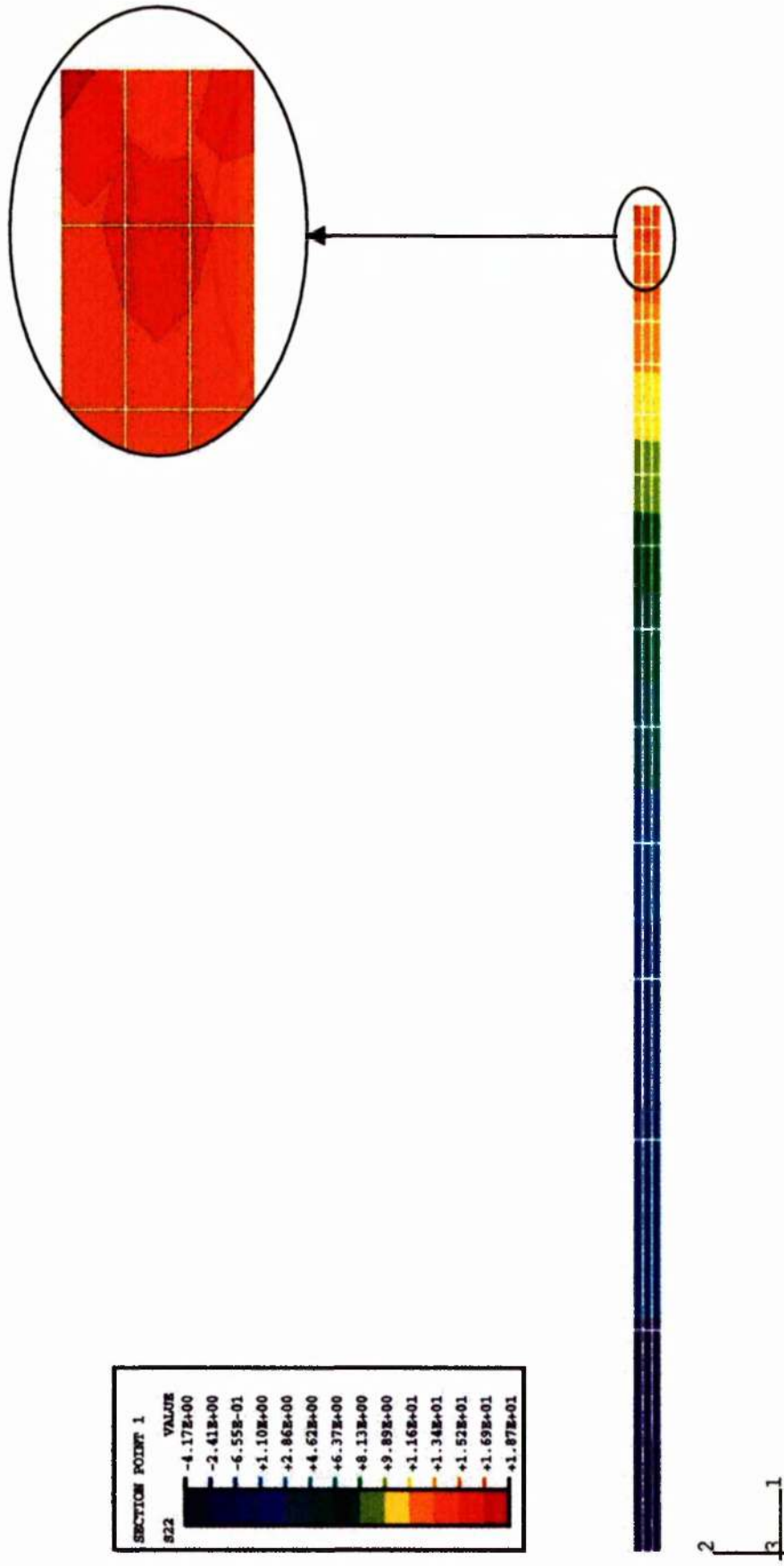


Figure 7.18 Contour plot of normal stress ( $S_{22}$ ) in adhesive line of Model H

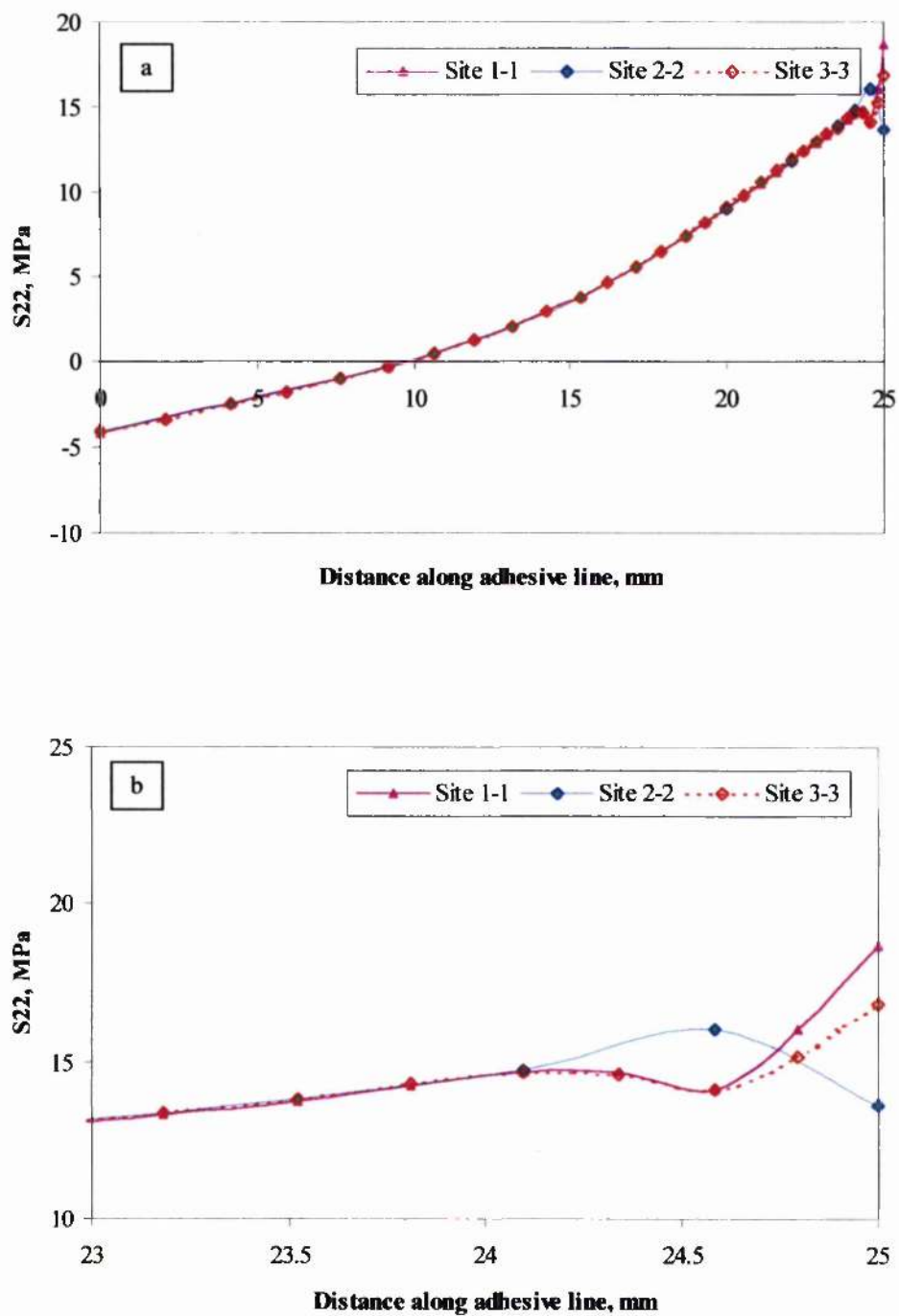


Figure 7.19 Normal stress distribution in adhesive line of Model H (with isotropic laminate properties) (see Fig. 7.16) (a) full length; (b) initial 2mm

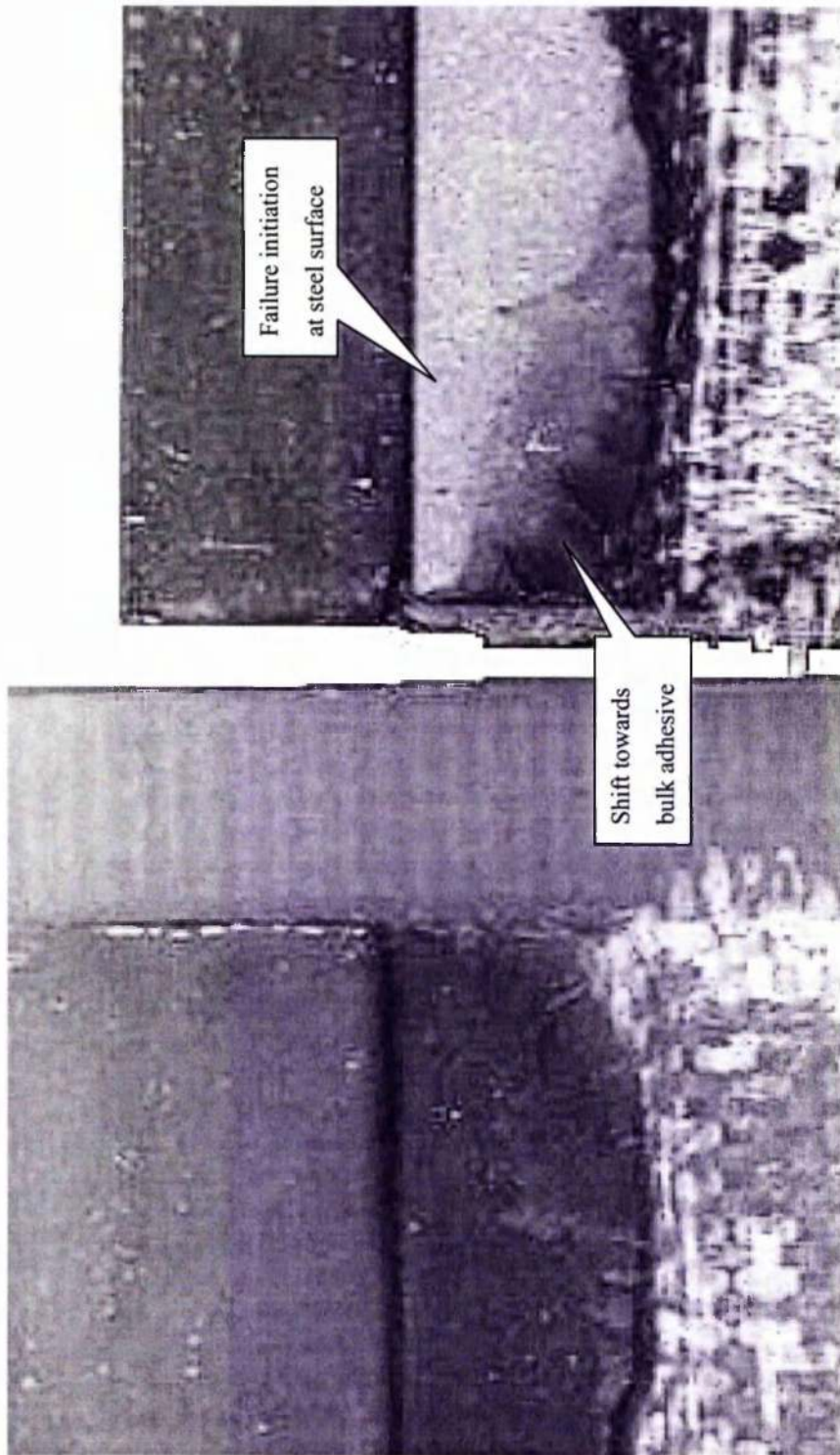


Figure 7.20 Fractured surfaces of hybrid cleavage specimen showing failure initiation at steel surface and then apparent shift towards bulk adhesive layer

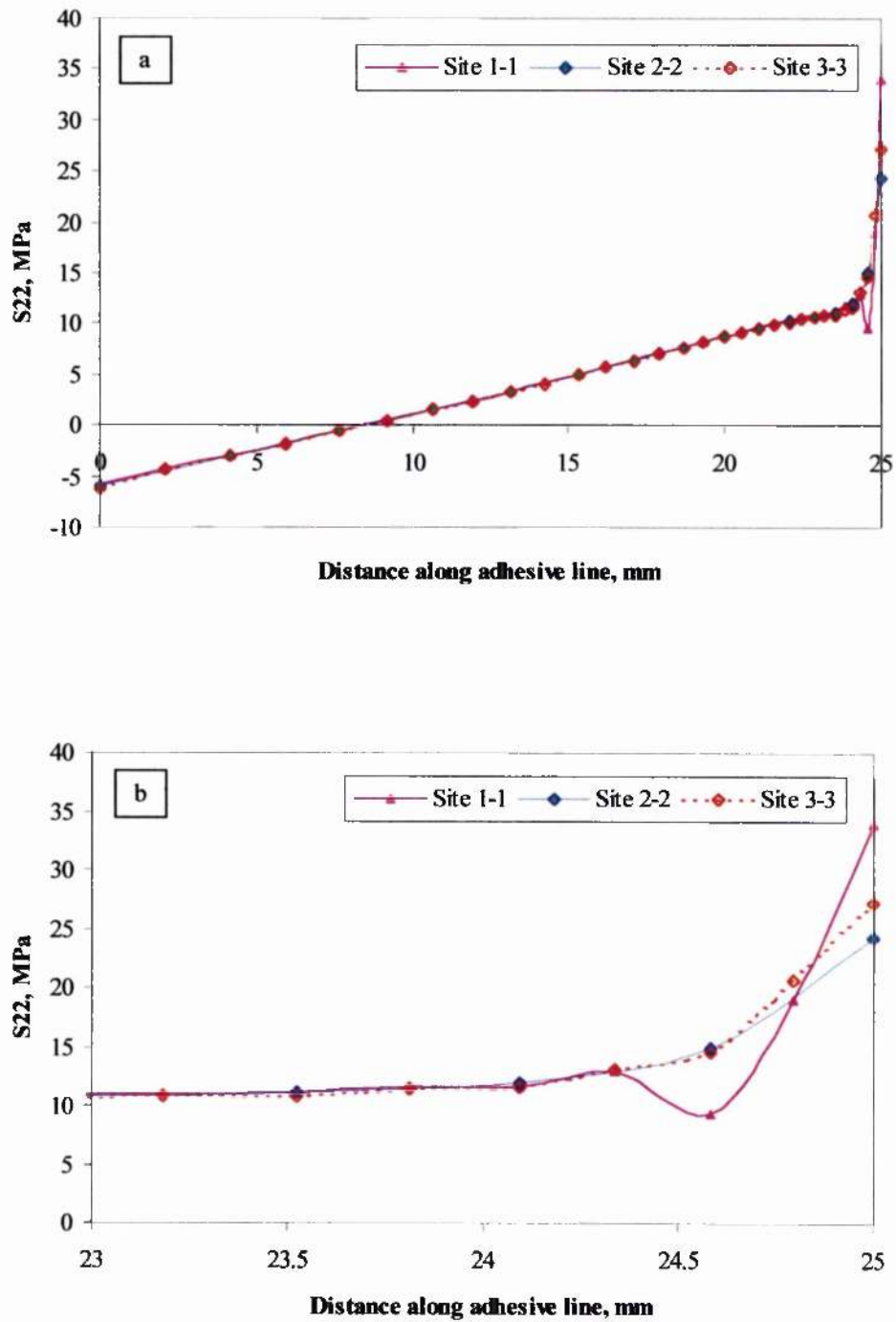


Figure 7.21 Normal stress distribution in the adhesive line of Model H (with orthotropic properties) (see Fig. 7.16) (a) full length; (b) initial 2mm

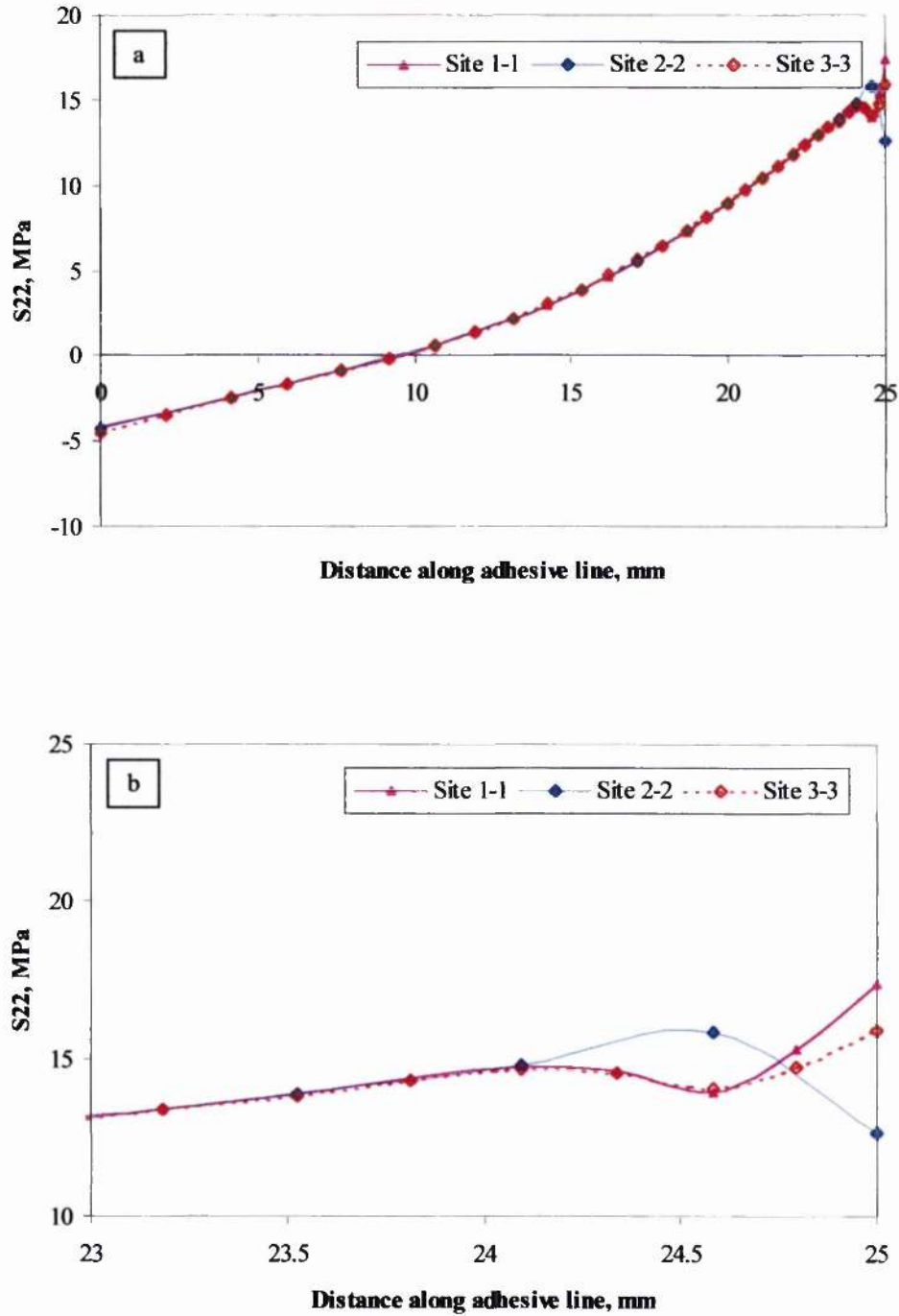


Figure 7.22 Tensile stress ( $S_{22}$ ) distribution in adhesive line of Model H (with steel insert - see Fig. 7.16) (a) full length; (b) initial 2mm

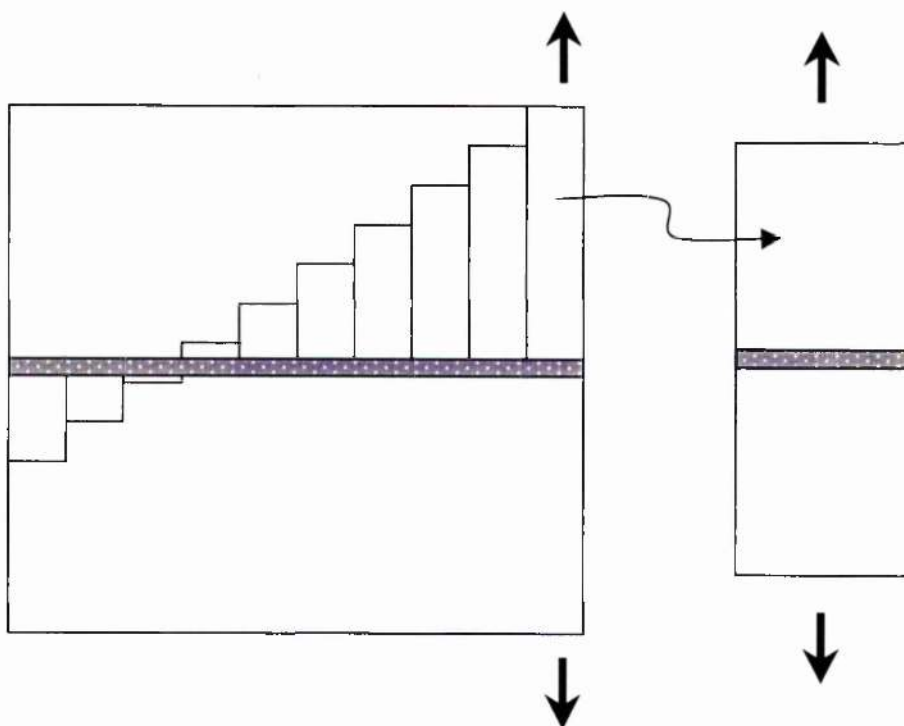


Figure 7.23 Representation of cleavage joint as multiple butt joints

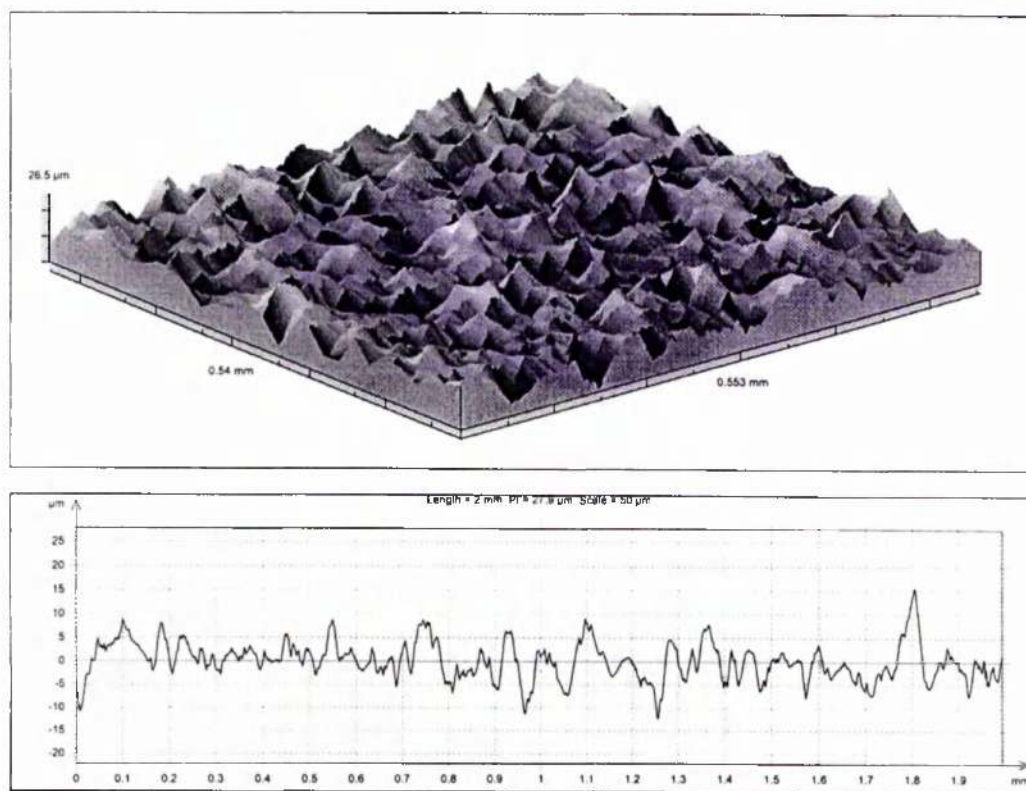


Figure 7.24 Actual surface profile of grit-blasted surface as seen by Talysurf

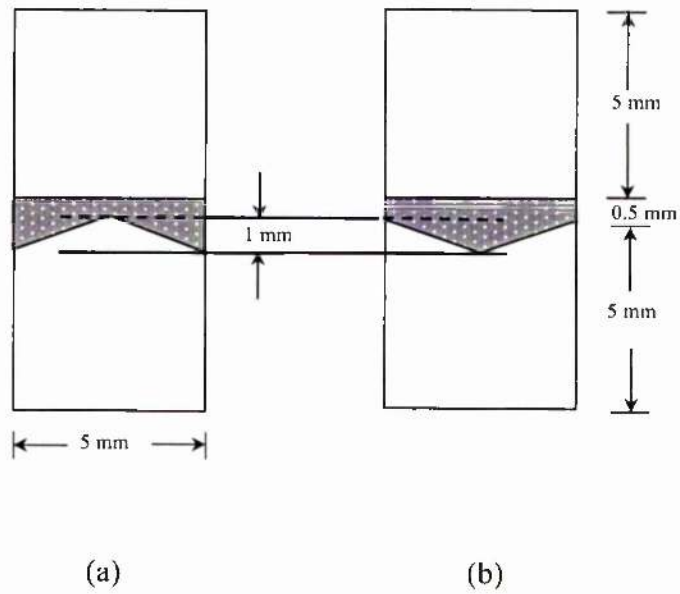


Figure 7.25 Schematic diagram of the roughness models (a) Model P1; (b) Model P2

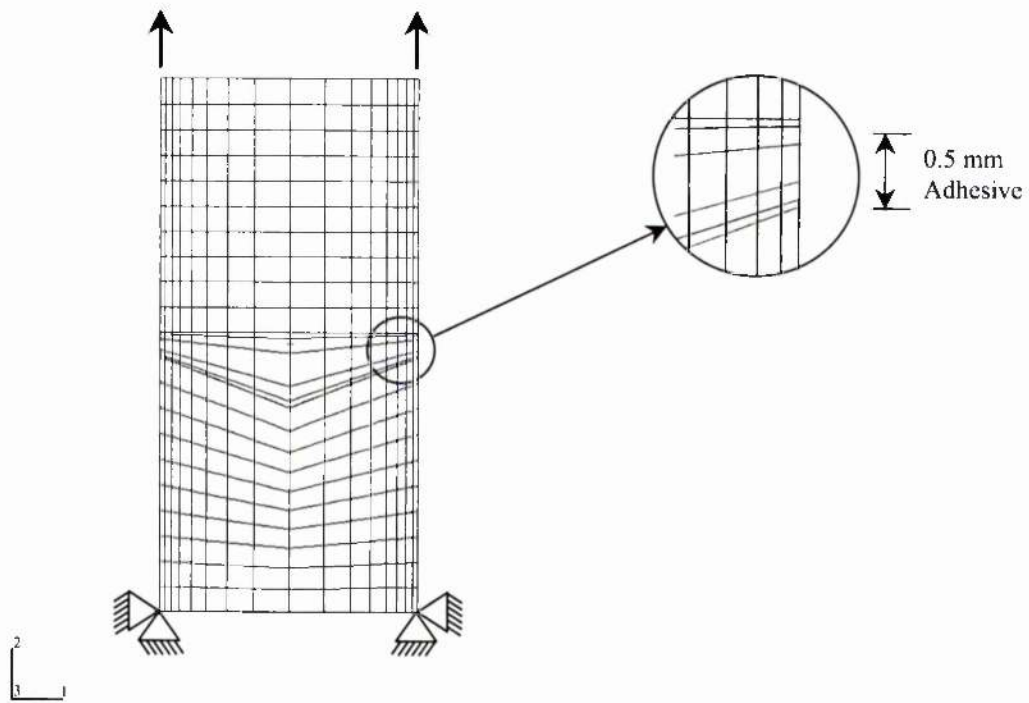


Figure 7.26 Numerical model of the surface roughness (Model P2)

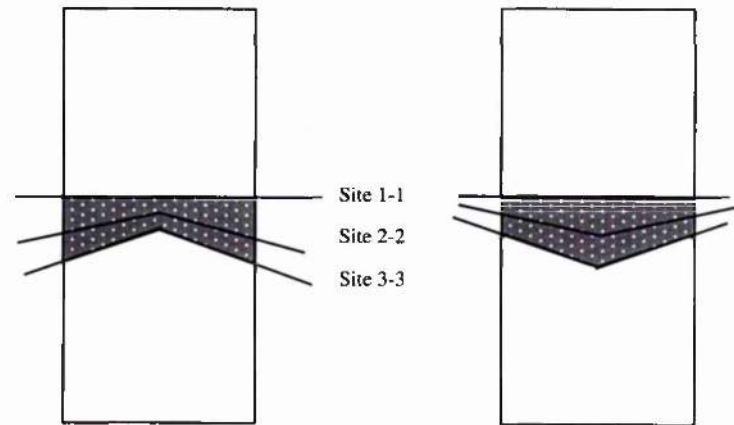


Figure 7.27 Possible failure sites in the roughness models (Models P1 and P2)

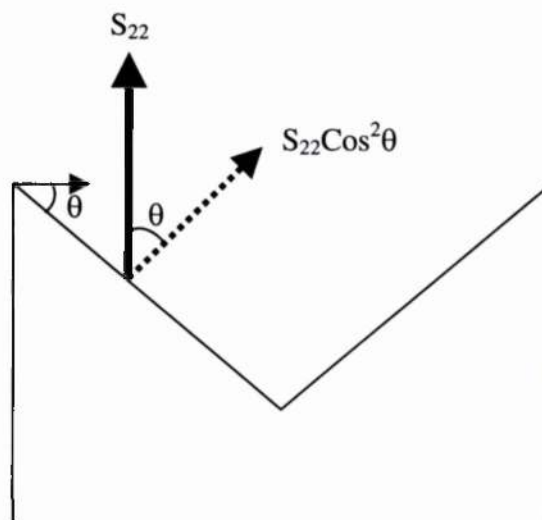


Figure 7.28 Transformation of normal stress at the rough surface

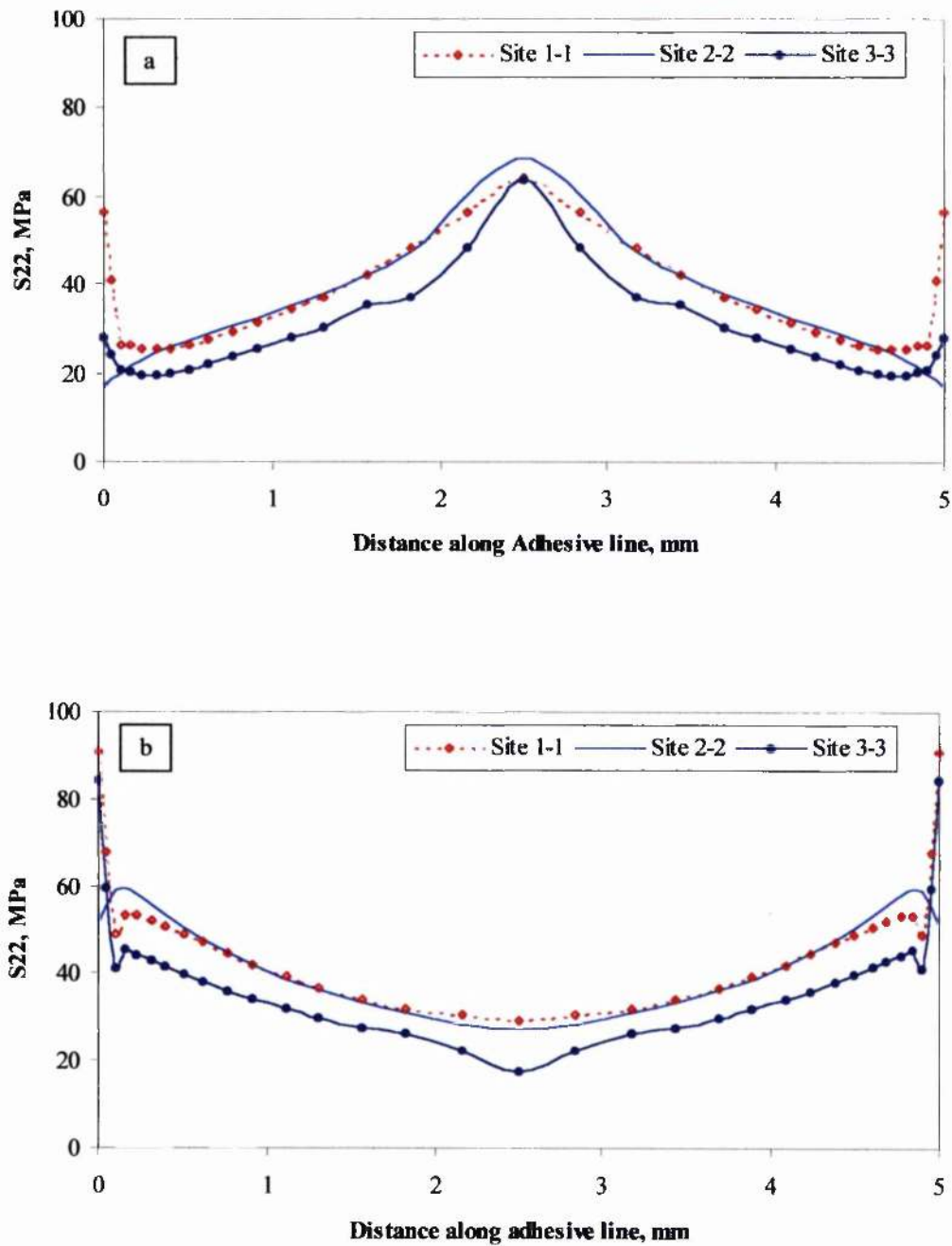


Figure 7.29 Normal stress distribution in adhesive line (see Figure 7.27) (a) Model P1; (b) Model P2

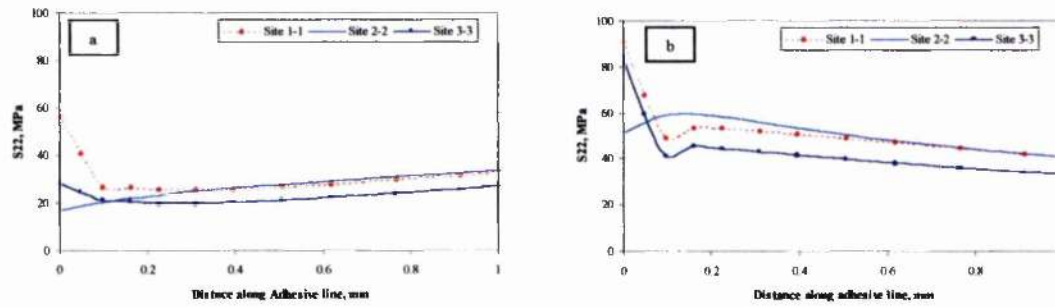


Figure 7.30 Normal stress distribution in the first millimetre of adhesive line (a) Model P1; (b) Model P2

Table A Comparison of stresses in roughness models (Models P1 and P2)

Node	Site	Stress (MPa)		Average stress (MPa)	Stress Increase due to roughness (%)
		Model P1	Model P2		
1st	1-1	56.43	91.08	73.76	31.5
	3-3	28.02	84.15		
2nd	1-1	40.86	67.52	54.19	29.4
	3-3	24.31	59.45		

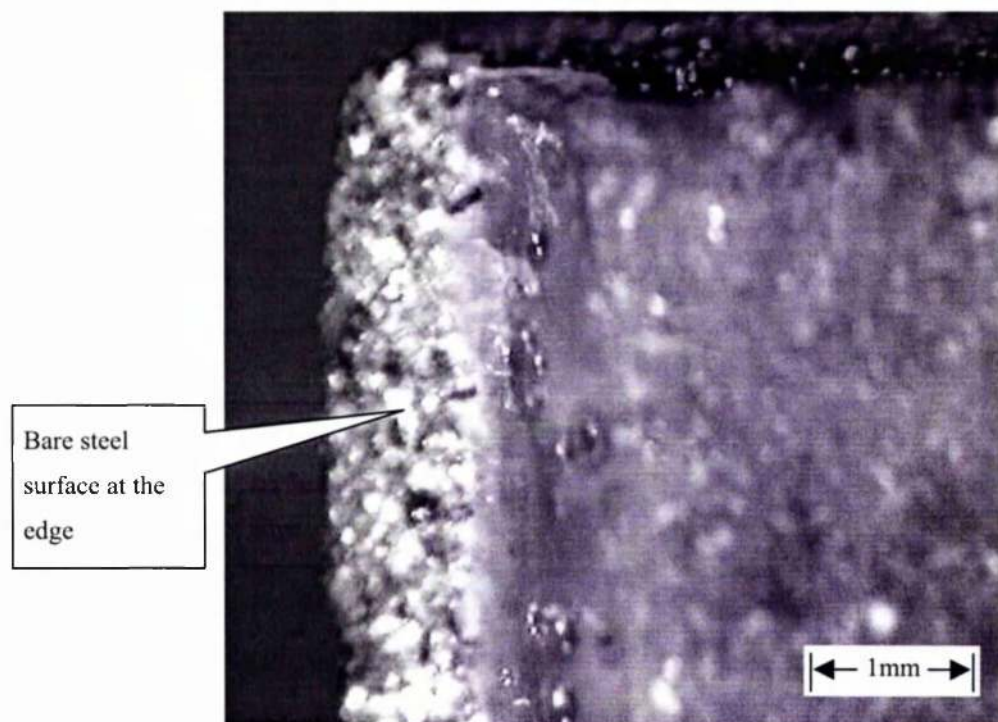


Figure 7.31 Fractured surface of grit-blasted cleavage joint showing failure initiation at the loaded edge

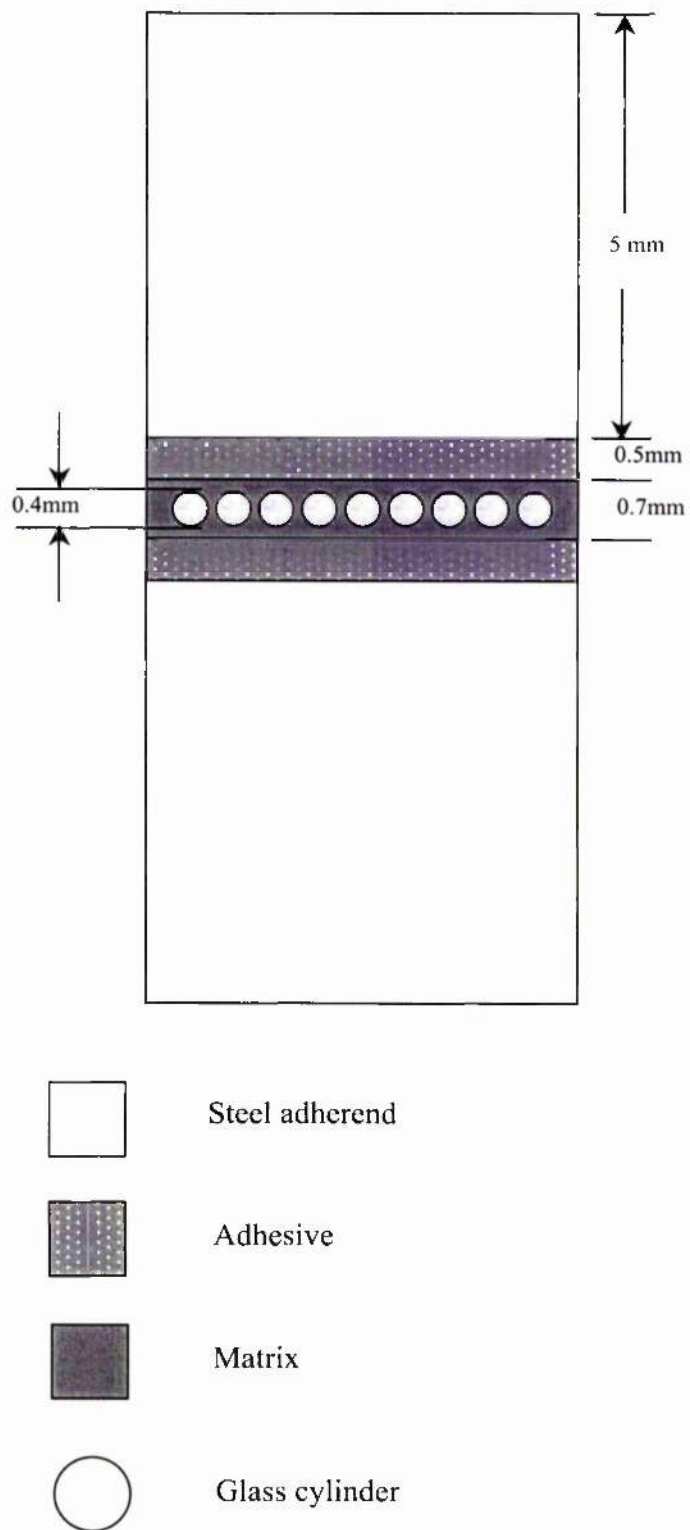


Figure 7.32 Details of partial hybrid model (Model P3)

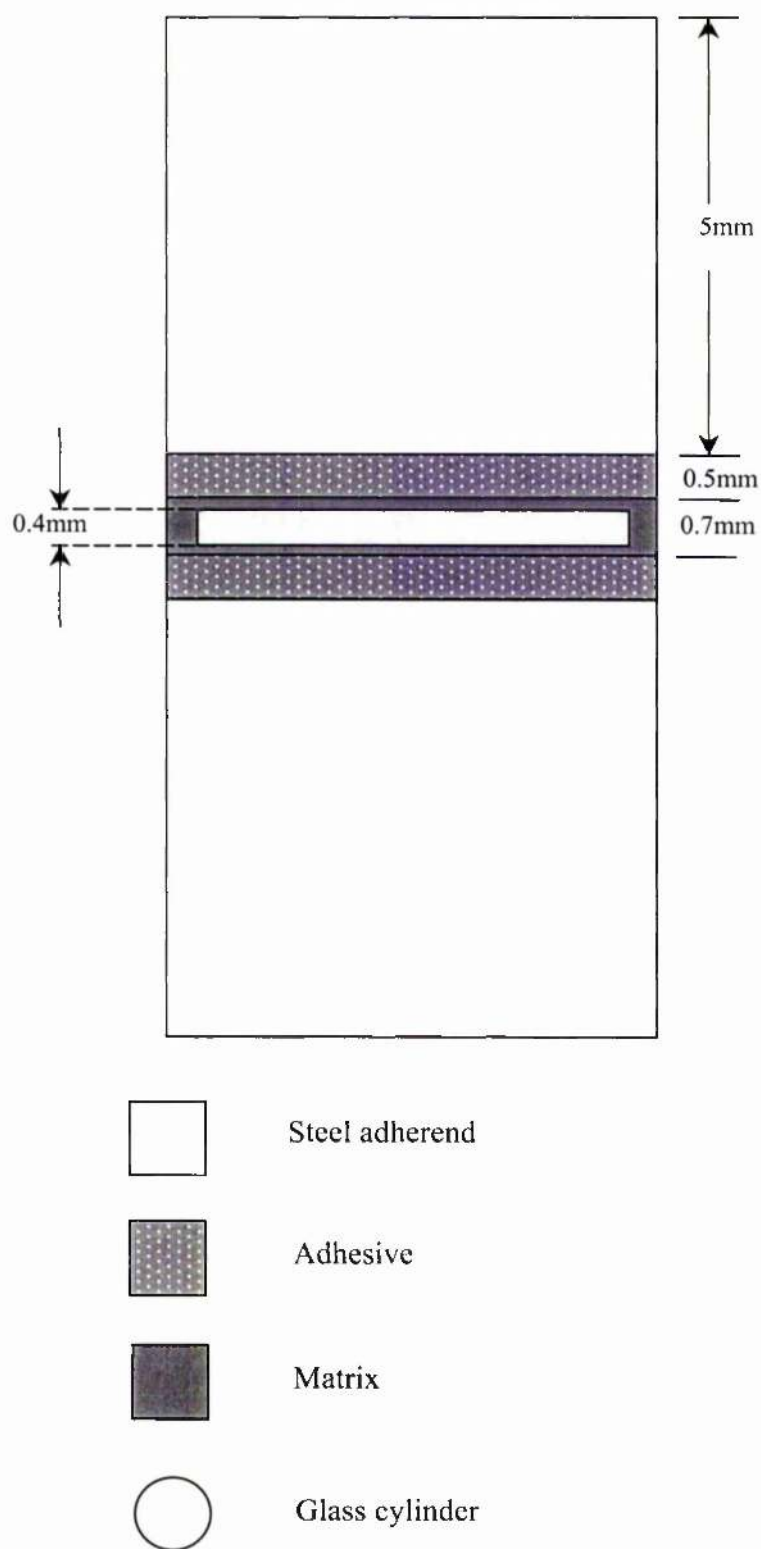


Figure 7.33 Schematic diagram of partial hybrid model (Model P4)

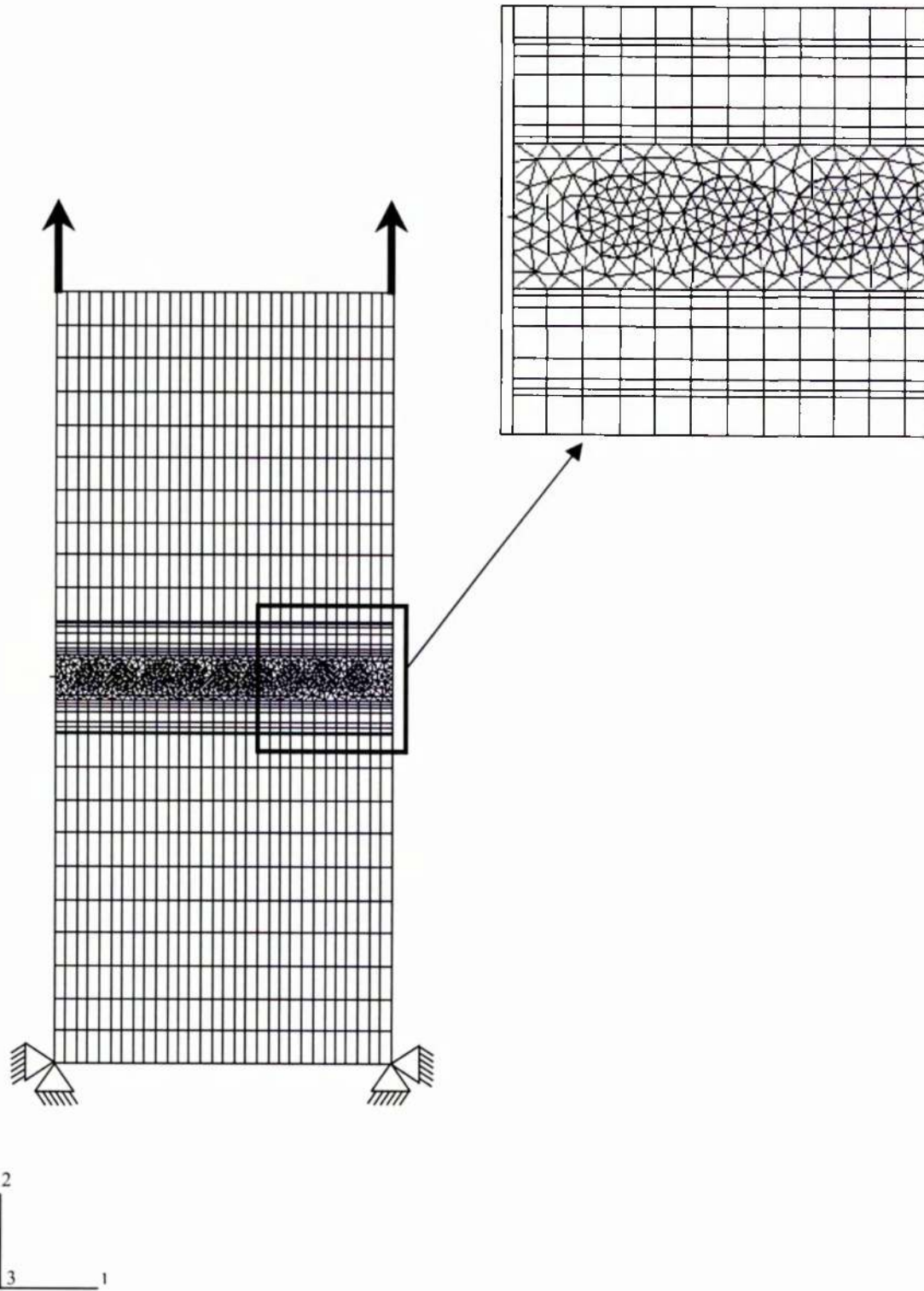


Figure 7.34 Model P3 (Numerical model)

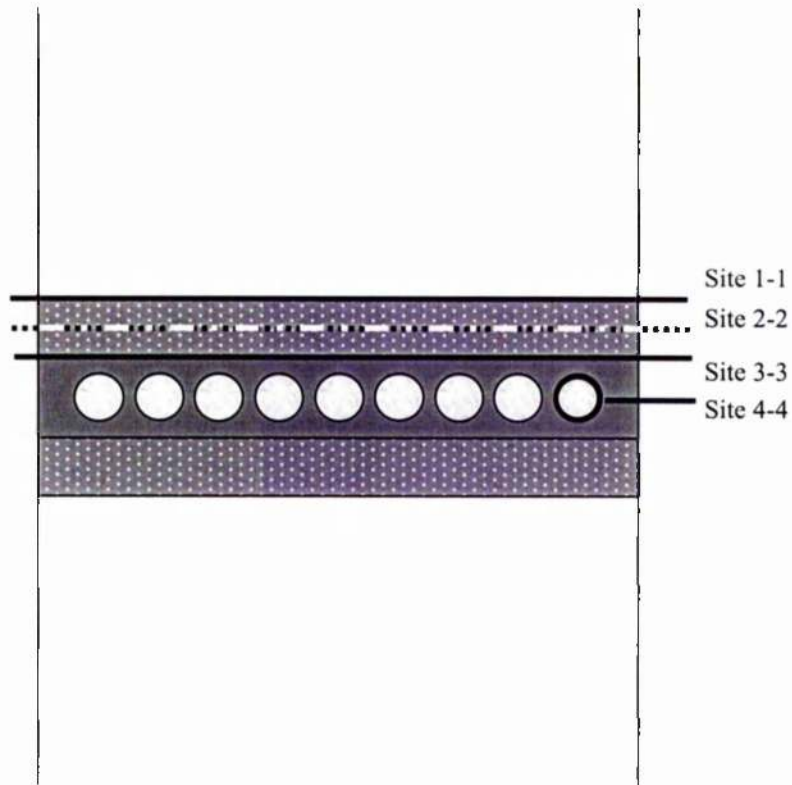


Figure 7.35 Possible failure sites in Model P3

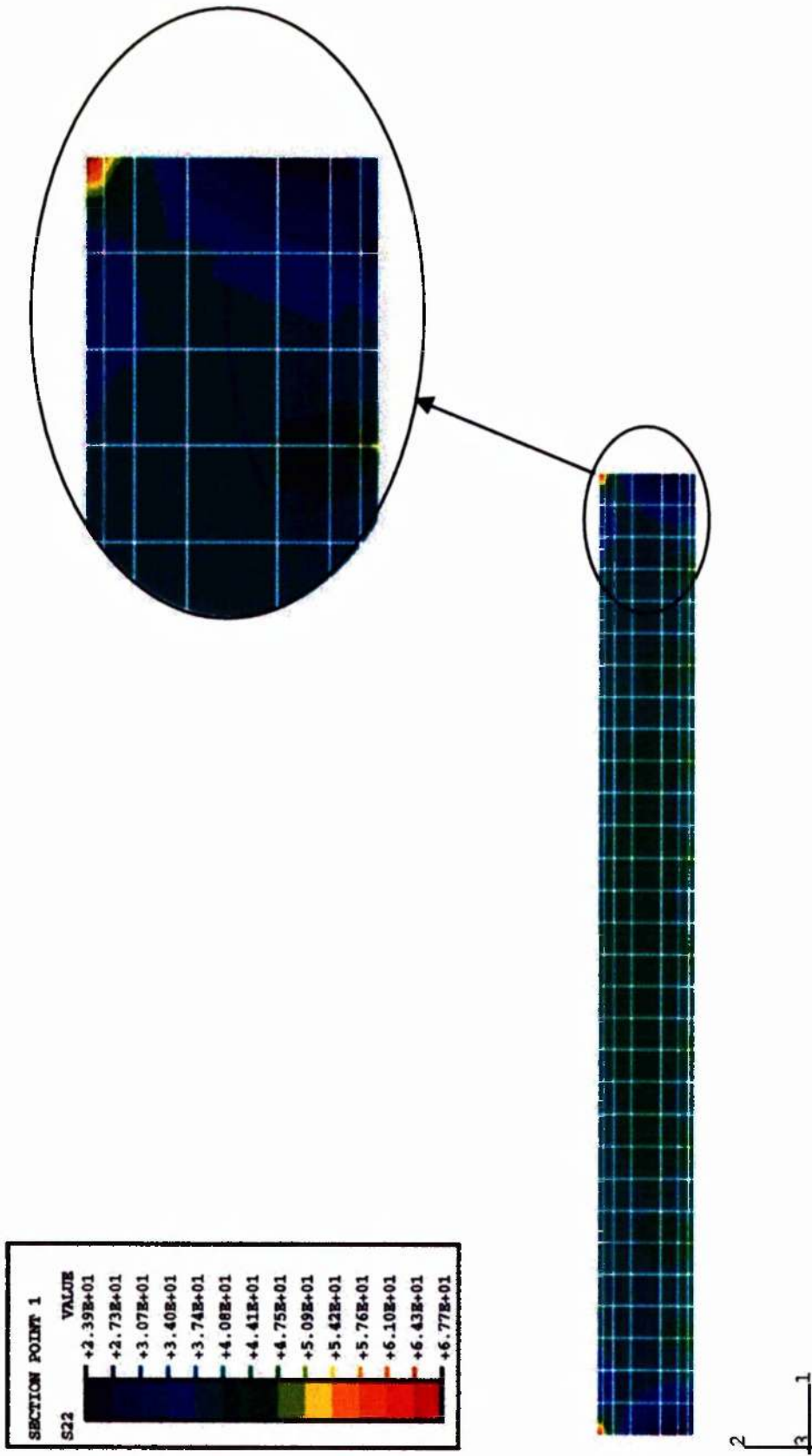


Figure 7.36 Contour plot of normal stress ( $S_{22}$ ) in the adhesive line of Model P3

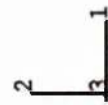
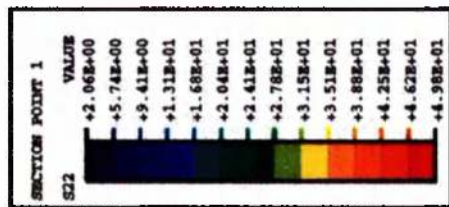


Figure 7.37 Contour plot of normal stress ( $S_{22}$ ) in the laminate matrix of Model P3

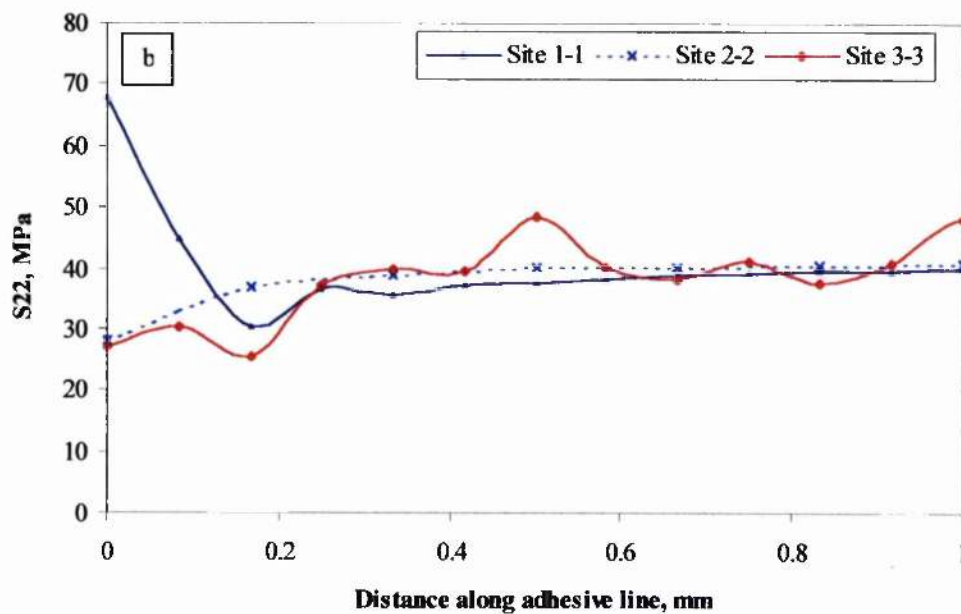
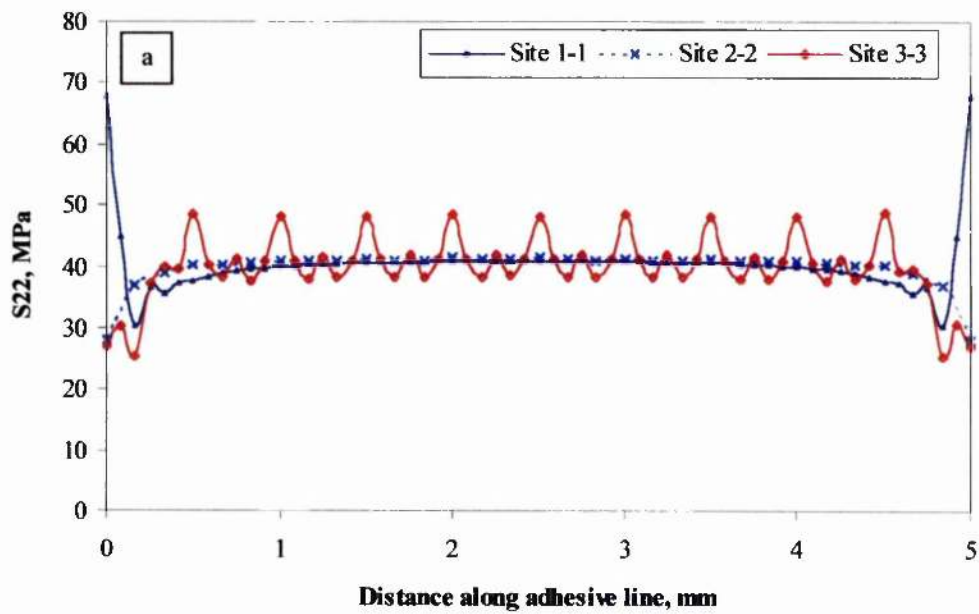


Figure 7.38 Normal stress ( $S_{22}$ ) distribution in adhesive line of Model P3 (see Fig. 7.35) (a) full length; (b) initial 1mm

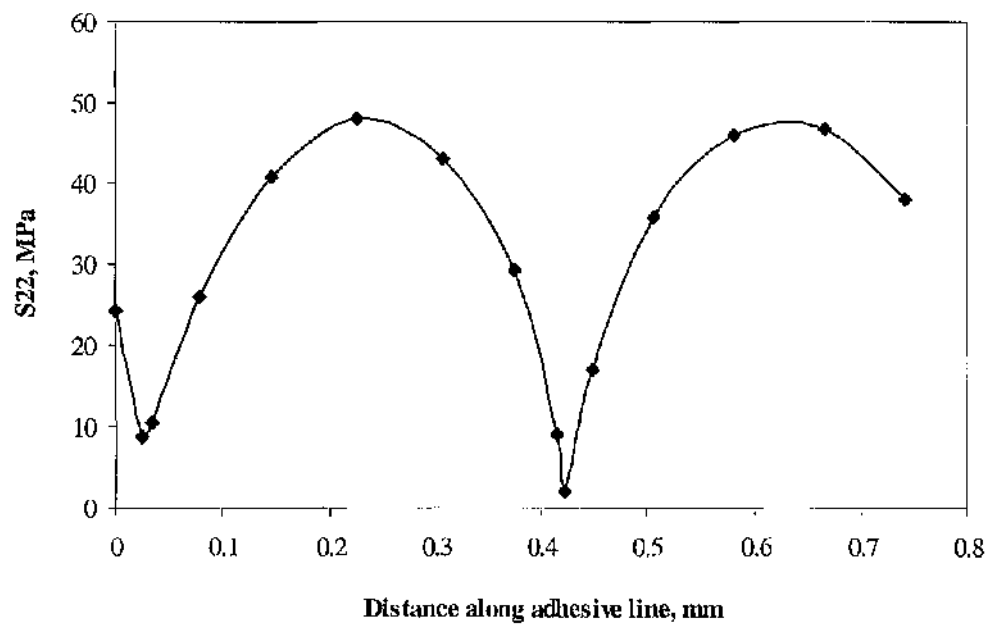


Figure 7.39 Normal stress ( $S_{22}$ ) distribution at the glass cylinder surface in Model P3

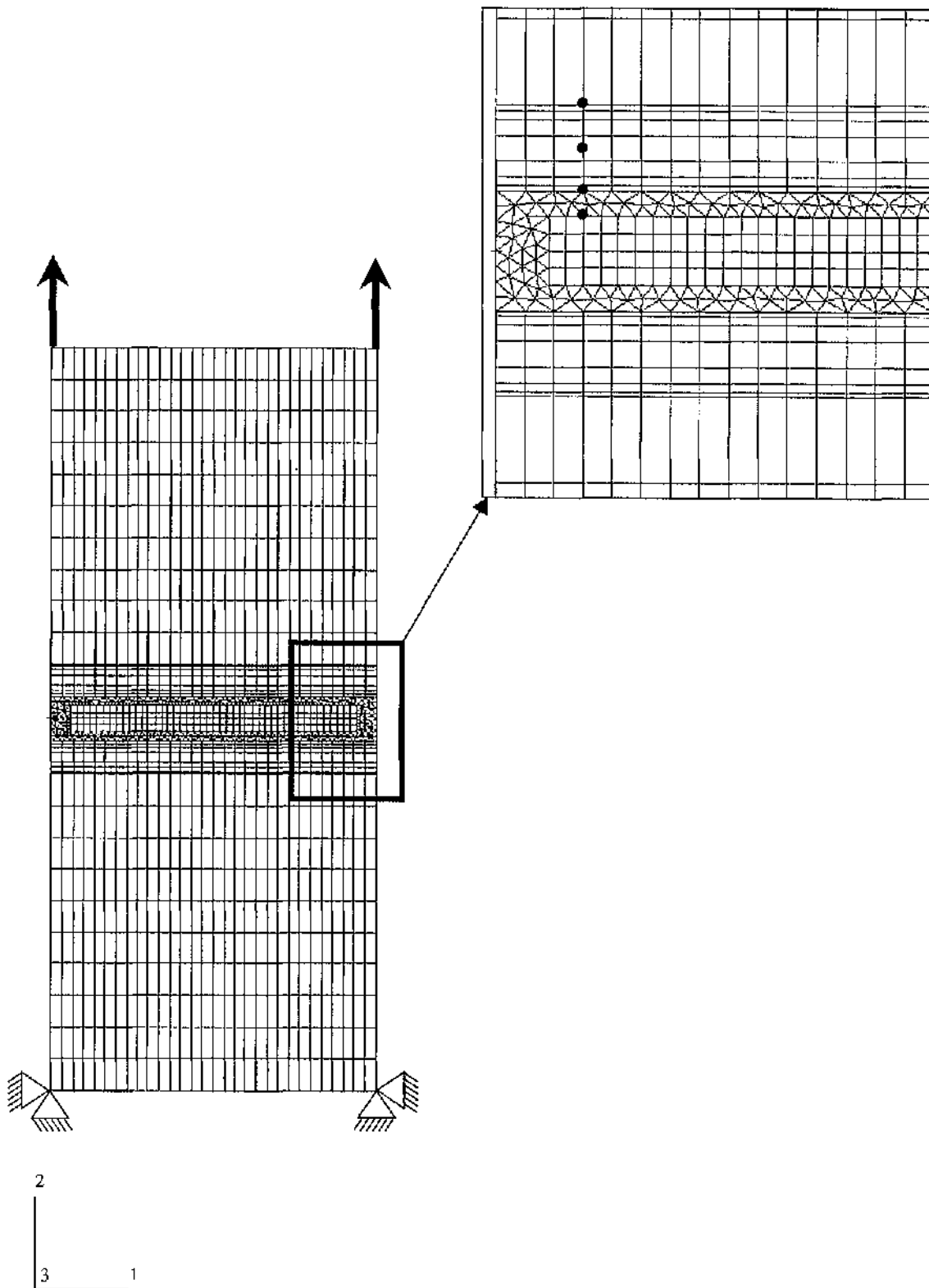


Figure 7.40 Model P4 (Black spots showing first matching nodes)

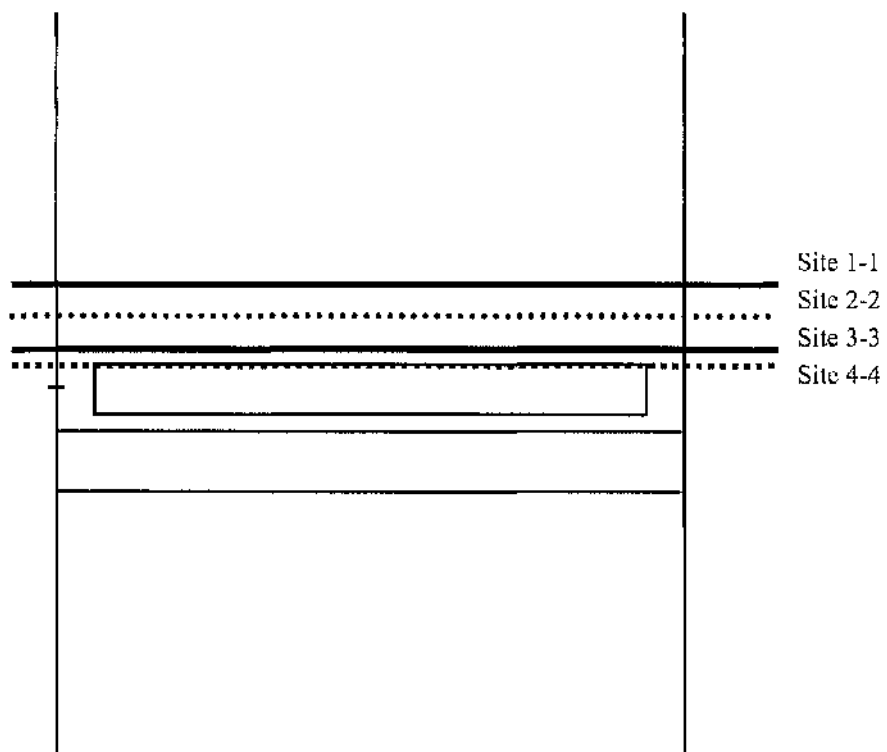


Figure 7.41 Possible failure sites (Model P4)

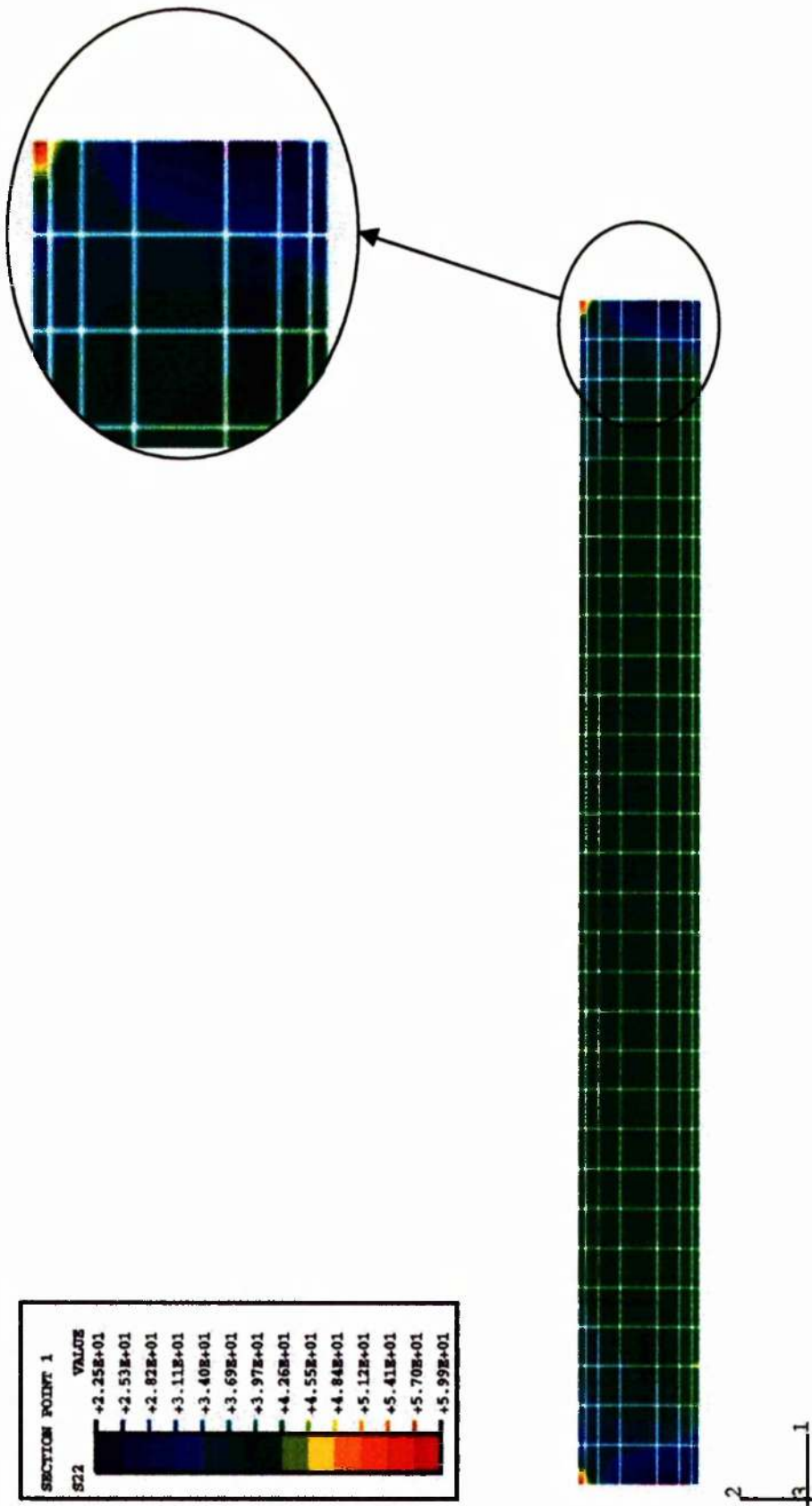


Figure 7.42 Contour plot of normal stress ( $S_{22}$ ) in the adhesive line of Model P4

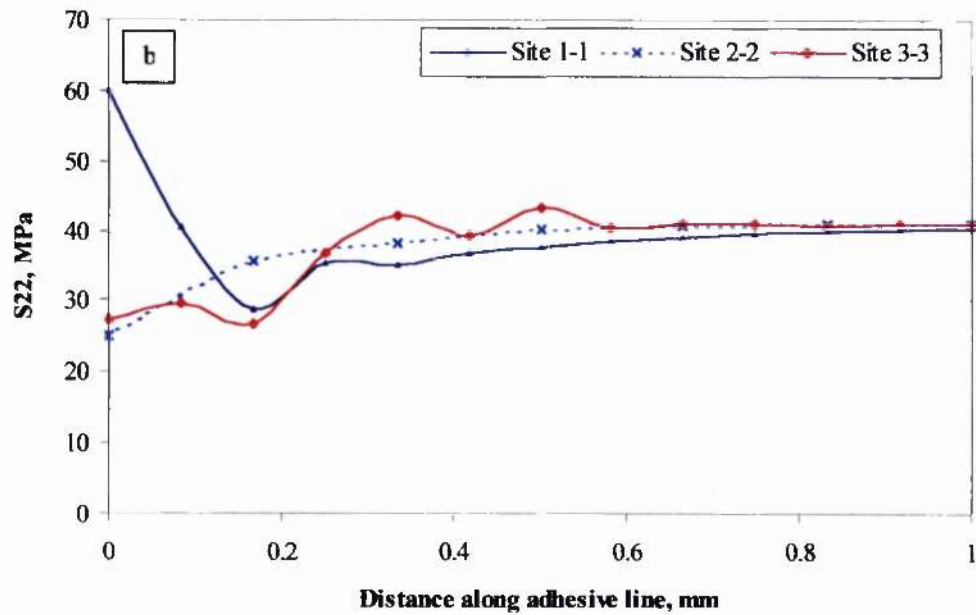
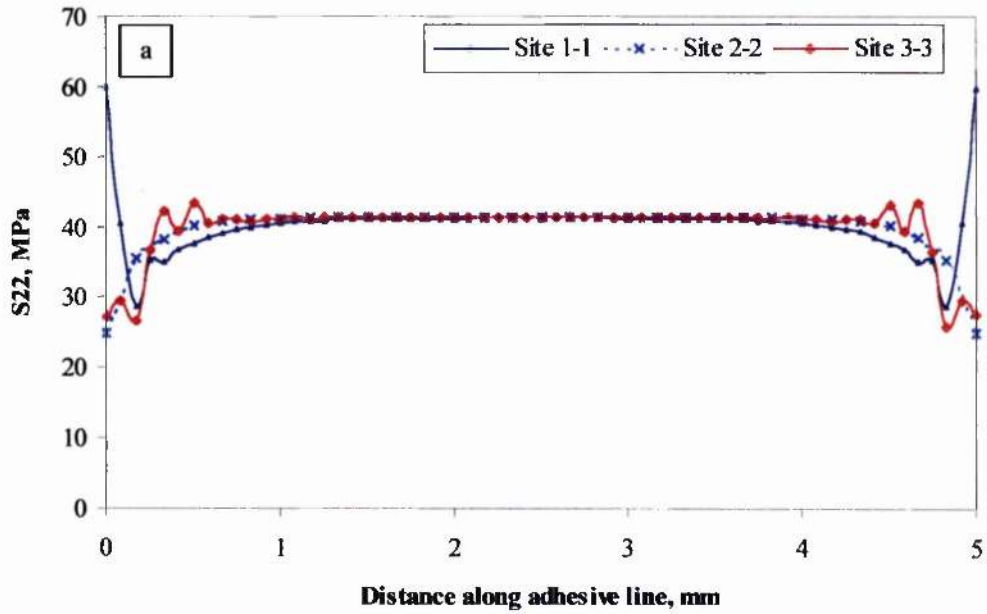


Figure 7.43 Normal stress ( $S_{22}$ ) distribution in adhesive line of Model P4 (see Fig. 7.41) (a) full length; (b) initial 1 mm

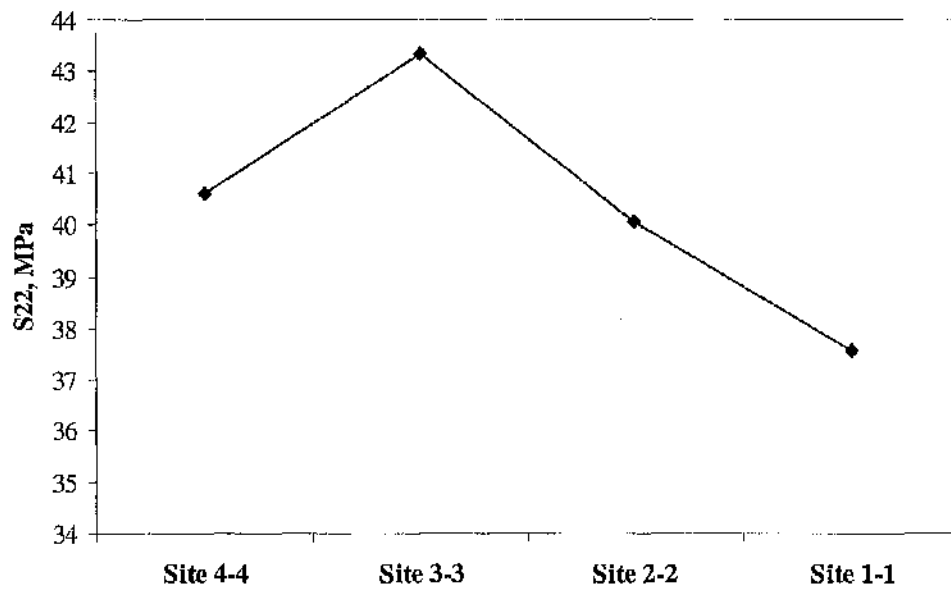


Figure 7.44 Stresses through thickness at first matching nodes in Model P4 (see Figures 7.40 and 7.41)

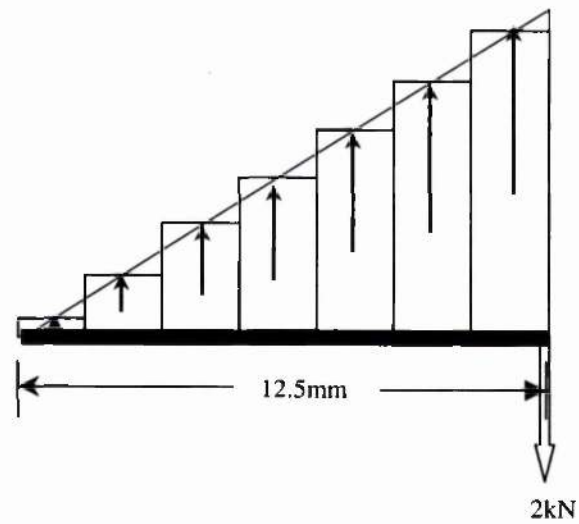
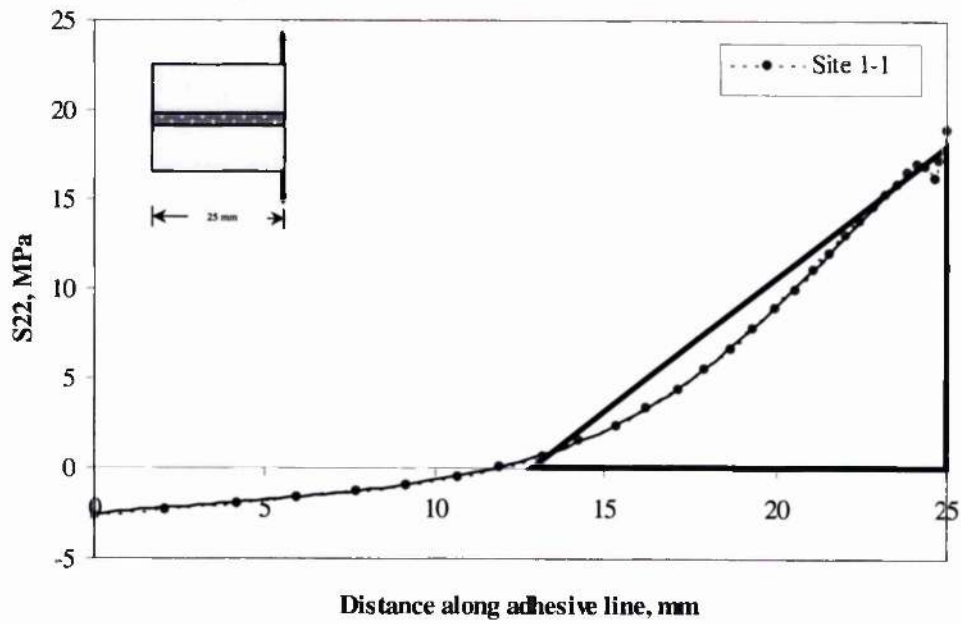


Figure 7.45 Idealisation of cleavage forces as triangular distributed load

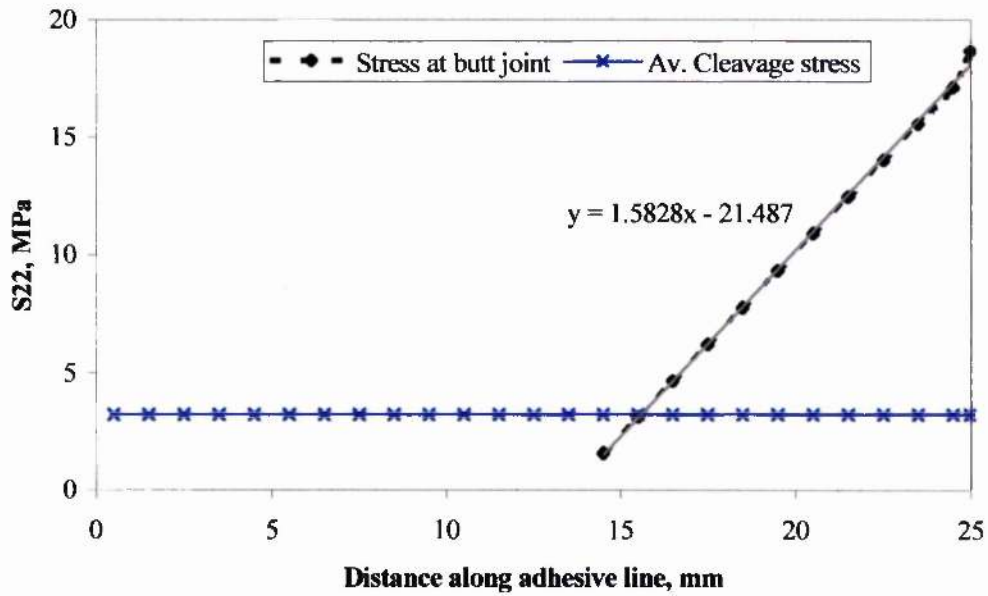


Figure 7.46 Calculated stress from triangular load in cleavage joint

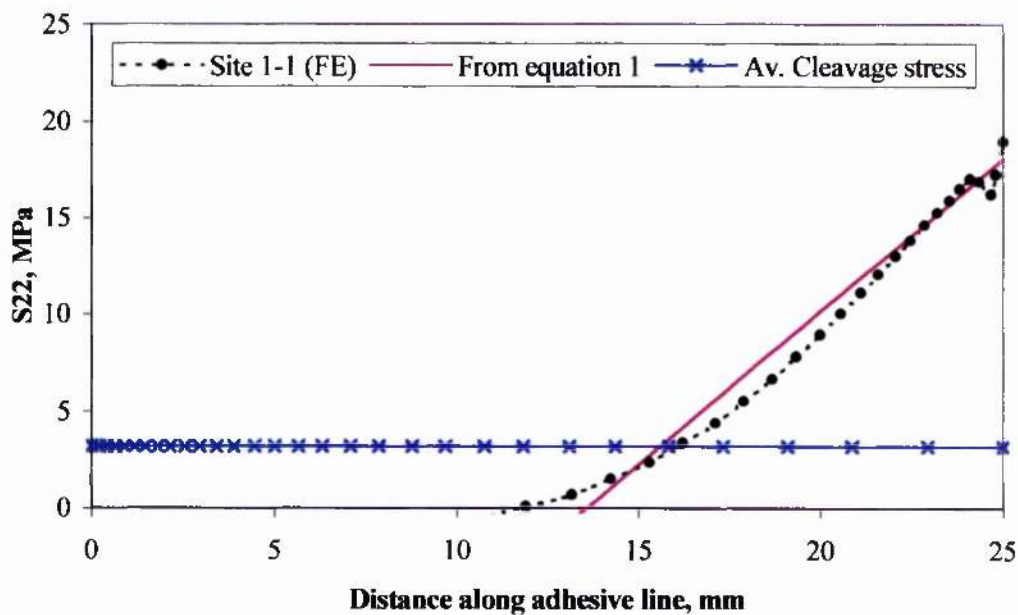


Figure 7.47 FE and calculated normal stresses in Model S

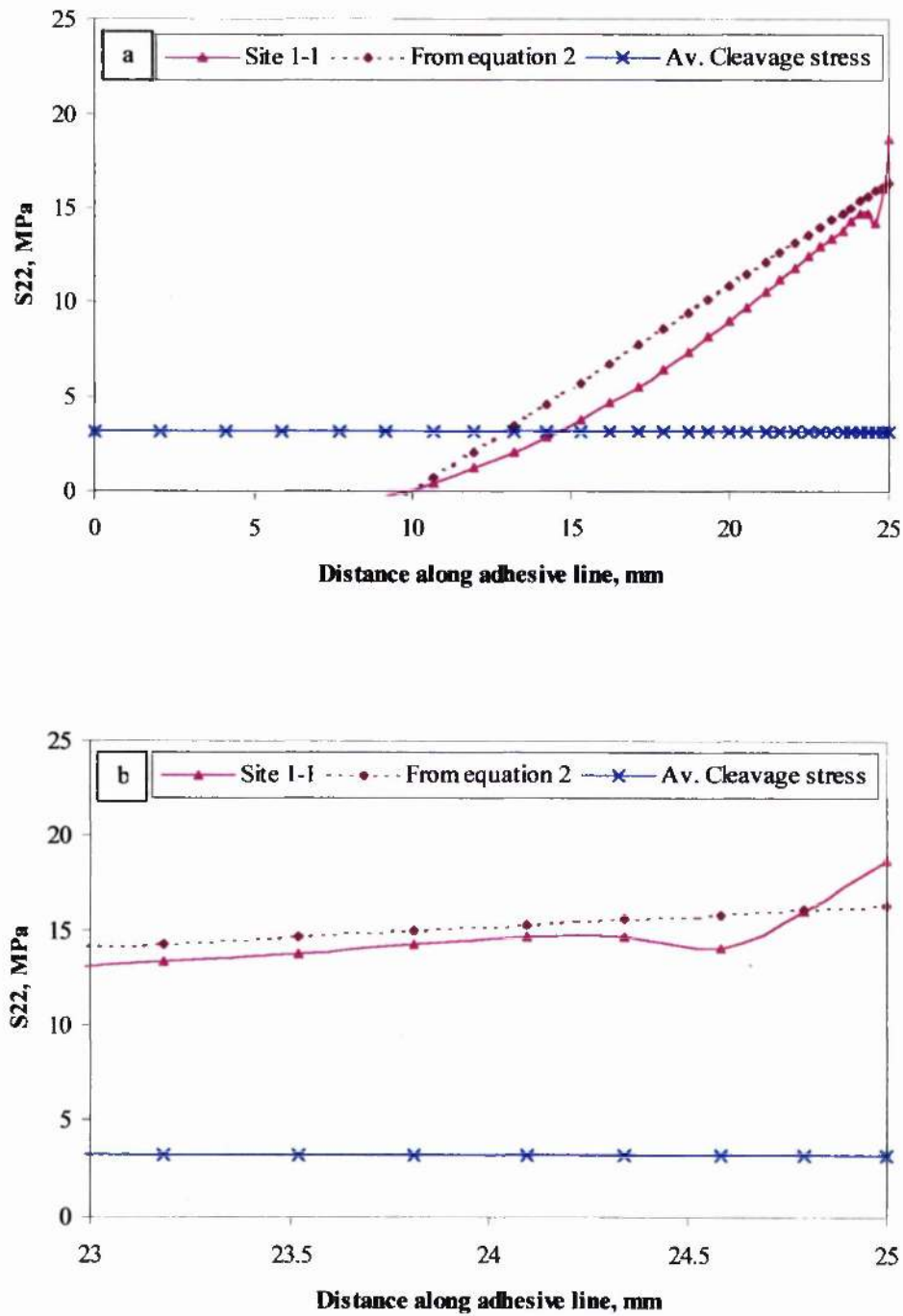


Figure 7.48 FE and calculated stresses in Model H (a) full joint length; (b) initial 2mm

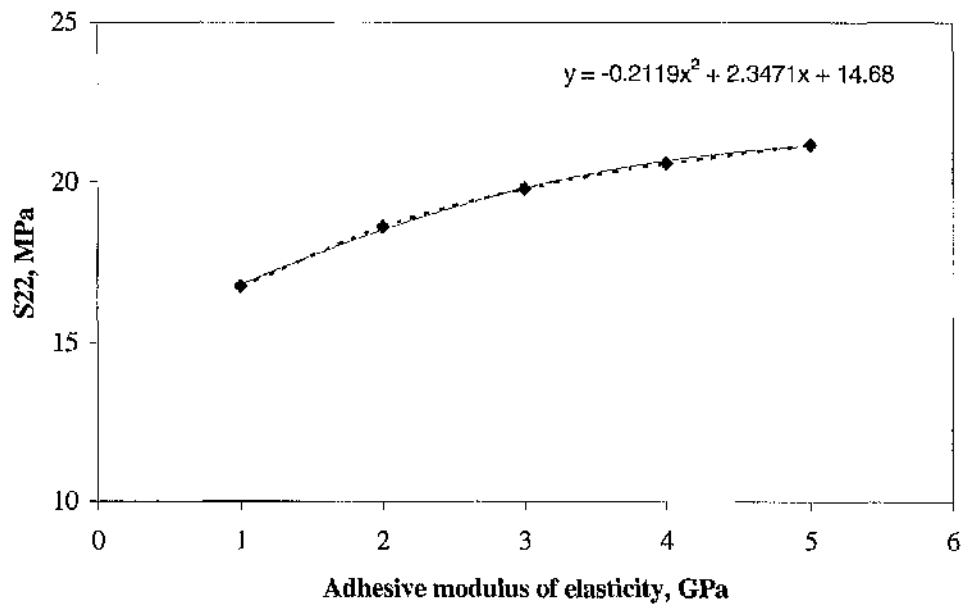


Figure 7.49 Variation of edge node stress with changing adhesive modulus of elasticity

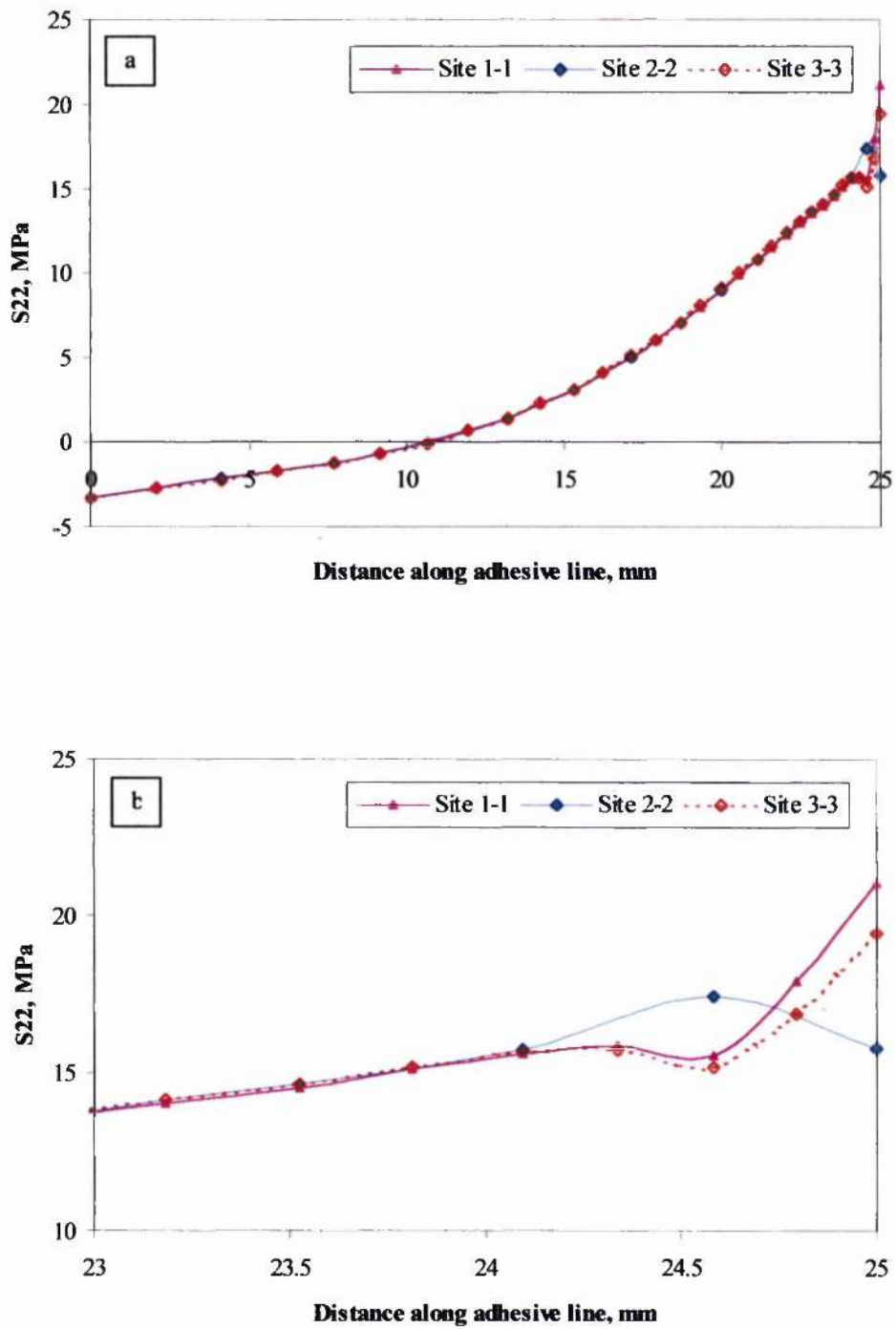


Figure 7.50 Normal tensile stress ( $S_{22}$ ) distribution in adhesive line of Model H with double adhesive modulus (see Fig. 7.16) (a) full length; (b) initial 2mm

Table 7.2 Properties of adherends and adhesive

<i>Material</i>	Young's modulus (GPa)	Poisson's ratio
Adhesive*	2.268	0.40
Steel <sup>212</sup>	207	0.29
Matrix <sup>211</sup>	3.6	0.40
Glass fibre <sup>202</sup>	72	0.30

\* Adhesive properties from supplier and experiment (Chapter 3)

Table 7.3 Isotropic properties of laminate<sup>†</sup>

<i>Parameter</i>	<i>Laminate</i> <i>(woven roving)</i>
E (MPa)	23000
$\nu$	0.25

† Assumed from the product data sheet<sup>210</sup>

Table 7.4 Orthotropic properties of laminate ‡

<i>Parameter</i>	<i>Laminate (woven roving)</i>
$E_1$ (MPa)	23000
$E_2$ (MPa)	9000
$\nu_{12}$	0.25
$G_{12}$ (MPa)	7000
$G_{13}$ (MPa)	4000
$G_{23}$ (MPa)	8000

‡ Approximate properties taken from various sources<sup>223,224</sup>

## CHAPTER EIGHT

### *DISCUSSION*

#### **8.1 Selection, Properties and Processing of Adhesive**

Several different types of adhesives are available on the market for the bonding of composites to steel. Acrylics, epoxies and polyurethanes are generally considered as good adhesives for the bonding of GRE to metals. The target in this study was to select an adhesive that can produce strong adhesive bonds to avoid cohesive failure in all testing, thus permitting an interfacial failure in response to varying surface/geometric conditions. In an earlier study<sup>209</sup>, six different adhesives from acrylics, epoxies and polyurethanes were tested for bonding GRP composites to steel and Redux<sup>®</sup> 420A/B, a modified room-temperature curing two-part epoxy adhesive from Ciba Chemicals, was found to give the best overall mechanical properties. It also gave the best cleavage strength compared to the other five, including a room-temperature curing epoxy adhesive, E32, from Permabond, UK. In addition to having good overall mechanical properties, long shelf life and room-temperature storage requirements, it also has the advantage of being less corrosive and safer for health than its earlier version (Redux 410A/B), whose hardener contained strontium chromate and was potentially carcinogenic. The packing of the adhesive was in a 200ml dual cartridge that allowed easy dispensing of the adhesive with minimum exposure and chances of skin contact. An inherent problem with this type of thixotropic adhesive is air entrapment during mixing and application. Limited pot life is another issue. Both of these may cause reliability problems, especially on polished surfaces, where wetting is a problem on its own.

Another consideration in the selection of this adhesive was that it has been formulated specifically for the bonding of composite materials and is being used by many end users for bonding epoxy fibreglass composites to itself and other adherends. Therefore, the data generated during this research will not only be of academic interest but may also be of direct interest to the adhesive users.

The Araldite<sup>®</sup> 420 adhesive (equivalent to Redux<sup>®</sup> 420, according to the manufacturer) has a wide range of curing temperature and time. The temperature varies from an ambient to as high as 150<sup>0</sup>C and the time varies from days to minutes, depending on the curing temperature. Although this study did not investigate the effects of these variations on the strength of the joints, these ought to have some effects. The choice, in this study, of a curing temperature and time of 70<sup>0</sup>C and two hours respectively, is considered to be realistic in terms of production factors. Some recent commercial prepregs require curing temperatures as low as 80<sup>0</sup>C.

To find the Young's modulus and the Poisson's ratio of the adhesive, several dog-bone bulk adhesive specimens were made, but due to the thixotropic nature of the adhesive, air bubbles got entrapped in many of them. However, it was possible to find at least one apparently bubble-free specimen for testing. The presence of any sizeable air bubble would cause a different rate of elongation than in a bubble-free specimen. The Poisson's ratio and the Young's modulus measured from the testing was in line with that obtained in an earlier study<sup>209</sup> and supplied by the resin supplier.

## 8.2 Process Variables for Composite Moulding

Attempts were made to utilise an existing fixed frame mould for making laminates from the prepregs, by hot press moulding. This however, proved extremely difficult to use due to difficulty in removing the moulded laminates. The old mould was then redesigned and the fixed frame was replaced with a removable one so that the fabricated laminate could be removed from the mould by dismantling the frame.

Adjusting the operating conditions for the making of laminate was another problem. Applying the pressure, recommended by the prepreg supplier, resulted in laminates with a number of surface holes (Figure 3.7). Attempts were therefore made to increase the pressure to a higher level, as recommended by some old data sheets for similar material. Higher pressures gave much better results (Figure 3.7) and it was possible to obtain smooth laminates with minimal resin loss during the moulding operation.

Mould release agents are used to assist in the removal of cured laminates from the moulds. Choices of internal and external mould release agents are available from a number of different chemistry types. Selection of an appropriate mould release agent is very important if the product (composite) is going to be adhesively bonded. An ideal mould release agent should not only help in the easy removal of the finished laminate from the mould but should also be easily and fully removable from the laminate surfaces. Trials were made to mould the laminates using a PTFE spray, the Mylar<sup>®</sup> Polyester film, and the nylon peel ply material. It proved very difficult to remove Mylar<sup>®</sup> film from the finished products. The PTFE and the nylon peel ply were satisfactory from the production viewpoint, but later in the testing peel ply did not perform up to expectation, as discussed in the following sections.

The GRE laminates used in this study have far superior resin matrix strength and interlaminar properties than the general-purpose laminates used in various non-structural or semi-structural applications. The adhesion characteristics of such well-prepared laminate are perhaps comparable with those of well-prepared steel.

### **8.3 Roughness Measurements**

Measured values of the surface roughness parameters, presented in Tables 4.1-4.3, are in line with those measured by other researchers<sup>71,74</sup>. For grit-blasted steel surfaces, roughness parameters do not depend on the direction of scanning and showed a complete isotropy. However, the woven roving glass fabric composite laminates showed a clear anisotropy for all surface conditions. Exceptions might be expected in the cases of resin-rich polished surfaces. Standard deviations in the measurements of the roughness of polished steel are typically high due to the difficulty in preparing a uniformly polished surface with manual techniques. Higher deviation was also noticed in the case of unidirectional fibre composites. The woven roving composites, on the other hand, did not show such a high standard deviation. There may be two possible reasons for this behaviour. First, the polished woven roving composite surfaces are already about five-times rougher than the polished steel surfaces and therefore the overall standard deviation is less. Second, the woven roving composites show, to some extent, an isotropy in the two perpendicular directions whereas the unidirectional composites show a clear anisotropy in the two

perpendicular directions. This is because the stylus keeps on changing its track between the fibres when the roughness is measured along the fibre direction. Lower standard deviations observed in the AFM measurements may be due to the fact that only one specimen was measured at different surface locations. In view of the difficulty in preparing uniformly polished surfaces, attempts were made to ensure that the frontal half of the specimen's surfaces were polished to the highest standard, as their contribution towards the total strength would be much larger than the rear half.

The Michelson's interferometer is very sensitive to surface variations and is suitable only for polished or nearly polished surfaces. In addition, the surface to be measured needs to be perfectly reflective in nature so that the incident light can reflect back and interfere with the reference light. Attempts were made to measure the roughness of the polished laminate surfaces using the interferometer but due to their non-reflective nature, such measurement was not possible. An available option was to gold-plate the laminate surface before measuring its roughness, but since another option (Talysurf) was available, this expensive alternative was discarded.

#### **8.4 Effect of Adhesive Thickness**

From the results presented in Chapter 5, it is evident that adhesive thickness affects joint strength differently in different types of specimen and surface finishes. In the case of grit-blasted cleavage specimens a small increase (approximately 4%) in the cleavage strength may be noted for a decrease in the adhesive thickness from 0.5mm to 0.1mm. However, the intensity of this effect diminishes further with a smaller coefficient of variation in the former case. This small increase in strength, as suggested by the results, may be due to the effects of triaxial constraint, adhesive defect populations and thermal shrinkage. This discovery of a small increase in the joint strength with decreasing adhesive thickness is in line with that of Adams et al<sup>96</sup>, who did not notice any prominent increase in T-peel joint strength with decreasing adhesive thicknesses. Gardon<sup>91</sup>, Williams<sup>92</sup> and Dukes and Bryant<sup>93</sup> also noticed this trend of increasing joint strength with decreasing adhesive thicknesses for butt joints in tension. Matsui<sup>97</sup>, on the other hand, reported an almost linear increase in theoretical and experimental strengths of standard cleavage specimens for adhesive

thicknesses from 0.1mm to approximately 1.5mm. These contradictory findings may well be due to different adhesives, curing conditions, surface pre-treatment and other chemical and physical conditions, which are difficult to match and compare, but may affect the joint strength. An example of one such condition is the change in surface chemistry of the adherend brought about by the grit-blasting process<sup>71</sup>.

In the case of polished steel cleavage specimens, however, strength decreased by approximately 11% for the same decrease in the adhesive thickness. This is in line with other findings<sup>5,97</sup> for peel and cleavage joints respectively. A possible reason for this decrease may be poor wetting of the polished steel surfaces in the case of small adhesive thickness, as shown in Figure 5.10. A similar trend was also observed in the cases of corroded, polished and grit-blasted specimens. However, due to the uncontrolled nature of the exposure and the limited number of specimens tested, it is difficult to quantify the end results.

The effect of adhesive thickness on the strength of thick adherend, steel lap-shear specimens (Table 5.2) was much more prominent. The reduction in shear strength with increase in the adhesive thickness was approximately 22%. This inverse relationship of adhesive thickness to joint strength is in line with the findings of Guha and EpeI<sup>70</sup> and Ojalvo and Eidinoff<sup>95</sup> in the case of single lap joints. Guha and EpeI<sup>70</sup> tested a range of adhesives using single-lap-shear joints and found that the increase in adhesive thicknesses from 0.25mm to 1mm led to a decrease in the strength of the adhesive joints by 1 to 25%, depending on the type of adhesive used. The increase in the adhesive thickness of lap-shear joints increases the bending moment and hence the cleavage stresses at the edge of the bond line<sup>96</sup>. It, therefore, appears that shear strength is more dependent on the adhesive thickness than cleavage strength.

Apart from the direct geometry dependent effects on the stresses, adhesive thicknesses may also indirectly affect the strength of the joints due to possible differences in the adhesive's chemical and physical properties near the interface with adherends and in the bulk. This difference has been studied and reported by several researchers<sup>84,100,99,101</sup> (Chapter 2). Some studies<sup>106,103,104,105</sup>, however, have not shown any difference in the thin film and bulk adhesive properties. Increase in the bond line

thickness generally results in decreased bond strength. In general, this effect is more prominent with adhesive thicknesses from 0.1mm to 0.5mm. For adhesive thicknesses more than 0.5mm, the cohesion forces in the bulk adhesive may determine the bond strength<sup>2</sup>.

Whatever the exact mechanism is, it may be concluded that the relationship between the bond strength and the adhesive thickness is not straightforward. This depends on a number of factors including, but not limited to, the nature and the properties of the adherends and adhesive, surface pre-treatment of the adherends and the geometry of the joint.

### **8.5 Effect of Corrosion**

Normal air forms about 3nm thick layer of  $\gamma\text{-Fe}_2\text{O}_3$  on plain-carbon steel surfaces<sup>225</sup>. Chemical composition of this oxide layer varies with the composition of steel alloy, presence of any inhibitor and the environmental conditions. The exact effect of these changing chemistries on the initial bond strength is unknown.

A small degree of thermal oxidation at 225°C was found to cause a drastic decrease in the adhesion of PVC organosol to mild steel<sup>226</sup>, but controlled oxidation treatment with dense blade-like growths increased peel adhesion of polyethylene to steel<sup>227,228</sup>.

Experiments were carried out with three main objectives. First, to confirm that uncontrolled oxidation in the natural environment could in no way improve the cleavage strength. Second, to test the sensitivity of cleavage strength towards steel corrosion and third, to look into the possible positive effects of grit-blasting (compared to polishing) when combined with rusting.

From the experimental results given in Chapter 5 (Tables 5.1 and 5.3), it can be seen that the initial cleavage strength drops considerably compared to the uncorroded specimens. This effect is more prominent in the case of specimens polished before corrosion. Absence of mechanical keying in the polished specimens appears to be the main difference that causes more reduction in the joint strength. However, the

possibility of any change in surface chemistry brought about by the grit-blasting, or any change in the chemistry of the oxide layer formed over the grit-blasted surface, may not be ruled out. It may also be suggested that the oxide layers formed as a result of the natural oxidation are not as strong as those formed under a controlled nitrogen environment. This effect may be similar to the much-researched controlled chemical anodising of the aluminium adherends compared to their oxidation in an open environment.

More work is needed for the correlation of joint strength with oxide chemistry, and also on the relationships between the surface topography and the long-term strength/durability in humid environments.

### **8.6 Effect of Surface Roughness**

Surface roughness has frequently been used as a design option for various adhesive joints. The relationship between roughness and adhesion is not very simple. Optimum adherend surface profile varies from one adhesive to another, and this also depends upon the type of stress applied<sup>78</sup>. A detailed literature review on the effects of surface roughness has already been presented in Chapter 2. Some aspects are, however, discussed again.

Almost all surface treatment methods bring some degree of changes in the surface roughness but grit-blasting is usually considered as one of the most effective methods in bringing the desired level of surface roughness. Actual roughness details of the surfaces greatly depend upon the way they are prepared. Variables in grit-blasting include the size, shape and the type of grit, the blast pressure, the treatment time, the blast angle and the distance from the blast nozzle to the surface<sup>11</sup>. Small particle sizes apparently leave greater percentages of contaminant residues on the surfaces. Particles of grit that remain on the surface after treatment may have a negative effect on their wetting<sup>71,229</sup>.

Should an adhesive be applied to the adherend surface immediately after grit-blasting or after some delay? This question was taken up by Brockmann<sup>18</sup>, who found that, for shot blasted mild steel specimens, initial and residual shear strength increased at

first with increasing 'open time' of the surfaces up to 24hrs and remained at a high level for up to 150hrs. Based on his finding, an open time of approximately 24hrs was selected in this study.

### *Steel Adherends:*

It can be seen from Table 5.1 that compared to diamond polishing, grit-blasting increases the cleavage strength by approximately 26% and 8% for adhesive thicknesses of 0.1mm and 0.5mm respectively. Improved performance of grit-blasted, steel cleavage specimens compared to polished ones are in line with the findings of Sargent<sup>76</sup>. Possible reasons for this strength improvement may be the increase in surface area, the creation of mechanical keying and the possible diversion of the failure path away from the interface into the bulk of the adhesive<sup>79,80</sup>, thus giving mini scarf joints on the adherend surfaces at a micro level. This is perhaps the reason for the better joint performance observed when the stainless steel surfaces were grit-blasted and degreased compared to the smooth 'ultra-clean' surfaces produced by the Argon ion etching in high vacuum<sup>68</sup>. On the other hand, Harris and Beever<sup>73</sup>, They et al<sup>230</sup> and Critchlow and Brewis<sup>72</sup> found no appreciable change in the joint strengths with increasing adherend surface roughnesses by mechanical treatment. These contrasting findings may be due to the fact that each researcher used a different set of adherends, adhesives and joints geometry. Moreover, the overall effect of grit-blasting is not limited to the removal of contamination or to an increase in surface area. This also relates to the changes in the chemical characteristics of the adherend surfaces<sup>71</sup> and to the inherent drawbacks of surface roughness, such as void formations<sup>82</sup> and in some cases, reduced wetting<sup>46</sup>. Decrease in wetting with increase in the surface roughnesses may be attributed to the hindrance effect of peaks, ridges and asperities to the spreading of the droplets. Huh and Mason<sup>36</sup> and Yost et al<sup>231</sup> noted that instead of flowing over ridges and peaks, the droplets seek out areas of the surface where they can flow more easily, particularly through troughs and valleys, probably as a result of capillary channelling.

The higher difference between the joint strength of grit-blasted steel compared with polished steel using 0.1mm adhesive thickness may be due to potential wetting

problems associated with the polished surfaces. Fracture surfaces of the polished joints showed bare steel and adhesive regions (Figure 5.14), which is in line with the findings of Jennings<sup>75</sup> and Bullet and Prosser<sup>84</sup>. They also observed that the areas of clean detachment were least on the rough surfaces, which was also seen in the grit-blasted cleavage specimens (Figure 5.11). The fracture mechanism may also be affected by surface roughness. A rougher surface promotes crack shielding that leads to a stick-slip crack propagation<sup>86</sup>.

Jennings<sup>75</sup> suggestion that random surface roughness could prevent alignment of the flaws or points of stress concentration seems to be in line with the present test results where some polished steel cleavage specimens, having void defects, failed at fairly low loads. On the other hand, the grit-blasted steel cleavage specimens containing similar void contents failed at about the same load as their almost bubble-free counterparts. In addition to the higher flaw content (void defects), which may result from exothermic reactions, alignment of flaws can also be expected where adherend surfaces have regular ridges. This maybe the reason for the failure of machine ground, steel cleavage specimens at lower loads compared to those made with the grit-blasted steel. This is also in line with the findings of Garnish and Haskins<sup>87</sup> who tested lap-shear specimens of aluminium and steel bonded with one-part, hot curing, epoxy adhesive and found higher strength in shot blasted specimens than those degreased only. This highlights the advantage of grit-blasting over machine grinding and diamond polishing of the steel adherends. However, Janarthanan et al<sup>85</sup> did find adhesion enhancement in a bi-layer construct through the introduction of oriented macroscopic surface roughness.

The effect of surface roughness also depends on the test temperature or the type of adhesive used. For example, at higher testing temperatures or with a low-modulus adhesive, where plastic or viscous flow is possible and flaws or points of stress concentration are less important to the strength of the joints, roughness would be expected to have a minor effect on the attainable joint strength. A low modulus nylon epoxy film adhesive (Metlbond<sup>®</sup> 1301) did not show any difference in joint strength between polished and grit-blasted specimens<sup>75</sup>. However, the modulus of the adhesive used in this study is reasonably high (approximately 2.5GPa) and we may,

therefore, expect some difference in the strength of polished and grit-blasted specimens, as shown by the experimental results.

It may be concluded that grit-blasting is an economical and simple surface preparation method for the bonding of steel surfaces, which gives a reliable and satisfactory initial joint strength. Long-term durability however, may be influenced by grit-blasted surfaces, but this may require further study.

### *Effects of roughness parameters $R_a$ and $R_{I_0}^2$*

Experimental results show that cleavage strength increases with the  $R_a$  values (Figure 5.21). This increasing trend is in line with the findings of Sargent<sup>76</sup>, who reported an increase in peel strength of aluminium test specimens with increasing surface roughness, and Arrowsmith<sup>83</sup>, who observed an increase in peel strength with increasing surface roughness of copper adherends. Kalnins et al<sup>81</sup> also found that the initial joint strength of polyethylene-steel adhesive joint increases with growth of the specific surface area of chemically treated substrate. Possible reasons for this increase in strength are the increase in surface area and the increase in plastic deformation of the adhesive in the interface region.

A rougher surface is expected to have a deeper roughness profile and hence the dispersed rubbery particles of a toughened adhesive may get entrapped in the roughness grooves. This effect was also observed by Gilibert and Verchery<sup>74</sup> who obtained the best results when the total depth of roughness was equal to the mean diameter of the dispersed toughening particles in the resin.

The experimental cleavage strength also appears to increase with the effective surface area ( $R_{I_0}^2$ ) of the adherend surfaces. It is however, realistic to believe that this increase in cleavage strength with the increase in surface area would be limited by the bulk adhesive strength i.e. until the failure becomes cohesive within the adhesive.

### ***Composite Adherend:***

The hybrid cleavage specimens made with grit-blasted composites appear to show approximately 18% lower strengths than those made with steel alone (Tables 5.1 and 6.1). It should, however, be noted that in the case of grit-blasted composites, failure initiated in the composite adherend (Figure 6.7) confirming the findings of Han and Koutsky<sup>192</sup>. This may be attributed to the fibre and resin damage caused by impact loading during the grit-blasting process. Diamond polishing outperformed grit-blasting, and in all specimen failures appear to initiate at the metal-adhesive interface (Figure 6.9). Possible reasons for the increased strength are the total removal of any mould release agent and the limited damage to the fibres and resin during the slow polishing operation compared to fast grit-blasting.

Due to the anisotropic roughness profile of polished or grit-blasted composite surfaces, a quantitative correlation of the roughness parameters,  $R_a$  and  $R_{10}^2$  with the strength values is very difficult. The difficulty in obtaining accurate measurements of roughness parameters also adds to this problem.

Stress concentration occurs in the vicinity of the peripheral edge of the bonded plane, which initiates the failure of the joint. Such stress concentrations are also thought to be a function of surface roughness. Because of so many parameters involved, it is very difficult to derive a generalised hypothesis for the relationship between surface roughness, surface energy and adhesion<sup>71</sup>.

### **8.7 Effect of Surface Pre-treatment of Composites**

In the case of fibre-reinforced epoxy resin adherends, the initial bond strength is related to the presence of contaminants on the adherend surfaces and is, therefore, directly related to its pre-treatment<sup>12</sup>. Some pre-treatment operations such as grit-blasting tend to cause debonding in the top ply of the laminates, due to the presence of underlying rigid glass fibres in the matrix. Therefore care should be taken in the pre-treatment of the composites.

In this study, the options considered for the pre-treatment of composites were: no pre-treatment; one side solvent (acetone) cleaning; both sides solvent cleaning; manual roughening; grit-blasting; diamond polishing and the application of peel ply.

The simplest method for removing contaminants from a surface is to wipe it with an appropriate solvent. There is however, a possibility that, rather than removing the contaminants, the process may just spread them over the surface. Such a smearing of contamination may be avoided by using fresh solvent and wipe or using vapour-degreasing equipment. The possibility of some chemical reaction between the cleaning solvent and the matrix resin should not be ruled out. From the results presented in Table 6.1, it can be seen that laminates with no surface pre-treatment or one-sided solvent cleaning failed at very low loads, and the coefficients of variation are very high. This result may be expected due to the remains of uncontrolled quantities of PTFE on the laminate surfaces and the known poor adhesion of epoxy adhesives to PTFE. Different results, however, might be expected from a different cleaning solvent, mould release agent and adhesive chemistry. A water-based mould release agent might be easier to clean from the laminate surfaces, and hence improved adhesion of the adhesive may be expected.

Double-sided solvent treatment did improve the joint strength by approximately 400% and reduced the coefficient of variation from 82% to 25% but still the limited cleaning power of acetone for PTFE allowed some of it to remain on the laminate surface and hence an adhesion/adhesive failure was observed.

Manual roughening of the solvent cleaned laminates with the emery paper appears to give satisfactory results, especially in comparison with grit-blasting. From Table 6.1 it may be noticed that manual roughening of the laminates produces joint strengths that are approximately 10% higher than those with grit-blasted laminates but still approximately 10% lower than those with diamond polished laminates. A possible reason for the improved strength obtained with manual roughening is that there is less chance of damage to the fibres and resin matrix compared to that resulting from the grit-blasting operation. Chances of such damage are minimum with diamond polishing, which also ensures complete removal of the top resin layer containing PTFE. It also helps in thinning the resin-rich layer formed during laminate formation.

From these results it is clear that in the case of epoxy fibreglass composites, it is not really the roughness that decides the joint strength, but the complete removal of impurities and the integrity of surface resin and fibres.

The motivations in using peel ply are to simplify the pre-treatment process, to protect the adherend surface during storage and handling and to ensure a contamination-free surface before bonding. The variables for peel ply treatment are the type of material, size of the ply, size of the weave and the nature of chemical finishes/release agents applied to the peel ply. In this study, laminates made with peel ply, recommended by the prepreg manufacturer, appeared to perform poorly compared to diamond polished laminates (approximately 42% lower joint strength). This is in contrast to the findings of Cowling et al<sup>232</sup>, carried out on a polyester matrix laminate. Lab testing on polyester laminates, with peel ply on one side and grit-blasting on the other, also showed that in all such specimens cleavage failure occurred on the grit-blasted side. This suggests that type of resin is an essential element in determining the joint strength. Although peel ply is good in providing fresh, clean surfaces, free from surrounding contamination, it may suffer from contamination originating from the peel ply material itself. The chemicals applied to the peel ply, during sizing and other manufacturing and finishing operations, are the key sources of these contaminants. The use of peel ply results in the formation of a resin-rich surface layer that may also reduce the actual strength achievable otherwise<sup>233</sup>. Peel ply may therefore be realistically considered as a source of contamination<sup>234</sup> and should be avoided when other better options are available.

In the case of composites, it is very difficult to manually control the grit-blasting operation and ensure a uniform removal of resin/contamination from the adherend surface. A small variation in grit-blasting time from one place of the surface to another may produce a visible depression that may not only cause more damage to the fibre but also result in an unexpected complex stress distribution at the surface.

## 8.8 Effect of Fibre Directions

Lower cleavage strengths were obtained (Table 6.1) in the case of specimens made with grit-blasted 90<sup>0</sup> unidirectional surface ply and woven fabric composite

laminates, compared to those made with grit-blasted  $0^\circ$  unidirectional surface ply. This may be attributed to the lower stiffness of the epoxy matrix compared to the reinforcing glass fibres.

From visual examination of the fractured surfaces (Figures 6.7 and 6.12) it can be seen that failure is taking place within the composite adherend. This may be attributed to the damage that may take place to the resin and fibres during the grit-blasting operation. In the case of composites made with unidirectional surface plies, some interlaminar failure within the unidirectional plies is also visible. The difference in cleavage strength of the hybrid cleavage joints made from the woven fabric laminate and the unidirectional laminates may also be due to the difference in their fibre volume fractions (52.85% in the case of UD laminate and 45% in the case of woven roving laminate).

Kairouz and Matthews<sup>194</sup> conducted a parametric study on the effects of the stacking sequence on peak stresses within the adhesive and composites in a single-lap joint. They performed linear elastic, small displacement and plane stress finite element analyses and found a good correlation between the observed positions of failure with the stress maxima from the finite element analysis. They concluded that a non-linear effect should be included in the analysis for prediction of the laminate failure. They also concluded<sup>195</sup> that although stacking sequence does not strongly influence joint strength, it does influence the failure mechanism that is dominated by bending stresses. On the other hand, Pradhan et al<sup>196</sup> and Ratwani and Kan<sup>197</sup> found sensitivity of joint strength to stacking sequence.

However, unlike the case of lap shear joints, the stacking sequence in the hybrid cleavage joints may not significantly influence the overall stiffness of the joint and its strength. The overall stiffness is dominated by the thick steel adherends.

Attempts were made to study the influence of fibre directions in the case of the polished specimens, but due to expired material, the unidirectional specimens failed at fairly low loads. It was therefore not possible to compare these values with those obtained from polished woven fabric composites.

From the experiments performed in this study it appears that fibre direction of the top ply does affect cleavage joint strength. However, to fully analyse the effect of stacking sequence on the strength of the hybrid cleavage joints more experimental work will be needed.

## 8.9 FE Modelling

The benefits that computer modelling brings to the designing of the adhesive bonded joints include reduction of designing process time, quick evaluation of the design alternatives and optimal product performance. The analyses in this work were carried out to substantiate some of the experimental findings, and several models (Figure 7.1) were developed and analysed as mentioned in Chapter 7.

The output of FE analysis is based on the reliability and accuracy of the input data, especially the detailed properties of the materials involved. In cases involving composites, it is often difficult to get accurate values of the parameters required and hence approximate values are taken. Quite often, a similar situation exists in the case of adhesives. These situations add to the approximate nature of solutions obtained from the FE analysis.

Although 3-D modelling would give a more accurate stress distribution, 2-D modelling was selected, as the main purpose of modelling was to perform a comparative study among different specimen models or different sites in the same specimen model. Some 3-D modelling was also performed in the case of steel/steel and hybrid cleavage specimens but the overall pattern of stress distribution was observed to be similar. Richardson et al<sup>170</sup> compared the 2- and 3-D finite element analysis of an adhesive joint as similar to the standard cleavage joint defined by ASTM D1062-78 (The cleavage strength of metal to metal adhesive bonds). They found that, with appropriate corrections, a 2-D finite element analysis could reproduce the conditions at various positions across the width of a 3-D joint.

A full-scale 2-D model based on the specifications defined in BS 5350: Part C1:1986<sup>1</sup> was made and analysed. The results were then compared with those obtained from the simplified model, Model S (Figure 7.1), to verify the stress

distribution patterns in the two models. The comparison showed that in both cases the stress distributions are the same. In addition, comparing analyses using 2-D shell elements and 2-D solid elements produced similar stress distribution patterns. Hence it seems fair to simplify the full model into a smaller, simplified and easy-to-analyse model.

Stress concentrations could occur at the end of the interface between the adherends and the adhesive layer. This observation can also be made in the case of Model S (Figure 7.8a) where higher normal stress may be observed at the steel interface. Possible reasons for this stress concentration are the differences in the elastic moduli of the adhesive and the adherends and unbond (trapped air bubbles) at the adhesive/adherends interface. As a result of higher stresses at the interface, it may be expected that failure will initiate at the steel surface, also observed from the experimental findings. Since failure occurs in the region of these very high stresses, it is clear that the averaged stresses in this region cannot give an accurate indication of the onset of failure. It can also be seen from Figure 7.8a that except within the first millimetres of the joint, the variation of stresses through the adhesive thickness is insignificant. The stresses at the interface were shown to be mesh dependent, especially in the absence of adhesive fillets<sup>10</sup>. Mesh dependency also existed even when non-linear analysis was considered<sup>174</sup>.

For the modelling of hybrid cleavage specimens, models based on Model H (Figure 7.1) were made and analysed by assigning isotropic and orthotropic properties to the laminates. Different sets of hypothetical properties were assigned to the laminates and the analyses were performed using 2-D and 3-D models. It was observed that in all cases, the critical value of the normal stress ( $S_{22}$ ) is highest at the steel/adhesive interface and shifts towards the laminate/adhesive interface. Further partial modelling of the joint also confirmed that the stresses at the steel interface are higher near the edges and it may, therefore, be expected that failure would initiate at the steel interface, as seen from the experimental findings (Figure 6.9).

Although the GRE laminate was modelled as an orthotropic solid material (Model II), the through thickness properties of the plies and the resin-rich layer at the top of the laminate were not taken into consideration. The tensile and compressive strength

of the overall laminate are often well known but it is difficult to measure the interlaminar strength. Attempts were made to find these properties from the composite supplier but the results were not available. Interlaminar tensile strength is more important in the case of cleavage, rather than tensile or compressive loading. The effect of interlaminar strength could be minimised by using laminates made from 3-D braided woven fabric. The resin-rich layer at the composite surface is expected to contribute more towards the overall strength/weakness of the joint in the case of GRP laminates than in GRE due to the brittleness of the polyester resin layer. Composite details with fibre orientation and resin layer were modelled in the partial models (Models P1 and P2).

Comparing the normal stress distributions in Model H with a steel insert to that with a GRE insert reveals that the stresses in the former case are lower by approximately 5%, hence an increase in joint strength would be expected. The experimental results (Tables 6.1 and 6.3) also showed that the cleavage specimens made with steel inserts performed approximately 7% better in strength compared to the hybrid cleavage specimens made with woven roving GRE.

Partial modelling of the cleavage specimen into small butt joints with triangular roughnesses is a good representation, as in practice the roughness profiles are made of a continuous series of concave and convex shapes. As an average of both models (Figure 7.1), stresses at Site 1-1 (flat top surface) are higher by about 30% than those at Site 3-3 (rough lower surface). The experimental results (Table 5.5) showed only 16% difference in the average cleavage strength between the polished and rough (24/30 mesh) surface conditions. Although these experimental conditions were assumed to represent Site 1-1 and Site 3-3 of the numerical models (Figure 7.27) respectively, the scatter between the numerical and experimental results is somewhat high. Beside the model representation problems, scatter is also possibly due to the lack of wetting in the bonded joints, and this could be more critical in the case of cleavage joints where stresses are highly concentrated at the edges. Surface profile can lead to the trapping of air beneath the adhesive and poor filling of the crevices. These voids can lead to stress concentrations and hence lower joint strength<sup>82</sup>. Depending on the nature of the roughness and the adhesive, the surface may not be wetted properly, and the adhesive may even start curing before going deeper into the

pore. Sargent<sup>76</sup> also analysed the contribution of increased area and surface roughness on the force required for detaching adhesives from the adherends. By considering a surface composed of spherical depressions, he found an increase of 15% in the normal tensile force required for detaching the adhesive from the adherend surfaces.

The results from the partial modelling of the hybrid Models P3 and P4 support the experimental results from the polished laminate specimens, where failure initiated at the steel interface. In the modelling, the adherend surfaces were considered as ideally smooth (flat) whereas in the actual experiments steel surfaces were grit-blasted with 40/60 mesh alumina grit. Because the focus here was on the composite interface, the detail of the steel interface was discarded. Perhaps it would very helpful to correlate the FEA results from the partial models with the corresponding experimental models (butt joints specimens). The problem, however, is the lack of reliability of test results from the butt joints specimens in general. Such experiments could produce a scatter as high as 60%<sup>113</sup>. Nevertheless this should be a subject of a future work.

The motivation in the development of equations for the calculation of cleavage stresses was the non-availability of a general mathematical expression which can be used directly to find the actual cleavage stresses in a cleavage joint. The assumption of using a triangular load distribution from FEA stress results seems to be a good approach. This, together with the classic mechanics, gave reasonable normal stress values that are in agreement with those found from finite element analysis. Therefore, it is now possible to estimate cleavage strength from the experimental results of standard cleavage specimens. This could help in the assessment of practical joint failure, rather than relying on average cleavage strength which is very misleading.

Although the stress results from forces and moments in Figure 7.45 could be achieved without using static equilibrium equations and Mathematica, the technique itself is a very useful one if the loading does not follow a linear triangular distribution. Should non-linearity and elasto-plastic behaviour be considered, a more sophisticated set of equations would have been generated. However, this was not realised due to the assumption of linear elastic behaviour of the joint.

## 8.10 Loci of Failure

Adhesive strength in a bonded joint can only be measured if the failure is exactly at the adhesive/adherend interface i.e. when the failure mode is purely adhesion. Otherwise, the result obtained shall be a measure of the tensile strength of the interfacial layer where the failure takes place. This layer may be the metal oxide, a contamination, or a mechanically weak component of the applied adhesive. Knowledge of the precise location of failure is, therefore, of prime importance for understanding the causes of failure.

Most brittle adhesives fail by a flaw-initiated crack mechanism. The first crack is caused by the local high concentration in the adhesive, as a consequence of the joint geometry, loading and mechanical properties of the adhesive and adherend. This first crack normally leads to total failure as the tip of the crack forms stress concentration higher than the original stress that caused it. Alignment problems in the case of cleavage joints could also result in failure at a far lower load. Cohesive failure in a polymer does not imply that it has failed at its bulk strength. The ultimate cohesive stress can vary with the adherend, its metallurgical state and the surface preparation<sup>75</sup>. Joint strengths higher than the corresponding reported bulk polymer strength have been reported<sup>75,119,235</sup>. It may be due to several factors, such as lateral constraint offered by the higher modulus adherend, nature of the polymer formed in the joint i.e. change in polymer surface morphology due to adherend, and the types, numbers and distribution of flaws in the adhesive layer.

It is well known that the fractured surfaces of the joints bonded with elastomer toughened epoxy resin may show stress whitening zones from the starting of cracks. This effect is related to local plastic deformation at the crack tip. Stress whitening was also observed in the fractured surfaces of the specimens in the current study (Figure 5.19).

The distinction between cohesive (cohesion) and adhesive (adhesion) failures may not always be clear and may not be that important when the greater part of the adhesive layer has been dislocated from the adherend. In this study, upon visual and light microscopic examination, it appeared that the specimens prepared by grit-

blasting steel adherends with coarser grit have shown significantly higher crazing (stress whitening zones due to micro-cracking) in the initial areas of the joint compared to those prepared with the finer grit. In both cases, however, failure was near the interfacial region with steel and was apparently in a mixed adhesion/cohesion mode. From the intensity of whitening it appeared that the failure initiated from one of the corners of the adherend, a point of theoretical singularity. This is in line with the findings of Crocombe et al<sup>178</sup>. On the other hand, in the case of polished specimens, the fractured surfaces of the joints showed no signs of crazing and bare steel and adhesive regions were clearly visible, showing an apparent adhesive failure (Figure 5.14). It is difficult to confirm, without using more sophisticated techniques such as electron microscopy and x-ray diffraction, if the bare portions of fractured surfaces were completely free from the adhesive residues or not. However, the results from the numerical analysis clearly indicate an adhesive failure mode and hence it may be said that the failure initiation in all these cases was adhesive (adhesion) failure. These observations may only apply to specific cases including loading conditions and type of adhesives and adherends.

In the case of GRE based hybrid cleavage specimens, edge delaminations had been eliminated by extending the laminate from the boundaries of the joint and except in a few specimens with unidirectional surface ply, no edge delamination had been observed. In the case of glass reinforced polyester laminate, this strategy did not seem to work and the locus of failure was clearly within the composite adherend. The main reason for such failure pattern would be the much weaker interlaminar strength of polyester-based composites compared to the epoxy-based composite laminates.

In the case of grit-blasted GRE hybrid cleavage specimens, failure appeared to initiate within the top ply of the composite laminate. The most obvious reason is the possible damage taking place to the resin and fibres during the grit-blasting process. However, in the diamond polished laminates, with minimal or no damage to the fibre and possible complete removal of the mould release agents, the locus of failure appeared to shift from the laminate surface to the point of theoretical higher stress (from FE analysis) at the steel surface.

Correct identification of the loci of failure helps in improving the areas of weaknesses in a joint and therefore results in improving the joint strength to the level where the adhesive may be utilised to its maximum potential i.e. where a cohesive failure would take place within the adhesive.

### 8.11 Final Comments

It has been seen that the evaluation and characterisation of an adhesive bonded joint is a complex task and a large number of variables related to adherend, adhesive, processing and surface preparation and geometry are involved. This makes it very difficult to generalise any findings. This is also why it is difficult to compare the results of various workers, because each of them uses different materials and operational variables. Each case, therefore, need to be tested and evaluated on an individual basis.

Although throughout this study small standard or modified cleavage specimens have been tested and modelled, it is believed that the results should equally be applicable to the local effect of larger structures. It is perhaps worthwhile to pursue the possibility of adopting the hybrid cleavage specimen in standard testing methods, and hence further work is necessary.

Due to non-homogeneity of composites through their thickness, special consideration needs to be given while analysing composite bonded structures. Areas of concern at micro-level are the fibre/matrix interface, at macro-level are the interfaces between the layers, and at structural level are the interfaces between the composite and other components of the adhesive joints.

The failure criteria applicable to isotropic, homogeneous materials are often not applicable to composite materials. For composites, the commonly applicable failure criteria are the Tsai-Hill<sup>236</sup> failure criteria and the Tsai-Wu<sup>237</sup> method that considers composite lamina as being anisotropic yet homogeneous. They assume that the behaviour of a single, unidirectional ply within the laminate is the same as that of an isolated ply. This assumption is not strictly valid for composites where adjacent plies provide constraints and modify the overall composite behaviour. Composites often

suffer from interfacial cracking between the matrix and the reinforcing fibres. This cracking may be due to manufacturing defects, impacts or high stress concentration at geometric or material discontinuities, and could be a limiting factor irrespective of the mode of loading. Due to these constraints, no universally acceptable failure theory has been established for the composites. Chandler et al<sup>238</sup> has proposed a way out of this problem. They feel that a simple failure criterion could be made on the basis that fibre failure occurs when the strain or stress in the fibres reaches a critical value. Failure in the matrix can be considered in terms of a suitable isotropic failure criterion. Matrix tensile failure normal to the fibre axis is to be governed by the stress concentrating effects of the fibres.

The effect of the adhesive fillet has not been considered in this study but their presence, size and shape may well effect the stress distribution and hence the ultimate strength of the cleavage joints. Its removal was necessary for controlling the bonding process quality. On the other hand, this could have caused local damage at highly stressed locations. Furthermore, the elasto-plastic natures of adhesive and composites have not been considered, as all bonded joints are designed and operated well within their elastic region.

Non of the five adhesive bulk specimens tested showed plastic behaviour which is uncharacteristic of such an adhesive. Increases in both void population and stiffness were noticed possibly due to warm curing at 70°C. There is also the possibility of change to the adhesive formulation due to commercial factors. Traditionally this adhesive is known as Redux<sup>®</sup> 420A/B (now Araldite<sup>®</sup> 420A/B). A previous departmental test on the adhesive gave a much lower modulus of elasticity<sup>209</sup>. No strain data were available from Ciba Chemicals for comparison but their experiments gave a similar tensile modulus of elasticity to this work. Future work to obtain a relevant curve is needed.

From this study it is clear that unlike adhesive bonding of GRP composites, where interlaminar strength is the main issue in the joint performance and not the surface pre-treatment or the adhesive, a well prepared GRE composite can perform comparably to a well prepared steel surface.

## CHAPTER NINE

***CONCLUSIONS AND RECOMMENDATIONS FOR FUTURE WORK*****9.1 Conclusions**

The conclusions drawn from the present study are summarised below:

1. The modified cleavage specimen provides a good methodology for testing composite/metal joints.
2. Cleavage strength is not strongly dependent upon the adhesive thickness within the practical range of thick adherend applications.
3. While a thicker adhesive line appears to contain a larger void population, it also appears to provide a better wetting condition, especially on polished steel.
4. Grit-blasting of steel shows better and more consistent results compared to polishing.
5. Cleavage strength of steel/steel joints appears to increase with the average roughness and the roughness profile area of the steel adherends.
6. The mode of failure initiation in steel cleavage joints under quasi-static loading and ambient conditions may be classified as “adhesive (adhesion) failure”. This mode seems to be independent of the level of roughness.
7. Oxidation of mild steel in a natural environment provides a very weak oxide layer for adhesive bonding. Moreover, highly corroded grit-blasted surfaces give a better adhesion than the equivalent polished ones.
8. Adhesive stresses at the interface with the composite are lower than those with the steel. Hence, in a steel/composite joint, where the composite matrix has high strength, adhesive failure initiates at the interface with the steel.
9. Grit-blasting of GRE composite results in fibre and resin damage and thus gives lower strength than that in the case of diamond polishing.
10. A polished epoxy composite produces a joint strength consistently higher than that of polished steel.

11. Laminates with a surface ply of  $0^0$  unidirectional fibre give slightly higher cleavage strengths than those with a  $90^0$  unidirectional surface ply or with a woven roving one.
12. Type of resin matrix is an essential element in determining the joint strength of a steel/composite joint. Specifically, laminates based on epoxy resin are significantly more suitable for adhesive bonding than polyester-based laminates.
13. A simplified numerical butt model with macro-roughness provides good correlation and representation of adhesion in the standard cleavage joint.
14. Normal tensile stresses in the case of rough steel surfaces are lower by 30% than those in the case of polished ones.
15. Developed design equations may be used to calculate cleavage stresses in the cleavage joints with fair accuracy.

## **9.2 Recommendations for Future Work**

More experimental and modelling work is recommended in the following areas to improve our understanding of the behaviour of cleavage joints between similar and dissimilar adherends.

1. The effect of stacking sequence on cleavage strength of the steel/composite cleavage joints.
2. Better mould release agents, preferably water-based, that can be easily and completely removed from the composite surfaces.
3. Correlation between the effects of particle size of the dispersed toughening agent/filler on the cleavage strength of steel/steel cleavage joints.
4. Detailed 3-D modelling and sub-modelling of hybrid steel/composite cleavage joints.
5. Quantitative study of the adhesive defects and joint strength.
6. Correlation of rust chemistry and joint strength.
7. Effect of high temperature oxidation on the cleavage strength of steel/steel cleavage joints.
8. Long term durability of cleavage joints in wet environments with the various surface conditions.

9. The effect of the adhesive fillet and the elasto-plastic properties of the adhesive and composite adherend.
10. Formulation of mechanical testing of specimens representing the partial models of P1, P2, P3, and P4.
11. Feasibility of adopting the modified hybrid cleavage specimen in the standard testing methods for adhesives.

## *References*

1. BS 5350:Part C1:1986, '*Determination of cleavage strength of adhesive bonds*', British Standards Institution, London, UK (1986).
2. Semerdjiev, S., '*Metal-to-Metal Adhesive Bonding*', Business Books Limited (1970).
3. Hart-Smith, L. J., 'A peel-type durability test coupon to assess interfaces in bonded, co-co-bonded, and co-cured composite structures', *Int. J. Adhesion Adhesives*, Vol. 19 (1999) pp 181-191.
4. Pocius, A. V., '*Adhesion and Adhesives Technology An Introduction*' Hanser Publishers, Munich (1997).
5. Lees, W. A., '*Adhesives in Engineering Design*', The Design Council, London (1984).
6. Aitken, D. F. and Blitt, M. A., '*Engineers Handbook of Adhesives*', The Machinery (1972).
7. McGarth, G., 'Not sticking to traditions- A guide to adhesive bonding', *TWI Bulletin* 3, (May/June 1991) pp 64-67.
8. *User's Guide to Adhesives*, Publication No. A17c-GB, Ciba Speciality Chemicals Plc. (1997).
9. Hashim, S.A., Winkle, I.E., Knox, E.M. and Cowling, M.J., 'Advantages of adhesive bonding in offshore and marine structural applications', *Chapter 19, Integrity of Offshore Structures - 5*, eds. Faulkner, D., Cowling, M.J., Incecik, A. and Das, P.K., EMAS Publishers (1993).
10. Tong, L. and Steven, G. P., '*Analysis and Design of Structural Bonded Joints*', Kulwer Academic Publisher, Massachusetts, USA (1999).
11. Wingfield, J. R. J., 'Treatment of composite surfaces for adhesive bonding' *Int. J. Adhesion Adhesives*, Vol. 13, No. 3 (1993) pp 151-156.
12. Parker, B. M., 'Adhesive bonding of fibre-reinforced composites' *Int. J. Adhesion Adhesives*, Vol. 14, No. 2 (1994) pp 137-143.
13. '*The use of continuous fiber composites in driveshafts*', (<http://www.addax.com/SAEPaper.htm>).
14. Kinloch, A. J., 'Fibre composites-joining', in *Handbook of Adhesion*, ed. Packham, D. E., Longman Group (FE) Ltd. (1992) pp 167-169.

15. D 907-96a, 'Standard terminology of adhesives', American society of Testing Materials, Philadelphia, PA (1996).
16. Shields, J., 'Adhesives Handbook', 3<sup>rd</sup> edition, Butterworth & Co. Ltd. (1984).
17. Skiest, I., 'Hand book of Adhesives', Reinhold Publishing Corp., New York (1962).
18. Brockmann, W., 'Steel adherends' in *Durability of Structural Adhesives*, ed. Kinloch, A. J., Elsevier Applied Science Publishers (1983) pp 281-315.
19. Bihsop, J. A., 'The chemistry and properties of a new generation of toughened epoxy matrices', *Int. J. Adhesion Adhesives*, Vol. 12, No. 3 (1992) pp 178-183.
20. Moulton, R. J. and Ting, R. Y., 'Effect of elastomeric additives on the mechanical properties of epoxy resin and composite systems', in *Composite Structures*, ed. Marshall, I. H., Applied Science Publishers Ltd, Essex, England (1981) pp 674-689.
21. Powell, P. C., 'Engineering with Fibre-Polymer Laminates', Chapman & Hall, London (1994) p 5.
22. Strong, A. B., 'Plastics: Materials and Processing', 2<sup>nd</sup> edition, Prentice-Hall Inc., New Jersey, USA (2000) p 643.
23. Brewis, D. M. and Briggs, D., 'An overview' in *Industrial Adhesion Problems*, eds. Brewis, D. M. and Briggs, D., Orbital Press, Oxford (1985) pp 1-14.
24. Gillespie Jr., J. W., Mertz, D. R., Edberg, W. M. and Ammar, N., 'Steel girder rehabilitation through adhesive bonding of composite materials', *Proc. Annual Tech. Conf. Soc. Plast. Engs.*, Vol. 1, No. 55 (1997) pp 1171-1175.
25. 'Adhesive bonding technologies key to developing fuel-efficient vehicles' (Taken from the summer 1997 newsletter), United States Council for Automotive Research ([www.uscar.org](http://www.uscar.org)) Specific Technologies.
26. Eley, D. D., and Tabor, D., 'Adhesion', ed. Eley, D. D., Oxford University Press (1961) p 9.
27. Kinloch, A. J., 'Adhesion and Adhesive, Science and Technology', Chapman & Hall, London (1987) pp 363-366.
28. Allen, K. W. 'Theories of adhesion surveyed' in *Aspects of Adhesion 5*, ed. Alner, D. J, University of London Press, London (1969) pp 11-24.
29. Wake, W. C., 'Theories of adhesion and uses of adhesives: a review', *Polymer* Vol. 19 (1978) pp 291-308.

30. Hull, D., '*An Introduction to Composite Materials*', Cambridge University Press, Cambridge (1981).
31. Johnson, Jr., R. E., and Dettre, R. H., in *Surface and Colloid Science*, ed. Matijevic, E., Vol. 2, Wiley-Interscience, New York (1969).
32. Wenzel, R. N., 'Resistance of solid surfaces to wetting by water', *Ind. Eng. Chem.* Vol. 28, No. 8 (1936) pp 988-994.
33. Mittal, K. L., in *Adhesion Science and Technology*, ed. Lee, L. H., Vol. 9A, Plenum Press, New York (1975).
34. Shuttleworth, R., and Bailey, G. L. J., 'The spreading of a liquid over a rough solid', *Disc. Farad. Soc.* Vol. 3, No. 16 (1948) pp 16-22.
35. Johnson, R.E. and Dettre, R.H., 'Contact angle hysteresis I. Idealized rough surfaces', *Adv. Chem. Ser.* No. 43 (1964) pp 112-135.
36. Huh, C., and Mason, G. S., 'Effect of surface roughness on wetting (theoretical)', *J. Colloid Interf. Sci.* Vol. 60, No. 1 (1977) pp 11-38.
37. Johnson, R. E., and Dettre, R. H., 'Wettability and contact angles', *Surf. Colloid Sci.*, Vol. 2 (1969) pp 85-153.
38. Carre, A., and Schultz, J., 'Polymer-aluminium adhesion, I. The surface energy of aluminium in relation to its surface treatment', *J. Adhesion*, Vol. 15 (1983) pp 151-62.
39. Zisman, W. A., in *Adhesion Science and Technology*, Vol. 9A, ed. Lee, L. H., Vol. 9A, Plenum Press, New York (1975) pp 55-91.
40. Levine, M., Ilkka, G., and Weiss, P., 'Relation of the critical surface tension of polymer to adhesion', *Polymer Letters*, Vol. 2 (1964) pp 915-919.
41. Barbarisi, M. J., 'Relationship between wettability and adhesion of polyethylene', *Nature*, Vol. 215 (1967) pp 383-384.
42. Bartell, F. E and Shepard, J. W., 'Surface roughness as related to hysteresis of contact angles I. The system paraffin-water-air', *J. Phys. Chem.*, Vol. 57 (1953) pp 211-215.
43. Dettre, R. H., and Johnson R. E., 'II. Contact angle measurements on rough surfaces', *Adv. Chem. Ser.*, No. 43 (1964) pp 136-144.
44. Tamai, Y., and Aratani, K., 'Experimental study of the relation between contact angle and surface roughness', *J. Phys. Chem.*, Vol. 76 (1972) pp 3267-3271.

45. Oliver, J. F. and Mason, S. G., 'Liquid spreading on rough metal surfaces', *J. Mater. Sci.* 15 (1980) pp 431-437.
46. Hitchcock, S. J., Carroll, N. T. and Nicholas, M. G., 'Some effects of substrate roughness on wettability', *J. Mater. Sci.*, Vol. 16 (1981) pp 714-732.
47. McBain, J. W. and Hopkins, D. G., 'On adhesives and adhesive action', *J. Phys. Chem.*, Vol. 29 (1925) pp 188-204.
48. Maxwell, J. W., 'Shear strength of glue joints as affected by wood surfaces and pressures', *Trans. Amer. Soc. Mech. Engs.*, Vol. 67 (1945) pp 104-110.
49. Bickerman, J. J., 'The fundamentals of tackiness and adhesion', *J. Colloid Sci.*, Vol. 2 (1947) pp 163-175.
50. Borroff, E. M. and Wake, W. C., 'II. Factors influencing the load required to strip rubber from fabric and foil surfaces', *Trans. Inst. Rubber Industry*, Vol. 25 (1949) pp 190-198.
51. Derjaguin, B. V., 'Problems of adhesion', *Research*, Vol. 8 (1955) pp 70-74.
52. Skinner, S. M., Savage, R. L. and Rutzler, J. E., 'Electrical phenomenon in adhesion, I. Electron atmospheres in dielectrics', *J. Appl. Phys.*, Vol. 24 (1953) pp 438-450.
53. Huntsberger, J. R., in *Treatise on Adhesion and Adhesives*, Vol. 1, ed. Patrick, R. L., Marcel Dekker, New York (1967).
54. Voyutskii, S. S., 'Autohesion and adhesion of high polymers', *Inter-science*, New York, Vol. 4 (1963) p 138.
55. Schonhorn, H., in *Adhesion: Fundamentals and Practices*, Ministry of Technology, Maclaren, London (1969).
56. Dickinson, J. T., Jenson, L. C., Lee, S., Scudiero, I. and Langford, S. C., 'Fracto-emission and electrical transients due to interfacial failure', *J. Adhesion Sci. Technol.*, Vol. 8, No. 11 (1994) pp 1285-1309.
57. Horn, R. G., and Smith, D. T., 'Contact electrification and adhesion between dissimilar materials', *Science*, Vol. 256 No. 5055 (1992) pp 362-364.
58. Vasenin, R. M., in *Adhesion: Fundamentals and Practice*, Ministry of Technology, Maclaren, London (1969).
59. Iyenger, Y., and Frickson, D. E., 'Role of adhesive-substrate compatibility in adhesion', *J. Appl. Polymer Sci.*, Vol. 11 (1967) pp 2311-2324.
60. Packham, D. E., 'Adhesion-fundamental and practical', in *Handbook of Adhesion*, ed. Packham, D. E., Longman Group (FE) Ltd. (1992) pp 21-24.

61. Brockmann, W. G., 'The importance of surface pretreatment prior to bonding' *Proc. Conf. IMechE.* (1986) pp 61-70.
62. Chang, W. V., 'Enhancement of adhesive joint strength by surface texturing', *J. Appl. Polymer Sci.*, Vol. 26, No. 6 (1981) pp 1759-1776.
63. CP3012, '*Cleaning and preparation of metal surfaces*', British Standards Institution, London, UK (1972).
64. BS 5350 Part A1, '*Methods of test for Adhesives: adherend preparation*', British Standards Institution, London, UK (1976).
65. Hong, S. G. and Boerio, F. J., 'Adhesive bonding of oil-contaminated steel substrates', *J. Adhesion*, Vol. 32 (1990) pp 67-88.
66. Brewis, D. M., and Briggs, D., 'Adhesion to polyethylene and polypropylene', *Polymer*, Vol. 22, No. 1 (1980) pp 7-16.
67. Kozma, L. and Olefjord, I., 'Surface treatment of steel for structural adhesive bonding', *Material Sci. Technol.*, Vol. 3 (1987) pp 954-962.
68. Baker, F. S., 'Effect of ultra-clean stainless steel surfaces on the strength of epoxide-stainless steel butt joints', *J. Adhesion*, Vol. 10, No. 2 (1979) pp 107-122.
69. Perry, H. A., '*Adhesive Bonding of Reinforced Plastics*', McGraw-Hill Book Co., Inc., 1959.
70. Guha, P. K. and Epel, J. N., 'Adhesives for the bonding of graphite/glass composites', *Society of Automotive Engineers, Inc.* 790149 (1980) pp 566-572.
71. Harris, A. F. and Beevers, A., 'The effect of grit-blasting on surface properties for adhesion', *Conf. Proc. Structural Adhesives in Engineering V*, Institute of Materials, Bristol (1998) pp 162-167.
72. Critchlow, G. W. and Brewis, D. M., 'Influence of surface macroroughness on the durability of epoxide-aluminium joints', *Int. J. Adhesion Adhesives*, Vol. 15, No. 3 (1995) pp 173-176.
73. Harris, A. F. and Beevers, A., 'Grit blasting of surfaces for adhesive bonding', *Int. J. Adhesion Adhesives*, Vol. 19 (1999) pp 445-452.
74. Gilibert, Y. and Verchery, G., 'Influence of surface roughness on mechanical properties of joints', in *Adhesive Joints Formation, Characteristics, and Testing*, ed. Mittal, K. L., Plenum Press (1982) pp 69-84.
75. Jennings, C. W., 'Surface roughness and bond strength of adhesive', *American Chem. Soc. Div. Org. Chem.*, Vol. 31, No. 2 (1971) pp 184-192.

76. Sargent, J. P., 'Adherend surface morphology and its influence on the peel strength of adhesive joints bonded with modified phenolic and epoxy structural adhesives', *Int. J. Adhesion Adhesives*, Vol. 14, No. 1 (1994) pp 21-30.
77. Venables, J. D., 'Adhesion and durability of metal-polymer bonds', *J. Mater. Sci.*, Vol. 19, No. 8 (1984) pp 2431-2453.
78. Sykes, J. M., 'Surface treatments for steel' in *Surface Analysis and Pretreatment of Plastics and Metals*, ed. Brewis, D. M., Applied Science Publishers, London, 1982, pp 153-74
79. De Bruyne, N. A., 'Aero Research Technical Notes', *Bulletin No.168*, Aero Research Ltd., Cambridge, 1958.
80. Packham, D. E., 'Roughness of surfaces', in *Handbook of Adhesion*, ed. Packham, D. E., Longman Group (FE) Ltd., 1992, pp 379-382.
81. Kalnins, M., Sirmacs, A, and Malers, L., 'On the importance of some surface and interface characteristics in the formation of the properties of adhesive joints' *Int. J. Adhesion Adhesives* 17 (1997) pp. 365-372.
82. Wake, W. C. in *Adhesion*, Ed. Eley, D. D., Oxford University Press, London, (1961) p 191.
83. Arrowsmith, D. J., 'Adhesion of electroformed copper and nickel to plastic laminates', *Trans. Inst. Met. Finish.*, Vol. 48 (Pt.2) (1970) pp 88-92.
84. Bullet, T. R. and Prosser, J. L., 'Factors affecting the adhesion of paint films to metal substrates', *VIII th Fatigec Congress* (1966) pp 374 -381.
85. Janarthanan, V., Garrett, P. D., Stein, R. S., and Srinivasarao, M., 'Adhesion enhancement in immiscible polymer bilayers using oriented macroscopic roughness', *ACS Div. Polymer Chem. Preprints*, Vol. 37, No. 2 (1996) pp 92-93.
86. Zhang, Y. L. and Spinks, G. M., 'An atomic force microscopy study of the effect of surface roughness on the fracture energy of adhesively bonded aluminium', *J. Adhesion Sci. Technol.*, Vol. 11, No. 2 (1997) pp 207-223.
87. Garnish, E. W. and Haskins, G. C., 'The effect of surface conditions when bonding with epoxy adhesives' in *Aspects of Adhesion 5*, ed. Alner, D. J, University of London Press, London (1971) pp 259-278.
88. Bijlmer, P. F. A., 'Influence of chemical pretreatments on surface morphology and bondability of aluminium', *J. Adhesion*, Vol. 5, No. 4 (1973) pp 319-331.

89. Kinloch, A. J., Bishop, H. E. and Smart, N. R., 'Surface analysis and bonding of aluminium-magnesium alloys', *J. Adhesion*, Vol. 14, No. 2 (1982) pp 105-118.
90. Anderson, G. P., Bennet, S. J. and DeVries, K. L., in *Analysis and Testing of Adhesive Bonds*, eds. Anderson et al, Academic Press, New York (1977) pp 198-213.
91. Gardon, J. L., in *Treatise on Adhesion and Adhesives*, ed. Patrick, R., Dekker, New York (1967).
92. Williams, M. L., 'Fracture threshold for an adhesive interlayer', *J. Appl. Polymer Sci.*, Vol. 14 (1970) p 1121-1126.
93. Dukes, W. A. and Bryant, R. W., 'The effect of adhesive thickness on joint strength', *J. Adhesion*, Vol. 1 (1969) pp 48-53.
94. Minnetyan, L., Chamis, C. C., and Murthy, P. L. N., 'Effect of adhesive thickness on the durability of a stiffened composite panel', *Proc. 39<sup>th</sup> Int. SAMPE Symposium*, (1994) pp 2044-2053.
95. Ojalvo, I. U. and Eidinoff, H. L., 'Bond thickness effects upon stresses in single lap adhesive Joints', *Society of Automotive Engineers, Inc.*, 770090 (1978) pp 347-356.
96. Adams, R. D., Grant, L. D. and Pavier, M., 'The influence of bond line thickness on the strength of structural adhesive joints', *Conf. Proc. Structural Adhesives in Engineering III*, Institute of Materials, Bristol (1992) pp 12/1-12/4.
97. Matsui, K., 'Effects of size on nominal ultimate tensile stresses of adhesive-bonded circular or rectangular joints under bending or peeling load'. *Int. J. Adhesion Adhesives* Vol. 10, No. 2 (1990) pp 90-98.
98. Matsui, K., 'Size-effects on average ultimate shear stresses of adhesive-bonded rectangular or tubular lap joint under tension-shear', *J. Adhesion*, Vol.10, No. 2 (1990) pp 81-89.
99. Peretz, D., 'Shear stress-strain characteristics of adhesive layers', *J. Adhesion*, Vol. 9 (1978) pp 115-122.
100. Brinson, H. F., 'The viscoelastic constitutive modelling of adhesives', *Composites*, Vol. 13 (1982) pp 377-382.
101. Hercules, D. M., 'Electron spectroscopy for chemical analysis', *J. Electron Spectrosc. Rel. Phen.*, Vol. 5 (1974) pp 811-826.

102. Dolev, G. and Ishai, O., 'Mechanical characterisation of adhesive layer in-situ and as bulk material', *J. Adhesion*, Vol. 12 (1981) pp 282-294.
103. Lilleheden, L., 'Mechanical properties of adhesives in situ and in bulk', *Int. J. Adhesion Adhesives*, Vol. 14, No. 1 (1994) pp 31-37.
104. Jeandreau, J. P., 'Intrinsic mechanical characterisation of structural adhesives', *Int. J. Adhesion Adhesives* Vol. 6, No. 4 (1986) pp 229-231.
105. Jeandreau, J.P., 'Analysis and design data for adhesively bonded joints', *Int. J. Adhesion Adhesives*, Vol. 11, No. 2 (1991) pp 71-79.
106. Adams, R. D. and Coppedale, J., 'The elastic moduli of structural adhesives', in *Adhesion-I*, ed. Allen, K., Applied Science Publishers, London, UK (1997) pp 1-17.
107. Gali, S., Dolev, G., and Ishai, O., 'An effective stress/strain concept in the mechanical characterisation of structural adhesive bonding', *Int. J. Adhesion Adhesives*, Vol. 1, No. 3 (1981) pp 135-140.
108. Adams, R. D., and Peppiatt, N. A., 'Stress analysis of adhesive-bonded lap joints', *J. Strain Anal.*, Vol. 9 No. 3 (1974) pp. 185-196.
109. Crocombe, A. D., and Adams, R. D., 'Influence of the spew fillet and other parameters on the stress distribution in the single lap joint', *J. Adhesion*, 13 (1981) pp 141-155.
110. Rispler, A. A., Tong, L., Steven, G. P. and Wisnom, M. R., 'Shape optimisation of adhesive fillets', *Int. J. Adhesion Adhesives*, 20 (2000) pp 221-231.
111. Hadavinia, H., Steidler, S., Durodola, J. and Beevers, A., 'Stiffness Sensitivity of Adhesive Bonded Coach Joints in Automotive', *Conf. Proc. Structural Adhesives in Engineering V*, Institute of Materials, Bristol (1998) pp 156-161.
112. Hashim, S. A., 'Assessment of Adhesive Bonding for Structural Design with Thick Adherends' *Ph.D. Thesis*, University of Glasgow (1992).
113. Anderson, G. P., DeVries, K. L. and Sharon, G., 'Evaluation of Adhesive Test Methods' in *Adhesive Joints Formation, Characteristics, and Testing*, ed. Mittal, K. L., Plenum Press (1982) pp 269-284.
114. 1990 Annual Book of Standards, Section 15, Volume 15.06, American society of Testing Materials, Philadelphia, PA.
115. BS 5350, *British Standard Methods of test for Adhesive*', British Standards Institution, London, UK.

116. ASTM D 3165-95 'Strength properties of adhesives in shear by tension loading of single-lap-joint laminate assembly', American society of Testing Materials, Philadelphia, PA.
117. ASTM D5041-93b 'Fracture strength in cleavage of adhesives in bonded joints', American society of Testing Materials, Philadelphia, PA.
118. ASTM D5573-94 'Classifying failure modes in fibre-reinforced-plastic (FRP) joints', American society of Testing Materials, Philadelphia, PA.
119. Wegman, R. F. and Tanner, W. C., 'Strength of epoxy adhesives when stressed to failure in milliseconds', ASTM Special Technical Publication, No. 360 (1964) pp.163-176.
120. Meissner, H. P. and Baldauf, G. H., 'Strength behaviour of adhesive bonds', *Tran. Am. Soc. Mech. Eng.*, Vol. 73 (1951) pp 697-704.
121. Failure analysis and prevention, Vol. 11, *ASM Handbook*, ASM International, (1986) pp 15-46
122. Hart-Smith L. J., 'Adhesive bond stresses and strains at discontinuities and cracks in bonded structures', *ASME J. Eng. Mater. Technol.*, Vol. 100 (1978) pp 16-24.
123. Rossettos, J. N., and Zhang, E., 'On the peak shear stresses in adhesive joints with voids', *ASME J. Appl. Mech.* Vol. 60 (1993) pp 559-560.
124. Heslehurst, R. B., 'Observations in the structural response of adhesive bondline defects', *Int. J. Adhesion Adhesives* Vol. 19 (1999) pp 133-154.
125. Papini, M., Fernlund, G., and Spelt J. K., 'The effect of geometry on the fracture of adhesive joints', *Int. J. Adhesion Adhesives*, Vol. 14, No. 1 (1994) pp 5-13.
126. Volkersen, O., 'Die Nietkraftverteilung in Zugbeanspruchten Nietverbindungen Mit Konstanten Laschenquerschnitten' *Luftfahrtforschung*, vol. 15 (1938) pp 41-47.
127. Goland, M. and Reissner, E., 'The stresses in cemented joints', *Transactions of ASME, J. Appl. Mech.*, Vol. 11 (March 1944) pp A17-A27.
128. Sneddon, I., 'The distribution of stress in adhesive joints' in *Adhesives*, ed. Eley, D. D., Oxford University Press (1961) ch-9.
129. Adams, R. D., and Peppiatt, N. A., 'Effect of Poisson's ratio strain in adherends on stresses of an idealised lap joint', *J. Strain Anal.*, Vol. 8, No. 2 (1973) pp 134-139.

130. Carpenter, W. C., 'Communication: Goland and Reissner were correct', *J. Strain Anal.* Vol. 24, No. 3 (1989) pp 185-187.
131. Tsai, M. Y. and Morton, J., 'An evaluation of analytical and numerical solutions to the single-lap joint', *Int. J. Solids Structures*, Vol. 31, No.18 (1994) pp 2537-2563.
132. Allman, D. J., 'A theory for elastic stresses in adhesive bonded lap joints', *Quart. J. Mech. Appl. Math.*, Vol. 30 (1977) pp 415-436.
133. Chen, D., and Cheng, S., 'An analysis of adhesive-bonded single lap joints', *ASME J. Appl. Mech.*, Vol. 50 (1983) pp 109-115.
134. Adams, R. D., and Mallick, V., 'A method of stress analysis of lap joints', *J. Adhesion*, Vol. 38 (1992) pp 199-217.
135. Renton, W. J., and Vinson, J. R., 'Analysis of adhesively bonded joints between panels of composite materials', *ASME J. Appl. Mech.* (March 1977) pp 101-106.
136. Hart-Smith L. J., 'Adhesive-bonded single-lap joints', NASA CR-112236, NASA Langley Research Centre, Hampton, Virginia, USA (1973).
137. Oplinger, D. W., 'A layered beam theory for single lap joints', Army Material Technology Laboratory Report MTL TR91-23 (1991).
138. Hahn, K. F., 'Photostress investigation of bonded lap joints. Part II: Analysis of experimental data', Douglas-Aircraft Company Research Report SM4000-1 (1960).
139. Adams, R. D., Chambers, S. H., Del Strother, P. J. A., and Peppiatt, N. A., 'Rubber model for adhesive lap joints', *J. Strain Anal.*, Vol. 8, No. 1 (1973) pp 52-57.
140. Hart-Smith L. J., 'Adhesive-bonded double-lap joints', NASA CR-112235, NASA Langley Research Centre, Hampton, Virginia, USA (1973).
141. Hart-Smith L. J., 'Adhesive-bonded scarf and stepped-lap joints', NASA CR-112237, NASA Langley Research Centre, Hampton, Virginia, USA (1973).
142. Hart-Smith L. J., 'Non-classical adhesive-bonded joints in practical aerospace production', NASA CR-112238, NASA Langley Research Centre, Hampton, Virginia, USA (1973).
143. Hart-Smith L. J., 'Stress analysis: A continuum mechanics approach', in *Developments in Adhesives-2*, ed. Kinloch, A. J., Elsevier Applied Science Publisher, London (1981) pp 1-44.

144. Engineering Science Data Unit, 'Inelastic shear stresses and strains in the adhesives bonding lap joints loaded in tension or shear', *Item No. 79016* (1979) London.
145. Engineering Science Data Unit, 'Elastic adhesive stresses in multistep lap joints loaded in tension', *Item No. 80039* (1979) London.
146. Roberts, T. M., 'Shear and normal stresses in adhesive joints', *J. Eng. Mech.*, Vol. 115, No. 11 (1989) pp. 2460-2479.
147. Bigwood, A., and Crocombe, A. D., 'Elastic analysis and engineering design formulac for bonded joints', *Int. J. Adhesion Adhesives*, Vol. 9, No. 4 (1989) pp 229-242.
148. Wang, C. H. and Rose, L. F. R., 'Determination of triaxial stresses in bonded joints', *Int. J. Adhesion Adhesives* 17 No. 1 (1997) pp 17-25.
149. Adams, R. D., Coppendale, J., Mallick, V. and Al-Hamdan, H., 'The effect of temperature on the strength of adhesive joints', *Int. J. Adhesion Adhesives*, Vol. 12, No. 3 (1992) pp 185-190.
150. Volkersen, O., 'Recherches sur la theoric des assemblages colles', *Construction Metallique*, Vol. 4 (1965) pp 3-13.
151. Tong, L., 'Bond shear strength of adhesively bonded double lap joints', *Int. J. Solids Structures*, Vol. 31, No. 21 (1994) pp 2919-2931.
152. Lubkin, J. L., 'A theory of elastic scarf joints', *ASME J. Appl. Mech.*, Vol. 24 (1957) pp 255-260.
153. Erdogan, F. and Rawani, M., 'Stress distribution in bonded joints', *J. Composite Materials*, Vol. 5, 1971, pp 378-393
154. Chang, M. D., Devries, K. L., and Williams, M. L., 'The effects of plasticity in adhesive fracture', *J. Adhesion*, Vol. 4 (1972) p 221.
155. Gent A. N, and Hamed G. R., 'Peel mechanics for an elastic-plastic adherend', *J. Appl. Polymer Sci.*, Vol. 21, (1977) p 2817.
156. Kim, K. S. and Aravas, N., 'Elastoplastic analysis of the peel test', *Int. J. Solids Structures*, Vol. 24, pp 417-435.
157. Lubkins, J. L., and Reissner, E., 'Stress distribution and design data for adhesive lap joints between circular tubes', *Transaction of ASME*, 78 (1956) pp 1214-1221.
158. Kukovyakin, V. M., and Skory I, A., 'Estimating the strength of bonded cylindrical joints', *Russ. Engng. J.*, Vol. 52, No. 4 (1972) pp 40-43.

159. Alwar, R. S., and Nagaraja, Y. R., 'Viscoelastic analysis of an adhesive tubular joints', *J. Adhesion*, Vol. 8 (1976) pp 79-92.
160. Shi, Y. P., and Cheng, S., 'Analysis of adhesive-bonded cylindrical lap joints subjected to axial load', *ASCE J. Eng. Mech.*, Vol. 119, No. 3 (1993) pp 584-602.
161. Ikegami, K., Sugibayashi, T., Matsui, K., 'Strength of cylinder joint adhesive bonded by coupling', *Arch. Appl. Mech.*, Vol. 65, No. 1 (1995) pp 44-53.
162. Chon, C. T., 'Analysis of tubular joint in torsion', *J. Composite Materials*, Vol. 16 (1982) pp 268-284.
163. Zhou, H. M., and Rao, M. D., 'Viscoelastic analysis of bonded tubular joints under torsion', *Int. J. Solids Structures*, Vol. 30, No. 16 (1993) pp 2199-2211.
164. Sawa, T. and Uchida, H., 'A two-dimensional stress analysis and strength evaluation of band adhesive butt joints subjected to tensile loads', *J. Adhesion Sci. Technol.*, Vol. 11, No. 6 (1997) pp 811-833.
165. Nakano, Y., Temma, K. and Sawa, T., 'A stress analysis of adhesive butt joints of dissimilar materials subjected to cleavage loads', *J. Adhesion*, Vol. 34 (1991) pp 137-151.
166. Wooley, G. R., and Carver, D. R., 'Stress concentration factors for bonded lap joints', *J. Aircraft*, Vol. 8, No. 10 (1971) pp 817-820.
167. Barker, R. M. and Hatt, F., 'Analysis of bonded joints in vehicular structures', *AIAA J.*, Vol. 11, No. 12 (1973) pp 1650-1654.
168. Carpenter, W. C., 'Finite element analysis of bonded connections', *Int. J. num. Meth. Engng.*, Vol. 6 (1973) pp. 450-451.
169. Carpenter, W. C., 'Stresses in bonded connections using finite elements', *Int. J. num. Meth. Engng.*, Vol. 15 (1980) pp 1659-1680.
170. Richardson, G., Crocombe, A. D., and Smith, P. A., 'A comparison of two- and three-dimensional finite element analysis of adhesive joints', *Int. J. Adhesion Adhesives*, Vol. 13 No. 3 (1993) pp 193-200.
171. Delale, F., Erdogan, F. and Aydinoglu, M. N., 'Stresses in adhesively bonded joints: A closed-form solution', *J. Composite Materials*, Vol. 15 (1981) pp 249-271.
172. Crocombe, A. D., and Adams, R. D., 'An elasto-plastic investigation of the peel test', *J. Adhesion*, Vol. 13 (1982) pp 241-267.

173. Crocombe, A. D., and Adams, R. D., 'Peel analysis using the finite element method', *J. Adhesion*, Vol. 12, No. 2 (1981) pp 127-139.
174. Sheppard, A., Kelly, D. W. and Tong, L., 'A damage zone model for the failure analysis of adhesively bonded joints', *Int. J. Adhesion Adhesives*, Vol. 18 No. 6 (1998) pp 385-400.
175. Adams, R. D., Coppedale, J. and Peppiatt, N. A., 'Stress analysis of axisymmetric butt joints loaded in torsion and tension', *J. Strain Anal.*, Vol. 13, No.1 (1978) pp 1-10.
176. Adams, R. D., and Harris, J. A., 'The influence of local geometry on the strength of adhesive joints', *Int. J. Adhesion Adhesives* 7 No. 2 (1987) pp 69-80.
177. Adams, R. D., Comyn, J. and Wake, W. C., '*Structural adhesive joints in engineering*' 2<sup>nd</sup> edition, Elsevier Applied Science Publishers, London (1997).
178. Crocombe A. D., Bigwood, D. A., and Richardson, G., 'Analysing structural adhesive joints for failure', *Int. J. Adhesion Adhesives* 10 No. 3 (1990) pp 167-178.
179. Hashim, S.A. and Cowling, M.J., 'Aspects of Testing and Failure Surface Analysis Related to Thick Adherend Steel Bonded Joints'. *Proc. Structural Adhesives in Engineering IV*, Bristol (1995) pp 245-250.
180. Li, W., 'Analysis of adhesive bonded tee joint by finite element method', Ph.D. Thesis, University of Birmingham (1998).
181. Hattori, T., 'A stress-singularity-parameter approach for evaluating the adhesive strength of single-lap joints', *JSME Int. J. Series I*, Vol. 34, No.3, pp 326-331.
182. Groth, H. L., 'Stress singularities and fracture at interface corners in bonded joints', *Int. J. Adhesion Adhesives*, Vol. 8, No. 2 (1988) pp 107-113.
183. Lang, T. P. and Mallick, P. K., 'The effect of recessing on the stresses in adhesively bonded single-lap joints', *Int. J. Adhesion Adhesives*, Vol. 19 (1999) pp 257-271.
184. Katona, T. R. and Batterman, S. C., 'Surface roughness effects on the stress analysis of adhesive joints', *Int. J. Adhesion Adhesives*, Vol. 3, No. 2 (1983) pp 85-91.
185. Smith, C. B., 'Some new types of orthotropic plates laminated of orthotropic materials', *J. Appl. Mech.* Vol. 20 (1953) pp 286-288.

186. Pyror, C. W., Jr., and Barker, R. M., 'Finite element analysis of bending-extensional coupling in laminated composites', *J. Composite Materials*, Vol. 4 (1970) pp 549-552.
187. Liu, J., Sawa, T. and Toratani, H., 'A two-dimensional stress analysis and strength of single-lap adhesive joints of dissimilar adherends subjected to external bending moment', *J. Adhesion*, Vol.12, No.8 (1998) pp 795-812.
188. Surace, G. and Brusa, E., 'A parametric study of structural adhesive joints for aerospace applications', in *Advance technology for design and fabrication of composite materials and structures: applications to the automotive, marine, aerospace and construction industry*, ed. Sih, G. C., Carpinteri, A. and Surace, G., Kluwer Academic Publishers, Netherlands (1995) pp 393-408.
189. Pickett, A. K., and Hollaway, L. 'The analysis of elastic-plastic adhesive stress in bonded lap joints in FRP structures', *Composite Structures*, Vol. 4 (1985) pp 135-160.
190. Herakovich, C. T., 'Edge effects and delamination failures', *J. Strain Anal.*, Vol. 24, No. 4 (1989) pp 245-252.
191. Ripling, E. J., Santner, J. S. and Crosley, P. B., 'Fracture of Composite-Adhesive-Composite System', in *Adhesive Joints Formation, Characteristics, and Testing*, ed. Mittal, K. L., Plenum Press (1982) pp 755-787.
192. Han, K. S. and Koutsky, 'Interlaminar Fracture Energy of Glass Fibre Reinforced Polyester Composites', *J. Composite Materials*, Vol. 15 (1980) pp 371-388.
193. Williams, J. G., 'The fracture mechanics of delamination tests', *J. Strain Anal.*, Vol. 24, No. 4 (1989) pp 207-214.
194. Kairouz, K.C. and Matthew, F. L., 'A finite element analysis of the effect of stacking sequence on the failure mode of bonded composite single lap joints', in *Composite Materials. Design and Analysis*, ed. De Wilde, W. P. and Blain, W. R., Computational Mechanics Publications, Southampton (1990) pp 549-564.
195. Kairouz, K. C. and Matthews, F. L., 'Mechanism of failure in bonded CFRP single lap Joints with different Stacking Sequences', *Conf. Proc. FRC'90*, Liverpool, Institution of Mechanical Engineers, UK (1990) pp 47-59.

196. Pradhan, S. C., Iyengar, N. G. R. and Kishore N. N., 'Parametric study of interfacial debonding in adhesively bonded composite joints', *Composite Structures*, Vol. 29 (1994) pp 119-125.
197. Ratwani, M. M. and Kan, H. P., 'Effect of stacking sequence on damage propagation and failure modes in composite laminates', *Damage in Composite Materials, ASTM STP 775*, ed. Reifsnider, K. L., American Society for Testing and Materials (1982) pp 211-228.
198. Lu, T. J., Ji, X. and Gu, X. R., 'The effect of resin properties on the strength of filamentary structures', *J. Strain Anal.*, Vol. 24, No. 2 (1989) pp 107-113.
199. Talreja, R., 'Damage development in composites: Mechanics and modelling', *J. Strain Anal.*, Vol. 24, No. 4 (1989) pp 215-222.
200. Lin, T. H., Salinas, D. and Ito, Y. M., 'Elastic-plastic analysis of unidirectional composites', *J. Composite Materials*, Vol. 6 (1972) pp 48-60.
201. Lakshminarayana, H. V. and Viswanath, S., 'A correlation study of finite element modelling for the stress analysis of composite-material laminates', *J. Strain Anal.*, Vol. 13, No. 4, (1978) pp 205-212.
202. Naik, N. K., 'Numerical modelling of woven fabric composite materials' in *Numerical Analysis and Modelling of Composite Materials*, ed. Bull, J. W., Blackie Academic & Professional, Glasgow (1996) pp 400-438.
203. Ducept, F., Davies, P. and Gamby, D., 'Mixed mode failure criteria for a glass/epoxy composite and an adhesively bonded composite/composite joint', *Int. J. Adhesion Adhesives*, Vol. 20 (2000) pp 233-244.
204. Yamada, Y. and Okumura, H., 'Analysis of local stress in composite materials by the 3D finite element', in *Composite Materials: mechanics, mechanical properties and fabrication*. ed. Kawata, K and Akasaka, T., Appl. Sci. Publisher for JSCM (1982) pp 55-64.
205. Dorn, L, 'TALAT lectures 4700: Adhesive bonding of aluminium', *European Aluminium Association* (1994).
206. Minford, J. D., 'Adhesives' in *Durability of Structural Adhesives*, ed. Kinloch, A. J., Elsevier Applied Science Publishers (1983).
207. Hashim, S. A., Cowling, M. J. and Lafferty, S., 'The Integrity of Bonded Connections in Large Composite Pipes', *Int. J. Adhesion Adhesives*, Vol. 18 (1998) pp 421-429.

208. Jeandrau, J. P., 'Adhesive mechanical characterisation-The user's need for structural applications', Conf. Proc. Structural Adhesives in Engineering III, Institute of Materials, Bristol (1992) pp 18/1-18/8.
209. Knox, E. M., 'Marine Applications for Structural Adhesives', *Ph.D. Thesis*, University of Glasgow (1996).
210. Product data sheets for Fibredux 913G/30%/E-5 and Fibredux 913G/37%/7781, Hexcel Corporation.
211. "Test methods for composite materials" seminar (Basel, Switzerland) notes, June 1993, Technomic Publishing Company, Pennsylvania, USA.
212. Shigley, J. E. and Mitchell, I. D., 'Mechanical engineering design', 4th ed., McGraw-Hill, New York (1983).
213. Sarkar, A. D., 'Surface Topography', in *Wear of Metals*, Pergamon Press, Oxford (1976) pp 8-13.
214. Bhushan, B., 'Micro/nanotribology using atomic force microscopy/friction force microscopy: state of the art', *Conf. Proc. IMechE*. Vol. 212, Part J (1998).
215. Help file of "Ultra" software, Taylor and Hobson.
216. Dagnall, H., 'Exploring surface texture', 3<sup>rd</sup> edition, Taylor Hobson Ltd., Leicester (1998).
217. <http://polymer.physics.bristol.ac.uk/spm>
218. <http://wintermute.chemie.uni.mainz.de/>
219. Instruction manual 'OPTIPHOT metallurgical microscope interference system', 59(89.2.c)H.E-3R, Nikon Corporation.
220. Patran V9.0, *The MacNeal-Schwendler Corporation*, Surrey, UK.
221. 'Abaqus V 5.5', *Hibbitt, Karlsson and Sorensen*, Providence, Rhode Island, USA.
222. Mathematica 4, *Wolfram Research Inc.*, Champaign, Illinois, USA.
223. Takada, S. and Kimpara, I., 'Analysis of flexural failure process of hybrid composite materials', *Conf. Proc. IMechE* (1990) pp 35-45.
224. LExcellent, C. and Nwokoye, D. O., 'Tri dimensional calculation of stratified composite plates elastically loaded in bending: experimental verifications' in *'Composite Materials. Design and Analysis'*, ed. De Wilde, W. P. and Blain, W. R., Computational Mechanics Publications, Southampton (1990) pp 293-314.

225. Bancroft, G. M., Mayne, J. E. O., and Ridgway, P., 'Moessbauer (sic) spectra and the structure of oxide films present on iron after exposure to dry air and to chromate solutions at pH4', *Brit. Corr. J.*, Vol. 6 (1971) pp 119-121.
226. Sherlock, J. C., in *Aspects of Adhesion 6*, ed. Alner, D. J, University of London Press, London (1971) pp 112-119.
227. Gardner, M. K., 'Adhesion of coatings to steel', *Ph.D. thesis*, University of Oxford (1987).
228. Evans, J. R. G., and Packham, D. E., 'Adhesion of polyethylene to metals: the role of surface topography', *J. Adhesion*, Vol. 10 (1979) pp177-191.
229. Schultz, R. D., Possart, W., Kamusewitz, H., Bischof, C., 'Young's equilibrium contact angle on rough solid surfaces, Part I. An empirical determination', *J. Adhesion. Sci. Technol.*, Vol. 3, No. 1 (1989) pp 39-48.
230. They, S., Legros, A., and Balladon, P., 'Study of parameters influencing the mechanical behaviour of and damage to steel-polymer interfaces' in *Mechanics and Mechanisms of Damage in Composites and Multi-Materials*, ESIS11(Edited by D. Baptiste) (1991) Mechanical Engineering Publications, London, pp 339-350.
231. Yost, F. G., Micheal, J. R., and Eisenmann, E. T., 'Extensive wetting due to roughness', *Acta Metall Mater*, Vol. 43, No. 1 (1995) pp 299-305.
232. Cowling, M. J., Hashim, S. A., Knox, E. M. and Winkle, I. E., 'Adhesive bonding for marine structural applications', *Proc. 3rd Int. Conf. on Polymers in a Marine Environment, London, IMarE*, (October 1991).
233. "Redux bonding technology", Publication No. RGU 034b, Hexcel Composites (Dec. 1997).
234. Hart-Smith, L. J., Redmond, G. and David, M. J., 'The curse of the nylon peel ply', *41<sup>st</sup> Intl. SAMPE Symposium* (March, 1996) pp 303-317.
235. Meissner, H. P. and Baldauf, G. H., *Tran. Amer. Soc. Mech. Eng.* (1951) p 697.
236. Agarwal, B. D. and Broutman, L. J., '*Analysis and performance of fibre composites*', 2<sup>nd</sup> edition, Wiley, New York, USA (1990).
237. Tsai, S. W. and Wu, E. M., 'General theory of strength for anisotropic materials', *J. Composite Materials*, Vol. 5 (1971) pp 58-80.
238. Chandler, II. D., Campbell, I. M. D. and Stone, A. N., 'Assessment of failure criteria for fibre reinforced composite laminate', *Int. J. Fatigue*, Vol. 17, No. 7 (1995) pp 513-518.

Appendix 1

Owing to the difficulty in making bubble-free bulk adhesive dog-bone specimens, as mentioned in section 3.4, the bulk adhesive specimen tested in the laboratory failed at about 50% of the maximum tensile strength (40.29 MPa) reported by the resin supplier, Ciba Chemicals. However, the part of stress-strain curve obtained during the testing was sufficient for calculating the Poisson's ratio and the Young's modulus.

Table A Stress-strain measurements from bulk adhesive specimen

<i>Axial stress</i> (MPa)	<i>Axial strain</i> (%)	<i>Transverse strain</i> (%)
-0.00311	0	0
0.142755	0	-0.0008
0.28862	-0.0006	-0.0001
2.688839	0.1068	-0.0445
2.778591	0.1113	-0.0464
2.883302	0.1223	-0.0505
5.349611	0.2145	-0.088
5.433706	0.2187	-0.0899
5.531818	0.2252	-0.0927
8.010975	0.3291	-0.1342
8.235118	0.3332	-0.1359
8.327412	0.3372	-0.1376
10.64658	0.4329	-0.1757
10.7216	0.4369	-0.1771
10.80912	0.4409	-0.1788
13.30811	0.5476	-0.2201
13.37861	0.5545	-0.2229
13.51961	0.5575	-0.2244
15.93828	0.666	-0.2661
16.00297	0.6694	-0.2674
16.07845	0.6735	-0.2698
18.5772	0.7939	-0.3142
18.63481	0.8003	-0.3166
18.7494	0.8039	-0.3176
21.29897	0.9327	-0.3645
21.36581	0.9359	-0.3659

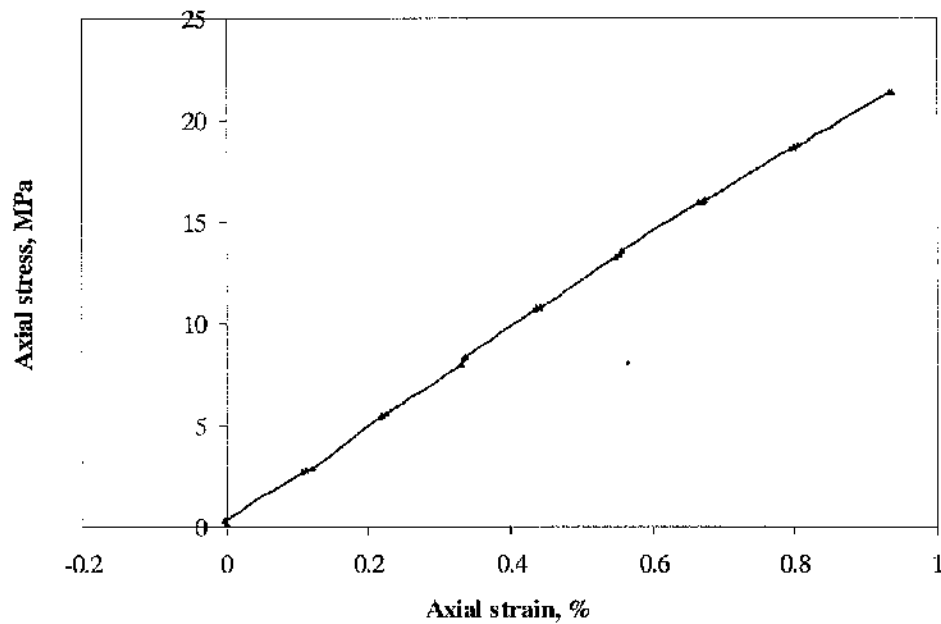


Figure A1 Stress-strain curve obtained from the tensile testing of bulk adhesive dog-bone specimen

$$\text{Young's modulus} = \frac{\text{Stress}}{\text{Strain}} = \frac{5.531818}{0.002252} = 2456 \text{ MPa}$$

$$\text{Poisson's ratio} = \frac{\text{Lateral strain}}{\text{Axial strain}} = \frac{0.2201}{0.5476} = 0.40$$

The calculated value of Young's modulus is in line with the value provided by the resin supplier. The calculated Poisson's ratio is also in line with the value reported earlier<sup>209</sup>.

Appendix 2

Figure A2 illustrates the triangular load distribution along a beam of 12.5mm length, representing a steel/steel cleavage joint (Model S). The beam is assumed to consist of a series of 12 butt joints of 1mm width and a half joint.

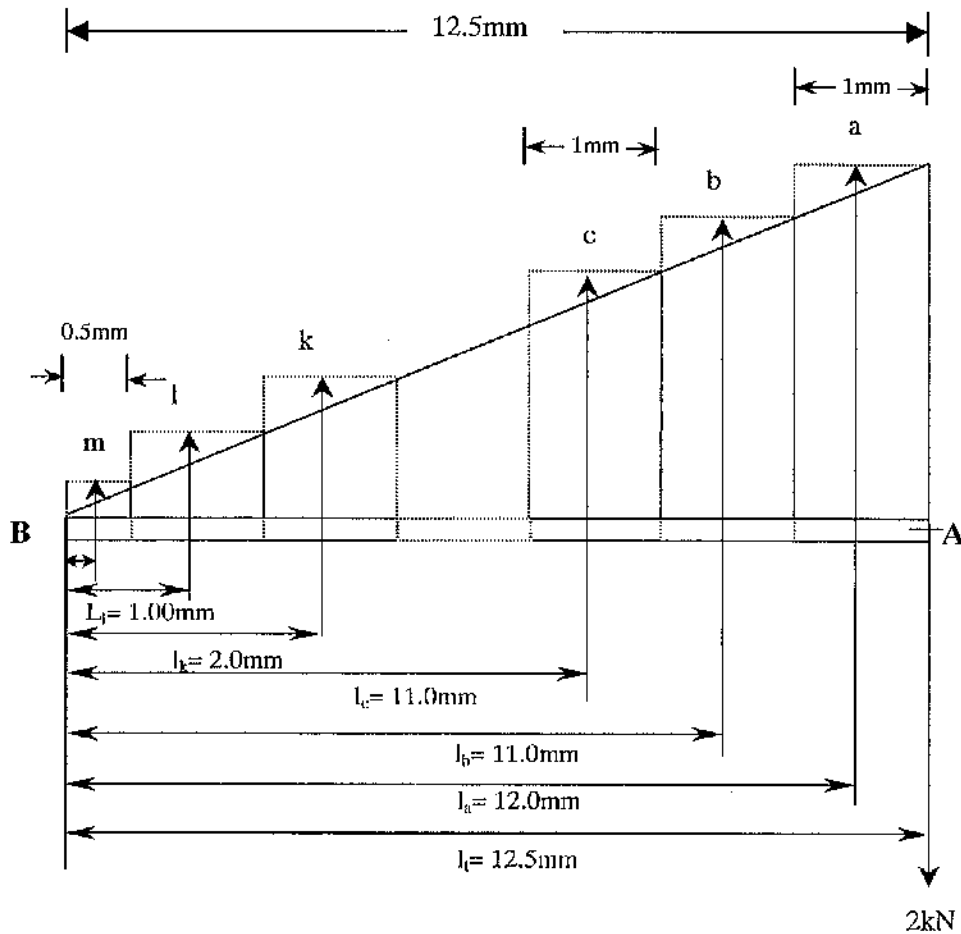


Figure A2 Triangular load distribution along a 12.5mm beam (Model S)

A nominal downward load of 2kN is applied at end A, that creates reaction tensile forces in each butt element represented here by a, b, c and so on. These reaction forces are assumed to act at the centre of the butt joints i.e. the first reaction force shall be acting at a distance of 0.5mm from end A.

Applying  $\sum F_y=0$  gives the following equation:

$$a + b + c + d + e + f + g + h + I + j + k + l + m = 2000 \quad (1)$$

Applying  $\sum M_A=0$  gives,

$$0.5a + 1.5b + 2.5c + 3.5d + 4.5e + 5.5f + 6.5g + 7.5h + 8.5I + 9.5j + 10.5k + 11.5l + 12.25m = 0 \quad (2)$$

By applying a similar triangle method, we get,

$$\frac{a}{b} = \frac{l_a}{l_b} \quad (3)$$

Substituting the known values in the above equation, we get,

$$\begin{aligned} \frac{a}{b} &= \frac{12.0}{11.0}, & \frac{a}{c} &= \frac{12.0}{10.0}, & \frac{a}{d} &= \frac{12.0}{9.0}, & \frac{a}{e} &= \frac{12.0}{8.0}, \\ \frac{a}{f} &= \frac{12.0}{7.0}, & \frac{a}{g} &= \frac{12.0}{6.0}, & \frac{a}{h} &= \frac{12.0}{5.0}, & \frac{a}{i} &= \frac{12.0}{4.0}, \\ \frac{a}{j} &= \frac{12.0}{3.0}, & \frac{a}{k} &= \frac{12.0}{2.0}, & \frac{a}{l} &= \frac{12.0}{1.0} \end{aligned} \quad (4-14)$$

Solving these equations using Mathematica gives the following results:

$$\begin{aligned} a &= 466.297, b=427.439, c=388.58, d=349.722, e=310.864, \\ f &= 272.006, g=233.148, h=194.29, i=155.432, j=116.574, \\ k &= 77.7161, l=38.858, m=-1030.93 \end{aligned}$$

### Appendix 3

Similar to the one mentioned in Appendix 2, a triangular load distribution along a beam of 15mm length is considered to represent a hybrid cleavage joint (Model H). The beam is assumed to consist of a series of 15, 1mm wide butt joints (Figure A3).

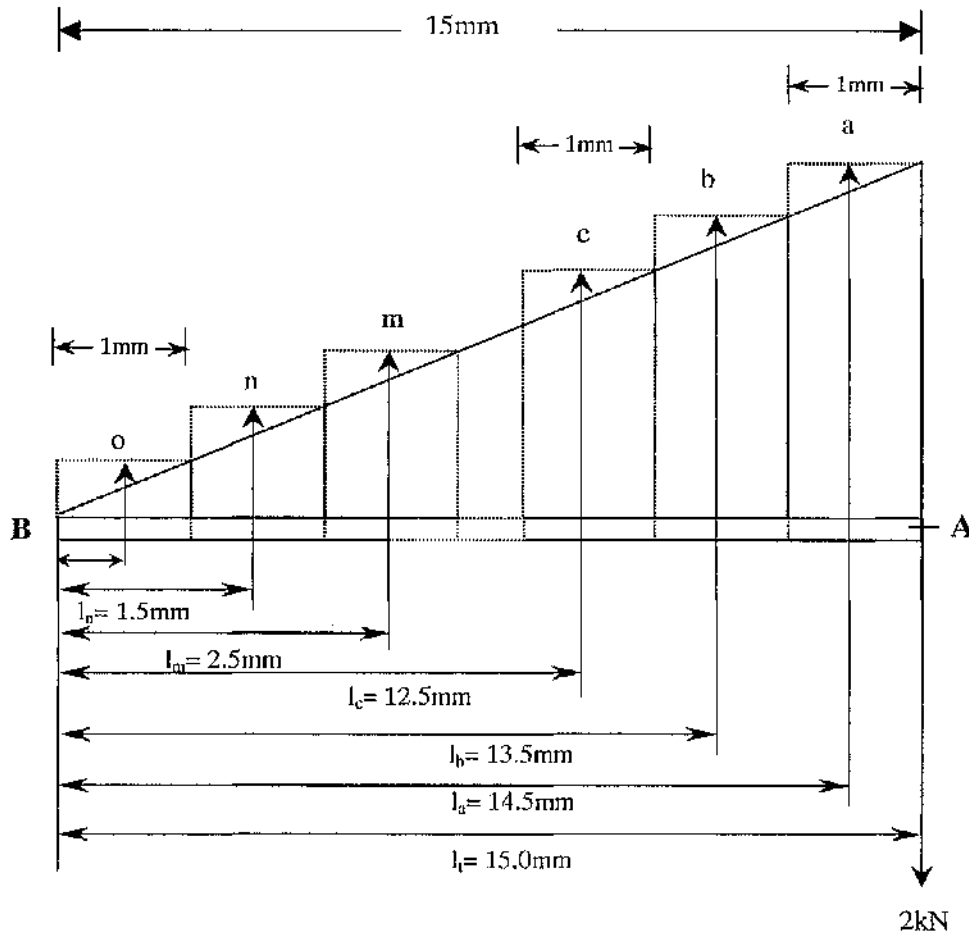


Figure A3 Triangular load distribution along a 15mm beam (Model II)

Again a nominal downward load of 2kN is applied at end A, that creates reaction tensile forces in each butt element represented here by a, b, c and so on. These reaction forces are assumed to act at the centre of the butt joints so that the first reaction force is acting at a distance of 0.5mm from end A.

Applying  $\sum F_V=0$ ,  $\sum M_A=0$  and a similar triangle method gives the following equations:

$$a + b + c + d + e + f + g + h + i + j + k + l + m + n + o + p = 2000 \quad (15)$$

$$0.5a + 1.5b + 2.5c + 3.5d + 4.5e + 5.5f + 6.5g + 7.5h + 8.5i + 9.5j + 10.5k + 11.5l + 12.5m + 13.5n + 14.5o = 0 \quad (16)$$

$$\begin{aligned} \frac{a}{b} &= \frac{14.5}{13.5}, & \frac{a}{c} &= \frac{14.5}{12.5}, & \frac{a}{d} &= \frac{14.5}{11.5}, & \frac{a}{e} &= \frac{14.5}{10.5}, \\ \frac{a}{f} &= \frac{14.5}{9.5}, & \frac{a}{g} &= \frac{14.5}{8.5}, & \frac{a}{h} &= \frac{14.5}{7.5}, & \frac{a}{i} &= \frac{14.5}{6.5}, \\ \frac{a}{j} &= \frac{14.5}{5.5}, & \frac{a}{k} &= \frac{14.5}{4.5}, & \frac{a}{l} &= \frac{14.5}{3.5}, & \frac{a}{m} &= \frac{14.5}{2.5}, \\ \frac{a}{n} &= \frac{14.5}{1.5} \end{aligned} \quad (17-29)$$

Solving the above equations using Mathematica gives the following solution:

$$\begin{aligned} a &= 393.911, & b &= 366.745, & c &= 339.578, & d &= 312.412, \\ e &= 285.246, & f &= 258.08, & g &= 230.913, & h &= 203.747, \\ I &= 176.581, & j &= 149.415, & k &= 122.248, & l &= 95.082, \\ m &= 67.9157, & n &= 40.7494, & o &= -1042.62 \end{aligned}$$